THE DEVELOPMENT OF MODIFIED ELECTRODES

A thesis submitted for the degree of Doctor of Philosophy of the University of London and for the Diploma of Membership of Imperial College.

by

Andrew Raymond Mount B. Sc., A.R.C.S.

Chemistry Department

Imperial College

London SW7 2AY

December 1986

ABSTRACT

The aims of the work presented in this thesis are twofold.

The first objective was the development of novel polymer modified electrodes for electrocatalysis. Lead(IV) carboxylate species have been widely used as batch oxidants for the specific oxidation of organic substrates in solution. The object of this part of the thesis was the synthesis of a polymer coat containing a lead(II)/lead(IV) carboxylate redox couple with the aim of producing an electrocatalytic modified electrode mimicking this reactivity. The preparation and characterisation of conducting polymer modified electrodes containing pendant carboxylic acid functional groups and the conversion of these moieties to form lead(II) carboxylate species is described. Data for the electrooxidation of redox couples and organic molecules at these films is presented and the applicability of these coats to electrocatalytic oxidation reactions discussed.

Secondly, the oxidation and reduction of the thionine coated electrode has been studied. Information concerning the flux of protons and counteranions throughout this reaction has been obtained by the novel use of potentiometric ring electrode sensors. Also presented are spectroelectrochemical results for these reactions. These results are interpreted in terms of the kinetics and mechanism of the coat redox reactions.

To Mum and Dad

I would like to thank:

the SERC for financial support

John Albery for his supervision

Wendy Flavell for her much appreciated help in typing parts of this thesis

Keith Parsons and Mark Neville for their excellent proof reading

Joe Przeworski, Pete Tebbutt, Keith Parsons and Hugh Middleton for helpful discussions during the course of this work

all members of Professor Albery's research group, past and present, who have made life so much fun over the past three years

Jeff, my brother, for his support

Jim Smith and his blue and white army

LIST OF CONTENTS

page

CHAPTER 1 INTRODUCTION

1.1 Polymer Modified Electrodes 23

1.1.1 Polymer Types 25

1.2 Methods Of Preparation 30

1.2.1 Covalent Chemical Linkage 30

1.2.2 Surface Adsorption 30

1.2.3 Plasma Discharge 32

1.2.4 Electrochemical Coating 33

1.3 Applications 34

1.3.1 Selective Redox Reactions 34

1.3.2 Batteries 41

1.3.3 Electrochromic Devices 41

1.3.4 Photoelectrodes 43

1.3.5 Other Applications 44

1.4 Outline Of The Rest Of This Thesis 46

CHAPTER 2 THEORY OF RING-DISC TECHNIQUES

2.1 The Rotating Disc Electrode 48

2.1.1 Current-Voltage Curves 57

2.2 The Rotating Ring-Disc Electrode 60

2.2.1 Amperometric Ring Sensors 60

2.2.2 Potentiometric Ring Sensors 63

2.2.2.1 The Silver/Silver Ion Electrode 64

2.2.2.2 The Silver/Silver Chloride Electrode 67

page

2.2.2.3 The Bismuth/Bismuth Oxide Electrode 69

2.2.2.3.1 General Theory For The Bismuth/Bismuth Oxide Ring Sensor Involving Proton and Hydroxide Ion Titration 72

CHAPTER 3 EXPERIMENTAL

3.1 Circuitry 92

3.2 Electrodes 95

3.2.1 Working Electrodes 95

3.2.2 Counter Electrodes 95

3.2.3 Reference Electrodes 96

3.3 Rotation System And Cell Assembly 97

3.4 Solvents 99

3.5 Background Electrolytes 100

3.6 Chemicals 101

3.6.1 Heteroaromatic Monomers 101

3.6.2 Miscellany 101

3.7 Spectrometry 102

3.7.1 Laser Raman Spectrometry 102

3.7.2 X-Ray Photoelectron Spectroscopy (XPS) 104

3.7.3 Scanning Electron Microscopy (SEM) 104

3.7.4 Fourier Transform Infra-Red Spectroscopy (FTIRS) 105

3.7.5 In Situ Visible Spectroscopy 105

3.8 Deoxygenation Systems 108

page

3.9 Bismuth Oxide Ring Experiments 109

3.9.1 Apparatus 109

3.9.2 Chemicals 109

3.9.3 Sensor Preparation 110

3.10 Siver/Silver Chloride Experiments 111

CHAPTER 4 CONDUCTING POLYMERS FOR ELECTROCATALYTIC OXIDATION

4.1 Introduction 112

4.1.1 Conducting Polymer Modified Electrodes 113

4.1.2 Selective Organic Oxidants For Electrocatalysis 116

4.1.2.1 Lead(IV) Acetate 116

4.1.2.2 Thallium(III) Acetate 116

4.1.3 Preparation Of Substituted Conducting Polymers 118

4.2 Synthesis And Electrochemistry Of 3- and 4-Carboxylated Pyrroles 122

4.3 Copolymerisation Of Thiophenes 125

4.3.1 Introduction 125

4.3.2 Polymerisation Of Thiophene 126

4.3.3 Formation Of TP/TPAA copolymers 132

4.3.3.1 Evidence For The Formation Of TP/TPAA copolymers 135

4.3.3.2 The Structure Of TP/TPAA Copolymers 143

page

4.3.4 Formation Of Thiophene And 3-Thiophene Carboxylic Acid Copolymers 145

4.3.4.1 Evidence For The Formation Of TP/TPCA copolymers 148

4.4 Incorporation Of Lead Into TP/TPAA and TP/TPCA Copolymers 151

4.4.1 TP/TPAA Copolymers 151

4.4.2 The Leading Of TP/TPCA Copolymers 154

4.5 Electrochemistry Of Leaded TP/TPAA Copolymers 157

4.5.1 Cyclic Voltammetry 157

4.5.2 Redox Reactions 159

4.5.2.1 The Oxidation Of Quinol 159

4.5.2.2 The Oxidation Of Ethylene Glycol And Other Diols 164

4.6 Discussion 168

Appendix- Experimental Details Of The TosMIC Reaction 171

CHAPTER 5 CHARGING AND DISCHARGING THE THIONINE COATED ELECTRODE

5.1 Introduction 172

5.1.1 Reaction Kinetics Of Polymer Modified Electrodes 172

5.1.2 The Thionine Coated Electrode- The Story So Far 175

5.2 Chronoamperometric Studies 181

page

5.3 Mechanisms Of The Charging/Discharging Process 187

5.3.1 Bismuth/Bismuth Oxide Experiments 187

5.3.2 Silver/Silver Chloride Experiments 199

5.3.3 Reactions Of Coated Thionine At pH > pK_{a3} 208

5.3.3.1 In Situ Visible Spectroscopic Experiments 209

5.3.3.2 'Disconnect' Experiments 209

5.4 Kinetics Of Large Step Chronoamperometric Experiments 215

5.4.1 Effects Of Mechanistic Change 215

5.4.2 Effect Of Step Size 217

5.4.3 Effect Of Anion Size 221

5.5 In Situ Laser Raman Spectroscopic Studies 224

5.6 Discussion- The Formation Of A General Model For Chronoamperometry At A Thionine Modified Electrode 233

5.7 The Applicability Of The Techniques Presented In This Chapter 238

APPENDIX 240

REFERENCES 245

LIST OF FIGURES

page

Figure 1.1 Schematic representation of mediated oxidation of a substrate (S) to a product (P) at a modified electrode. 24

Figure 1.2 Conduction in polyvinyl polymers via an electron hopping mechanism. 27

Figure 1.3 Examples of polymers and polymerisable monomers which produce modified electrodes for which electronic conduction occurs by electron hopping. 28

Figure 1.4 Some aromatic monomers which produce conducting polymer modified electrodes. 29

Figure 1.5 Examples of surface derivatising reactions for the preparation of modified electrodes. 31

Figure 1.6 The proposed reaction scheme for photoassisted electrochemical reduction using polyvinylferrocene electrodes. 38

Figure 1.7 The 'all polymer' cell. 42

Figure 2.1 The rotating disc electrode (RDE). 49

Figure 2.2 The cylindrical polar co-ordinates and fluid flow vectors used to model the RDE. 50

Figure 2.3 The functions B, G and H. 50

Figure 2.4 Flow patterns for an RDE. 52

Figure 2.5 Calculated concentration profiles at an RDE. 52

page

Figure 2.6 Movement from charge transfer control to mass transfer control for reduction of O to R at an RDE. 55

Figure 2.7 The rotating ring-disc electrode (RRDE). 61

Figure 2.8 The schematic variation in concentration of an electroactive species at an RRDE. The species is being produced at the disc and destroyed at the ring. 62

Figure 2.9 The concentration of electrogenerated species as a function of radial distance for a potentiometric ring sensor with low exchange current density. The gap and ring dimensions shown are for the electrodes used in this work. 71

Figure 2.10 Schematic concentration profile for the titration of A produced at the disc by B from the bulk. 73

Figure 2.11 Schematic variation of the concentration of A with x, the distance from the disc, with and without titration of A by B. In both cases, the flux of A at the disc is the same. 81

Figure 2.12 The effect of titration of A by B in the radial direction. 82

page

Figure 2.13 Theoretical plot of the flux of proton or hydroxide ion at a disc electrode as a function of the pH at the disc (pH_0) and in the bulk (pH_∞) for W=1 Hz. The flux values are given in mol cm^{-2} s^{-1}. 89

Figure 3.1 Some electronic units based on the operational amplifier used in the construction of electrochemical circuits.
(a) voltage follower
(b) summing inverting amplifier
(c) subtractor
(d) inverting amplifier 93

Figure 3.2 Schematic diagrams of three electrode and four electrode potentiostatic circuits. 94

Figure 3.3 The electrochemical cells.
(a) aqueous
(b) non-aqueous 98

Figure 3.4 The in situ laser Raman electrochemical cell. 103

Figure 3.5 The MIRΓTIRS set-up. 106

Figure 4.1 Pyrrole, thiophene and furan. 114

Figure 4.2a The structure of polypyrrole, polythiophene and polyfuran. 115

page

Figure 4.2b Oxidation and reduction of the polymer. 115

Figure 4.3a The oxidation of diols by lead(IV) acetate. 117

Figure 4.3b The oxidation of aromatic compounds by thallium(III) acetate. 117

Figure 4.4 The proposed mechanism of the TosMIC reaction. 123

Figure 4.5 Current-voltage data for the oxidation of thiophene (75 mM) at W = 4 Hz, $v = 20\ mVs^{-1}$. 127

Figure 4.6 Current-time data for the electrooxidation of a thiophene solution (500 mM) at 1.6 V. 128

Figure 4.7 A cyclic voltammogram of a polythiophene modified electrode in $MeCN/LiClO_4$ (0.1 M) at $v = 50\ mV\ s^{-1}$. 130

Figure 4.8 Variation of the peak currents for oxidation and reduction of a polythiophene coat with the potential sweep rate. 131

Figure 4.9a Current-time data for the electropolymerisation of a 150mM TP/100 mM TPAA solution at 1.6 V. 133

Figure 4.9b Cyclic voltammogram of the resulting coat ($v = 50\ mVs^{-1}$). 133

page

Figure 4.10 Variation of the observed peak currents for oxidation and reduction of the TP/TPAA polymer with potential sweep rate. 134

Figure 4.11a FTIR spectrum of a TP/TPAA copolymer. The peak positions are given in wavenumbers. 137

Figure 4.11b IR spectrum of TPAA monomer. 137

Figure 4.12 FTIR spectrum of polythiophene. 138

Figure 4.13 ESCA spectrum of a polythiophene coated platinum flag. 140

Figure 4.14a ESCA spectrum of a coated platinum flag prepared by polymerising a solution of 300 mM TP/75 mM TPAA. 141

Figure 4.14b ESCA spectrum of a coated platinum flag prepared by polymerising a solution of 300 mM TP/150 mM TPAA. 141

Figure 4.15 Typical SEM photograph of a TP/TPAA copolymer coated electrode. 144

Figure 4.16 Cyclic voltammogram of a TP/TPCA copolymer produced by oxidation of a 300 mM TP/200 mM TPCA solution at 1.85 V (v = 10 mV s^{-1}). 147

Figure 4.17 FTIR spectrum of a TP/TPCA copolymer. 149

Figure 4.18 The canonical forms of a TP/TPCA copolymer. 150

page

Figure 4.19a FTIR spectrum of copolymer produced from a 300mM TP/200mM TPAA solution. The coat was soaked in saturated aqueous lead(II) nitrate solution for six hours. 152

Figure 4.19b IR spectrum of lead(II) acetate. 152

Figure 4.20 Typical SEM photograph of a leaded TP/TPAA copolymer coated flag. 155

Figure 4.21 FTIR spectrum of a TP/TPCA copolymer after soaking in saturated lead(II) nitrate solution for ten hours. 156

Figure 4.22 Cyclic voltammogram of a leaded TP/TPAA coat ($v = 50$ mV s^{-1}) (a) first cycle (b) after 5 cycles (c) after 30-40 cycles. 158

Figure 4.23 Cyclic voltammogram of a leaded TP coat ($v = 50$ mV s^{-1}) (a) first cycle (b) after 30-40 cycles. This coat was soaked in aqueous lead(II) nitrate for six hours. 158

Figure 4.24a Levich plot for the oxidation of quinol(5 mM) at a TP/TPAA copolymer film. 160

Figure 4.24b Tafel plot for the same data. 160

Figure 4.24c Koutecky-Levich plot for the oxidation of quinol (5 mM) at a leaded TP/TPAA copolymer film. 161

page

Figure 4.25 Current-voltage data for the oxidation of ethylene glycol (1 M; $v = 20$ mV s^{-1}; W = 9 Hz; a, b, c, d refer to the first, second, third and thirtieth to fourtieth cycles)

(i) at a leaded TP/TPAA electrode 165

(ii) at a leaded polythiophene electrode 165

(iii) at a platinum electrode. 166

Figure 5.1 Schematic representation of the oxidation of a modified electrode in the absence of redox reaction with solution species.

(a) transport of polymer redox species and counterions.

(b) field distribution across the layer. 173

Figure 5.2 The two possible types of intermolecular bonding for thionine in the coat. 176

Figure 5.3 Typical cyclic voltammogram of polythionine in H_2SO_4 (50 mM; $v = 50$ mV s^{-1}). 178

page

Figure 5.4 The scheme of squares for thionine. The values to the left of the equilibria are for the coated species. Those to the right refer to thionine in solution. 179

Figure 5.5 Current versus $t^{-1/2}$ plots for small step chronoamperometry at thionine modified electrodes.
(a) in H_2SO_4 (50 mM; step 190 mV to 210 mV; $D/l^2 = 1.82\ s^{-1}$)
(b) in glycylglycylglycine buffer (0.1 M, pH 8.0; step -75 mV to -175 mV; $D/l^2 = 0.66\ s^{-1}$) 183

Figure 5.6 Large step chronoamperometry at a thionine modified electrode in aqueous $NaClO_4$ (0.1 M) solution.
(a) Th ——> L 184
(b) L ——> Th 185

Figure 5.7 Response of a bismuth/bismuth oxide ring electrode to solutions of varying pH (W = 10 Hz). 188

Figure 5.8 Electronic and protonic flux for the reactions Th ——> L and L ——> Th in unbuffered $NaClO_4$ (0.1 M) solution, bulk pH 3. 190

page

Figure 5.9 Electronic and protonic flux for the reactions Th ——> L and L ——> Th in unbuffered $NaClO_4$ (0.1 M) solution, bulk pH 4. 191

Figure 5.10 Electronic and protonic flux for the reactions Th ——> L and L ——> Th in unbuffered $NaClO_4$ (0.1 M) solution, bulk pH 5. 193

Figure 5.11 Electronic and protonic flux for the reactions Th ——> L and L ——> Th in unbuffered $NaClO_4$ (0.1 M) solution, bulk pH 6. 195

Figure 5.12 Electronic and protonic flux for the reactions Th ——> L and L ——> Th in unbuffered $NaClO_4$ (0.1 M) solution, bulk pH 9. 197

Figure 5.13 Typical response of an Ag/AgCl potentiometric ring sensor to variation of the bulk chloride concentration (W = 9 Hz). 200

page

Figure 5.14 Typical Ag/AgCl ring response to large step chronoamperometry at a thionine coated electrode in 100μM NaCl/50mM $NaClO_4$ solution (W = 2 Hz)
(a) Th ——> L
(b) L ——> Th. 203

Figure 5.15 The normalised simulated ring response, i_R^S, and the normalised amperometric ring current, i_{R,Cl^-}, for the reaction Th ——> L from Figure 5.14. 204

Figure 5.16 The visible spectrum of an oxidised thionine coated electrode in glycine buffer (0.1 M, pH 9.4). 210

Figure 5.17 Change in the absorption of a thionine coated electrode with time after the imposition of a potential step to bring about complete coat oxidation or reduction
(a) Th ——> L 211
(b) L ——> Th. 212

page

Figure 5.18 Evolution of the potential of a thionine coated electrode with time after disconnection of the applied potential. The electrode had been oxidised for one second prior to disconnection by the application of a potential step to bring about the reaction L ——> Th.
(a) glycine buffer (0.1 M, pH 9.4)
(b) H_2SO_4 (50 mM). 213

Figure 5.19 Large step chronoamperometric data for the reaction L ——> Th in glycine buffer (0.1 M). 218

Figure 5.20 The effect of the magnitude of the potential step when performing large step chronoamperometry on a thionine coated electrode in $HClO_4$ (0.1 M) solution.
(a) Th ——> L 219
(b) L ——> Th. 220

Figure 5.21 The large anion biological buffers used in these experiments. 222

Figure 5.22 Large step chronoamperometric data for the reaction Th ——> L at a coated electrode.
(a) in MES buffer (0.1 M; pH 5.5)
(b) in $HClO_4$ (0.1 M). 223

page

Figure 5.23 SERR spectrum of an oxidised thionine coat in H_2SO_4 (50 mM). 225

Figure 5.24 The variation in intensity of the 479 cm^{-1} Raman peak throughout the coat reactions Th ——> L and L ——> Th in H_2SO_4 (50 mM). 226

Figure 5.25 SERR spectrum of an oxidised thionine coat in glycine buffer(0.1 M, pH 9.4). 228

Figure 5.26 The variation in intensity of the 479 cm^{-1} Raman peak throughout the coat reactions Th ——> L and L ——> Th in HEPES buffer (0.1 M, pH 8.1). 231

Figure 5.27 The variation in intensity of the 479 cm^{-1} Raman peak throughout the coat reactions Th ——> L and L ——> Th in KCl (0.1 M, pH 6.2). 232

Figure 5.28 Schematic representation of the proposed initial reaction on performing complete coat reduction at pH 1 and the electrostatic field produced across the layer. 235

LIST OF TABLES

	page
Table 1.1 Selected Polymer Modified Electrodes	35
Table 1.2 Polymer Modified Electrodes For Gas Reduction	39
Table 2.1 Calculated Values For a_0/b_∞, F And F' As A Function Of ϱ	79
Table 2.2 The Majority Species At The Disc And Ring And In the Bulk For The Four Limiting Cases Of Equation (2.67)	84
Table 4.1 Oxidation Potentials For Some 3-Substituted Thiophenes And The Oxidation Potential Of The Resulting Polymers	120
Table 4.2 Summary Of Data For The Electrochemical Copolymerisation Of TP and TPAA	136
Table 4.3 ESCA Data For Thiophene	142
Table 4.4 Summary Of Data For The Electrochemical Copolymerisation Of TP and TPCA	146
Table 4.5 Kinetic Data For The Oxidation Of Quinol	162
Table 5.1 In Situ SERR Data For Oxidised Thionine Coats Normalised With Respect To The Intensity Of The Peak At 479 cm^{-1}	229

CHAPTER 1 INTRODUCTION

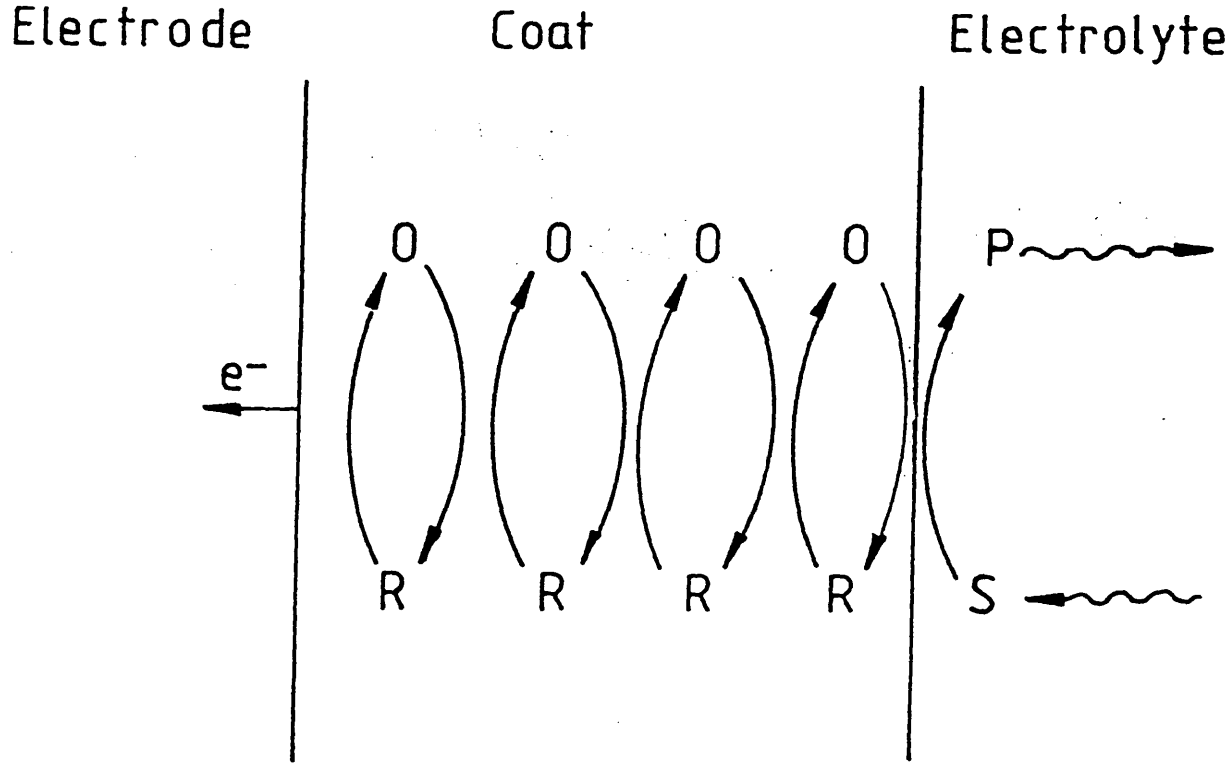
1.1 Polymer Modified Electrodes

The electrochemical oxidation or reduction of a substrate in solution is relatively insensitive to the the electrode material used. This is because reaction involves direct electron transfer between the Fermi level of the metal and the ion or neutral molecule. Thus the reactivity of the electrode- its strength as an oxidising or reducing agent- is directly related to the applied potential[1]. The planar nature of the electrode surface also means that it is extremely insensitive to substrate geometry.

In order to achieve greater kinetic specificity at the electrode, surface modification of the metal is desirable. Chemical modification of a bare electrode is the immobilisation of a thin film of a chosen substance onto the electrode surface. This coating prevents direct electrode-electrolyte contact, so that electron transfer between metal and solution is mediated by the redox groups present in the coat (Fig. 1.1). It was hoped that careful selection of these groups would control the catalysis or inhibition of a solution redox reaction, thus allowing electrode reactivity to be tailored to suit the application. This accounts for the growth in interest in chemically modified electrodes since the initial experimental work by Murray et al[2].

The work described in this thesis is concerned with the surface derivatisation of metal electrodes with polymeric species. Polymer modified electrodes typically

Figure 1.1 Schematic representation of mediated oxidation of a substrate (S) to a product (P) at a modified electrode.



contain a very high concentration of redox active centres (of the order of 0.1-5 Molar[4]) and may be many layers thick. This means that these coats could have the further advantage that electrochemical response may be many times greater than that of a bare or monolayer coated electrode. It is this potential for sensitivity and selectivity which has made polymer modified electrodes of considerable interest to the research chemist, particularly for the development of new electrocatalysts and sensors (section 1.3). However, the success of this strategy has been limited; few working systems have been developed, in spite of many man-hours of research. The objective of the work presented in this thesis is the realisation of some of this potential and a fuller understanding of the reactions of these surface films.

1.1.1 Polymer Types

Many different types of surface bound redox polymers have been synthesised. These generally can be sub-divided into groups according to the nature of the redox species present in the coat and the mechanism by which charge conduction occurs through the polymer. Firstly, the electrochemically active groups may form part of the polymer backbone itself, as in the case of polythionine (Chapter 5), or may be chelated or bound electrostatically to groups on the polymer. An example of this would be the use of inorganic ions incorporated into polymers for electro-organic oxidations (Chapter 4). Secondly, the coats can be classified according to the nature of electronic conduction.

In the case of polyvinyl compounds, the transport of electrons throughout the coat generally takes place via an "electron hopping" mechanism[14,15] (Figure 1.2). For these polymers, the conductivity of the backbone is poor due to the high degree of bond saturation. Electron propagation occurs by hopping between neighbouring redox sites, with the possibility of co-ordinated polymer motions facilitating this process by decreasing the jump distance, λ. Examples of this type of polymer are given in Figure 1.3. However, some aromatic compounds (Figure 1.4), when electropolymerised, yield coats which possess a backbone with a degree of unsaturation, forming a delocalised π-system. Electron transport through this π-system is facile when the polymer is in its oxidised form and conductivities of the order of 10 S/cm have been measured[16]. These are widely referred to as conducting polymers. This type of coat is further discussed in Chapter 4.

Further information concerning polymer modified electrodes can be found in the comprehensive reviews by Albery and Hillman[3] and Murray[4].

Figure 1.2 Conduction in polyvinyl polymers via an electron hopping mechanism.

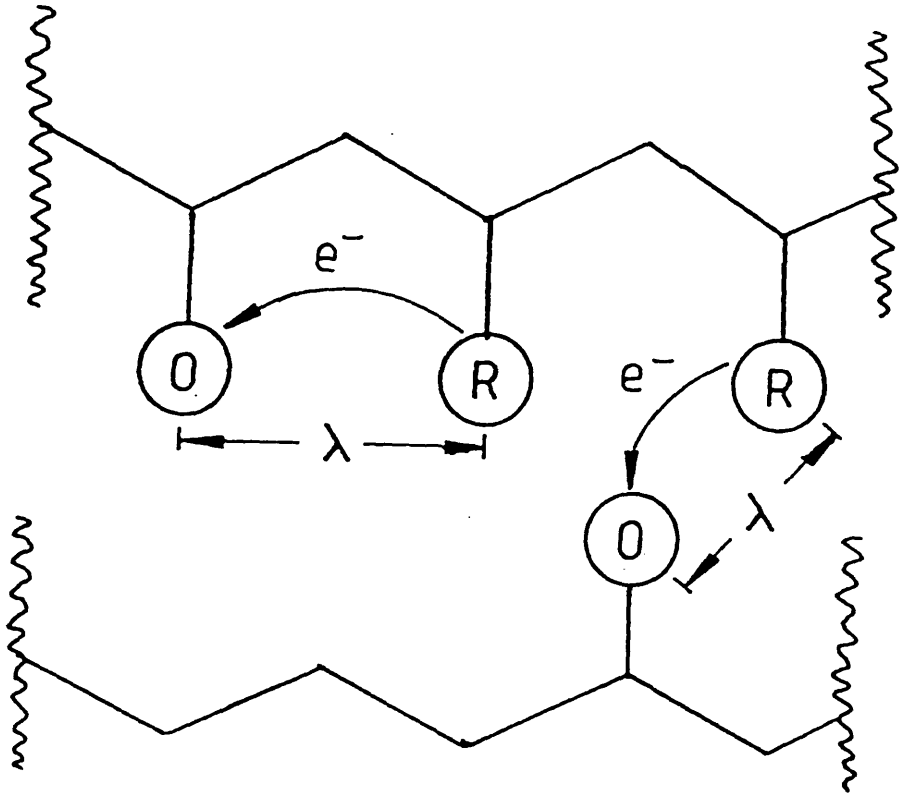
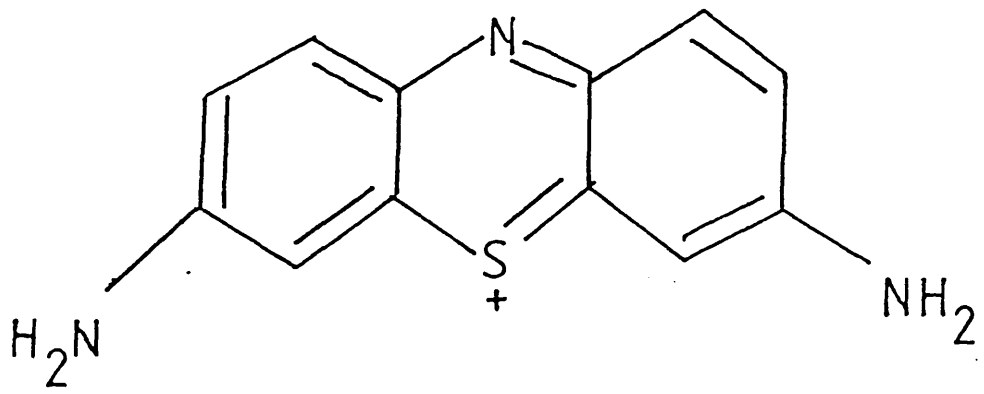
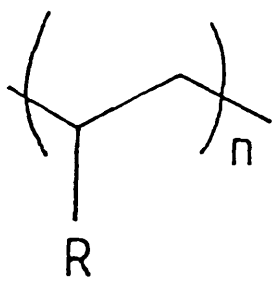
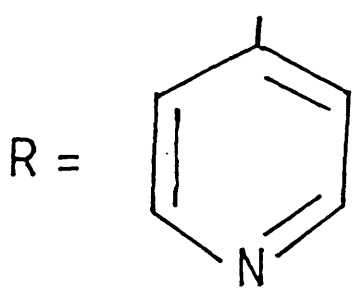


Figure 1.3 Examples of polymers and polymerisable monomers which produce modified electrodes for which electronic conduction occurs by electron hopping.

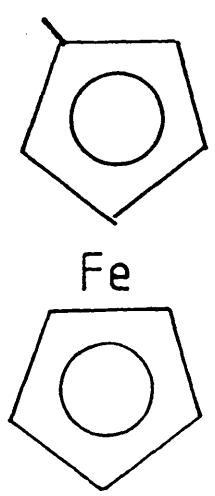


Thionine



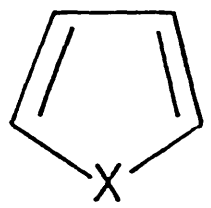


Polyvinylpyridine

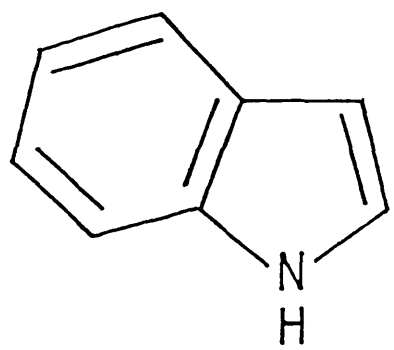


Polyvinylferrocene

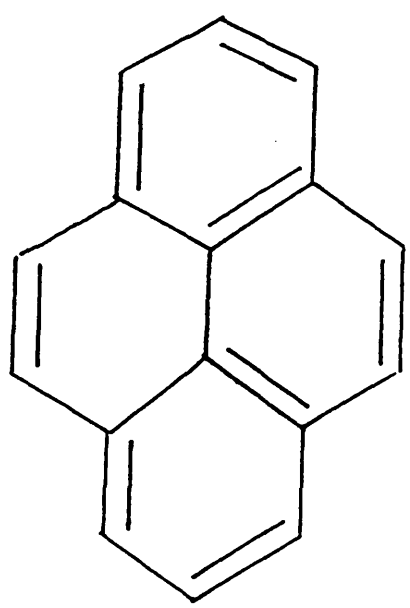
Figure 1.4 Some aromatic monomers which produce conducting polymer modified electrodes.



X = NH Pyrrole
S Thiophene
O Furan



Indole



Pyrene

1.2 Methods Of Preparation

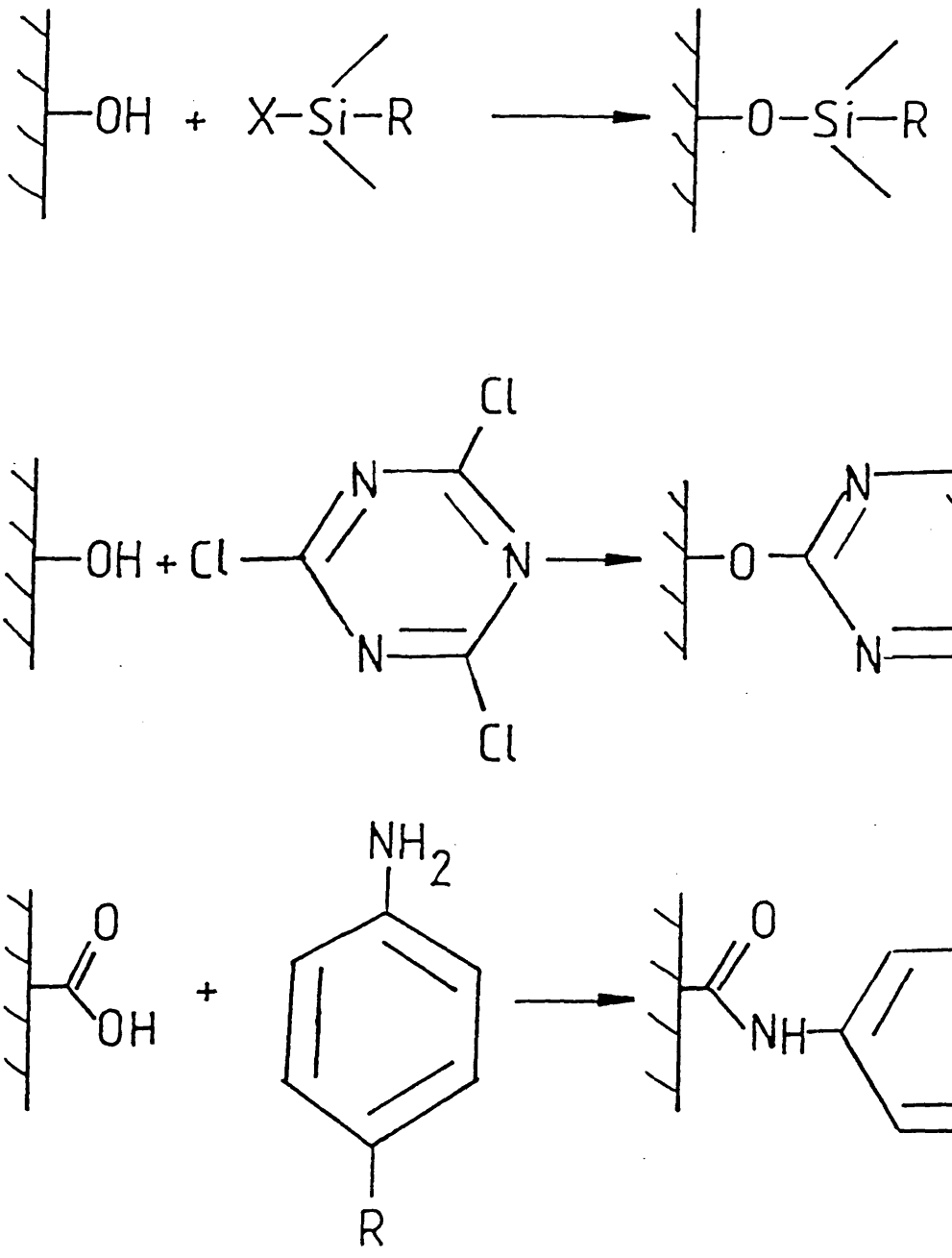
1.2.1 Covalent Chemical Linkage

This technique involves the surface derivatisation of hydroxyl, carboxyl and ketonic groups of the oxidised surface of glassy carbon and metal electrodes. Examples of these reactions are given in Figure 1.5. The derivatising species typically contains a group, R, possessing a reactive moiety such as -Cl, $-NH_2$ or $-CO_2H$ which allows for further surface modification through chemical reaction. This method has the disadvantage of requiring several synthetic steps, generally involving moisture-sensitive covalent linking agents. The technique is ideally suited for producing monolayers, but not for multilayer or polymer electrodes - other than polymers or copolymers of the derivatising reagent[13] - due to the inordinate amount of synthesis involved.

1.2.2 Surface Adsorption

Surface adsorption can be utilised by using one of two techniques. In the first, polymeric adsorbed species are in dynamic equilibrium with the species in solution. The disadvantages of this method are that the coating substance present in solution may interfere with the solution redox reaction and that long-term electrode stability may be poor, due to competitive adsorption by electrode products. There is also no control of the coat thickness and the number of polymers soluble in electrochemical solvents is limited. The second method is that of irreversible

Figure 1.5 Examples of surface derivatising reactions for the preparation of modified electrodes.



adsorption - a solution of the polymer is deposited onto the electrode surface and the solvent is allowed to evaporate off. This can be achieved by dropping the solution onto the electrode (drop coating), dipping it into the solution (dip coating) or dropping the dissolved polymer on and spinning the electrode to remove the solvent (spin coating). The coat is stable in the bulk electrolyte due to its insolubility. Control of the amount of substance immobilised is possible through variation of the solution concentration and the volume deposited. This is the chosen method for the immobilisation of functionalised polyvinyl compounds[5,6,7,8].

Problems with this technique can be the stability of the electrode-coat bonding and the control of coat porosity, including the elimination of pin-holes which leave the electrode exposed. These phenomena often depend upon the nature of the solvent and its rate of evaporation.

1.2.3 Plasma Discharge

This is a method best suited to polymer modified electrodes formed by the polymerisation of radicals. Monomer vapour is polymerised by a radio frequency plasma beam and polymer product is deposited onto the electrode surface[9,10]. This provides an even coat, with a thickness which can be easily controlled. However, the main drawbacks are the need for a specialist UHV plasma machine and coat damage during deposition caused by the beam.

1.2.4 Electrochemical Coating

This is the preparative method used for polythionine and the conducting polymers (Chapters 4 & 5). Oxidation or reduction of redox monomers in solution may result in anionic, cationic or radical polymerisation at the electrode surface to yield a polymer modified electrode. The use of a working electrode with controlled hydrodynamics (e.g. the rotating-disc electrode) and the control of coating potential or current allows facile optimisation of the coating conditions. Film thicknesses may be varied by changing the coating time[11]. These modified electrodes generally contain few, if any, pinholes through which electrolyte can penetrate to the electrode, as polymerisation generally occurs preferentially at these sites[12]. This decreases the importance of direct reaction at the electrode (section 4.5.2.1).

A limitation on this method is that for polymer films which cannot oxidise or reduce fresh monomer electrocatalytically and which block the diffusion of monomer to the electrode surface, the film growth will halt and electrode passivation may occur.

1.3 Applications

1.3.1 Selective Redox Reactions

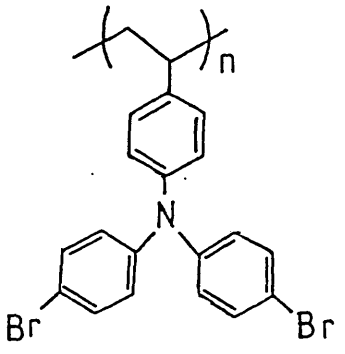
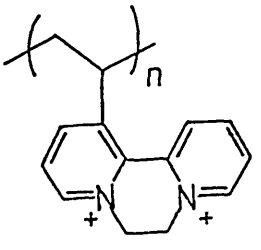
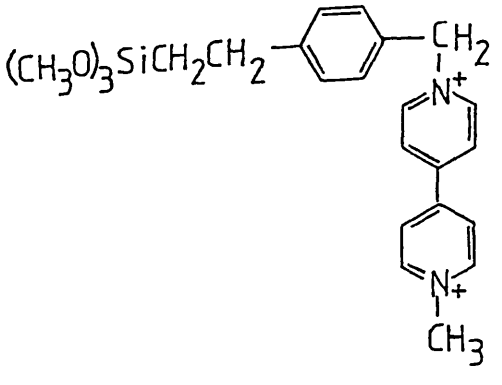
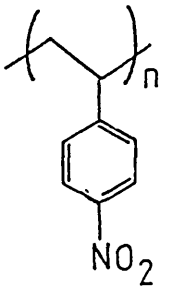
There is much interest in the oxidation of organic compounds for electrocatalysis and of large biological molecules for use in biosensors. This type of redox reaction is often extremely unselective at a bare electrode and poisoning often occurs, due to the formation of carbonaceous deposits. Kulys and coworkers have oxidised enzymes containing FAD and haem centres by using poly-(o-quinone) and poly-(p-quinone) modified electrodes, as well as protonated polyvinylpyridines containing electrostatically bound ferricyanide[17]. The oxidation of NADH by quinonoid coats has also been investigated by Arai et al[18], whilst catalytic oxidation of ascorbic acid has been accomplished by the use of a polyvinylferrocene film[19].

As well as large biological molecules, small organic species have also been oxidised. Moutet[20] has used the amine cation radical of polymer I (Table 1.1) to cleanly oxidise acetate and octanoate according to the equation

$$RCO_2^- \xrightarrow{-e^-} R^\cdot + CO_2$$

Excellent use of the power of ruthenium(IV) as an oxidising agent has been made in the work of Meyer and Samuels[21]. A film of polyvinylpyridine, when doped with aquobis(2,2'-bipyridyl)ruthenium(II), yields a coat which can be oxidised electrochemically to produce ruthenium(IV). This can then be

Table 1.1 Selected Polymer Modified Electrodes

Polymer/Monomer Structure	Number
	I
	II
	III
	IV

used to carry out the following reactions

$$(CH_3)_2CHOH \xrightarrow[-2H+]{-2e^-} (CH_3)_2C{=}O$$

$$H_3CPhCO_2^- \xrightarrow[+2H_2O]{-6e^-,-7H^+} {}^-O_2CPhCO_2^-$$

$$H_3CPhCH_3 \xrightarrow[+4H_2O]{-12e^-,-14H^+} {}^-O_2CPhCO_2^-$$

The currents produced by this electrode were disappointingly small (less than 10 $\mu A/cm^2$) and electrode lifetimes were very short i.e. of the order of minutes. However the concept of using two-electron oxidants to minimise radical side-products is one that will be discussed further in Chapter 4.

The application of polymer modified electrodes to mediated electroorganic reductions has been extremely limited. Murray and Willman[22] have investigated the photo-assisted reduction of 1,2-dibromo-1,2-diphenylethane to stilbene at the viologen polymer II and polymerised monomer III (table 1.1).

$$PhCHBrBrCHPh + 2e^- + h\nu \longrightarrow PhCH{=}CHPh$$

Kerr, Miller and Van De Mark[23] showed that this reaction could be carried out at a polynitrostyrene electrode (polymer IV, Table 1.1). They showed that, provided the solvent used was dry acetonitrile, stilbene could be produced on the preparative scale. Photo-assisted electrochemical reduction has also been performed on chloroform and tetrachloromethane, using polyvinylferrocene

electrodes[24]. The proposed reaction scheme is given in Figure 1.6.

As well as electrocatalytic reduction of organic and solvent species, much work has been published on the reduction of gases. This is desirable for the development of new electroanalytical gas sensors and in the case of oxygen, for the improvement of existing fuel cell technology. some examples of polymer electrodes used for electrocatalytic gas reduction are shown in Table 1.2. Most O_2 electrodes are quinone based. They suffer from two major problems. Firstly, incomplete reduction of oxygen to hydrogen peroxide usually occurs. Secondly, there is a relatively small drop in reduction potential compared with a bare electrode. These deficiencies reduce the energy available from the fuel cell. Currents are typically of the order of 10 $\mu A/cm^2$, even for the polypyrrole electrode, as the polymer is a poor electronic conductor in its reduced form (Chapter 4).

The efficient production of hydrogen from protons in solution has been of interest to electrochemists, as hydrogen has been proposed as a useful and convenient chemical energy store of the electrical energy produced by solar cells. Wrighton and Harrison[31] have produced a catalytic electrode for this process by dispersing palladium aggregates in a silylated viologen polymer. We have further investigated this strategy using electrically conducting polymers[32].

Figure 1.6 The proposed reaction scheme for photoassisted electrochemical reduction using polyvinylferrocene electrodes.

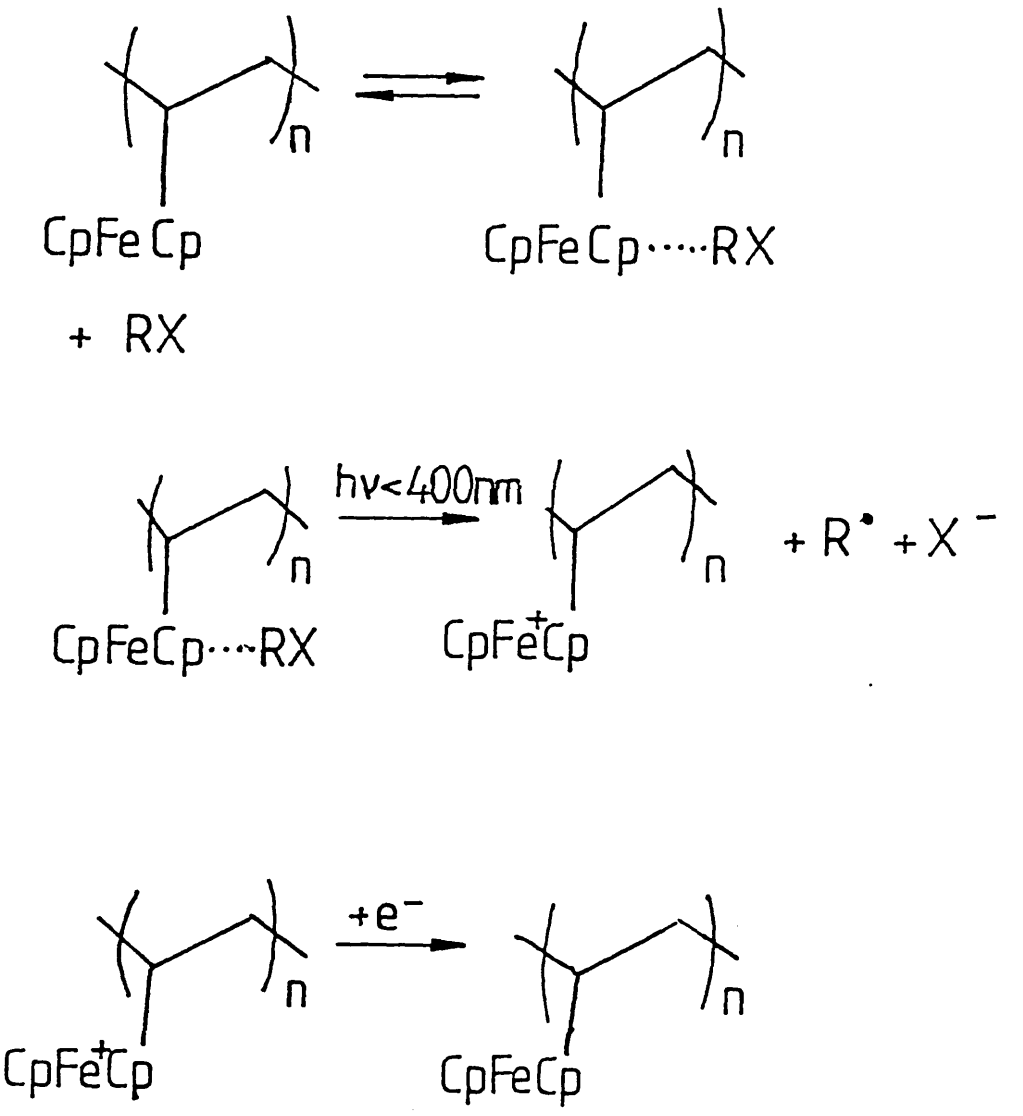
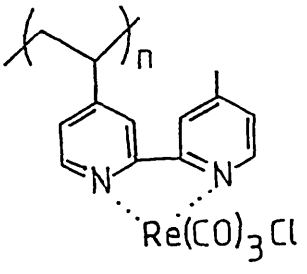
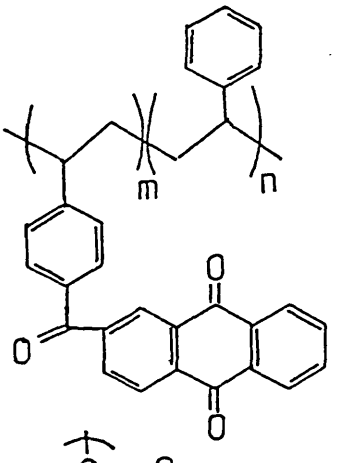
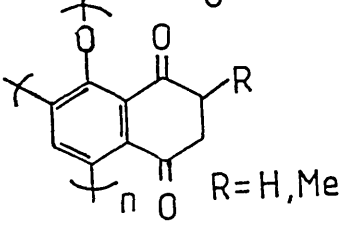
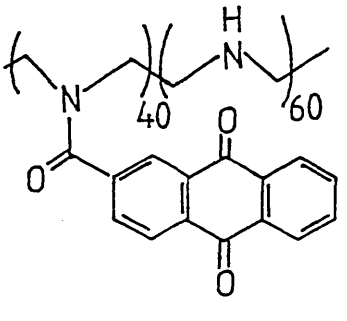
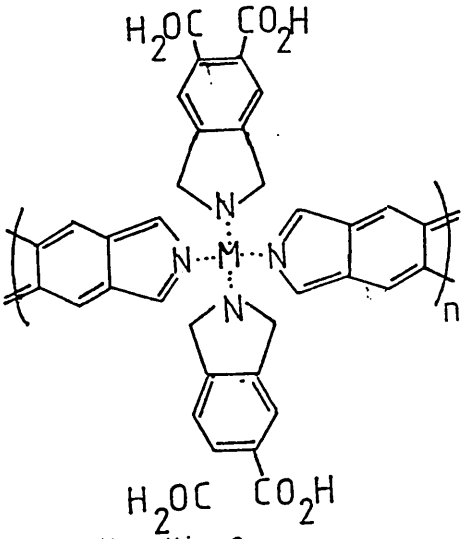
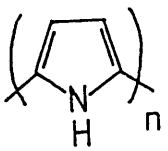


Table 1.2 Polymer Modified Electrodes For Gas Reduction

Polymer Structure	Substrate	Product	Reference
	CO_2	CO	23
	O_2	$O_2^{-(a)}$	24
	O_2	H_2O_2	25
	O_2	H_2O_2	26

Polymer Structure	Substrate	Product	Reference
 M = Ni, Co	O_2	H_2O_2,	27
M = Fe		H_2O, H_2O_2	
 + added Co(II) complexes	O_2	H_2O_2	28

(a) In DMSO, as the system was inactive in aqueous solution.

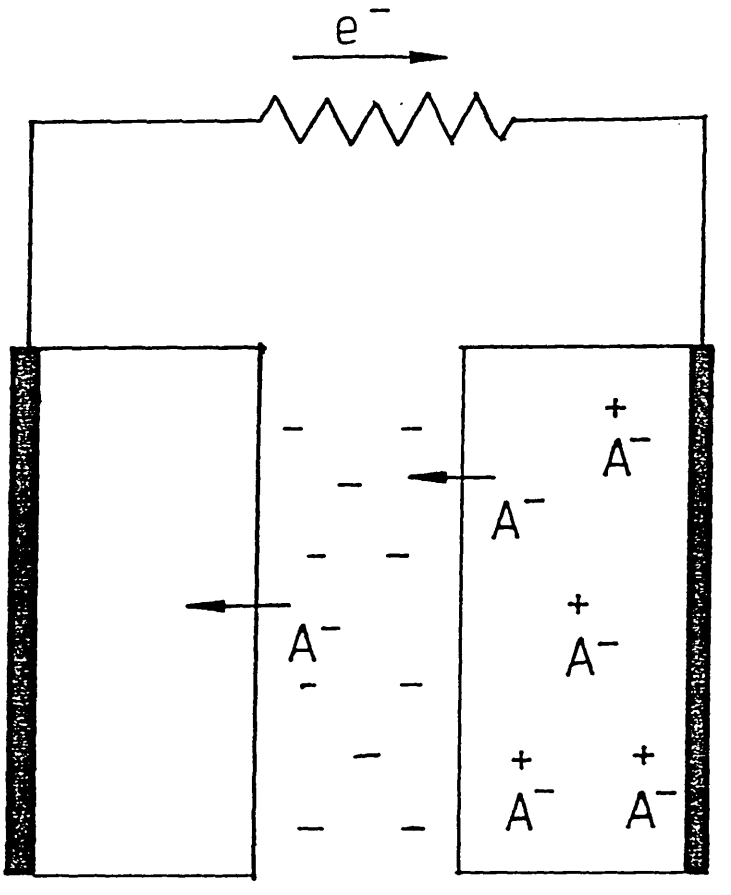
1.3.2 Batteries

Conducting polymer electrodes possess high electronic conductivity and a high concentration of redox sites (Section 1.1.1). This means that efficient charge storage and high discharge currents are possible with these modified electrodes and so they have been investigated for use in battery cells. A typical cell consists of an oxidised and neutral, reduced conducting polymer film, each deposited onto a platinum electrode, as the anode and cathode respectively (Figure 1.7). During discharge, anion is incorporated into the cathode film from the background electrolyte in order to maintain coat electroneutrality and a corresponding loss of anion occurs at the anode. This system has been used in the construction of conducting polymer cells of polyacetylene[33,34,35], polyazulene[36] and polythiophene[36]. Open circuit voltages are in the range 0.5-2.3 V and short-circuit currents of up to 3 mA/cm^2 have been measured. Short-term experiments performed on the polyazulene cells revealed good reproducibility of these properties upon recharging[36].

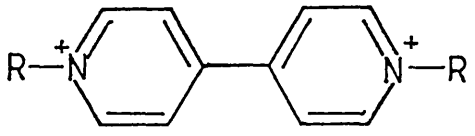
1.3.4 Electrochromic Devices

There has been much recent interest in the synthesis of electrochemical display devices to replace LED and LCD displays with a cheaper system which is easy to manufacture, operates at low voltages and has a long

Figure 1.7 The 'all polymer' cell.



lifetime. One class of compounds of particular interest is the viologens



The V^{2+} oxidation state shown can be reversibly reduced to form the cation radical, $V^{+\cdot}$, which possesses a strong absorption band in the visible. When R is an alkyl chain with an end-group amenable to condensation polymerisation, copolymers containing viologen groups can be obtained and these can be coated onto electrodes[37,38,39]. Yamana and Kawata[40] have studied viologen polymers formed from monomers with terminal vinyl groups. However, these coats are kinetically slow to react.

Garnier et al[41,42] have investigated the electrochromic behaviour of polythiophene and the variation of colour with oxidation state (potential), chemical structure and the nature of the counterion. The switching times are very much faster than for the polyviologen coats - of the order of tens to hundreds of milliseconds, depending upon the film thickness. Colour contrast can be observed on a platinum electrode for films thicker than 0.1 μm.

1.3.4 Photoelectrodes

With the limited availability of fossil fuels, attention has recently switched to alternative energy sources, such as solar power. The development of more efficient photoelectrodes for the conversion of solar energy to electrical energy is therefore of prime importance.

Doped inorganic semiconductors such as gallium arsenide, silicon and gallium phosphide have proved to be effective photoelectrodes, but these suffer from photocorrosion reactions, which lead to a drop in the photocurrent. Surface coating of conducting polymers such as polypyrrole[43-51] and polyaniline[49] have been shown to block ion and solvent transport to the semiconductor electrode and so prolong photocell lifetimes by up to several hundred hours.

Semiconductor photosensitive polymer modified electrodes have also been produced. Examples of these are the modified polyvinylchloride and polytetrafluoroethylene polymer[52] and thin films of polythiophene and poly(3-methylthiophene)[53].

Another type of photocell uses organic dyes as the photoactive species. There are two possible methods used for coat fabrication. The first relies on entrapment of dye molecules within a polymer coat. An example of this is croconoate violet in poly(4-vinylpyridine), which produces cathodic photocurrents under illumination[54]. The second type of film utilises modified electrodes consisting entirely of polymerised dye molecules, such as polyviologens[55].

1.3.5 Other Applications

Conducting polymers can be made to take up and expel anions reversibly by cycling between the oxidised and reduced forms (Chapter 4) and it is this feature which has

led to the development of a poly(3-methoxythiophene) film for the controlled release of anionic drugs[56]. Facile control of the release rate is possible by control of the magnitude of the coat reduction current.

When a film of polypyrrole is exposed to a gas such as ammonia in air, gas molecules are incorporated into the film. This leads to a change in conductivity of the film directly related to the concentration of ammonia and so polypyrrole modified electrodes can be used as ammonia sensors[57].

1.4 Outline Of The Rest Of The Thesis

Chapter 2 will deal solely with the theory for the ring-disc electrochemical techniques used in this thesis. Novel theory will be developed for the use of potentiometric ring sensors to obtain fluxes at the surface of a rotating disc electrode by deconvoluting the change in the observed ring potential. The use of chronoamperometry and cyclic voltammetry, performed at planar, stationary electrodes for the study of redox reactions is well-known. Theory has been developed for the study of the redox reactions of solution species at modified electrodes, to which the interested reader is referred[3,4].

Chapter 3 will consist of the experimental details for the work presented in Chapters 4 and 5. Among the items included will be details of the electrochemical and spectroscopic apparati used, chemical purification procedures and electrode fabrication.

The development of conducting polymer modified electrodes for electrocatalytic oxidation of organic compounds will be discussed in Chapter 4. This will contain a general discussion on conducting polymers, results for the electropolymerisation and characterisation of novel conducting copolymers and studies concerning the incorporation of lead(II) ions into these coats . The applicability of these films to electrocatalysis will be discussed in the light of the results presented for the oxidation of organic molecules and solution redox species at

these modified electrodes.

Chapter 5 will concern the kinetics and mechanism of reaction of a polymeric dye modified electrode, polythionine. Spectroscopic and electrochemical data will be presented along with results collected using potentiometric ring electrode sensors, for the flux of proton and counteranion throughout these reactions. The kinetics and mechanism of the coat reaction will be discussed in the light of this information.

CHAPTER 2 THEORY OF RING-DISC TECHNIQUES

2.1 The Rotating Disc Electrode

When an electroactive species reacts at an electrode, the rate of electron transfer is directly proportional to the concentration of the substance at the electrode surface. Irreproducible results are obtained for electrochemical reactions in an unstirred solution. This is due to the effects of depletion of reactant near the electrode, coupled with stray solution convection resulting from thermal gradients.

In order to alleviate these problems, forced convection systems have been developed. These give a well-defined reproducible flow of electrolyte to the electrode. However, the transport of solution has proved very difficult to model theoretically for many of these systems. One type of electrode which has been found to be amenable to such treatment is the rotating disc electrode (RDE).

The RDE consists of a disc-shaped electrode surrounded by coplanar insulating material (Figure 2.1). This is suspended in the electrolytic solution and rotated at a controlled rate. Von Karman[58] was the first to describe the solution flow pattern induced by the rotating disc. Using the cylindrical polar co-ordinate system given in Figure 2.2, the fluid velocity components can be represented by

$$v_\phi = r\omega B(x/x_{Hy}) \qquad \ldots.(2.1)$$

$$v_r = r\omega G(x/x_{Hy}) \qquad \ldots.(2.2)$$

$$v_x = (\omega/\nu)^{1/2} H(x/x_{Hy}) \qquad \ldots.(2.3)$$

Figure 2.1 The rotating disc electrode (RDE).

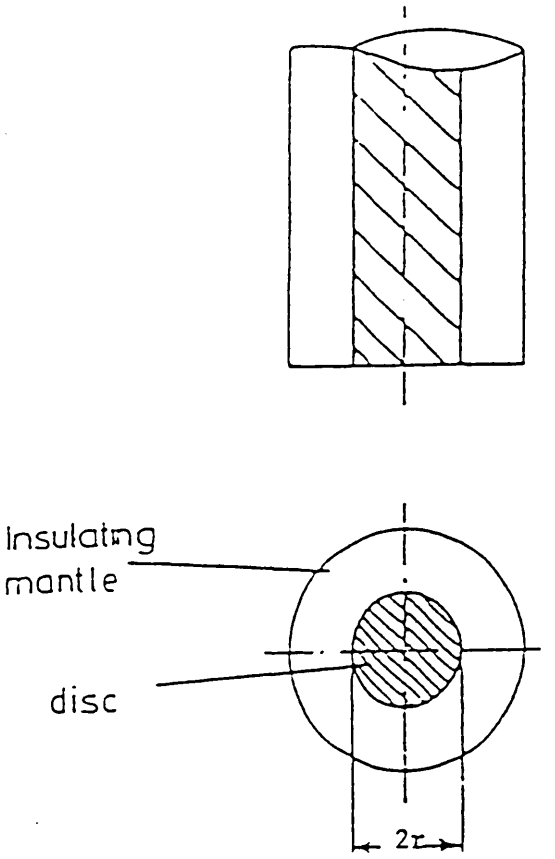


Figure 2.2 The cylindrical polar co-ordinates and fluid flow vectors used to model the RDE.

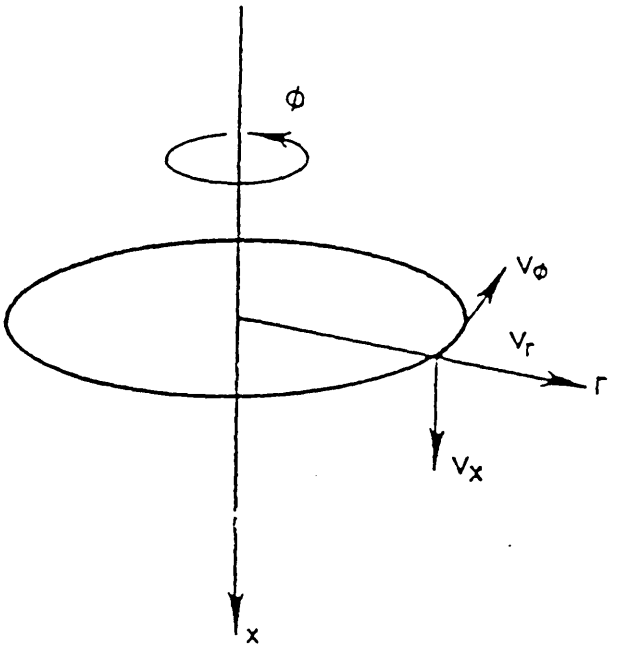
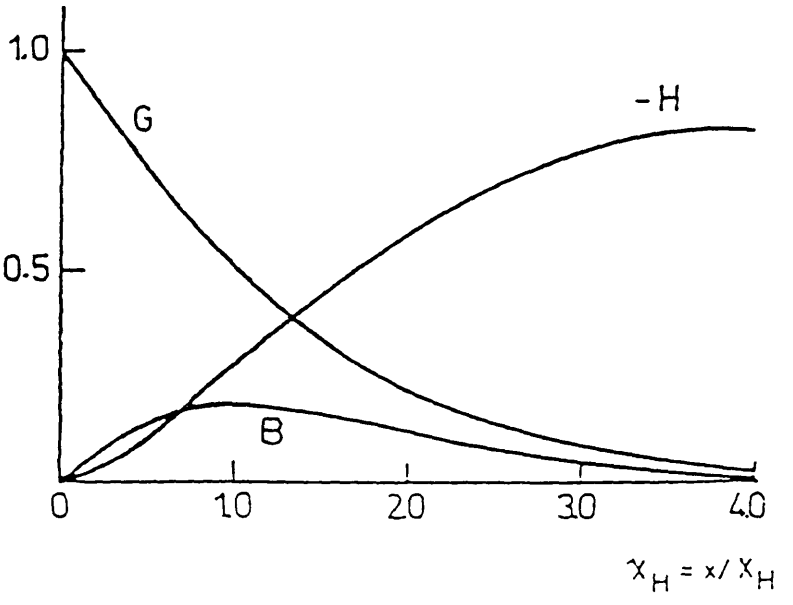


Figure 2.3 The functions B, G and H.



where v is in cm s^{-1}

ω is the rotation speed in rad s^{-1}

v is the kinematic viscosity in cm^2 s^{-1}

and $$x_{Hy} = (v/\omega)^{1/2} \qquad \ldots.(2.4)$$

The functions B, G and -H are plotted in Figure 2.3. It can be seen that v_x is independent of r. This means that the surface of the disc is uniformly accessible to solution species, so simplifying mathematical modelling. The flow pattern produced is shown in Figure 2.4. The electrode acts as a pump, drawing up solution to the disc and flinging it out laterally.

Levich[59] used these streamlines to model mathematically transport to the RDE. Under conditions of transport by diffusion and convection with no migration, the steady state differential equation for the system is

$$D \frac{\partial^2 c}{\partial x^2} = v_x \frac{\partial c}{\partial x} \qquad \ldots.(2.5)$$

where c is the concentration of the electroactive species (mol cm^{-3})

D is its diffusion coefficient (cm^2 s^{-1})

These conditions apply if excess background electrolyte is present. Integration of equation (2.5) with the boundary condition $x \longrightarrow \infty$ $c \longrightarrow c_\infty$ (where c is the bulk concentration of the redox substance) and comparison with Fick's first law gives

Figure 2.4 Flow patterns for an RDE.

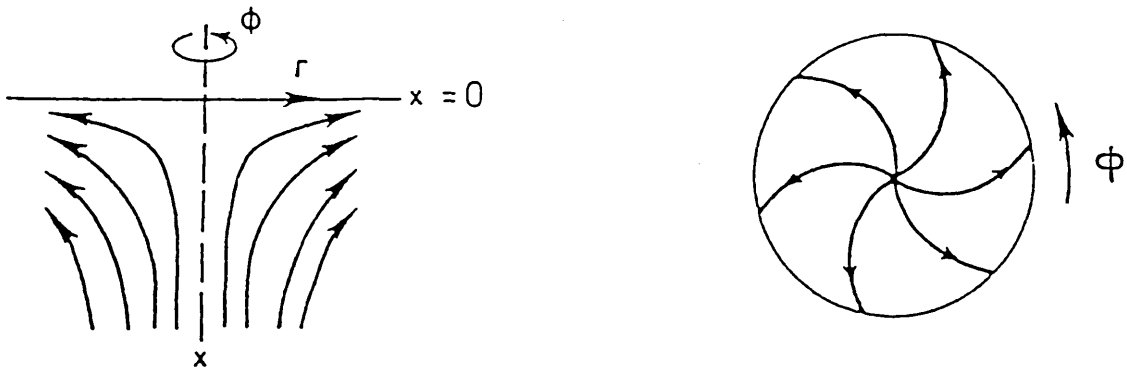
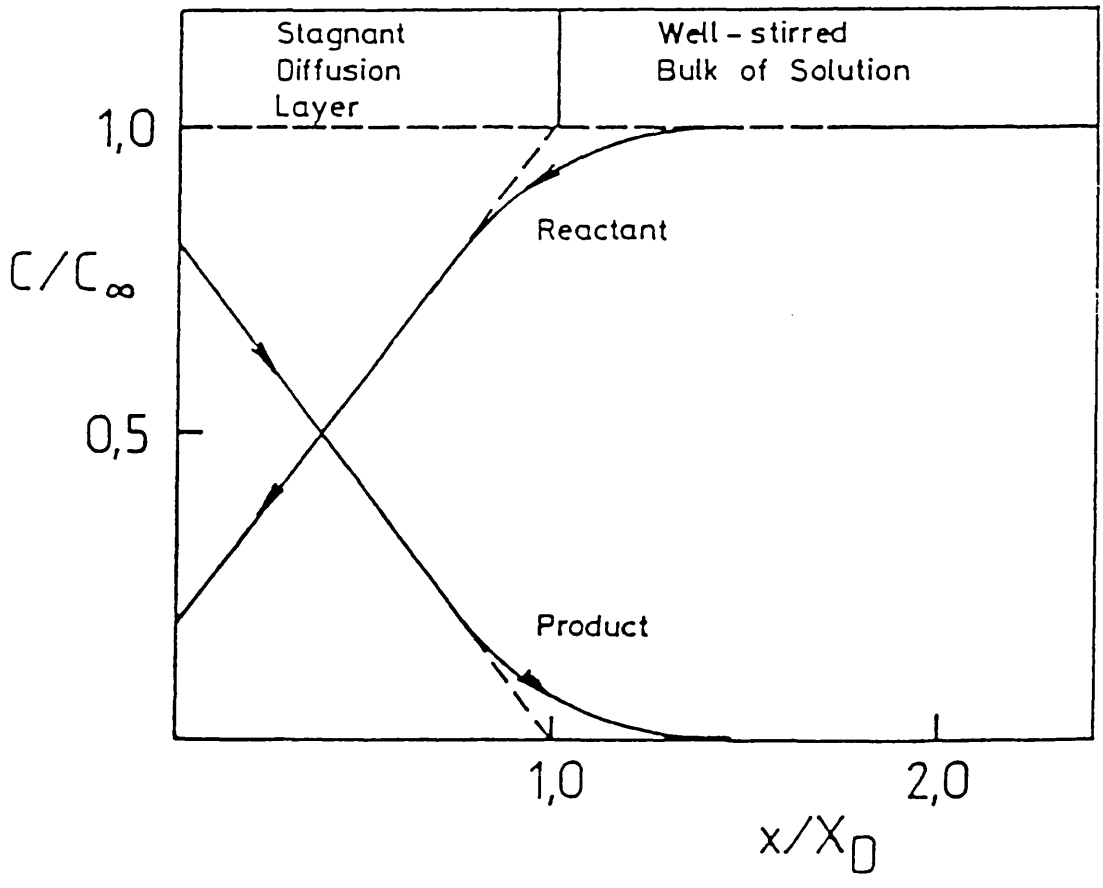


Figure 2.5 Calculated concentration profiles at an RDE.



$$\frac{j}{D} = \left\{ \frac{\partial c}{\partial x} \right\}_{x=0} = \frac{c_\infty - c_0}{X_D} \qquad \ldots.(2.6)$$

where c_0 is the concentration at x = 0

j is the flux at the electrode (mol cm^{-2} s^{-1})

and $$X_D = 0.643\ W^{-1/2} \nu^{1/6} D^{1/3} \qquad \ldots.(2.7)$$

where W is the rotation speed (Hz)

Figure 2.5 gives a typical concentration profile with distance from the RDE. At distances of x greater than X_D from the electrode, the solution is well-stirred and transport is by diffusion and convection. however for $x < X_D$ transport by diffusion is dominant. In this region, known as the diffusion layer, the solution rotates with the disc.

At the disc surface, the rate of reaction is also governed by the electrode kinetics. For the reaction

$$O \xrightarrow{+ne^-} R$$

the rate constant for reaction at the electrode surface, k', is given by

$$k' = k_0' \exp(-\alpha F(E-E^\ominus)/RT)$$

where α is the electron transfer coefficient[1]

k_0' is the standard electrochemical rate constant i.e. the value of k' at $E = E^\ominus$ (cm s^{-1})

F is Faraday's constant (C mol^{-1})

The electrode flux is

$$j = k' c_0 \qquad \ldots.(2.8)$$

and by substituting for c_0 in equation (2.6) and

rearranging, one obtains

$$\frac{1}{j} = \frac{1}{k'c_\infty} + \frac{1}{k_D'c_\infty} \qquad \ldots.(2.9)$$

where $k_D' = D/X_D$ $\ldots.(2.10)$

k_D' is the second order rate constant describing mass transfer of the electroactive species to the electrode surface (cm s^{-1}).

One can see that equation (2.9) has two limiting forms, depending on which of the terms on the right-hand side of the equation dominates.

(i) If $k'c_\infty \ll k_D'c_\infty$

$$j = k'c_\infty$$

In this case charge transfer is slow and rate determining and only a small fraction of the species arriving at the electrode reacts.

(ii) If $k'c_\infty \gg k_D'c_\infty$

$$j = k_D'c_\infty$$

The flux is therefore mass-transfer controlled, with charge transfer being so fast that the transport of reactant to the electrode determines the rate.

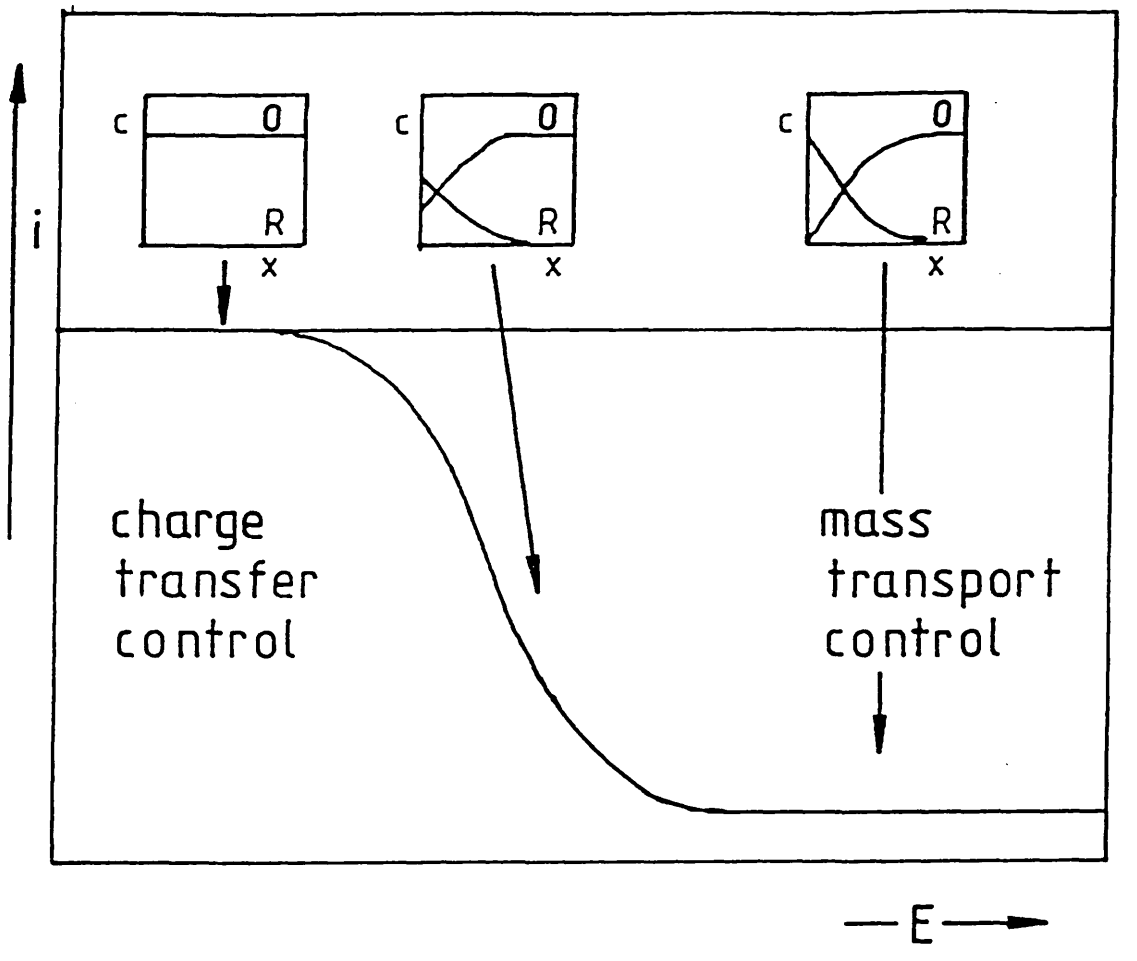
Movement from case (i) to case (ii) can be effected by making the electrode more reducing. This is shown schematically in Figure 2.6. The current observed for case (ii) is termed the mass transport limiting current, i_L.

Since $i = nFAj$ $\ldots.(2.13)$

$$i_L = 1.554nFAc_\infty D^{2/3}\nu^{-1/6}W^{1/2} \qquad \ldots.(2.14)$$

where A is the electrode area (cm^2)

Figure 2.6 Movement from charge transfer control to mass transfer control for reduction of O to R at an RDE.



Thus, a plot of i_L against $W^{1/2}$ should give a straight line through the origin. This is termed a Levich plot.

However, this treatment assumes a rate-determining electron transfer step at the electrode. Many systems involve some second step that is independent of potential prior to electron transfer i.e.

$$O \xrightarrow{k_?'} O^* \xrightarrow[k_1']{+ne} R$$

In this scheme, the rate constant for the mass transport independent step is denoted by $k_?'$. The observed electrochemical rate constant, k', is given by

$$\frac{1}{k'} = \frac{1}{k_?'} + \frac{1}{k_1'} \qquad \ldots.(2.15)$$

and the smaller of the two rate constants $k_?'$ and k_1' will be rate limiting. Thus the equation for the mass transport limiting current in this case is

$$\frac{nFAc_\infty}{i_L} = \frac{0.643D^{-2/3}\nu^{1/6}}{W^{1/2}} + \frac{1}{k_?'} \qquad \ldots.(2.16)$$

This means that the Levich plot will not be straight, as at high rotation speeds $k_?'$ will become rate limiting. However, a plot of i_L^{-1} against $W^{-1/2}$ will give a straight line with a y-intercept of $k_?'$. This is termed a Koutecky-Levich plot[60].

2.1.1 Current-Voltage Curves

A general expression can be derived[61,62] for the current-voltage relationship of the reaction

$$A + ne^- \underset{k'_{-1}}{\overset{k'_1}{\rightleftharpoons}} B$$

at the RDE. In this case both forward and reverse reactions are important. The following equation can be derived, relating the limiting fluxes of A (j_A) and B (j_B) to the total flux observed at the electrode, j.

$$j = \frac{1}{k'_{D,A}} \left[k'_1 (j_A - j) - k'_{-1} (j - j_B) \left\{ \frac{D_A}{D_B} \right\}^{2/3} \right] \quad \ldots.(2.17)$$

Using $k'_1 = k'_0 \exp(-\alpha(E-E^{\circ})F/RT)$

and $k'_{-1} = k'_0 \exp((n-\alpha)(E-E^{\circ})F/RT)$

where k'_0 is the value of the electrochemical rate constant at $E = E^{\circ}$

and $i_{O,L} = nFAj_B$

$i_{R,L} = nFAj_A$

from equations (2.13) and (2.14)

where $i_{O,L}$ and $i_{R,L}$ refer to the mass transport limiting oxidation and reduction currents respectively at the electrode.

Substitution of these expressions into equation (2.17) and rearrangement gives the general expression

$$\ln\left\{\frac{k'_{D,A}}{k'_0}\right\} + \frac{\alpha(E-E^{\sigma})F}{RT} =$$

$$\ln\left[\left\{\frac{i_{R,L}}{i} - 1\right\} + \left\{\frac{i_{O,L}}{i} - 1\right\}\left\{\frac{D_A}{D_B}\right\}^{2/3} \exp\left\{\frac{n(E-E^{\sigma})F}{RT}\right\}\right] \quad \ldots.(2.18)$$

where i is the observed current.

For an irreversible system, E must be much greater or less than E^{σ} to produce a current. For a reduction $E << E^{\sigma}$ and equation (2.18) reduces to

$$\ln\left\{\frac{i_{R,L}}{i} - 1\right\} = \ln\left\{\frac{k'_{D,A}}{k'_0}\right\} + \frac{\alpha(E-E^{\sigma})F}{RT}$$

whereas for an oxidation, the equation simplifies to

$$\ln\left\{\frac{i_{O,L}}{i} - 1\right\} = \ln\left\{\frac{k'_{D,B}}{k'_0}\right\} + \frac{\beta(E-E^{\sigma})F}{RT}$$

when $E >> E^{\sigma}$. These are Tafel equations corrected for mass transport. In each of these cases, a plot of $\ln(i_L/i - 1)$ vs. $(E - E^{\sigma})$ will yield α or β from the slope and k'_0 from the y-intercept. This is termed a Tafel plot.

For reversible systems, $k'_0 >> k'_{D,A}$. Thus equation (2.18) can be simplified, giving

$$\ln\left\{\frac{i - i_{R,L}}{i_{O,L} - i}\right\} = \frac{n(E - E^{\sigma})F}{RT} + \frac{2}{3}\left\{\frac{D_A}{D_B}\right\}$$

For many systems $D_A \approx D_B$ and in this case a plot of the

left hand side of the above equation against E allows one to find n and E° from the gradient and y- intercept. In fact, $E^{\circ} \approx E_{1/2}$, where $E_{1/2}$ is the potential at which

$$i = \frac{1}{2} (i_{O,L} + i_{R,L}) .$$

2.2 The Rotating Ring-Disc Electrode (RRDE)

This electrode configuration consists of an RDE with the addition of a concentric ring electrode around the disc (Figure 2.7)[61]. The ring and disc are coplanar and separated by an insulator. As can be seen from the flow patterns for the RDE (Figure 2.4), this geometry enables the ring to act as a downstream monitor of disc products. This section is concerned with the theory of both amperometric and potentiometric ring sensors.

2.2.1 Amperometric Ring Sensors

Let us consider the following reaction scheme.

Disc $\quad A \pm ne^- \longrightarrow B$

Ring $\quad B \pm ne^- \longrightarrow C$

In this reaction, A is converted to B at the disc. B then travels downstream to the ring where C is formed in a mass-transfer limited reaction. This means that the concentration of B in the bulk solution and at the ring is zero. The transport properties of this system have been modelled[64] and the RRDE streamline flow pattern is shown in Figure 2.8. The fraction of electrogenerated B that reaches the ring electrode is termed the collection efficiency, N_0, given by

$$N_0 = \frac{|i_R|}{|i_D|} \qquad \ldots.(2.19)$$

where i_R is the ring current

i_D is the disc current

N_0 has been obtained[65,66] and is given by

$$N_0 = 1 - f(\alpha/\beta) + \beta^{2/3}(1 - f(\alpha)) - (1 + \alpha + \beta)^{2/3}(1 - f\{(\alpha/\beta)(1 + \alpha + \beta)\} \qquad \ldots.(2.20)$$

Figure 2.7 The rotating ring-disc electrode (RRDE).

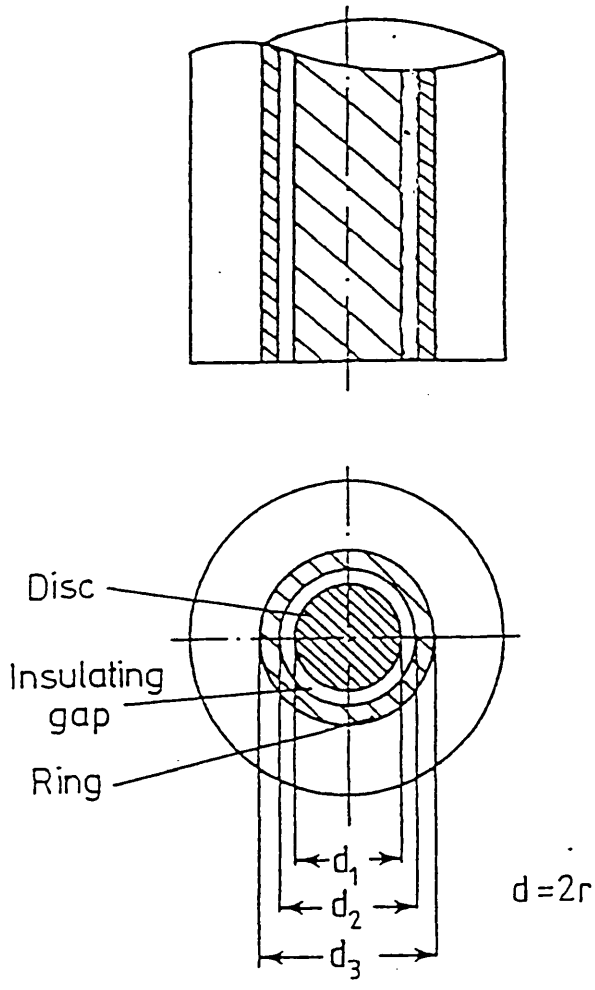
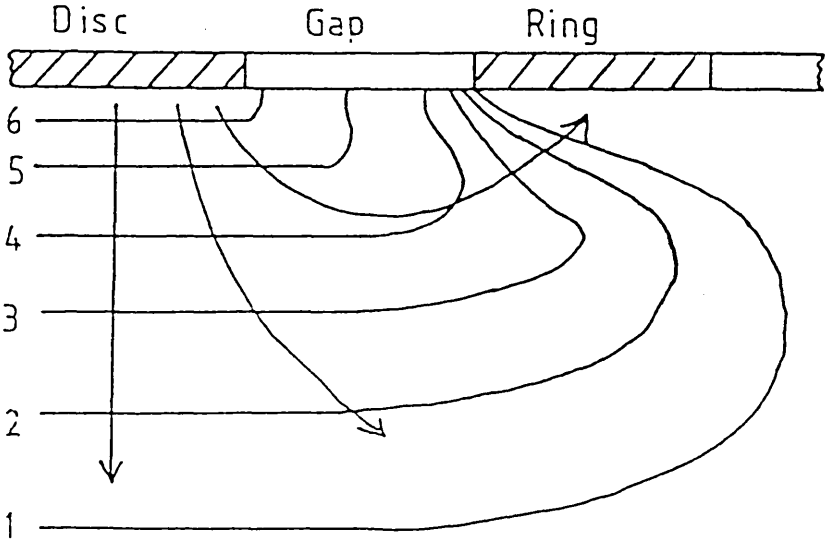


Figure 2.8 The schematic variation in concentration of an electroactive species at an RRDE. The species is being produced at the disc and destroyed at the ring.



where

$$f(\theta) = 3^{1/2}/4\pi \ln\{(1 + \theta^{1/3})^3/ [1 + \theta]\} + 3/2\pi \arctan[(2\theta^{1/3} - 1)/3^{1/2}] + 1/4 \quad ....(2.21)$$

and

$$\beta = \{(r_3/r_1)^3 - (r_2/r_1)^3\} \quad ....(2.22)$$

$$\alpha = \{(r_2/r_1)^3 - 1\} \quad ....(2.23)$$

Thus, the collection efficiency is merely a function of the three characteristic ring- disc radii r_1, r_2 and r_3 (Figure 2.7) and is independent of the rotation speed. This treatment assumes that B is stable on the time scale of the disc to ring traversal. If this is not the case, the observed collection efficiency is less than N_0.

2.2.2 Potentiometric Ring Sensors

An alternative to the use of a ring electrode in the amperometric mode is the potentiometric ring electrode. In this case, the ring is held at open-circuit ($i_R = 0$). In the presence of the reduced and oxidised forms of an electroactive species

$$A + ne^- \rightleftharpoons B$$

the equilibrium potential of the ring electrode with the disc at open-circuit will be given by the Nernst equation[1]

$$E = E^{\ominus}_{A,B} + \frac{2.3\ RT}{nF} \log_{10} \left\{ \frac{[A_R]}{[B_R]} \right\}$$

Production or destruction of A or B at the disc electrode will lead to variation of the ratio of the ring concentrations of A and B, A_R and B_R. This will result in a change in the measured ring potential.

Previous work has considered the theory of potentiometric detection on the ring for reversible[67] and irreversible[68] systems. This thesis presents work using two types of potentiometric ring sensor- the silver/silver chloride electrode for chloride ion detection and the bismuth/bismuth oxide pH sensor.

2.2.2.1 The Silver/Silver Ion Electrode

Albery, Bruckenstein and Napp[67] have developed a theoretical treatment for the current-voltage behaviour at the ring of the reversible system

$$A + ne^- \underset{\longleftarrow}{\longrightarrow} B$$

when these reactions are also occuring at the disc electrode. This treatment involves the solution of the convective-diffusion equation for the ring-disc electrode

$$D \frac{\partial^2 c}{\partial x^2} = -Cx \frac{\partial c}{\partial x} + Crx \frac{\partial c}{\partial r} \qquad ....(2.25)$$

where $C = 8.0\ W^{3/2} \nu^{-1/2}$ ....(2.26)

For a reversible reaction with a high exchange current density, such as Ag/Ag^+, since the ring electrode is an equipotential surface,

$$a_R^0 / b_R^0 = K_R \qquad ....(2.27)$$

across the whole of the ring, where

K_R is a constant

a_R^0 and b_R^0 are the surface concentrations of A and B at the ring.

The ring potential can be expressed by the following equation

$$E_R = E^{\sigma}_{A,B} - \frac{2.3\ RT}{nF}\left[\frac{2}{3}\log_{10}\left\{\frac{D_B}{D_A}\right\} + \log_{10}\left\{\frac{i^{\infty}_{R,A} - i_R - N_0 i_D}{i_R + N_0 i_D - i^{\infty}_{R,B}}\right\}\right] \quad \ldots.(2.28)$$

where $i^{\infty}_{R,A}$ and $i^{\infty}_{R,B}$ are the mass transport limited currents for reaction of A and B at the ring

and i_D, i_R are the currents at the disc and ring, respectively.

When $i_D = 0$, this equation reduces to the ring current-voltage equation.

Further development of equation (2.28) is possible. For the silver/silver ion reaction, if the ring is made of silver metal, b^0_R is constant and so the surface silver ion concentration must be constant across the ring, from equation (2.27). Also, $i^{\infty}_{R,Ag}$ must be very large and so

$$i^{\infty}_{R,Ag} >> (i_R + N_0 i_D)$$

Thus, equation (2.28) becomes

$$E_R = Q + \frac{2.3\ RT}{nF}\log_{10}\left[i_R + N_0 i_D - i^{\infty}_{R,Ag^+}\right] \quad \ldots.(2.29)$$

with

$$Q = E^{\sigma}_{Ag/Ag^+} - \frac{1.53\ RT}{nF}\left[\log_{10}\left\{\frac{D_{Ag^+}}{D_{Ag}}\right\} + \frac{3}{2}\log_{10} i^{\infty}_{R,Ag}\right]$$

being constant.

Equation (2.29) can be rearranged to give

$$E_R = S + \frac{2.3\ RT}{F} \log_{10} \left[1 - \frac{i_R + N_0 i_D}{i^{\infty}_{R,Ag^+}} \right]$$

....(2.30)

with the constant, S, given by

$$S = Q + \frac{2.3\ RT}{F} \log_{10} \left[- i^{\infty}_{R,Ag^+} \right]$$

For a potentiometric ring sensor, when $i_D = i_R = 0$, from equation (2.30)

$$E_R = S$$

Therefore

$$E_R = (E_R)_{i_D, i_R = 0} + \frac{2.3\ RT}{F} \log_{10} \left[1 - \frac{i_R + N_0 i_D}{i^{\infty}_{R,Ag^+}} \right]$$

....(2.31)

In the potentiometric mode, $i_R = 0$, and so one obtains

$$(E_R)_{i_R = 0} = (E_R)_{i_D, i_R = 0} + \frac{2.3\ RT}{F} \log_{10} \left[1 - \frac{N_0 i_D}{i^{\infty}_{R,Ag^+}} \right]$$

....(2.32)

which upon rearrangement, gives the following equation for i_D

$$i_D = - \frac{i^{\infty}_{R,Ag^+}}{N_0} \left[\exp \left\{ \frac{\Delta E_R F}{RT} \right\} - 1 \right] \quad ....(2.33)$$

where

$$\Delta E_R = (E_R)_{i_R = 0} - (E_R)_{i_R, i_D = 0}$$

Thus, it can be seen that a measurable shift in

ΔE_R can be produced when i_D is comparable to or greater than i^{∞}_{R,Ag^+}. Since i^{∞}_{R,Ag^+} can be made very small by having a small bulk concentration of Ag^+, this method can be used to detect very small disc fluxes.

2.2.2.2 The Silver/Silver Chloride Electrode

A silver/silver chloride electrode can be produced by chloridising a silver electrode in aqueous solution (section 3.10). This process results in a porous film of silver chloride being deposited onto the silver. On immersing this electrode in an aqueous solution, the local concentrations of silver and chloride ions will be given by the solubility product of silver chloride

$$K_{sp} = [Ag^+][Cl^-] \qquad \ldots.(2.34).$$

Also, the potential of the electrode will be determined by the Nernst equation (equation (2.24)) for the silver/silver ion couple. This mechanism has been shown to be the most important for the silver/silver chloride electrode. Direct electron transfer between the silver and silver chloride solids does not occur for thin, porous silver chloride films[72,73,74]. A combination of these two equations gives

$$E = E^{\ominus}_{Ag/Ag^+} + \frac{2.3\ RT}{F} \log_{10} K_{sp} - \frac{2.3\ RT}{F} \log_{10} [Cl^-] \qquad \ldots.(2.35)$$

This equation will hold as long as solid silver chloride is present. Also, the kinetics of the silver chloride dissociation and association must be fast enough for the equilibrium concentrations of silver and chloride ions to be maintained close to the electrode.

The previous section described the current-voltage characteristics of the silver/silver ion ring electrode when silver is produced or destroyed at the disc. From equation (2.35), it is evident that the silver/silver chloride ring electrode is sensitive to disc chloride fluxes. It is clear that as long as the chloride ion concentrations at the ring and in the bulk solution are greater than $K_{sp}^{1/2}$, chloride ion will be the majority ionic charge carrier. In this case, the concentration profiles for chloride ion will be exactly analagous to those for silver ion in Figure 2.8. Therefore, by analogy with equation (2.33), disc fluxes of chloride ion, i_{D,Cl^-}, can be related to the observed ring potential, ΔE_R, by the following expression

$$i_{D,Cl^-} = - \frac{i^{\infty}_{R,Cl^-}}{N_0} \left[\exp \left\{ - \frac{\Delta E_R F}{RT} \right\} - 1 \right] \quad \ldots.(2.36)$$

The change of sign of the exponent compared with equation (2.33) reflects the change in sign of the dependence of potential on concentration given by equation (2.35) in comparison with the Nernst equation for a silver/silver ion electrode.

If the chloride ion and silver ion concentrations are both of similar magnitude to $K_{sp}^{1/2}$, then this equation does not hold, as both ions are important in ionic charge transport. The equation will also not be applicable if the majority ion at the disc and in bulk solution differ. In this case, there will be a reaction zone at which silver and

chloride ions react to form solid silver chloride- thus the observed ring response will be less than that predicted by equation (2.36). The general theory for this situation is considered in section 2.2.2.3 for proton and hydroxide ion.

2.2.2.3 The Bismuth/Bismuth Oxide Electrode

Various metal/metal oxide systems can be used as pH electrodes. Examples are palladium[69], iridium[70], antimony[70] and bismuth. Of these, bismuth/bismuth oxide is the easiest to prepare- this can be done electrochemically, at room temperature (section 3.9).

The electrode senses the Nernstian potential set up between bismuth and hydrated bismuth oxide layers. The reaction can be represented by the general equation

$$\underset{BiOx}{[Bi_x(OH)_y]^{(2x-y)+}}\ (A^-)_{2x-y} \underset{\longleftarrow}{\overset{2xe^-}{\longrightarrow}} xBi + yOH^- + (2x-y)A^-$$

The potential of this electrode is given by

$$E = K_1 - \frac{2.3\ RTy}{2xF} \log_{10}[OH^-] \qquad ....(2.37)$$

where

$$K_1 = E^{\ominus}_{Bi/BiOx} - \frac{2.3\ RT}{F}(2x-y)\ \log_{10}[A^-]$$

K_1 is constant, independent of x and y, for high concentrations of anion, A^-. This is the case in electrochemical experiments, where background electrolyte is present.

The dissociation constant of water, K_w, is given

by

$$K_w = [H^+]\,[OH^-] \qquad ....(2.38)$$

and

$$pH = -\log_{10}[H^+] \qquad ....(2.39)$$

Therefore, combining equations (2.37), (2.38) and (2.39), one obtains

$$E = K_2 - \frac{2.3\ RTy}{2xF}\ pH \qquad ....(2.40)$$

In this equation, K_2 is another constant.

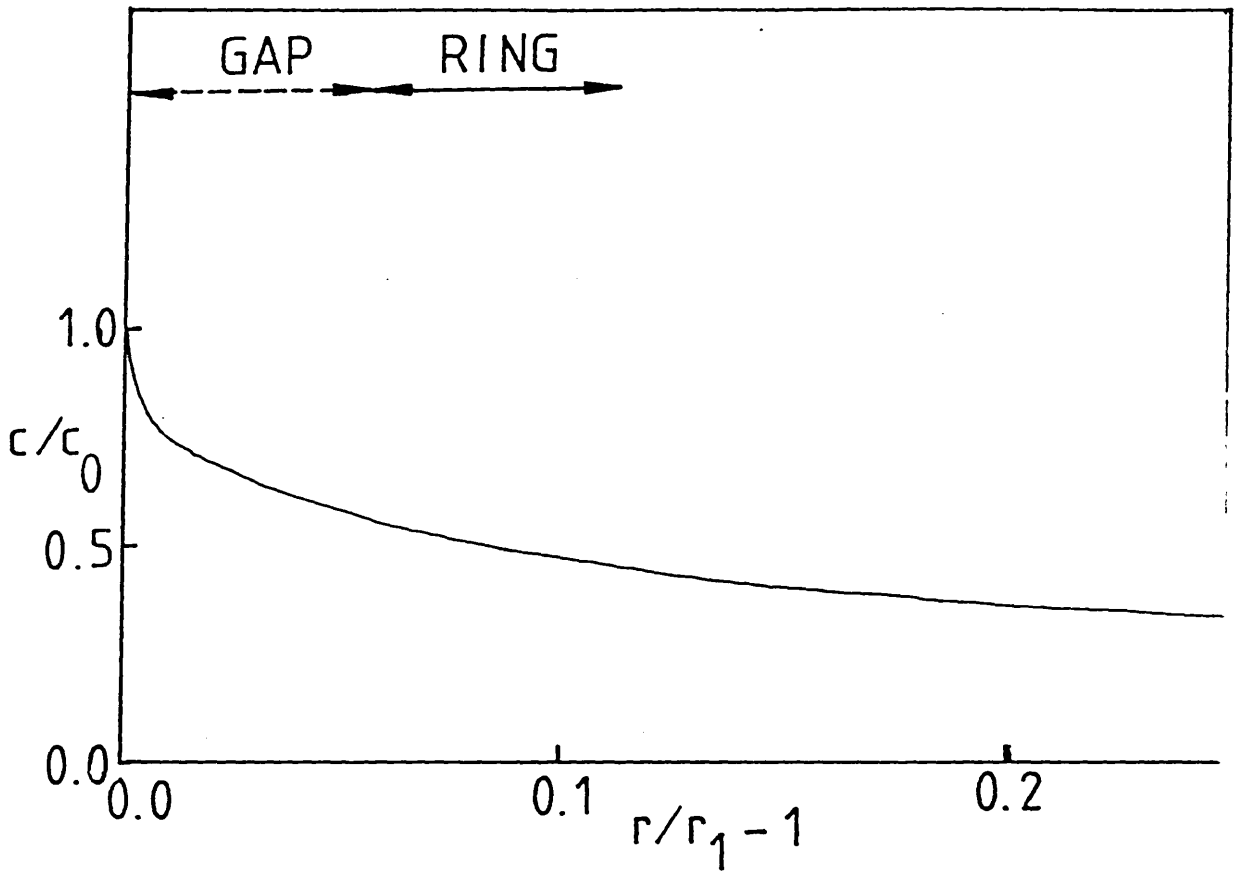
$$K_2 = K_1 - \frac{2.3\ RTy}{2xF}\ \log_{10}K_w$$

The magnitude of the response of this sensor to pH varies with x and y. Therefore, calibration of the ring response using solutions of known pH is necessary to allow conversion of ring potential to pH.

Unlike the silver/silver ion electrodes, this potentiometric sensor has a very low exchange current density[75]. This means that the flux of protons or hydroxide ions at the ring surface causes little perturbation to the radial concentration profile across the ring. Hence the concentration profile across the ring can be modelled in a similar way to the gap[75] (Figure 2.9).

The solution of the convective-diffusion equation for this system has been presented[75]. However, this treatment assumes that no titration of proton with hydroxide ion occurs in the gap. General theory incorporating this effect will be presented in this section.

Figure 2.9 The concentration of electrogenerated species as a function of radial distance for a potentiometric ring sensor with low exchange current density. The gap and ring dimensions shown are for the electrodes used in this work.



2.2.2.3.1 General Theory For The Bismuth/Bismuth Oxide Ring Sensor Involving Proton And Hydroxide Ion Titration

Throughout this treatment, A and B will be used for the majority and minority species in the bulk of solution. Above pH7, B is hydroxide, whereas below this value, B is taken as proton.

Figure 2.10 shows the concentration profile for the production of A at the disc and titration by B from the bulk. Lower case letters are used to denote concentrations. B diffuses in from the bulk of solution and reacts with A to produce water. X_R is the reaction layer thickness for A and X_D. is the diffusion layer thickness. It is assumed that where B is the majority ion (i.e.for $x > X_R$), $a = 0$ and where $x < X_R$, $b = 0$. This approximation will be valid for all but the smallest of disc fluxes.

At X_R, using Fick's first law and equating fluxes

$$j = \frac{D_A a_0}{X_R} = \frac{D_B b_\infty}{(X_D - X_R)} \qquad \ldots.(2.41)$$

from equation (2.6). Rearrangement of this equation yields

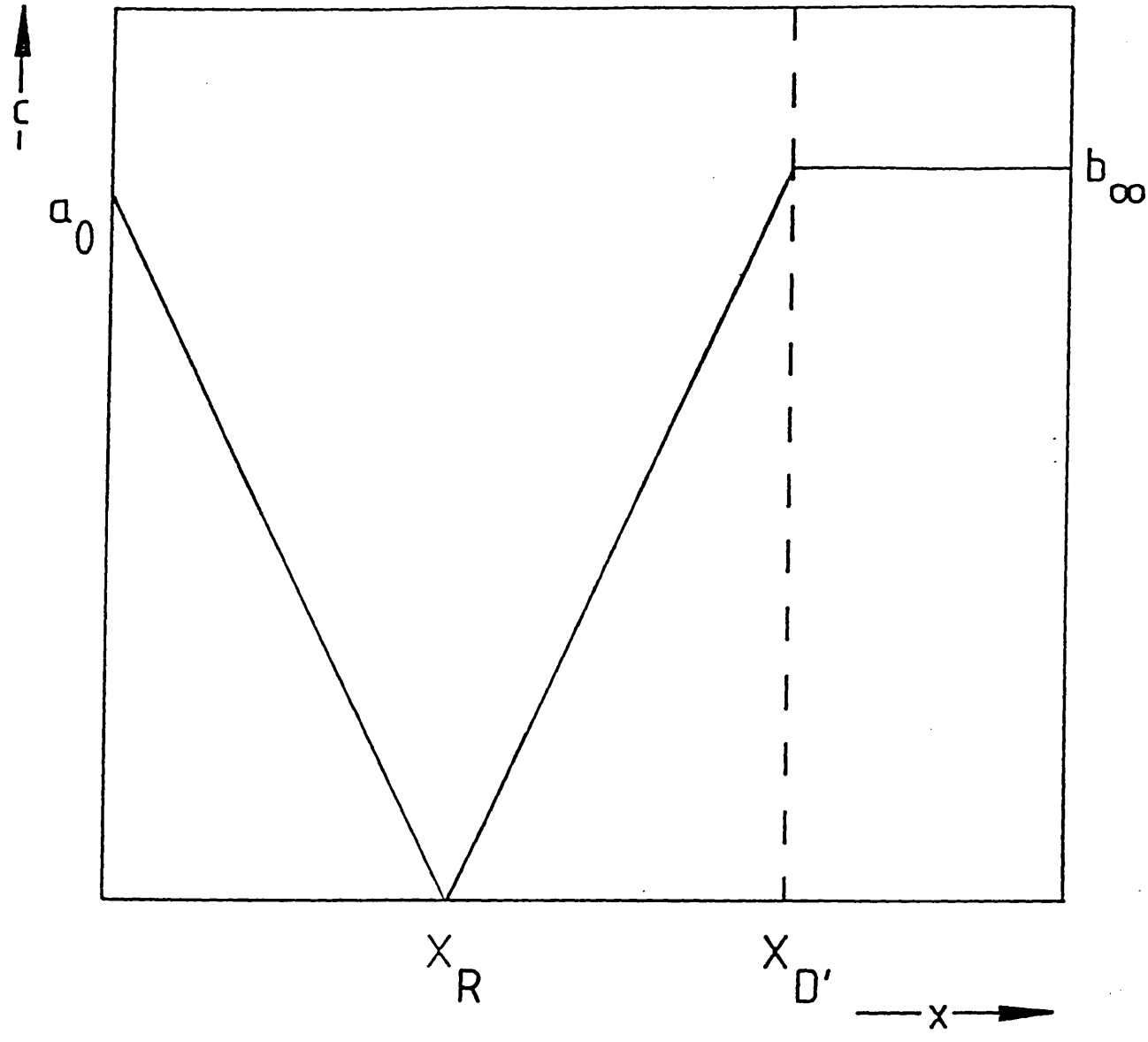
$$j = \frac{D_A a_0 + D_B b_\infty}{X_D} \qquad \ldots.(2.42)$$

X_D. will vary with a_0 and b_∞, as well as rotation speed.

The convective-diffusion equation for this system is (equation 2.10, reference 64)

$$D_A \frac{\partial^2 a}{\partial x^2} - Cx^2 \frac{\partial a}{\partial x} - D_B \frac{\partial^2 b}{\partial x^2} + Cx^2 \frac{\partial b}{\partial x} = 0 \qquad \ldots.(2.43)$$

Figure 2.10 Schematic concentration profile for the titration of A produced at the disc by B from the bulk.



At $x < X_R$

$$D_A \frac{\partial^2 a}{\partial x^2} - Cx^2 \frac{\partial a}{\partial x} = 0 \qquad \ldots.(2.44)$$

The boundary conditions for the solution of this equation are at $x = 0$; $a = a_0$ and

at $x = X_R$; $a = 0$

Similarly, for $X_R < x < \infty$

$$D_B \frac{\partial^2 b}{\partial x^2} - Cx^2 \frac{\partial b}{\partial x} = 0 \qquad \ldots.(2.45)$$

with at $x = X_R$; $b = 0$

$x \longrightarrow \infty$; $b \longrightarrow b_\infty$

Equation (2.44) has the solution[64]

$$\frac{\partial a}{\partial x} = \left\{ \frac{\partial a}{\partial x} \right\}_0 \exp \left[- \frac{1}{3} \left\{ \frac{x}{X_A} \right\}^3 \right] \qquad \ldots.(2.46)$$

where $X_A = (D_A/C)^{1/3}$.

Integration of this equation gives

$$a = a_0 + \left\{ \frac{\partial a}{\partial x} \right\}_0 \int_0^x \exp \left[- \frac{1}{3} \left\{ \frac{x}{X_A} \right\}^3 \right] dx \qquad \ldots.(2.47)$$

A value for a_0 can be found by substitution of the boundary condition for A at $x = X_R$.

$$a_0 = - \int_0^{X_R} \left\{ \frac{\partial a}{\partial x} \right\}_0 \exp \left[- \frac{1}{3} \left\{ \frac{x}{X_A} \right\}^3 \right] dx \qquad \ldots.(2.48)$$

Similarly, from equation (2.45)

$$\frac{\partial b}{\partial x} = \frac{j}{D_B} \exp \left[- \frac{1}{3} \left\{ \frac{x}{X_B} \right\}^3 \right]$$

....(2.49)

The multiplication term for the exponential in this equation is found by saying when x is small, i.e. $x < X_B$, transport is by diffusion and $j = D_B \, \partial b/\partial x$. Integration and application of the boundary condition for B at X_R gives

$$b_\infty = \int_{X_R}^{\infty} \frac{j}{D_B} \exp \left[- \frac{1}{3} \left\{ \frac{x}{X_B} \right\}^3 \right] dx$$

....(2.50)

whilst for any x,

$$b_x = \int_{X_R}^{x} \frac{j}{D_B} \exp \left[- \frac{1}{3} \left\{ \frac{x}{X_B} \right\}^3 \right] dx$$

....(2.51)

On combining equations (2.50) and (2.51) and making the substitution

$$\lambda = x/X_B$$

one obtains

$$b = - \frac{jX_B}{D_B} \int_{X/X_B}^{\infty} \exp \left\{ - \frac{\lambda^3}{3} \right\} d\lambda + b_\infty \qquad ....(2.52)$$

where

$$b_\infty = - \frac{jX_B}{D_B} \int_{X_R/X_B}^{\infty} \exp \left\{ - \frac{\lambda^3}{3} \right\} d\lambda \qquad ....(2.53)$$

For A, by making the substitutions

$$\lambda = x/X_A \text{ and } j = -D_A (\partial a/\partial x)_0$$

into equation (2.48),

$$a_0 = \frac{jX_A}{D_A} \int_0^{X_R/X_A} \exp\left\{ -\frac{\lambda^3}{3} \right\} d\lambda \qquad \ldots.(2.54)$$

From equations (2.53) and (2.54), one can see that there are certain limiting cases for this reaction.

(i) When $X_A = X_B$, the simple result

$$j = \frac{D_A a_0 + D_B b_\infty}{X_D}$$

can be derived. Thus, in this case, $X_{D,A} = X_D$, the diffusion layer thickness of both A and B at the RDE (equation (2.7)).

(ii) When $X_R << X_A, X_B$ i.e. $\lambda << 1$.

In this case,

$$\int_0^{\xi} \exp\left\{ -\frac{\lambda^3}{3} \right\} d\lambda \approx \xi$$

and so, from equations (2.53) and (2.54)

$$j \approx \frac{D_A a_0}{X_R} \approx \frac{D_B b_\infty}{X_B A - X_R} \qquad \ldots.(2.55)$$

where

$$A = \int_0^{\infty} \exp\left\{ -\frac{\lambda^3}{3} \right\} d\lambda = 1.288 \qquad \ldots.(2.56)$$

But $AX_B = X_{D,B}$

where $X_{D,B}$ is the diffusion layer thickness, X_D, for B.

Rearrangement gives

$$X_R = X_{D,B} \frac{D_A a_0}{D_A a_0 + D_B b_\infty}$$

and

$$j = \frac{D_A a_0 + D_B b_\infty}{X_{D,B}}$$

This treatment assumes the general solution for the disc flux to be of the form

$$j = \frac{F.(D_A a_0 + D_B b_\infty)}{X_{D,B}}$$

where the function, F, must be found.

Let $D_A/D_B = \alpha$

By rearrangement and substitution for $X_{D,B}$ from equations (2.53) and (2.56), one obtains

$$F. \left[\frac{\alpha_0}{b_\infty} + 1 \right] = \int_0^\infty \exp\left\{ -\frac{\lambda^3}{3} \right\} d\lambda \left[\int_\varrho^\infty \exp\left\{ -\frac{\lambda^3}{3} \right\} d\lambda \right]^{-1} \quad \ldots.(2.57)$$

where $\varrho = X_R/X_B$ i.e. $\varrho/(\alpha^{1/3}) = X_R/X_A$

Replacement of the denominator of this equation from equations (2.53) and (2.54) gives

$$F. \left[\frac{\alpha_0}{b_\infty} + 1 \right] = \alpha^{\frac{2}{3}} \left\{ \frac{a_0}{b_\infty} \right\} \int_0^\infty \exp \left[-\frac{\lambda^3}{3} \right] d\lambda \,.$$
$$\left[\int_0^{\varrho/\alpha^{1/3}} \exp \left\{ -\frac{\lambda^3}{3} \right\} d\lambda \right]^{-1} \quad \ldots.(2.58)$$

and, hence, one can produce an equation for a_0/b_∞ by comparing (2.57) and (2.58)

$$\frac{a_0}{b_\infty} = \alpha^{-\frac{2}{3}} \int_0^{\varrho/\alpha^{1/3}} \exp \left\{ -\frac{\lambda^3}{3} \right\} d\lambda \,.$$
$$\left[\int_\varrho^\infty \exp \left\{ -\frac{\lambda^3}{3} \right\} d\lambda \right]^{-1} \quad \ldots.(2.59)$$

Combination of this equation and (2.58) yields an expression for F

$$F = \alpha^{-\frac{1}{3}} \int_0^\infty \exp \left\{ -\frac{\lambda^3}{3} \right\} d\lambda \,.$$
$$\left[\int_0^{\varrho/\alpha^{1/3}} \exp \left\{ -\frac{\lambda^3}{3} \right\} d\lambda + \int_\varrho^\infty \exp \left\{ -\frac{\lambda^3}{3} \right\} d\lambda \right]^{-1}$$

$\ldots.(2.60)$

These functions can be solved analytically by the use of incomplete Gamma functions, which can be represented by power series. The theory for this is presented in an appendix to this chapter.

Calculated values for a_0/b_∞ and F are presented in Table (2.1). When A is H^+ and B is OH^-, $\alpha^{1/3}$ has a value of 1.217. For the reverse situation, $\alpha^{1/3}$ is 0.817. Also shown are the calculated values for a simple analytical approximation for F,

Table 2.1 Calculated Values For a_0/b_∞, F and F'

As A Function Of ϱ

$\alpha^{1/3} = 1.217$				$\alpha^{1/3} = 0.821$			
ϱ	a_0/b_∞	F	F'	ϱ	a_0/b_∞	F	F'
1.0	1.46	0.976	0.974	1.0	4.32	1.042	1.057
1.3	3.57	0.943	0.946	1.3	9.76	1.094	1.092
1.5	7.00	0.916	0.918	1.5	17.9	1.139	1.130
1.7	15.0	0.890	0.885	1.7	36.6	1.170	1.164
2.0	52.5	0.855	0.840	2.0	121	1.201	1.198

$$F' = \frac{1 + 0.1\ (a_0/b_\infty)}{1 + 0.1\ \alpha^{1/3}\ (a_0/b_\infty)} \qquad \ldots.(2.61)$$

It is evident that F' is a very good approximation to the function F.

Now, the effect titration with B has upon the disc concentration of A must be considered. From equation (2.46), $\partial a/\partial x$ is unaffected by titration with B at any given x if $(\partial a/\partial x)_0$ is constant. Hence, one may relate the concentration profile of A for any experiment to a hypothetical profile, with the same flux of A at the disc, where no titration by B occurs (Figure 2.11)

Therefore, one may write

$$j \approx F'. \left\{ \frac{D_A a_0 + D_B b_\infty}{X_{D,B}} \right\} = \frac{D_A a_0^*}{X_{D,A}} \qquad \ldots.(2.62)$$

where a_0^* is the hypothetical value of a_0 which would be observed for an experiment with no titration by B with the same value of $(\partial a/\partial x)_0$.

Rearrangement of equation (2.62) gives an expression for the drop in a at the disc.

$$\Delta = a_0^* - a_0 = b_\infty \left\{ \frac{D_B^{2/3}}{D_A^{2/3}} \right\} F' +$$

$$a_0 \left[F'. \left\{ \frac{D_A^{1/3}}{D_B^{1/3}} \right\} - 1 \right] \qquad \ldots.(2.63)$$

The concentration of A seen at the ring, a_R, in the absence of titration, is given by[73]

$$a_R^* = N_D\ a_0^* \qquad \ldots.(2.64)$$

Figure 2.11 Schematic variation of the concentration of A with x, the distance from the disc, with and without titration of A by B. In both cases, the flux of A at the disc is the same.

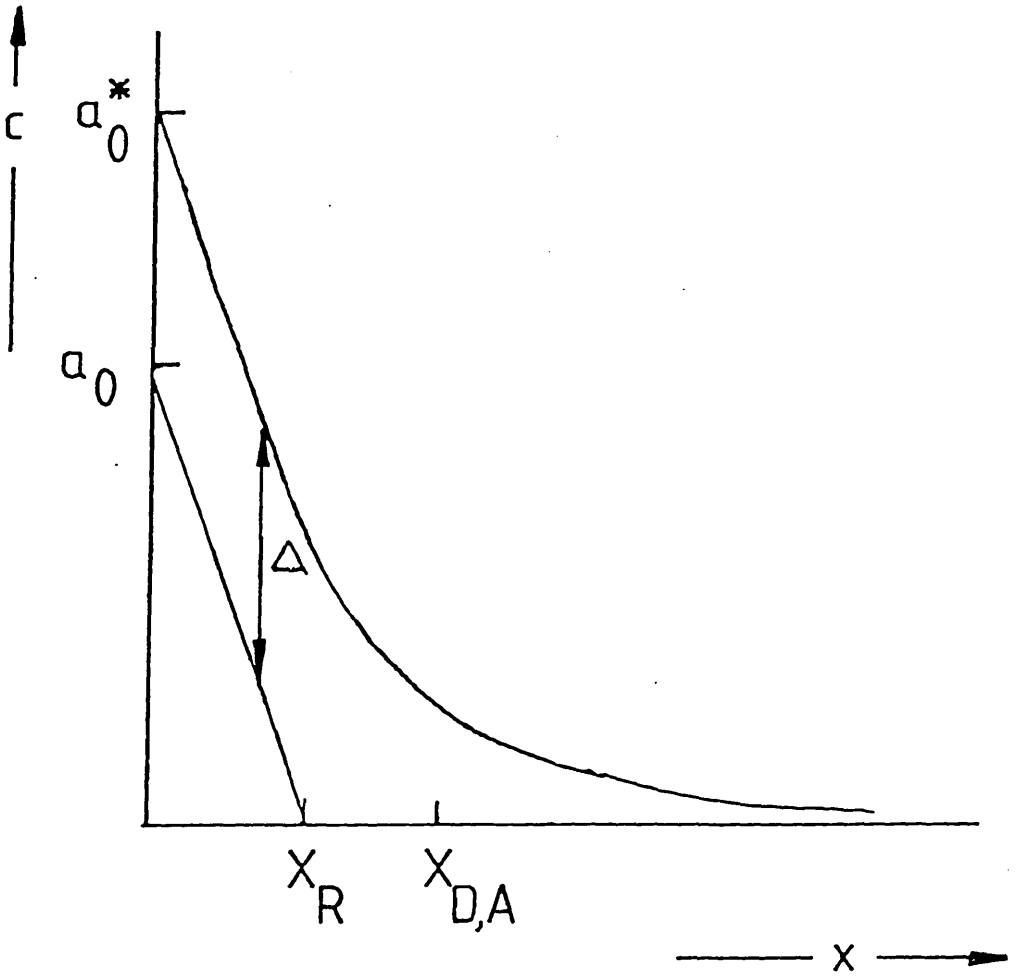
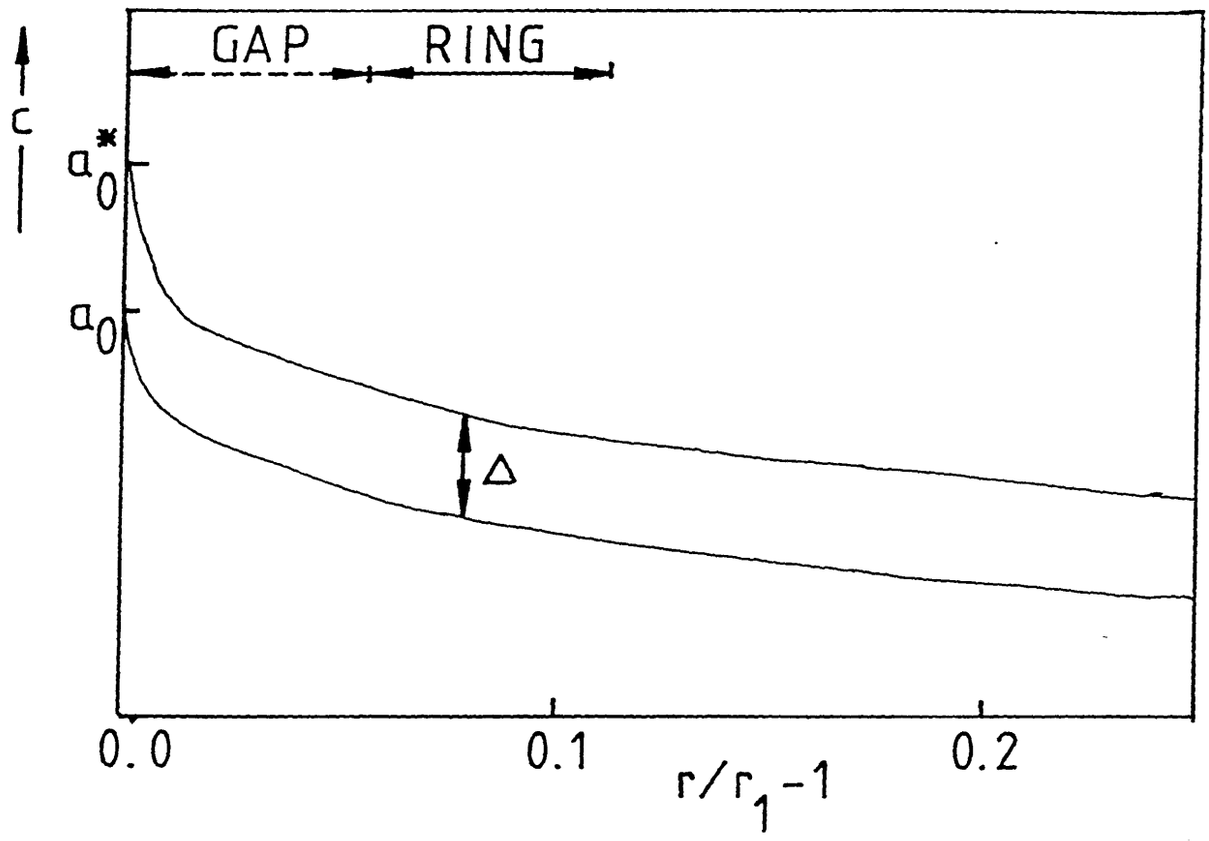


Figure 2.12 The effect of titration of A by B in the radial direction.



where

$$N_D = 1 - 1/6\ F[(r_2/r_1)^3 - 1] - 2/3\ F[\{(r_2 + r_3)/2r_1\}^3 - 1] - 1/6\ F[(r_2/r_1)^3 - 1]$$

and F(0) is given by equation (2.21)

Figure (2.12) shows the titration effect in the radial direction. Again, the observed ring concentration of A is reduced by Δ, independent of the radial distance.

$$a_R = N_D a_0^* - \Delta = N_D a_0^* - (a_0^* - a_0) \qquad ....(2.65)$$

Combination of equations (2.63) and (2.65) gives

$$a_R = a_0^* \left[N_D - 1 + \frac{1}{F'} \left\{ \frac{D_A}{D_B} \right\}^{1/3} \right] - \frac{D_B b_\infty}{D_A} \qquad ....(2.66)$$

On substitution of this equation into (2.62), the following general expression for the flux at the electrode is obtained.

$$j = \frac{1}{X_{D,A}} (D_A a_R + D_B b_\infty) \left[N_D - \left\{ \frac{1 - (D_B/D_A)^{1/3}}{1 + 0.1(a_0/b_\infty)} \right\} \right]^{-1} \qquad ....(2.67)$$

This equation has four limiting cases. These are classified in Table (2.2) by the majority species at the disc and ring and in the bulk.

Case I applies for a concentration step of A in the bulk. No titration occurs and

$$j = \frac{N_D D_A}{X_{D,A}} (a_R - a_\infty)$$

Table 2.2 The Majority Species At The Disc And Ring And In The Bulk For The Four Limiting Cases Of Equation (2.67)

Case	Disc	Ring	Bulk
I	A	A	A
II	A	A	B
III	A	B	B
IV	B	B	B

This is equation (17) of reference (75). Transport of A is dominant.

Case II requires the application of equation (2.67) in full. However, in order to calculate fluxes, one requires a value of a_0. From equations (2.63) and (2.67),

$$F' \left\{ \frac{D_A}{D_B} \right\}^{1/3} N_D \left[1 - \left\{ \frac{1 - (D_B/D_A)^{1/3}}{N_D(1 + 0.1(a_0/b_\infty)} \right\} \right] = \frac{D_A a_R + D_B b_\infty}{D_A a_0 + D_B b_\infty} \qquad \ldots.(2.68)$$

Substitution for F' and rearrangement leads to the following quadratic equation

$$0.1N_D\alpha^{4/3}y^2 + \{\alpha - \alpha^{1/3}(1 - N_D)[0.1 + \alpha] - 0.1\alpha^{4/3}y_R\}y - \{\alpha y_R + \alpha^{1/3}(1 - N_D)\} = 0$$

where $y = a_0/b_\infty$ and $y_R = a_R/b_\infty$

The positive root of this equation provides a value of a_0/b_∞ for equation (2.67).

Case IV applies when a_0 is negligible compared with b_∞. The flux in this case is given by

$$j = \frac{D_B(b_\infty - b_R)}{X_{D,B}N_D}$$

This applies when B is the majority ionic species throughout and titration by A is unimportant. This is the corresponding equation for B to case I for A.

Case III applies when the reaction layer for titration lies

between the disc and the ring. The equation for case III is found by derivation of a smooth function which applies both at the II/III and III/IV boundaries.

The boundary condition for case II/case III is $a_R = b_R = K_w^{1/2}$. Thus equation (2.67) becomes

$$j = \frac{D_B b_\infty}{X_{D,A}} \left[N_D - \left\{ \frac{1 - (D_B/D_A)^{1/3}}{1 + 0.1(a_0/b_\infty)} \right\} \right]^{-1} \quad ....(2.69)$$

In this case, $D_A a_0 << D_B b_\infty$ and $F' \approx 1$, so equation (2.62) can be approximated to

$$j \approx \frac{D_B b_\infty}{N_D X_{D,B}} \quad ....(2.70)$$

From equations (2.62) and (2.65), since a_R is small and can be approximated to zero

$$a_0 = a_0^* (1 - N_D) = \frac{X_{D,A} j}{D_A} (1 - N_D) \quad ....(2.71)$$

Combining equations (2.70) and (2.71), one obtains

$$\frac{a_0}{b_\infty} \approx \frac{(1 - N_D)}{N_D} \left\{ \frac{D_B}{D_A} \right\}^{2/3}$$

Typically, $N_D \approx 1/2$ and so if D_A and D_B are of similar magnitude,

$$1 + 0.1(a_0/b_\infty) \approx 1$$

This gives, from equation (2.69)

$$j = \frac{D_B b_\infty}{X_{D,A}} \left[N_D - \left\{ 1 - \left\{ \frac{D_B}{D_A} \right\}^{1/3} \right\} \right]^{-1}$$

or, converting $X_{D,A}$ to $X_{D,B}$

$$j = \frac{D_B b_\infty}{X_{D,B}} \left[1 - (1 - N_D) \left\{ \frac{D_A}{D_B} \right\}^{1/3} \right]^{-1} \quad \ldots.(2.72)$$

At the III/IV boundary, $b_0 = a_0 = 0$. Therefore, combining equations (2.65) and (2.38), $b_R = (1 - N_D)\, b_\infty$ and one has the mass transport limited flux of B at the disc. Therefore, from equations (2.13) and (2.14)

$$j = \frac{D_B b_\infty}{X_{D,B}}$$

It is necessary to find a function, g, that satisfies the equation

$$j = g \cdot \frac{D_B b_\infty}{X_{D,B}}$$

across the whole region of case III and the boundary conditions.

Let $h = b_R / \{(1 - N_D) b_\infty\}$

The function, h, nas a value of zero at the II/III boundary, rising to one at the III/IV boundary.

Therefore, to summarise previous results

when $D_A = D_B$; $h = 0$ $g = 1/N_D$

$h = 1$ $g = 1$

$D_A \neq D_B$; $h = 0$ $g = 1/\{1 - (D_A/D_B)^{1/3}(1 - N_D)\}$

$h = 1$ $g = 1$

A function which satisfies these conditions is

$$g = \frac{1 - h + h.\{1 - (D_A/D_B)^{1/3}[1 - N_D]}{1 - (D_A/D_B)^{1/3}[1 - N_D]}$$

Thus, by substitution for h, the full flux equation for case

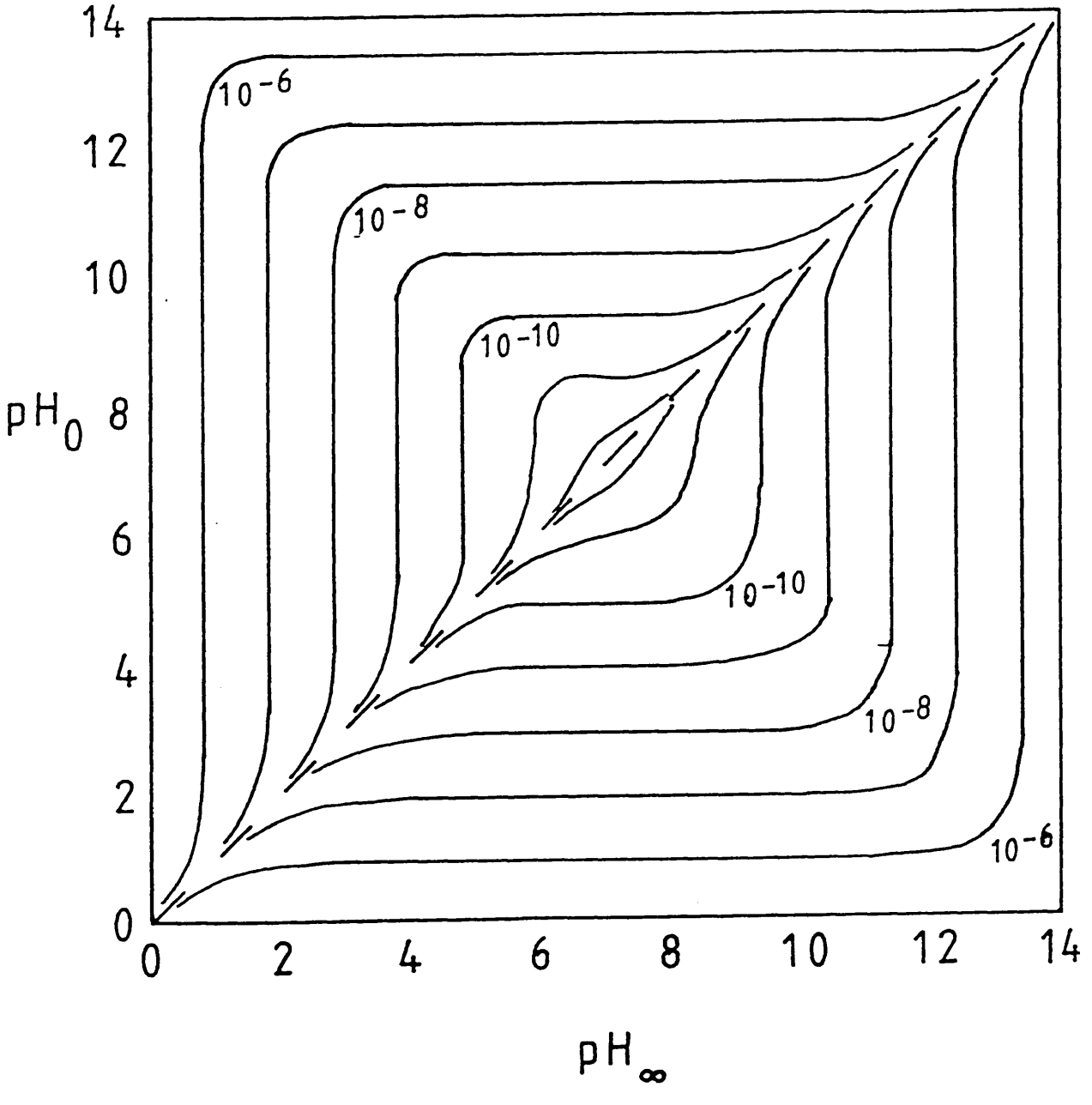
III is

$$j = \frac{D_B\{b_\infty - (D_A/D_B)^{1/3} b_R\}}{X_{D,B}\{1 - (D_A/D_B)^{1/3}[1 - N_D]\}}$$

It is therefore possible to calculate disc fluxes of proton and hydroxide ion for any given values of a_R, N_D and b_∞. Automation of these calculations has been facilitated by means of a BBC basic computer program, BISMUTH, to be found in an appendix to this thesis.

In addition, theoretical plots of proton and hydroxide flux as a function of disc and bulk pH are possible. This is achieved by setting the collection efficiency, N_D, equal to unity. Then, any ring concentrations used in these calculations are equivalent to those at the disc. An example of one of these plots is given in Figure (2.13), at W = 1 Hz.

Figure 2.13 Theoretical plot of the flux of proton or hydroxide ion at a disc electrode as a function of the pH at the disc (pH_0) and in the bulk (pH_∞) for W=1 Hz. The flux values are given in mol cm^{-2} s^{-1}.



Appendix

This appendix gives an analytical solution to the general expression

$$\int_0^z \exp\left\{ -\frac{\lambda^3}{3} \right\} d\lambda$$

By making the substitution $t = \lambda^3/3$, one obtains

$$I(z) = \int_0^z \exp\left\{ -\frac{\lambda^3}{3} \right\} d\lambda = \frac{1}{3^{2/3}} \int_0^{z^3/3} t^{-\frac{2}{3}} \exp(-t)\, dt$$

An analytical solution for this integral is[76]

$$\frac{1}{3^{2/3}} \int_0^{z^3/3} t^{-\frac{2}{3}} \exp(-t)\, dt = \frac{1}{3^{2/3}} \gamma(1/3,\ z^3/3) =$$

$$\frac{z\Gamma(1/3)\ \gamma^*(1/3,\ z^3/3)}{3} = z\Gamma(4/3)\ \gamma^*(1/3,\ z^3/3)$$

The incomplete gamma function, γ^*, can be represented by a power series[77], leading to a series for the integral

$$I(z) = \frac{z}{3} \sum_{n=0}^{\infty} \frac{(-z^3/3)^n}{n!(n+3)}$$

This converges rapidly for five terms of the expansion with $z < 1.8$.

An alternative expansion is

$$I(z) = \frac{1}{3^{2/3}} \gamma(1/3,\ z^3/3) = \frac{\Gamma(1/3)}{3^{2/3}} - \frac{\Gamma(1/3,\ z^3/3)}{3^{2/3}}$$

$$= A - \frac{\exp(-z^3/3)}{z^2} \left[1 - \frac{2}{z^3} + \frac{2.5}{z^6} - \frac{2.5.8}{z^9} + \ldots \right]$$

This converges rapidly for five terms for $z > 1.8$.

The value of A is given by equation (2.56).

Therefore these series can be used to determine the values of F and a_0/b_∞, as from equations (2.59) and (2.60)

$$F = \frac{A}{A + \alpha^{1/3}\, I(\varrho/\alpha^{1/3}) - I(\varrho)}$$

and

$$\frac{a_0}{b_\infty} = \frac{I(\varrho/\alpha^{1/3})}{\alpha^{2/3}\{A - I(\varrho)\}}$$

CHAPTER 3 EXPERIMENTAL

3.1 Circuitry

Modular electronic units were interconnected to produce a wide range of electrochemical circuits. All of these modules were based on the operational amplifier- examples are given in Figure 3.1. These units have been discussed in more detail in previous work[62,81,82]. Schematic diagrams of the three electrode disc and four electrode ring-disc circuits are shown in Figure 3.2. The potential of the working electrode is controlled with respect to the reference electrode, which is at earth. For these circuits

$$V_{O,2} = V_2 + i_2 R_{M,2} \qquad \ldots.(3.1)$$

$$V_{O,3} = V_3 + i_3 R_{M,3} \qquad \ldots.(3.2)$$

and so for both the ring and disc electrodes, the current can be found by subtracting the input and output of the operational amplifiers, knowing $R_{M,2}$ and $R_{M,3}$.

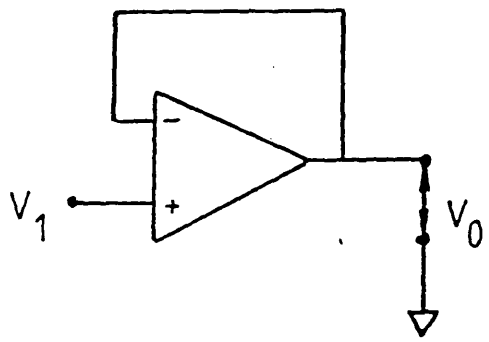
Experimental results were displayed on one or more of the following :-

(i) A digital voltmeter(Fluke 8000A)

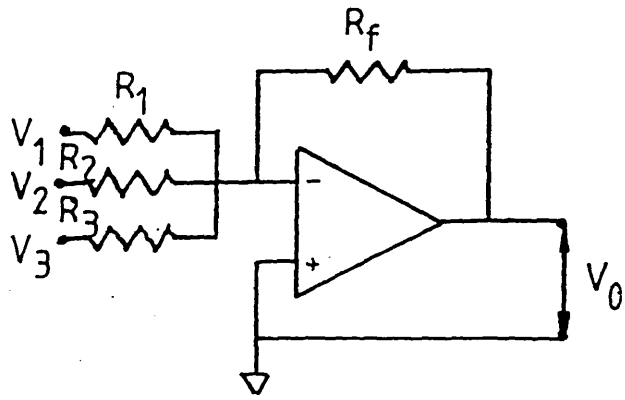
(ii) An x-y-t recorder(Bryans 29000 or 60000)

(iii) A digital storage oscilloscope (Gould OS4000 or OS4001)

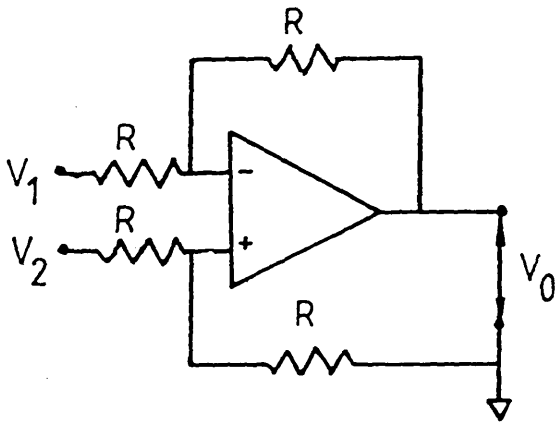
Figure 3.1 Some electronic units based on the operational amplifier used in the construction of electrochemical circuits.



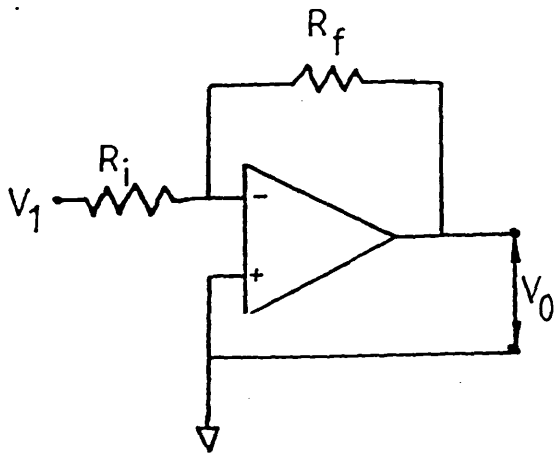
(a) voltage follower



(b) summing inverting amplifier

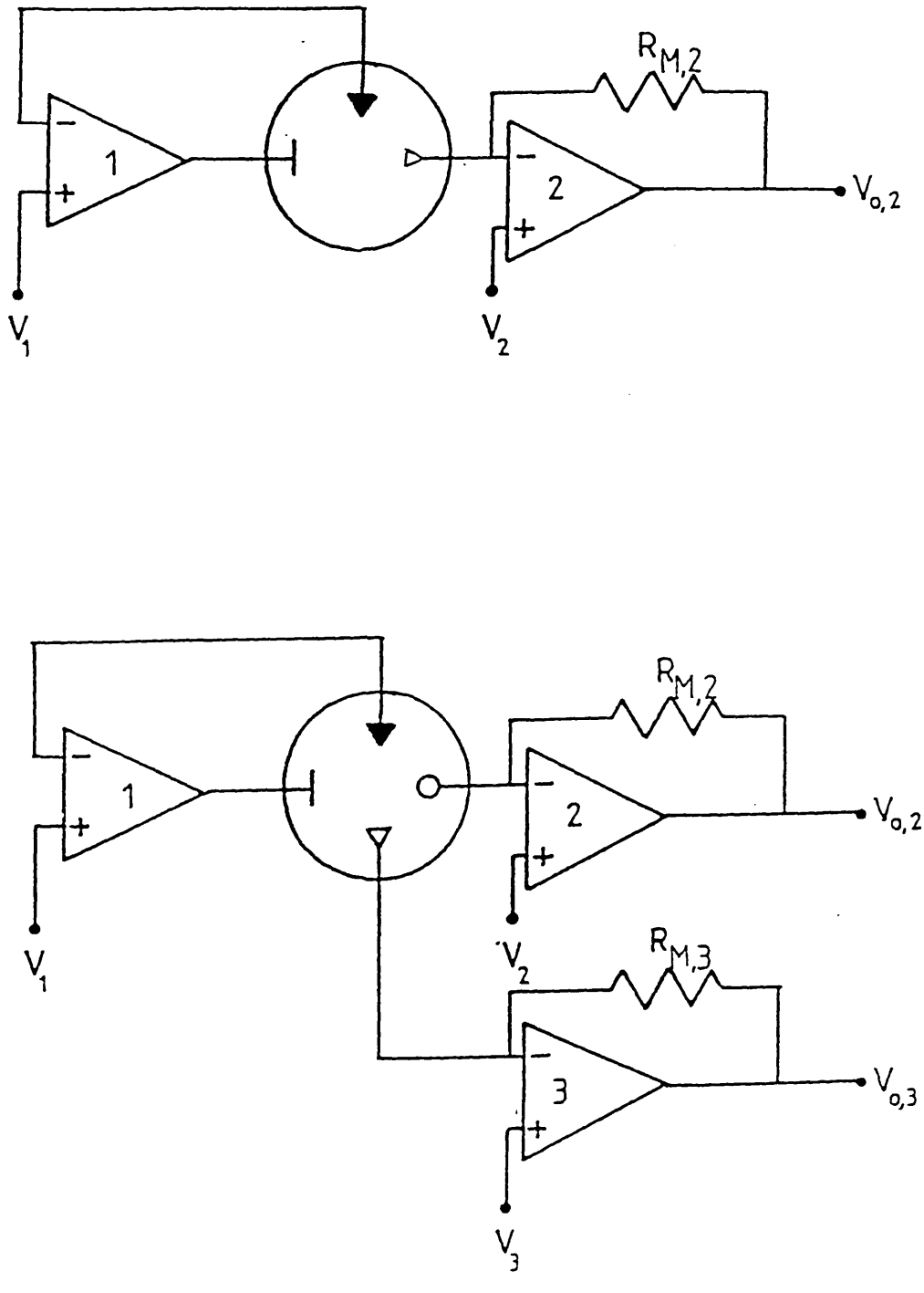


(c) subtractor



(d) inverting amplifier

Figure 3.2 Schematic diagrams of three electrode and four electrode potentiostatic circuits.



3.2 Electrodes

3.2.1 Working Electrodes

Working electrodes were manufactured in house by Mr. Mike Pritchard. Rotating disc and ring-disc electrodes were constructed from gold or platinum (Johnson-Matthey Ltd.). Insulating mantles were made of Kel-F (Fluorocarbon), Teflon (DuPont) or Araldite (Ciba-Geigy).

These electrodes were mechanically polished using 25 μm Alumina (Buehler Ltd.) lubricated with glycerol, followed by 6 μm and 3 μm diamond lapping compound (Engis Ltd.). This was followed by hand-polishing with a slurry of 1 μm Alumina (Banner Scientific) in doubly deionised water and then a slurry of 0.3 μm Alumina. Occasionally, electrodes were further cleaned by electrochemical cycling past the anodic and cathodic solvent limits in aqueous sulphuric acid (50 mM)[82].

Home-made platinum flag electrodes, typically 1 cm^2 in area, were used for spectroscopic analysis of modified electrodes. These were hand polished in the same way as RDE and RRDE electrodes.

3.2.2 Counter Electrodes

Counter electrodes were constructed in house from platinum gauze (Johnson-Matthey), typically of an area of approximately 2 cm^2. These were cleaned using nitrating mix (1:1 nitric acid and sulphuric acid) and rinsed with doubly deionised water.

3.2.3 Reference Electrodes

All aqueous electrochemical experiments were peformed using a home-made potassium chloride saturated calomel electrode (SCE). All potentials quoted in chapter 5 for the aqueous thionine experiments are with respect to the SCE. For non-aqueous experiments, an Ag/Ag^{+} electrode was used. This consisted of a silver wire dipping into a solution of silver perchlorate (0.01M) in the experimental background solution[82]. This electrode has a potential of +0.681V with respect to the standard hydrogen electrode and +0.437V with respect to SCE. All potentials quoted in chapter 4 are with respect to this electrode.

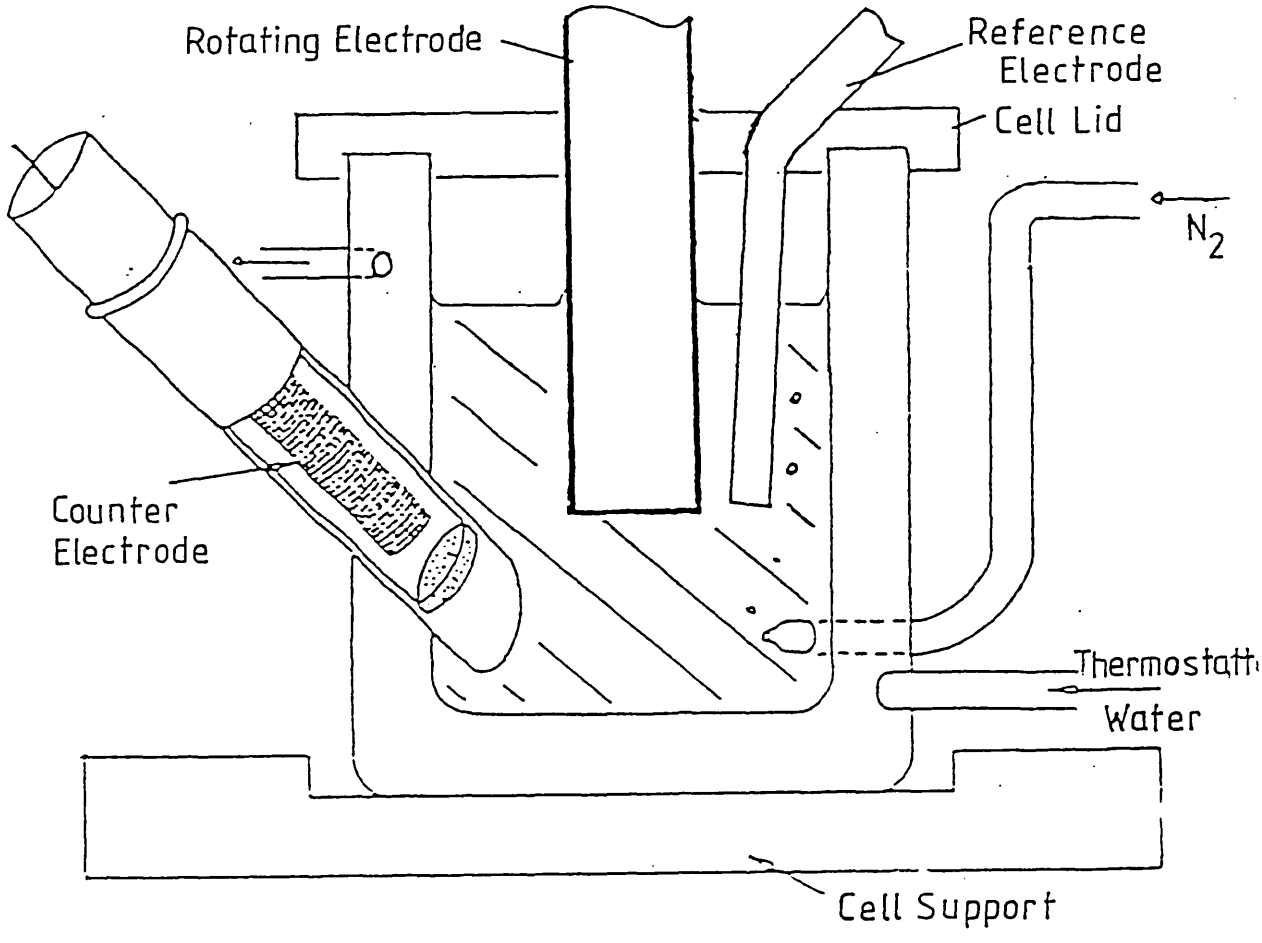
3.3 Rotation System And Cell Assembly

The rotation system used was that described previously[82].

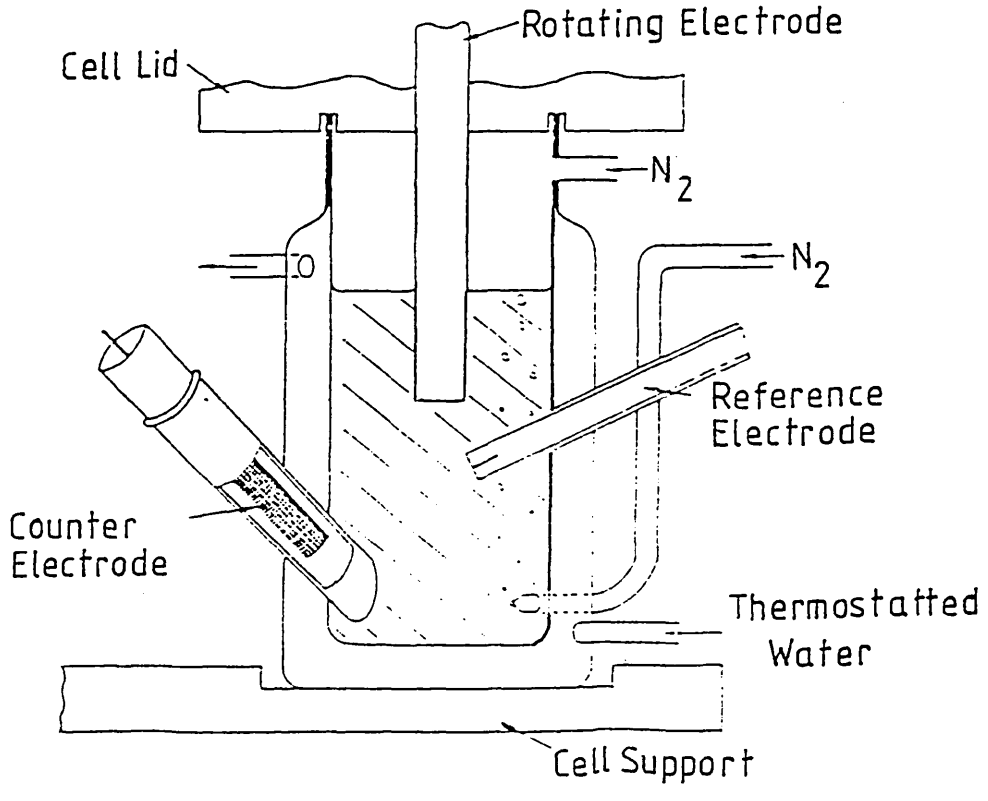
The two electrochemical cell assemblies used are shown in Figure 3.3. The first system is typically for aqueous work. Products of counter electrode reactions were excluded from bulk solution by means of a porous glass frit. The volume of the cell is approximately 200 cm^3. The second is utilised in non-aqueous work. This has a much smaller solution volume (25 cm^3) and has no counter frit. This is because the frit was found to give high resistances in organic solvents, leading to current saturation. An extra nitrogen inlet tube allows a stream of gas to be blown across the surface of the solution in conjunction with, or as an alternative to, normal purging.

Figure 3.3 The electrochemical cells.

(a) aqueous



(b) non-aqueous



3.4 Solvents

All water used for electrochemistry was doubly deionised by being passed through an amine ion-exchange resin (Houseman) and a Millipore Milli-Q filter system. Fison's dried, distilled acetonitrile was refluxed for two hours over calcium hydride (1% weight/volume) and then fractionally distilled under conditions of high reflux ratio. The middle fraction (~60%) was collected, boiling point 81 °C, and stored under dry Argon.

The purification procedure for dimethyl sulphoxide was that used by Mann[83]. AnalaR grade DMSO (BDH Ltd.) was slowly frozen. The remaining liquor (approximately 20% of the batch) was discarded. The frozen portion was distilled with 50 cm/dm^3 benzene to remove water as part of an azeotropic mixture. Purification was completed by distillation under vacuum (b.p. 189 °C at 760 mm Hg) and the solvent stored under dry argon.

3.5 Background Electrolytes

Lithium perchlorate (Aldrich Chemical Co.) was dried in vacuo at 60 °C and stored under dry argon. This was the chosen electrolyte for all non-aqueous experiments, in 0.1 M concentration, unless otherwise stated.

AnalaR tetrabutylammonium tetrafluoroborate (TBAT) (BDH) was recrystallised three times from an ethyl acetate/petroleum ether mixture and dried in vacuo at 50 °C.

Sulphuric and hydrochloric acids (Fison's Ltd.) were used without further purification. All other supporting electrolytes were of Analar grade (BDH) or puriss. grade (Fluka) and were used as obtained.

3.6 Chemicals

All chemicals in this section were supplied by Aldrich, unless otherwise stated.

3.6.1 Heteroaromatic Monomers

Thiophene (b.p. 84 °C) was distilled and stored under dry argon at 5 °C.

Thiophene-3-carboxylic acid and thiophene-3-acetic acid were used without further purification.

Saturated aqueous solutions of thionine (Fluka) were filtered prior to use.

3.6.2 Miscellany

All chemicals employed in syntheses were used as received. Details of pyrrole synthetic work are to be found at the end of chapter 4. Glassware was cleaned in a solution of Decon 90 (5%, BDH) in distilled water, rinsed several times with this water and then dried at 110 °C. All glycols and benzene (BDH) were dried over 3A molecular sieves and stored under dry argon. These sieves were activated at 300 °C for 24 hours in a stream of dry nitrogen.

3.7 Spectrometry

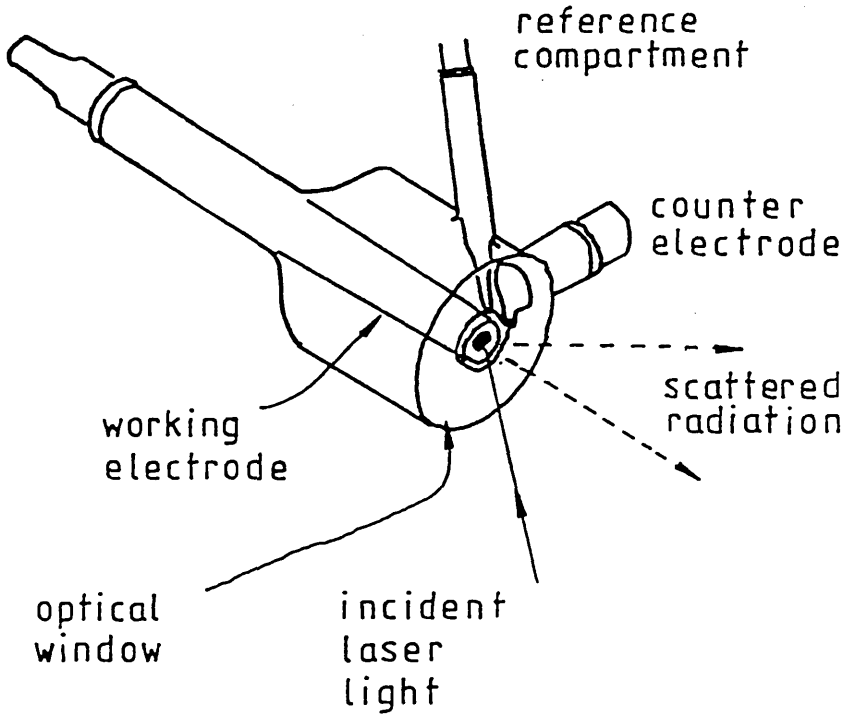
3.7.1 Laser Raman Spectrometry

Most of the in situ thionine chronoamperometric experiments were performed in collaboration with Professor R. E. Hester at the University of York. The design of the electrochemical cell and the gold working electrode have been reported previously[84,85]. This experimental set-up is shown in Figure 3.4. Incident light is reflected at the electrode surface after passing through the optical window and a thin layer of solution. The Raman signal is detected normal to the electrode.

The gold working electrode area used was 0.071 cm^2 in area and the electrode was positioned approximately 2 mm from the optical window. Experiments in York were carried out using a Chemical Electronics type TR40-3A potentiostat and WG-01/1 waveform generator in conjunction with a Hewlett-Packard 7015B x-y-t recorder. Spectra were recorded on a Spex 1403 spectrometer, with a cooled RCA C31034-A02 photomultiplier tube. This was linked to a Spex DPC-2 digital photometer. Computer control was by a Compudrive and Scamp minicomputer. A Spectra Physics 170 Krypton laser or a Coherent Radiation 590 Rhodamine 6G dye laser, pumped by a Coherent Radiation 52A argon laser was the excitation source.

All other experiments were performed in house. This experimental set-up consists of a Spex Ramalog V spectrometer fitted with a GaAs photomultiplier. Data handling is by a Spex Datamate computer. Early work used a

Figure 3.4 The in situ laser Raman electrochemical cell.



52 krypton laser (Coherent). Also used in later work was an Innova 90-K krypton laser and an Innova 70-4 argon laser (Coherent).

3.7.2 X-Ray Photoelectron Spectroscopy (XPS)

These ultra-high vacuum (UHV) experiments were performed on an Escalab Mark II spectrometer (VG Scientific). Peak integration was performed using VG software.

3.7.3 Scanning Electron Microscopy (SEM)

SEM experiments were carried out on a JEOL JSM T-200 electron microscope. Platinum flags coated with the substance of interest were immobilised onto an aluminium drum using perspex cement. These electrodes were sputtered with a 20 nm thickness of gold to prevent surface charging. A silver dag was applied to provide contact between the gold and the aluminium.

Spectra were taken under UHV at a working distance of 20 mm, with an accelerating voltage of 25 kV and at an angle of 30 ° with respect to vertical.

Two detectors were utilised. A camera was used to record SEM pictures. Printed on these are white scale lines. The length of these markers in microns is the first of the set of numbers printed on these pictures. The other available option was an energy dispersive analysis of X-rays (EDAX) detector. This allows the number of X-rays emitted over a range of energies to be followed with time as a means of elemental analysis.

3.7.4 Fourier Transform Infra-Red Spectrometry (FTIRS)

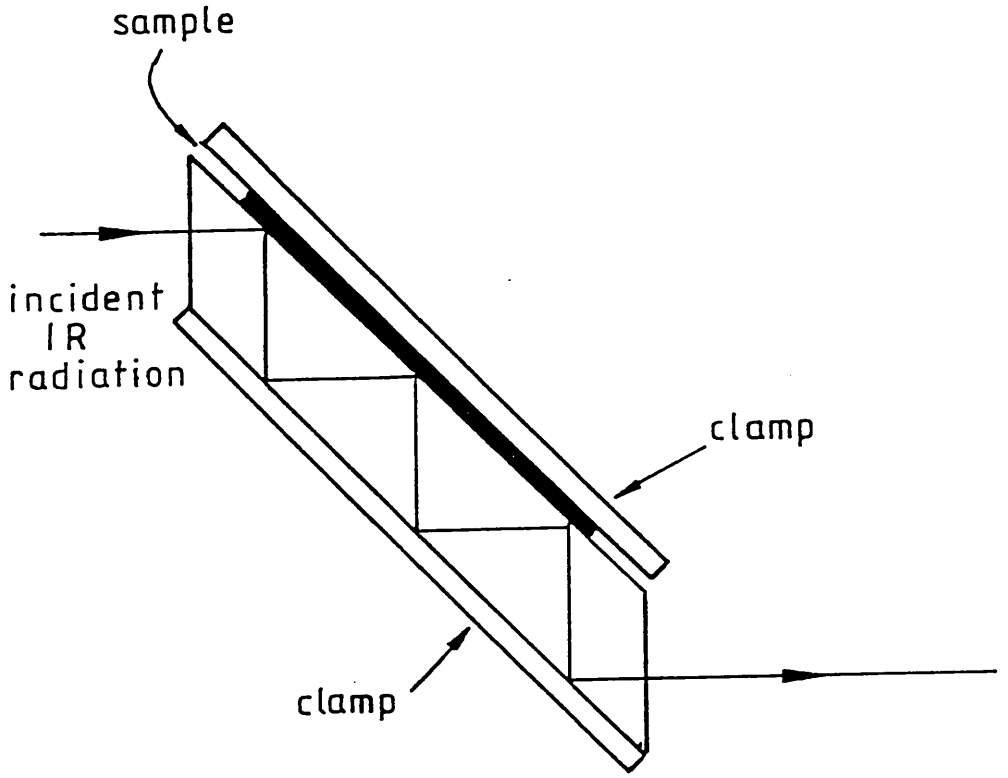
The technique performed was that of multiple internal reflection Fourier transform infra-red spectroscopy (MIRFTIRS)[86] (Figure 3.5). The coated platinum flag was firmly clamped to the outside of the prism. Infra-red radiation was then passed through the prism under conditions of multiple internal reflection. The evanescent wave penetrates a depth, d, into the modified electrode upon being reflected at the prism/coat interface. Typically this distance is of the order of the wavelength of the light ($\sim$10 μm)[87]. This technique therefore allows interrogation of the structure of the whole layer for all but the thickest of coats. It is also suitable for opaque samples such as polyheteroaromatics.

These ex-situ experiments were carried out using one of two machines. Initial results were obtained using a Nicolet 7000 spectrometer at Raychem Ltd. More recent work utilised a Mattson Sirius 100 spectrometer. Each was fitted with the Barnes attenuated total internal reflectance (ATR) accessory and a KBr beamsplitter. Generally, a cadmium-mercury telluride (CMT) detector, cooled with liquid nitrogen, was used in conjunction with a KRS-5 waveguide (Barnes).

3.7.5 In Situ Visible Spectroscopy

Experiments were performed using a Hewlett-Packard 8450A diode array spectrometer. Transparent working electrodes were fabricated in house, using glass slides (0.8 cm x 3 cm) coated with indium doped tin oxide. The

Figure 3.5 The MIRFTIRS set-up.



electrochemical cell was a Kartell dispolab 1939 UV grade disposable cuvette. This had a path length of 1 cm.

3.8 Deoxygenation Systems

Aqueous solutions were degassed using white spot nitrogen (BOC) for about twenty minutes before use. This had previously been deoxygenated by passage through three Dreschel bottles, each containing an aqueous, caustic solution of anthraquinone-2-sulphonate in contact with amalgamated zinc. A fourth bottle of doubly deionised water was used to presaturate the gas.

Non-aqueous solutions were purged with high purity argon (99.99%, BOC) for twenty minutes. Initial gas purification involved successive passage through calcium hydride for drying, a chromium oxide/silica column for deoxygenation and drying and two presaturation bottles containing dried organic solvent over 3A molecular sieves.

3.9 Bismuth Oxide Ring Experiments

3.9.1 Apparatus

Much of the experimental details for this pH-sensitive system has been described previously[75]. All solutions must be kept free of carbon dioxide and carbonate to minimise the effect of solution buffering between disc and ring.

Control of the solution pH was enabled by using a pH-stat system. This consisted of a PHM62 standard pH-meter, a TTT60 titrator and an ABU80 autoburette (Radiometer). This was calibrated daily across the pH range three to nine using various buffer solutions.

3.9.2 Chemicals

Alkaline doubly deionised water, with added potassium permanganate to oxidise organic compounds, was refluxed for two hours and then distilled under dry argon. The middle fraction (60%) of the distillate of b.p. 100 °C was collected, producing CO_2-free solvent. This was stored under dry argon. All solutions were made up and experiments performed in an Atmos dry bag filled with argon. The electrochemical solution was continually degassed throughout the experiment.

Control of the pH was effected by using $HClO_4$ (0.1M) and carbonate-free NaOH (0.1M, BDH) solutions, purged with argon. Sodium perchlorate (0.1M, BDH) was used as the background electrolyte. All reagents were of AnalaR grade.

3.9.3 Sensor Preparation

Bismuth ring plating was carried out according to the method of Harbaugh and Mathers[88]. The plating solution consisted of Bi_2O_3 (4g) dissolved in 20 ml of concentrated perchloric acid and diluted to 100 ml with water. Typical coating conditions were a current density of -2.2 mA cm^{-2} for thirty minutes. The electrode was then washed and left to partially oxidise in aqueous solution.

3.10 Silver/Silver Chloride Experiments

Prior to electroplating, ring electrodes were anodised in concentrated nitric acid for ten minutes at a current density of approximately 10 mA cm^{-2}. After washing with doubly deionised water, silver was electroplated using an aqueous solution of potassium silver cyanide (50 mM, BDH AnalaR). The current density was ~ -3 mA cm^{-2} and the plating time was typically two hours. Anodic chloridisation was effected in aqueous hydrochloric acid (10mM), passing 1 mA cm^{-2} for thirty minutes, or until the ring was plum in colour.

CHAPTER 4-CONDUCTING POLYMERS FOR ELECTROCATALYTIC OXIDATION

4.1 Introduction

Polymer modified electrodes have many advantages over bare electrodes in electrocatalytic reactions. In particular, the specificity of the electrode is extremely important. Also of value is the increase in effective surface area for reaction of a polymer with an open structure. Thus, a greater number of catalytic sites are available for reaction with the substrate and so faster reaction rates are possible.

Examples of such electrodes are given in section 1.3.1. Unfortunately, catalytic currents at these electrodes are small. Theoretical analysis has shown that, in order to produce a sufficiently high current at the electrode, the homogeneous second order rate constant for the reaction between polymer redox site and solution substrate must be greater than 10^3 M^{-1} s^{-1} [3,89]. This has been shown to be unattainable for polyvinyl and polystyrene coats, for which electron transport is via an electron hopping process. This limits the reaction to the layers closest to the electrode.

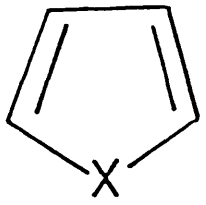
The aim of the work presented in this chapter was to produce electrocatalytic polymer modified electrodes with good electronic conductivity. The chosen group of polymers with this characteristic are the polyaromatics termed the conducting polymers.

4.1.1 Conducting Polymer Modified Electrodes

Electrochemical oxidation of selected aromatic monomers has been shown to result in the deposition of electronically conducting polymer films onto the electrode surface[90-94]. The most widely investigated monomeric species are the five-membered heterocycles: pyrrole, thiophene and furan (Figure 4.1).

These coats can be formed electrochemically. Oxidation of the monomers gives radical cations, which couple at the electrode surface to give polymer films. When formed, these coats are oxidised and counterions are present to maintain electroneutrality. Their schematic structure is given in Figure 4.2a. Coupling occurs primarily at the ring 2,5-positions, as these have the highest electron density in the radical cation[102]. The rings have a high degree of coplanarity and a delocalised π-system is formed along the polymer strands. Thus, these films exhibit high electronic conductivities of the order of 0.1-100 S cm^{-1}[36,95,96]. Electrochemical oxidation and reduction of the film is possible by cycling the electrode potential between suitable limits. This is shown schematically in Figure 4.2b. The neutral form of the coat is much less conducting, with a conductivity of 10^{-7}-10^{-8} S cm^{-1}. Thus, high catalytic currents will only be observed for reactions where the regeneration of the catalytic centre occurs at potentials where there is significant oxidation of the polymer.

Figure 4.1 Pyrrole, thiophene and furan.



X = NH Pyrrole
S Thiophene
O Furan

Figure 4.2a The structure of polypyrrole, polythiophene and polyfuran.

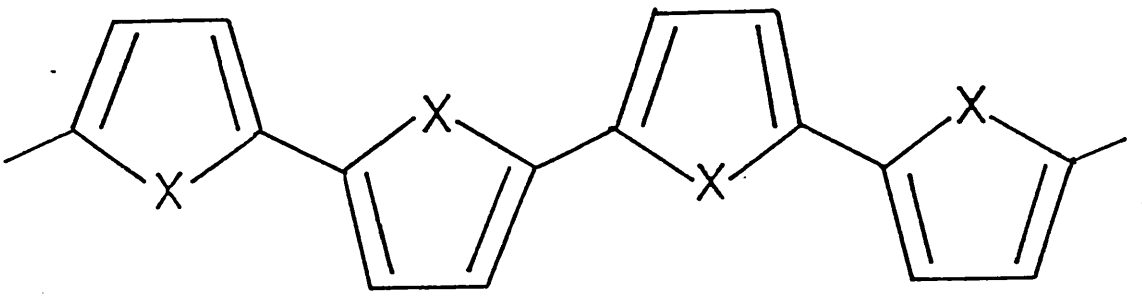
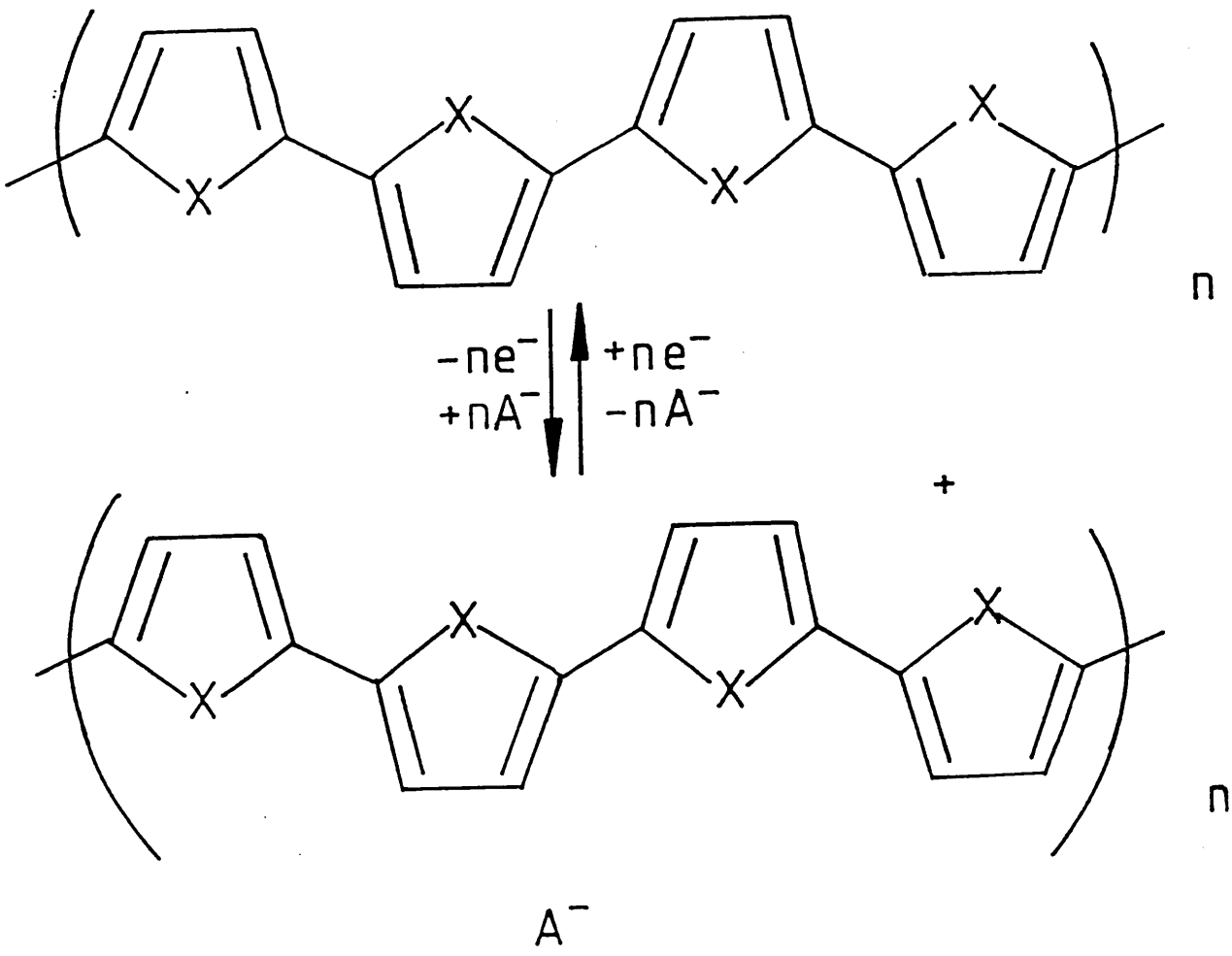


Figure 4.2b Oxidation and reduction of the polymer.



4.1.2 Selective Organic Oxidants For Electrocatalysis

The object of this work is to produce a modified electrode to perform selective organic oxidations. Two well-known oxidants used in batch synthesis are lead(IV) acetate and thallium(III) acetate. Two-electron redox couples were deliberately chosen to increase the likelihood of concerted two-electron oxidation. This minimises the possibility of side reactions involving the coupling of radical products.

4.1.2.1 Lead(IV) Acetate

This species is widely used in biochemistry for the selective carbon-carbon bond cleavage of vic-diols[97,98] (Figure 4.3a). Coordination of the diol occurs with the concomitant loss of two acetate groups. Subsequent reaction results in the formation of lead(II) acetate. For this reaction to be made electrocatalytic, electrooxidation of this reduced lead species to reform complex I or II is required.

4.1.2.2 Thallium(III) Acetate

Thallium(III) Acetate is extensively used in organic chemistry for aromatic ring functionalisation[99]. A typical reaction scheme for this process is shown in Figure 4.3b. Electrocatalysis would be enabled by reoxidation of species III to form complexes I or II.

Thus, the production of a conducting polymer film derivatised with lead(II) acetate or thallium(I) acetate species, which can be easily oxidised to regenerate the catalyst is required. This work researches the formation of

Figure 4.3a The oxidation of diols by lead(IV) acetate.

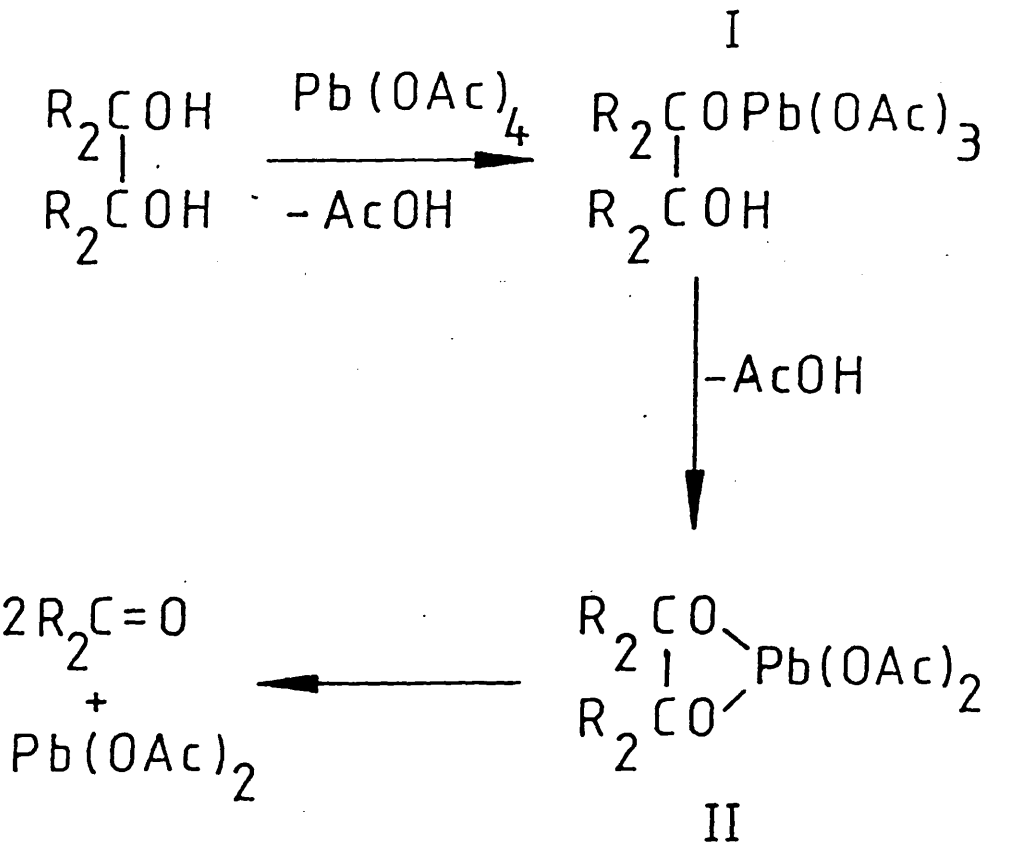
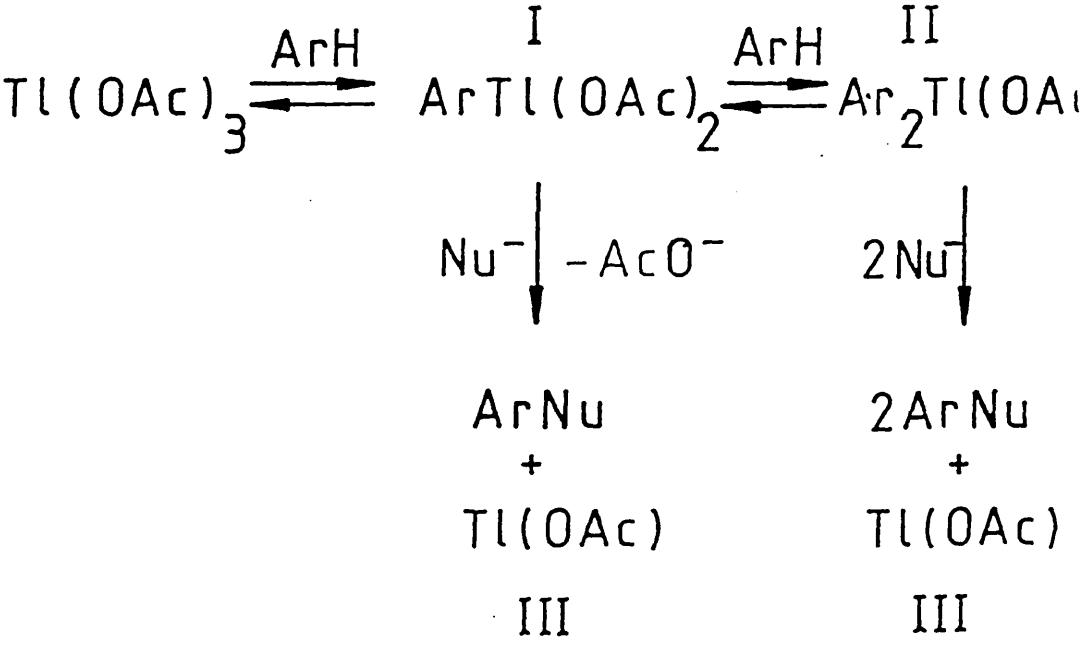


Figure 4.3b The oxidation of aromatic compounds by thallium(III) acetate.



novel conducting polymers with pendant acetic acid or carboxylic acid groups and their subsequent coordination with Pb(II) and Tl(III) as a method of producing just such a film. Primarily, the lead oxidation reaction was investigated, due to the great toxicity of thallium compounds. The catalytic oxidation of ethylene glycol to formaldehyde or formic acid was the target electrocatalytic reaction.

4.1.3 Preparation Of Substituted Conducting Polymers

The conducting polymer films (Figure 4.2a) consist primarily of linear chains of heteroaromatic rings linked at the 2,5- ring positions. It is not surprising, therefore, that 2,5-derivatisation of the monomers has been shown to inhibit polymerisation. Hence, substituents must be present in the 1-,3- or 4- ring positions.

Such modification can be carried out after polymerisation. For example, polypyrrole films can be nitrated, reduced and then acetylated to attach the desired group[100]. The disadvantage of this strategy is the need for several synthetic steps. These reactions may require extreme conditions, which may lead to coat degradation.

The most simple method is the one-step electrochemical polymerisation of substituted monomers. The conductivity of electropolymerised 1-alkyl substituted pyrroles has been measured[101]. Poly-1-methylpyrrole has a conductivity of 10^{-3} S cm^{-1}. This is 10^{5} times smaller than that of polypyrrole. Replacement of the methyl group with

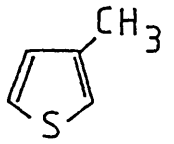
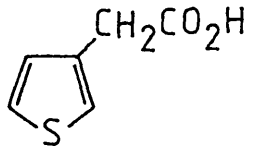
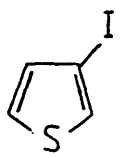
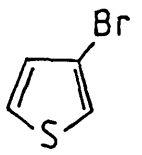
the more bulky isobutyl functionality results in a further hundredfold decrease in conductivity. Therefore, it can be concluded that steric effects due to N-substitution greatly affect the rate of electron propagation.

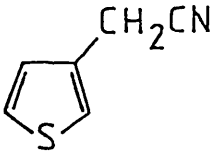
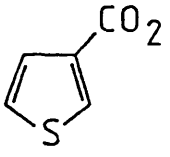
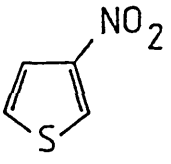
In contrast, films of 3-methylthiophene have measured conductivities comparable to polythiophene[36]. This implies that substitution in the ring 3- or 4- positions has less steric effect, making the formation of 3,4- or 3-carboxylated polymers desirable for this work.

Table 4.1 presents cyclic voltammetric data for the electropolymerisation of a series of 3-substituted thiophenes[102]. This shows potentials for the observed monomeric oxidation peak (E_{pa}) and for the oxidation of the resulting polymer (E_D). Monomeric oxidation results in the formation of a radical cation. The observed variation in the E_{pa} value has been interpreted in terms of the polar-mesomeric effects of the substituents. That E_{pa} has been found to be linearly related to E_D also infers that E_D for the polymer varies as a result of these effects. Thus, 3-derivatisation with these small substituents does not seem to produce significant steric barriers to polymerisation or oxidation.

It is disappointing, in the light of the objectives of this work, that the 3-carboxylate functionalised thiophenes shown do not form films upon electrooxidation. The reasons for this will be discussed further in section 4.3.1.

Table 4.1 Oxidation Potentials For Some 3-Substituted Thiophenes And The Oxidation Potential Of The Resulting Polymers

Monomer	E_{pa}/V	E_D/V
 Thiophene	1.62	0.52
 3-Methylthiophene	1.42	0.28
 3-Thiopheneacetic Acid (TPCA)	1.50	-
 3-Iodothiophene	1.59	-
 3-Bromothiophene	1.66	0.62

Monomer	E_{pa}/V	E_D/V
 3-Thiopheneacetonitrile	1.78	0.68
 3-Thiophenecarboxylic Acid (TPCA)	1.84	-
 3-Nitrothiophene	2.02	-

4.2 Synthesis And Electrochemistry Of 3- and 4-Carboxylated Pyrroles

Synthesis of these monomers utilised the TosMIC reaction of van Leusen[103]. The proposed mechanism is given in Figure 4.4. This was used to attempt the synthesis of the following compounds

(i) R_1 = Me R_2 = CO_2Me

dimethyl 3,4-pyrroledicarboxylate (DPDC)

(ii) R_1 = Me R_2 = Me

methyl 4-methylpyrrole-3-carboxylate (MMPC)

(iii) R_1 = Et R_2 = CH_2CO_2Et

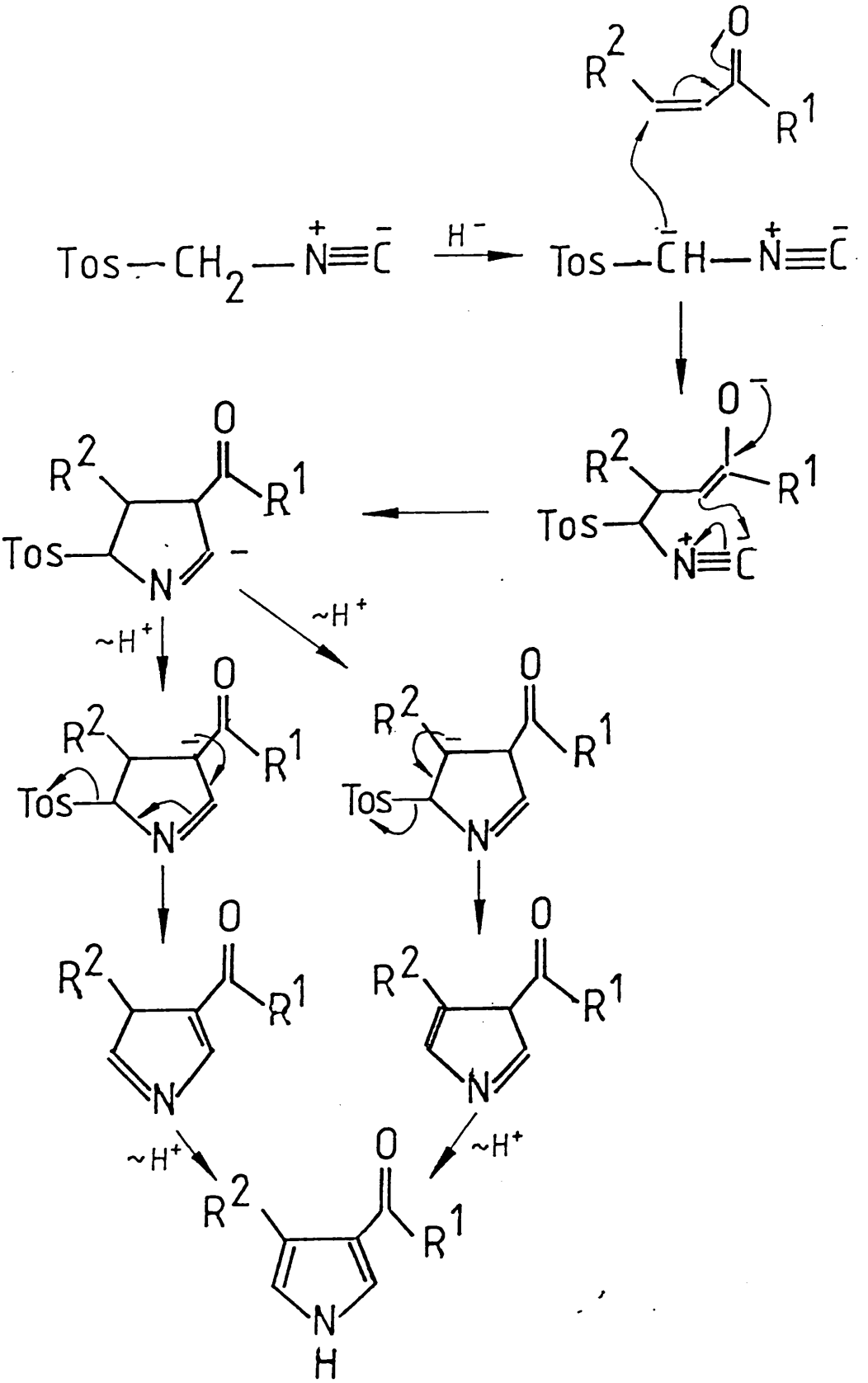
diethyl 4-acetylpyrrole-3-carboxylate (DAPC)

Experimental details for these reactions can be found in an appendix to this chapter.

Experimentally, it was found that only the synthesis of DPDC was possible. This is probably due the lack of a carbonyl α- to the vinyl group in R_2 for syntheses (ii) and (iii). This group will stabilise intermediates with a negative charge α- to R_2. Therefore, it seems that the right hand of the two mechanisms for the ejection of the Tosyl group and aromatisation of the ring is dominant.

Electrochemical studies at an RDE in MeCN/TBAT (0.1 M) solutions showed no peaks due to oxidation of the DPDC monomer within the solvent limits. Similar behaviour was observed when using dimethyl sulphoxide as solvent. Pyrrole has an E_{pa} of +0.76V[102]. Therefore, the addition of these two electron-withdrawing carboxyl substituents

Figure 4.4 The proposed mechanism of the TosMIC reaction.



results in a marked increase in the energy required to form the radical cation. However, these have already been shown to be a requirement of the TosMIC synthesis. This has also been illustrated by the failure to synthesise other pyrrole monomers via the TosMIC reaction[82]. In these reactions, other anion stabilising groups were used in R_2 in place of carbonyl. Thus, it appears that the groups required for successful TosMIC synthesis also inhibit polymerisation and film formation.

Any future work using this strategy would therefore require further synthetic modification of the CO_2R_1 or R_2 groups prior to electrooxidation in order to reduce their electronegativity. This should lead to a decrease in the ring oxidation potential.

4.3 Copolymerisation of Thiophenes

4.3.1 Introduction

In section 4.2, the failure of 3,4-dicarboxlated pyrroles to electropolymerise was explained in terms of the decrease in the thermodynamic stability of the radical cation. Similar arguments may be applied to thiophenes. However, this cannot be the only reason for lack of film formation. From Table 4.1, 3-thiopheneacetic acid (TPAA) has an oxidation potential similar to that of thiophene itself, but does not form polymer coats when electrooxidised. This can be explained by considering the proposed mechanism for film formation[102].

When a radical cation, $R^{+\cdot}$, is formed at the electrode, it can undergo one of three surface processes. Firstly, it can couple with another radical cation and polymerise. Secondly, it can diffuse away into bulk solution to react there. Finally, it can react with solvent, or a nucleophilic species. $R^{+\cdot}$ can be an oligomer or polymer chain of any length. For film formation, the first reaction must be dominant. This is the case for thiophene. The introduction of electron-withdrawing substituents reduces the stability of the radical cation, so increasing the rate of nucleophilic substitution. This results in a decrease in the surface concentration of $R^{+\cdot}$ and a reduction in the amount of surface polymerisation. Since the acetyl group is slightly electron donating, this effect is unimportant for TPAA.

A reduction in the importance of the film formation reaction can also be effected by increasing the importance of diffusion of $R^{+\cdot}$ from the electrode surface. This can be achieved by the attachment of polar groups to the thiophene monomer to increase the solubility of R and $R^{+\cdot}$. The acetate group of TPAA would be expected to be just such a solubilising functionality.

If this hypothesis is correct, a reduction in the solubility of the oligomer and polymer radical cations would be effected by reducing the number of acetate side-groups for a given chain length. This could be brought about by the copolymerisation of thiophene(TP) and TPAA.

4.3.2 Polymerisation Of Thiophene

Figure 4.5 shows the effect of sweeping the potential of a platinum RDE, rotating at 4Hz, in a thiophene solution (75mM). On increasing the applied potential, oxidation of the thiophene monomer begins at +1.4V and current saturation occurs at around +1.5V. Increased currents are observed on the return sweep, indicative of a surface nucleation process[104]. This cycling results in the deposition of a black film of polythiophene.

Coating can also be effected by jumping the electrode potential to +1.6V from 0V or open circuit. This results in a current-time transient similar to that shown in Figure 4.6. Oxidation occurs with a rapidly increasing current, again indicative of surface nucleation. Hillman[105] has analysed the shape of this part of the observed current transients, noting their similarity with the calculated

Figure 4.5 Current-voltage data for the oxidation of thiophene (75 mM) at W = 4 Hz, v = 20 mVs^{-1}.

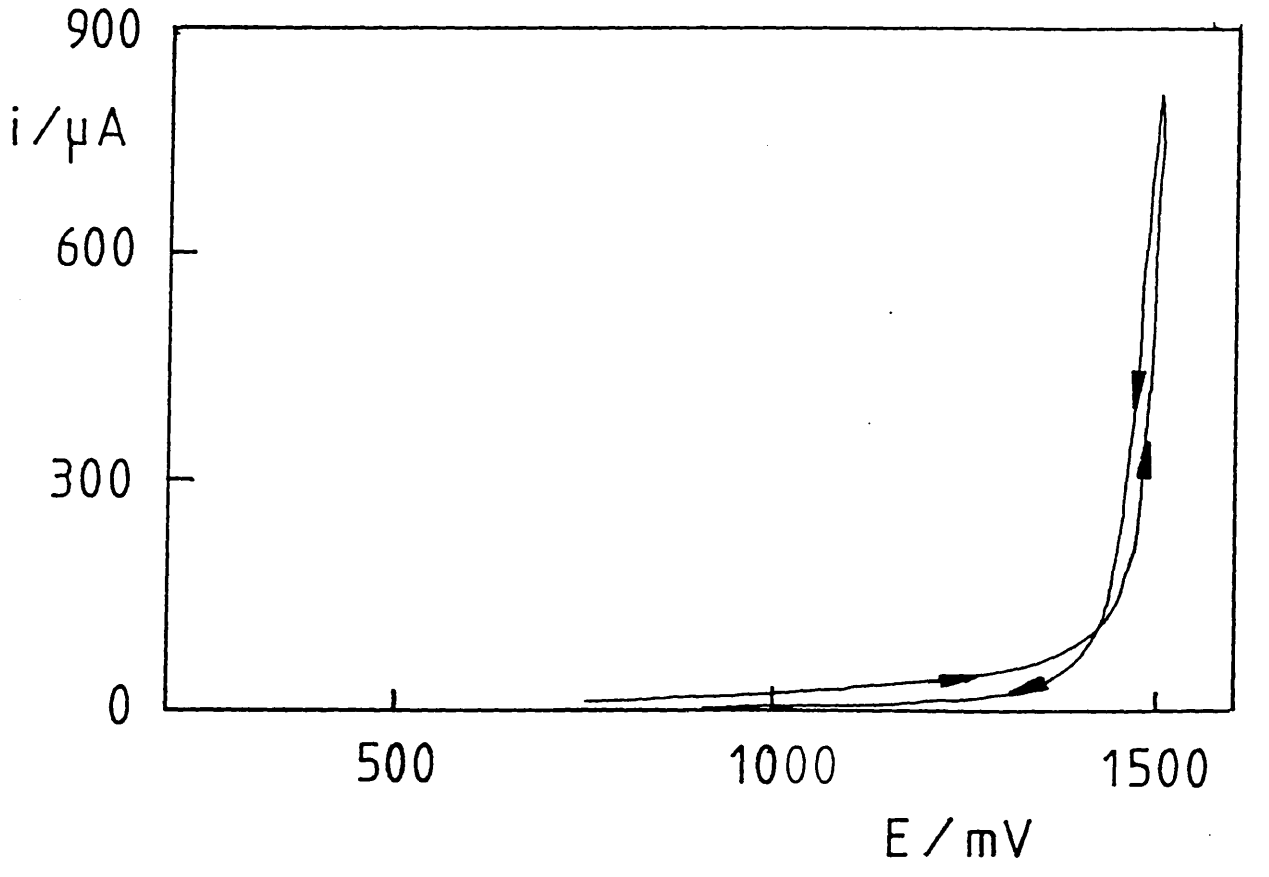
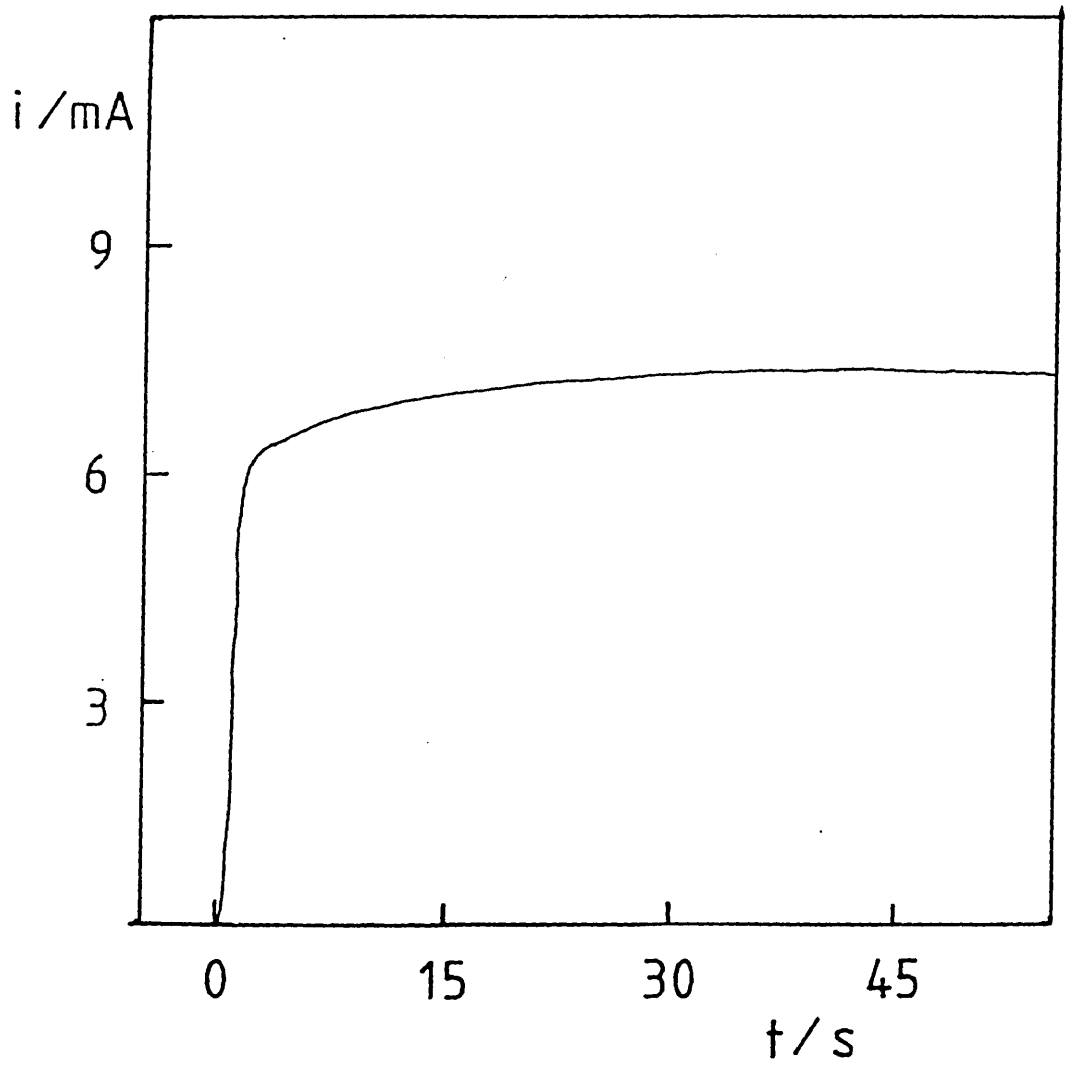


Figure 4.6 Current-time data for the electrooxidation of a thiophene solution (500 mM) at 1.6 V.



transients for three-dimensional instantaneous nucleation and growth of right circular cones[104]. Thus, thiophene polymerisation appears to occur with differing rate constants for growth normal to and parallel with the electrode surface. At long times the observed current is constant, independent of time. This is due to complete overlap of the nucleation centres, resulting in film growth normal to the electrode surface only. Such behaviour has also been observed for experiments involving polymerisation at +1.7V.

Figure 4.7 shows a cyclic voltammogram (CV) of the resulting modified electrode in background electrolyte solution. The observed oxidation and reduction peaks are due to the formation of the oxidised, conducting and reduced, insulating forms of the coat, respectively. These peak currents show a linear dependence upon potential sweep rate (v) (Figure 4.8). This is indicative of the complete oxidation and reduction of a surface bound species[4]. The area under each peak therefore gives the charge required to fully oxidise and reduce the polymer. For polymerisations using 150 mM thiophene, this is typically of the order of 3% of the charge passed during coating. This implies that the film coverage is linearly dependent on the charge passed during film formation, in agreement with previous work[96]. Results presented in this paper also indicate that on electropolymerisation, 2.25 electrons are removed per thiophene monomer. Of these, two electrons are lost during

Figure 4.7 A cyclic voltammogram of a polythiophene modified electrode in $MeCN/LiClO_4$ (0.1 M) at $v = 50\ mV\ s^{-1}$.

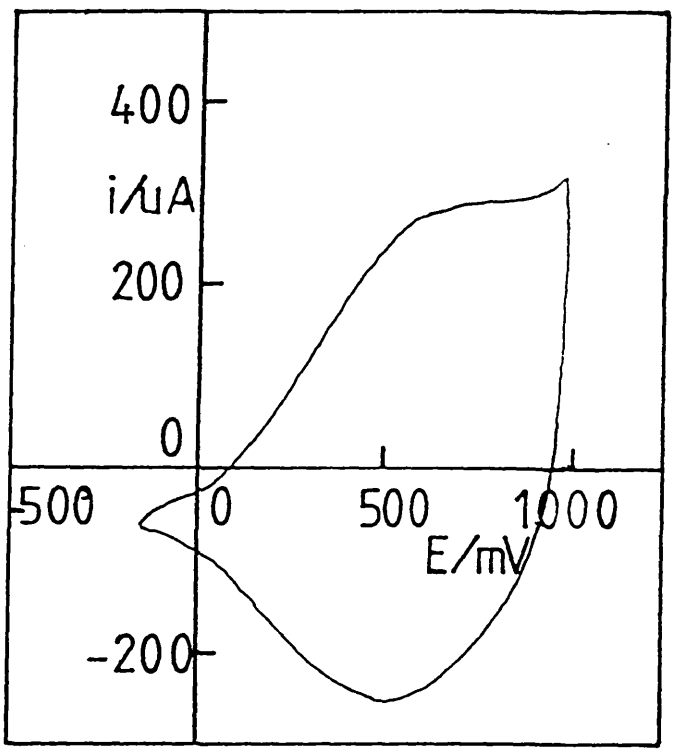
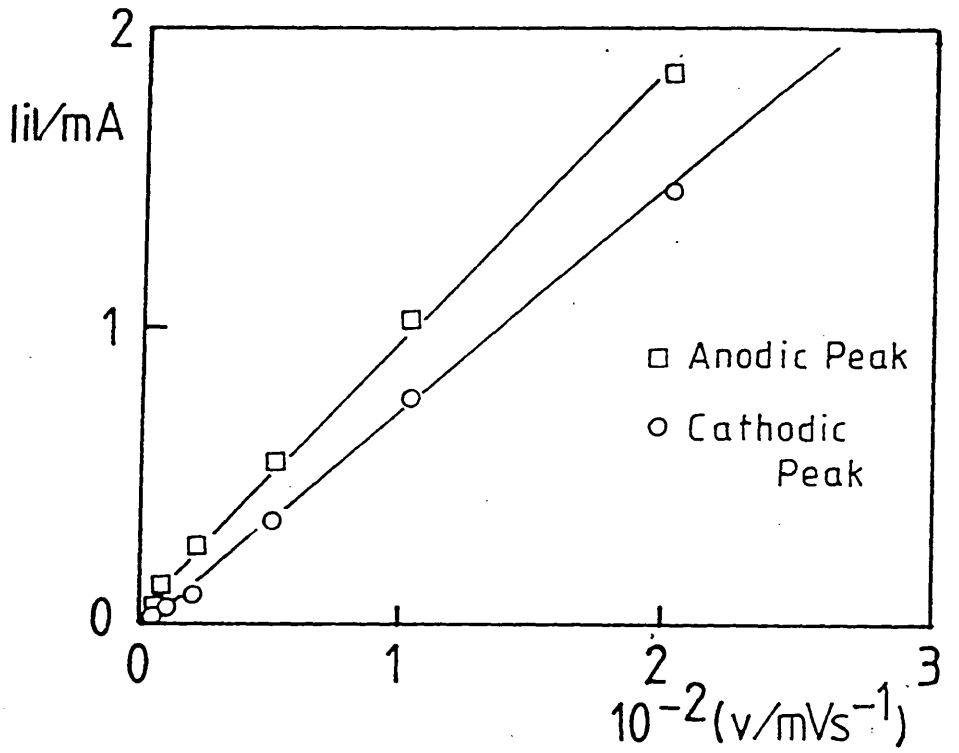


Figure 4.8 Variation of the peak currents for oxidation and reduction of a polythiophene coat with the potential sweep rate.



the coupling process. This indicates that polymer oxidation should require 11% of the electrooxidation charge. The discrepancy between the observed and theoretical percentages can be attributed to the effect of non-polymer forming side reactions of the radical cations (section 4.3.1). Indeed, increasing the solution concentration of thiophene does lead to an increase in the percentage of the thiophene oxidation current seen in the cyclic voltammogram.

Further oxidation of the coat in background electrolyte solutions occurs at potentials greater than +1.3V. This leads to degradation and the loss of film electroactivity.

4.3.3 Formation Of TP/TPAA Copolymers

These experiments were performed using identical coating conditions to those for polythiophene.

Current-time data for the electropolymerisation of a solution of 150mM TP and 100mM TPAA is presented in Figure 4.9a. The shape of the current transient is similar to that observed for pure thiophene, implying a similar electrooxidation process. However the magnitude of the oxidation currents is increased. At the applied potential of +1.6V, the radical cation of both monomers will be formed. CV data for the resulting film in background solution (Figure 4.9b) shows comparable peak positions to those of a polythiophene coat. The observed peak currents are proportional to the sweep rate (Figure 4.10), indicative of complete oxidation/reduction of the polymer. The charge passed in this process was found to be approximately 7% of

Figure 4.9a Current-time data for the electropolymerisation of a 150mM TP/100 mM TPAA solution at 1.6 V.

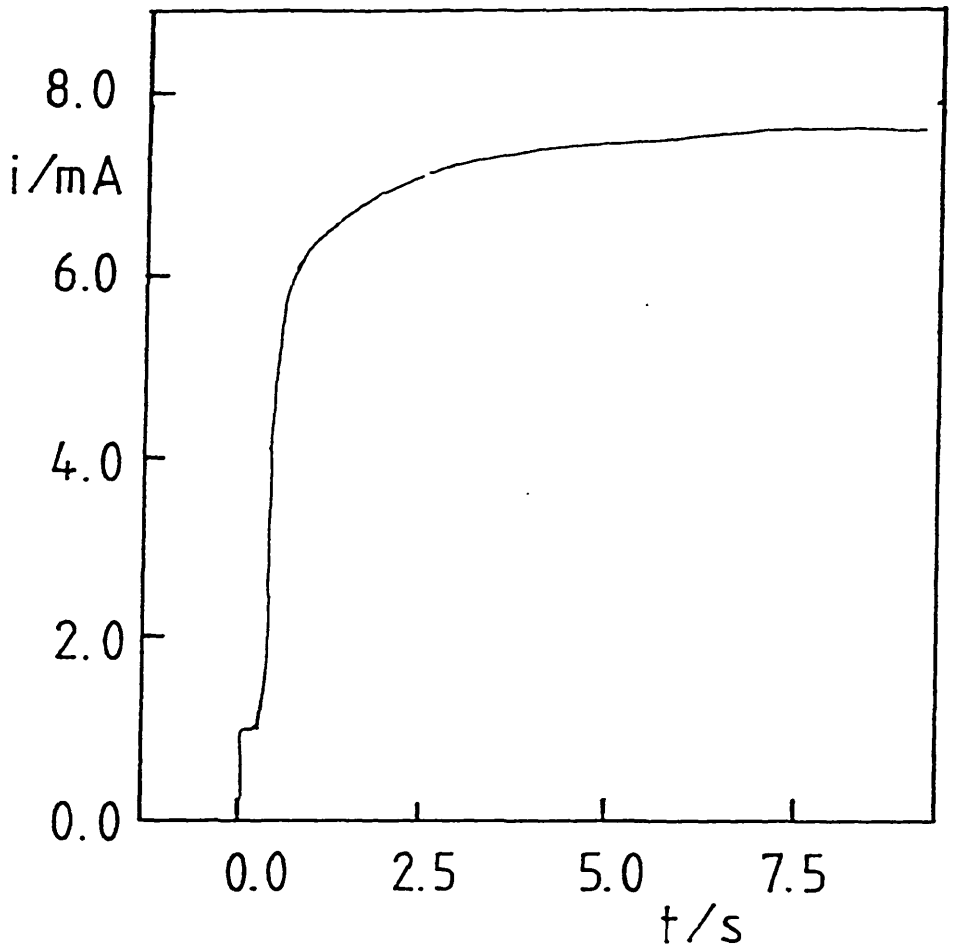


Figure 4.9b Cyclic voltammogram of the resulting coat ($v = 50\ mVs^{-1}$).

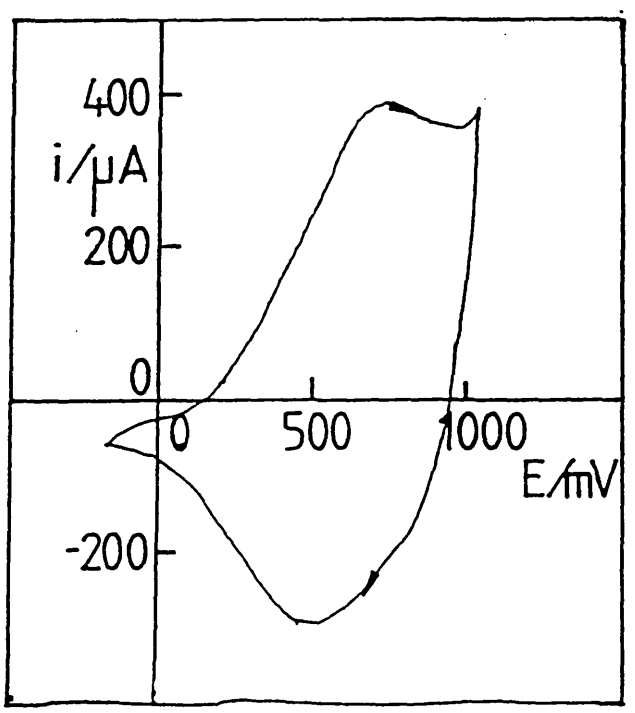
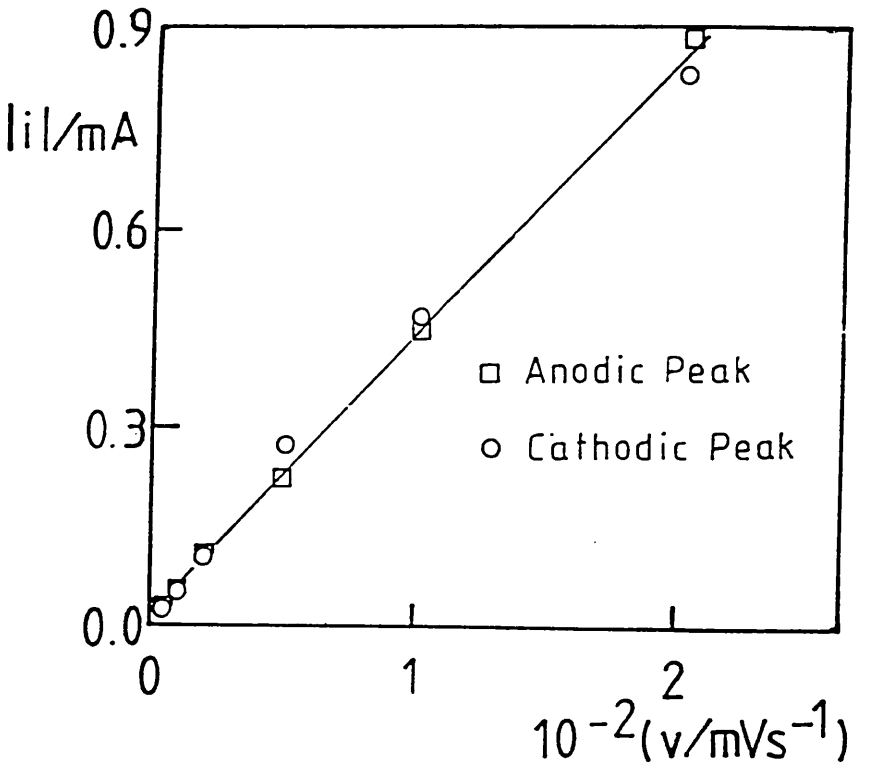


Figure 4.10 Variation of the observed peak currents for oxidation and reduction of the TP/TPAA polymer with potential sweep rate.



the charge passed in forming the film. This is a greater percentage than for the coats formed using pure TP (150 mM) solution.

This experiment was repeated with varying concentrations of TPAA. The data is summarised in Table 4.2. The observed oxidation currents increase when the concentration of TPAA is raised. This is further evidence for the oxidation of both monomeric species. In all cases, the observed CV peak currents were proportional to sweep rate. The fraction of electrooxidation charge that appears in the CV peak also increases with added TPAA. This can be attributed to the decreased importance of the radical cation side reactions. The rate of coupling at the surface will depend upon the square of the radical cation concentration. All other radical reaction rates are linearly dependent upon $[R^{+\cdot}]$. Therefore increasing the bulk monomer concentration will enhance polymer formation. However, the concentration of TP has remained constant- it is the concentration of TPAA which has been increased. Hence, this data is indicative of copolymerisation of TP and TPAA.

4.3.3.1 Evidence For The Formation Of TP/TPAA Copolymers

Figure 4.11a shows an FTIR spectrum of the copolymer coated onto a platinum flag. The major peaks correspond to those of the TPAA monomer[106] (Figure 4.11b). However, these are somewhat broadened in the polymer. These peaks are not present in a similar spectrum of pure polythiophene (Figure 4.12).

Table 4.2 Summary Of Data For The Electrochemical Copolymerisation Of TP And TPAA

[TP] /mM	[TPAA] /mM	Mean Oxidation Current/mA	Total Oxidation Charge/mC (A)	Polymer CV Peak Charge /mC (B)	B/A (%)
150	-	4.1	140	5.5±0.5	4.0±0.4
150	75	7.0	105	6.1±0.5	6.0±0.5
150	100	8.1	120	7.5±0.5	6.3±0.4
150	250	8.5	160	10.0±0.6	6.3±0.4

Figure 4.11a FTIR spectrum of a TP/TPAA copolymer. The peak positions are given in wavenumbers.

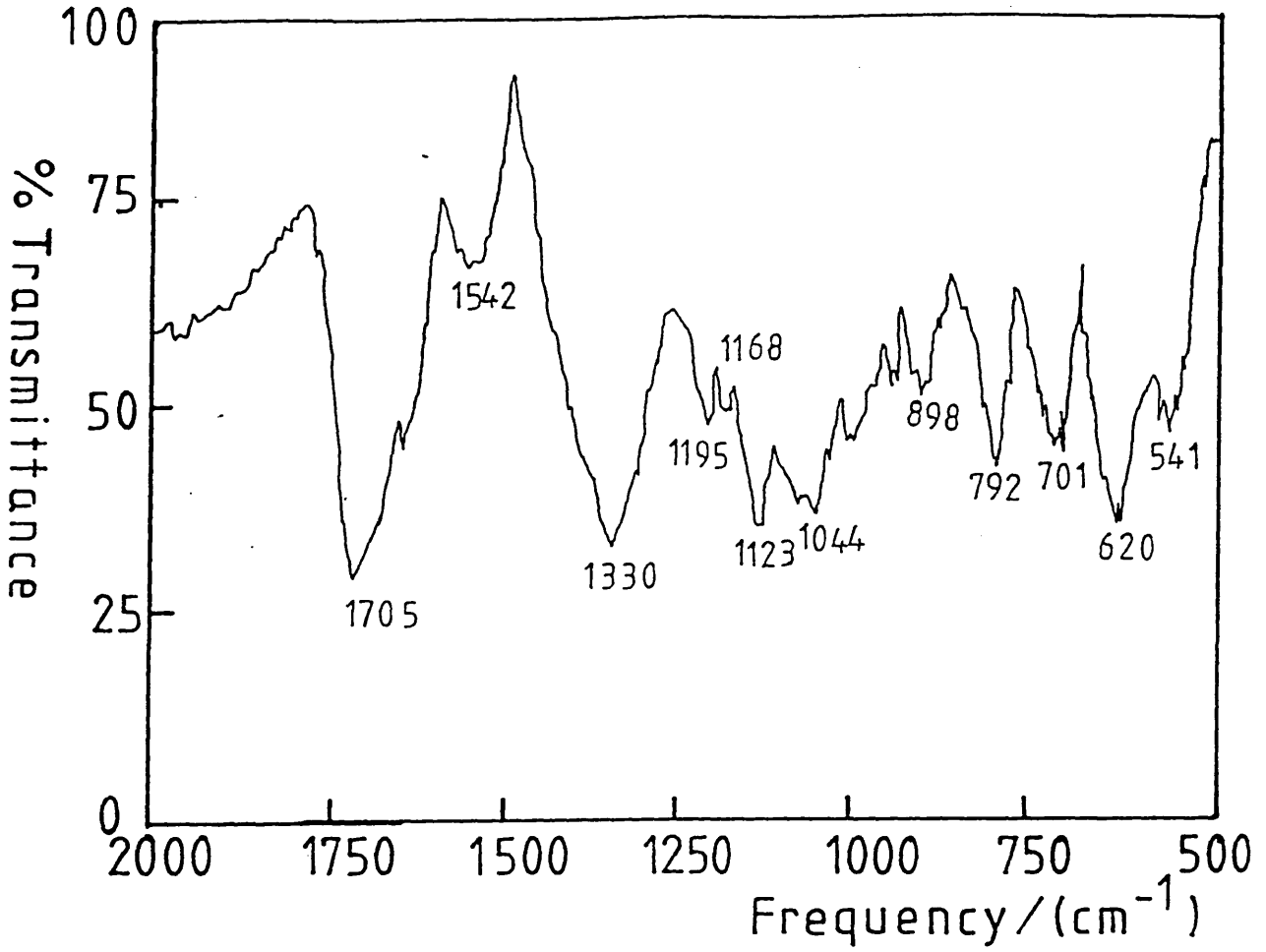
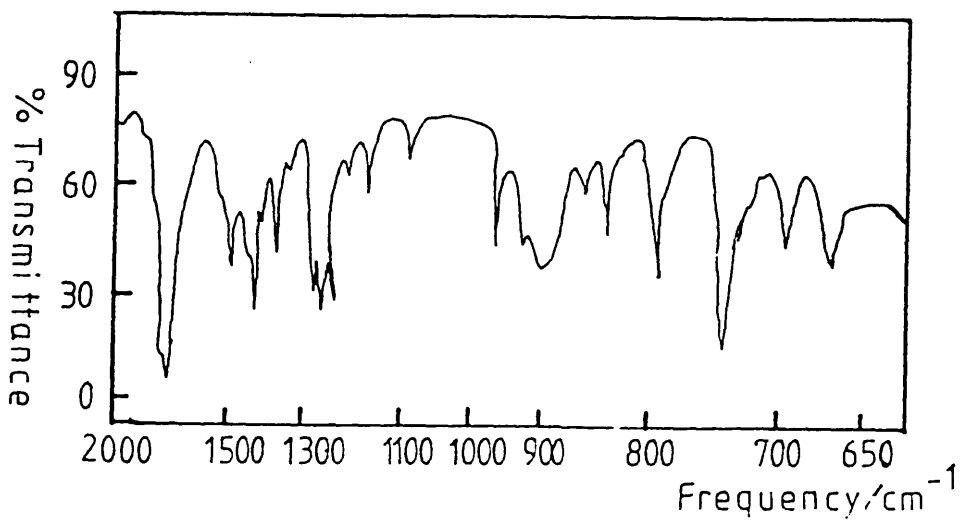
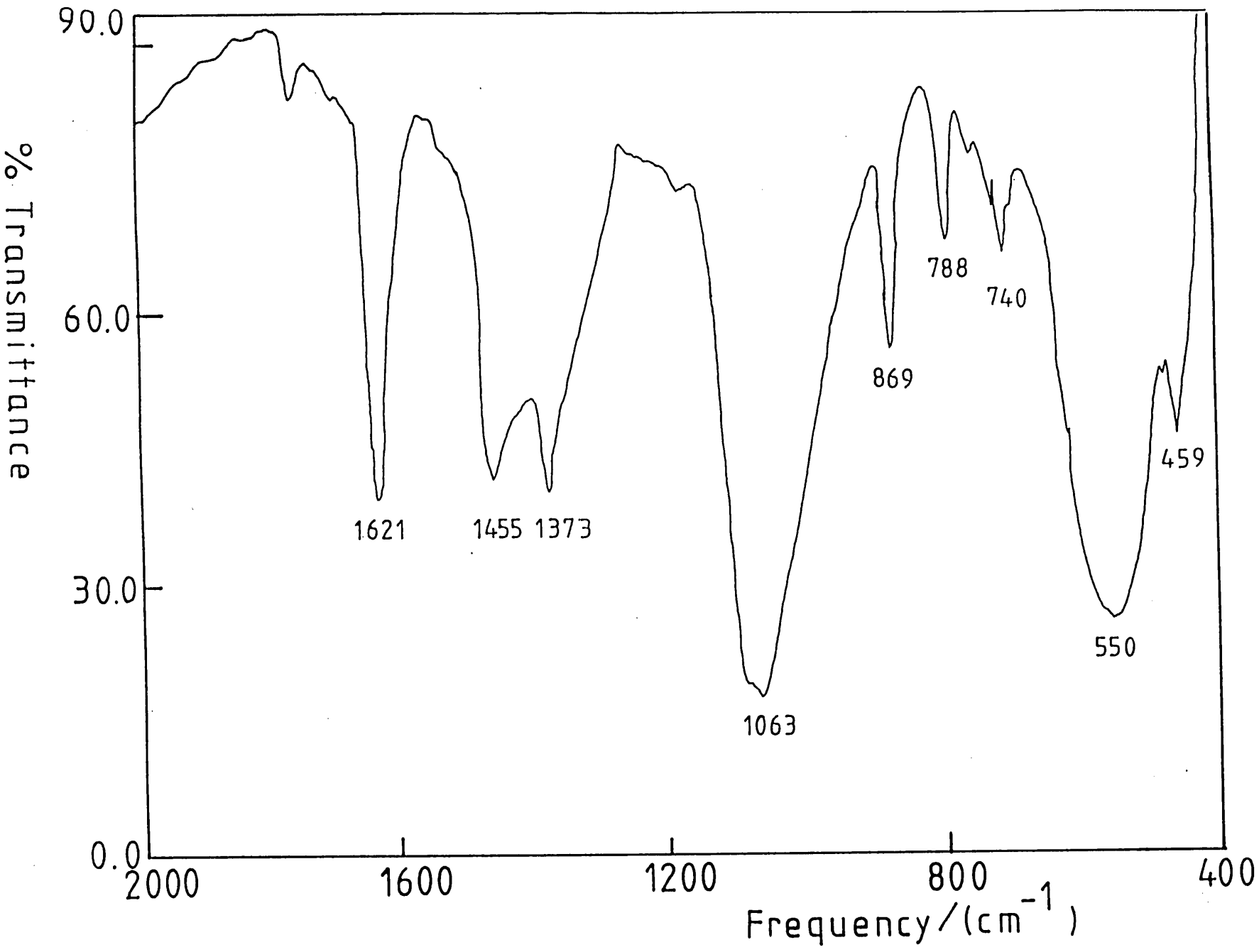


Figure 4.11b IR spectrum of TPAA monomer.




90.0
60.0
30.0
0.0
% Transmittance
1621
1455
1373
1063
869
788
740
550
459
2000
1600
1200
800
400
Frequency/(cm-1)

A typical ESCA spectrum of a polythiophene coated flag electrode is given in Figure 4.13. This can be contrasted with the spectra of TP/TPAA copolymers. Figures 4.14a and 4.14b show data for films prepared using solution concentrations of 300mM TP/75mM TPAA and 300mM TP/150mM TPAA respectively. The relevant peak assignments and observed core binding energies for the thiophene spectrum are given in Table 4.3. These are assigned by comparison with literature values[107,108]. Small deviations of the observed binding energies from these values can be attributed to surface charging of the sample. It is clear that for the copolymer spectra, an extra peak is present at 289.2eV. This is assigned to electrons from the C(1s) orbital of the carbonyl substituent of TPAA. The observed chemical shift[107] of this C(1s) peak when compared with that attributed to atoms from the polymer backbone is due to the greater electronegativity of the carbonyl carbon. The intensity of this peak can be seen to increase on raising the TPAA:TP concentration ratio.

Quantitative calculations of this ratio for the polymer were attempted by integration of the two C(1s) peaks. The results presented in Figure 4.14b indicate that one carbonyl group is present for every eleven other carbons. This gives a TPAA/TP ratio of 2:3 in the polymer. The corresponding ratio in the coating solution was 1:2. However, observed peak ratios will be sensitive to the presence of adventitious carbon on the surface of the sample. Further quantitative experiments to correlate the

Figure 4.13 ESCA spectrum of a polythiophene coated platinum flag.

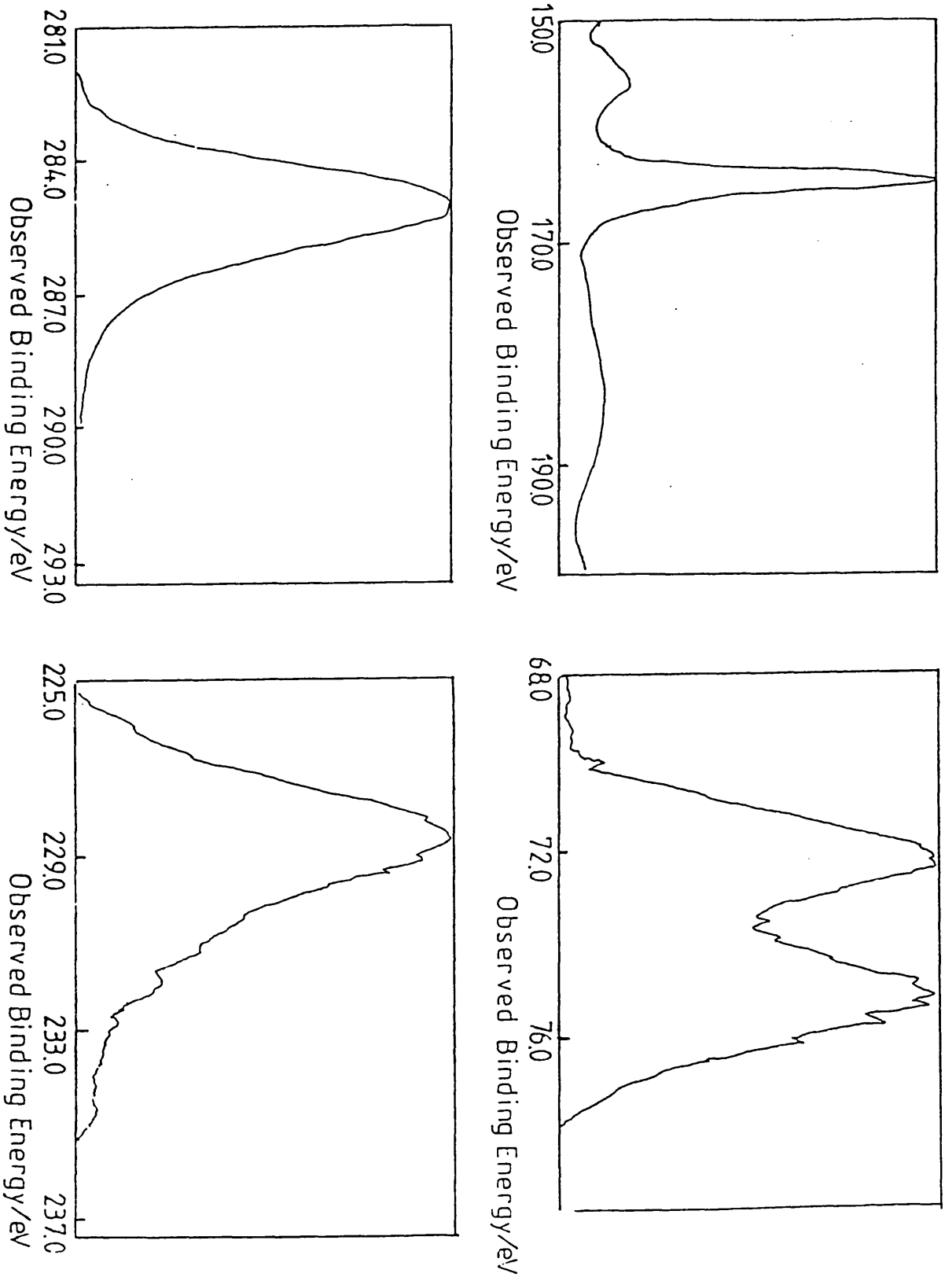


Figure 4.14a ESCA spectrum of a coated platinum flag prepared by polymerising a solution of 300 mM TP/75 mM TPAA.

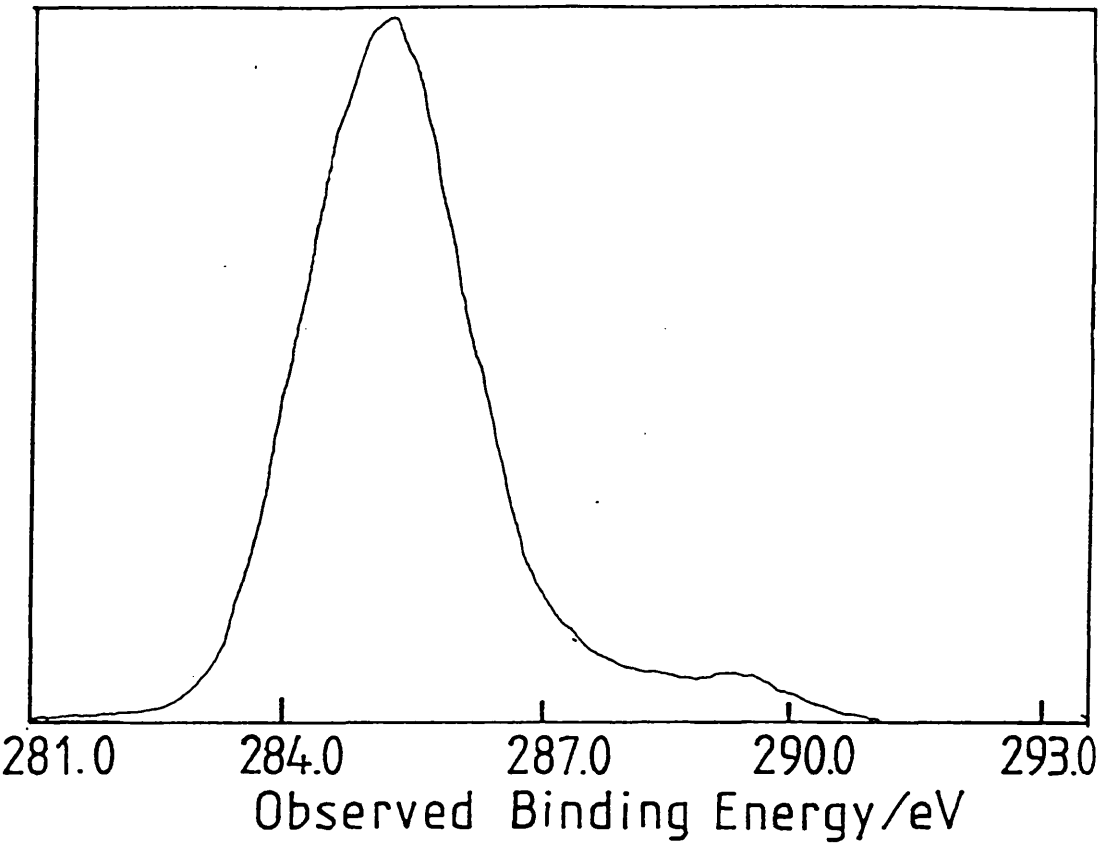


Figure 4.14b ESCA spectrum of a coated platinum flag prepared by polymerising a solution of 300 mM TP/150 mM TPAA.

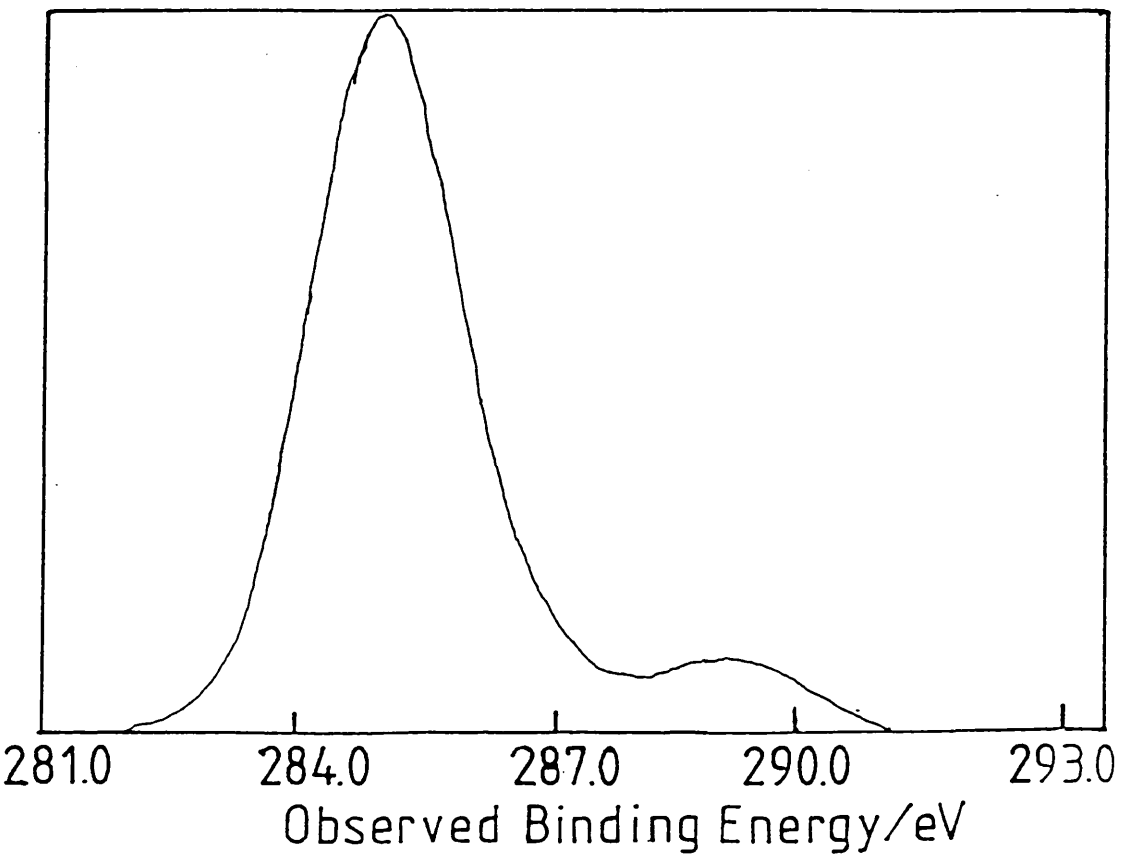


Table 4.3 ESCA Data For Thiophene

Apparent Binding Energy (±0.1)/eV	Core Electron Assignment[107,108]
72.3	$Pt(4f_{3/2})$
75.4	$Pt(4f_{5/2})$
164.7	$S(2p_{1/2}), S(2p_{3/2})$
229.0	$S(2s_{1/2})$
285.2	$C(1s_{1/2})$

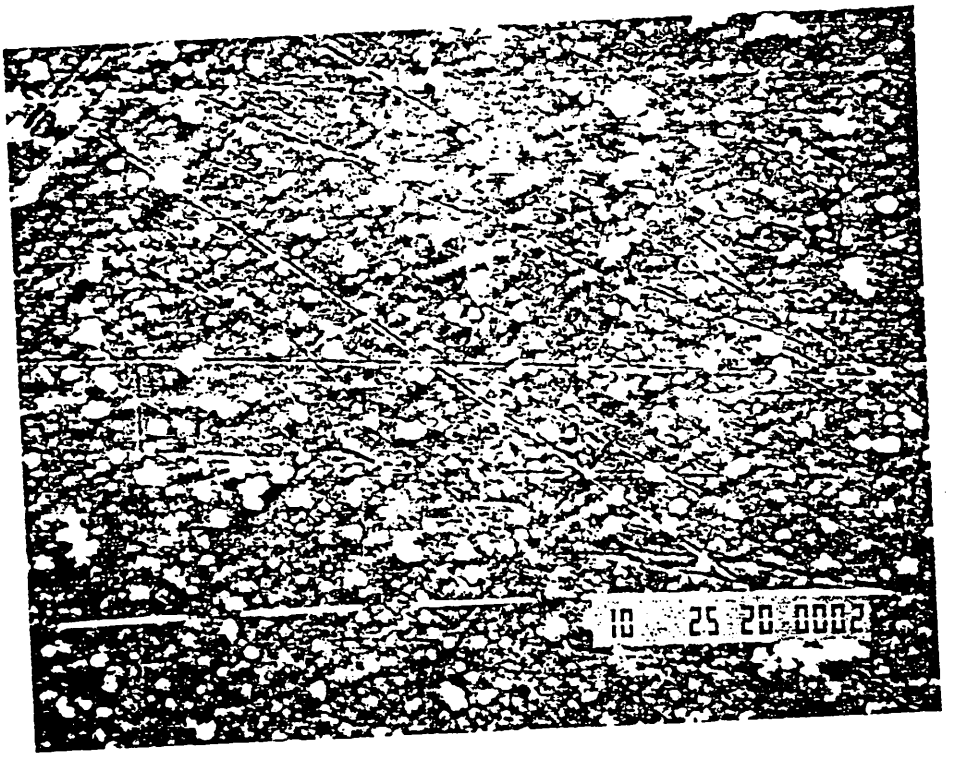
polymer composition with the solution concentrations of TP and TPAA await the development of an electrode with reproducible solution hydrodynamics that can be examined by the ESCA technique. Flag electrodes do not have fixed TP and TPAA concentrations at the electrode surface throughout polymerisation. This is a necessity for reproducible copolymerisation at any electrode.

Another important piece of evidence for copolymer formation is the observed solubility. Thick films (~ 0.1-1 mm) of TP and TP/TPAA polymers were prepared and peeled from the electrode surface. The polythiophene coats were found to be insoluble in a wide variety of organic solvents. The copolymer films, though, dissolved slowly in dimethylformamide. This is due to the increased polarity of the copolymer structure, brought about by the addition of polar acetate side groups. Solution IR experiments confirmed the presence of dissolved polymer.

4.3.3.2 The Structure Of The TP/TPAA Copolymers

The structure of these films was investigated, using SEM. Figure 4.15 shows a typical SEM photograph of a TP (300 mM)/TPAA (200 mM) copolymer coated flag electrode. The coat can be seen to be a homogeneous, densely packed polymer on the micron scale. Photographs of polythiophene coated flags indicate a similar morphology.

Figure 4.15 Typical SEM photograph of a TP/TPAA copolymer coated electrode.



4.3.4 Formation Of Thiophene And 3-Thiophenecarboxylic Acid Copolymers

Copolymerisation experiments were also performed using mixtures of TP and 3-thiophenecarboxylic acid (TPCA) (Table 4.1). Typical experimental results for the electrooxidation of TP/TPCA solutions at +1.6V are shown in Table 4.4. At this potential, the magnitude of the current and the percentage of oxidation charge apparent in the background electrolyte CV can be seen to be insensitive to any added TPCA. The FTIR spectra of these coats are similar to those for pure polythiophene (Figure 4.11a). Thus, it can be concluded that copolymerisation does not occur at this potential. The observed E_{pa} for TPCA was +1.84V (Table 4.1). This provides evidence that copolymerisation requires the formation of both radical cationic species.

In contrast, experiments performed at +1.85V are indicative of copolymerisation (Table 4.4). Similar electrooxidation behaviour was observed for TP/TPCA as for TP/TPAA solutions. There were corresponding increases in the oxidation current and the fraction of charge observed when performing cyclic voltammetry on the coat in background electrolyte solution. This is again indicative that copolymerisation has occured. Figure 4.16 shows CV data for a TP/TPCA copolymer. The oxidation peak is clearly broader than in the case of polythiophene or TP/TPAA copolymers. The reduction peak also appears slightly broader. The E_{pa} values for TP and TPCA (Table 4.1) are separated by of the order of 250 mV. Therefore, the E_D of TP and TPCA would be expected

Table 4.4 Summary Of Data For The Electrochemical Polymerisation Of TP and TPCA

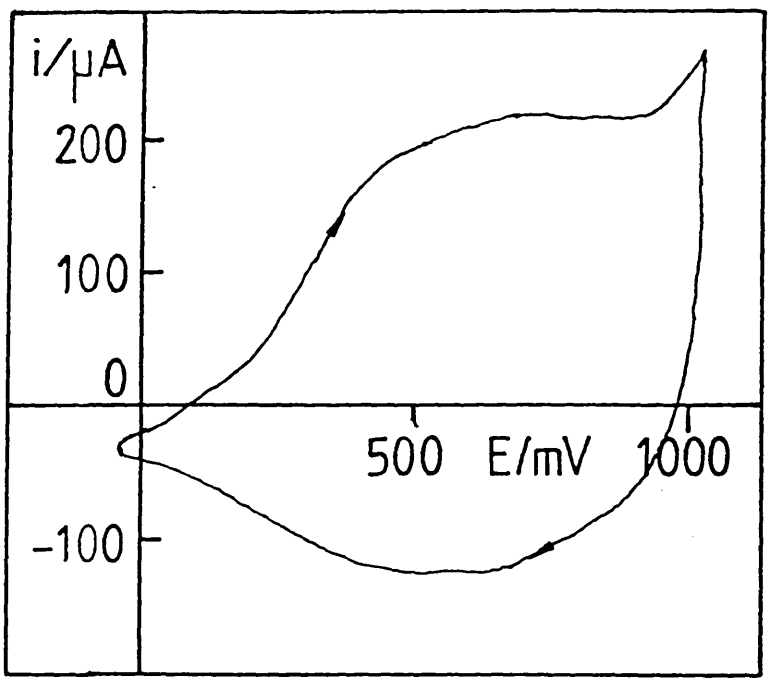
(a) at +1.6 V

[TP] /mM	[TPCA] /mM	Mean Oxidation Current/mA	Total Oxidation Charge/mC (A)	Polymer CV Peak Charge /mC (B)	B/A (%)
150	-	3.0	75	2.5±0.2	3.0±0.3
150	100	3.0	110	3.5±0.3	3.1±0.3
150	200	2.9	90	2.5±0.2	2.6±0.3

(b) at +1.85 V

[TP] /mM	[TPCA] /mM	Mean Oxidation Current/mA	Total Oxidation Charge/mC (A)	Polymer CV Peak Charge /mC (B)	B/A (%)
300	-	4.3	160	9.0±0.5	5.6±0.5
150	150	4.9	113	6.5±0.4	5.9±0.5
150	300	4.3	111	4.3±0.3	6.6±0.5

Figure 4.16 Cyclic voltammogram of a TP/TPCA copolymer produced by oxidation of a 300 mM TP/200 mM TPCA solution at 1.85 V (v = 10 mV s^{-1}).



to have a similar disparity (section 4.1.2). This would explain the wider range over which copolymers of these substances oxidise and reduce when compared with TP and TP/TPAA copolymers, for which the E_{pa} of the monomers is similar.

4.3.4.1 Evidence For The Formation Of TP/TPCA Copolymers

FTIR spectroscopy on platinum flags coated with TP/TPCA copolymer (Figure 4.17) show a broad peak at 1650-1610 cm^{-1}. This is assigned as being due to the stretching mode of a carbonyl group. However, solution spectra of TPCA monomer in chloroform show the carbonyl stretch to be at 1692 cm^{-1}. This shift in frequency may be due to partial delocalisation of the C=O bond into the π-system of the polymer backbone. This is shown schematically in Figure 4.18. The C-O bond order appears to be greater than one-and-a-half, as the asymmetric stretch of carboxylate anions occurs between 1550 cm^{-1} and 1610 cm^{-1}[109].

As with TP/TPAA copolymers, thick films have been shown to be soluble in DMF, producing a brown solution. Again, solution IR indicates the presence of dissolved copolymer.

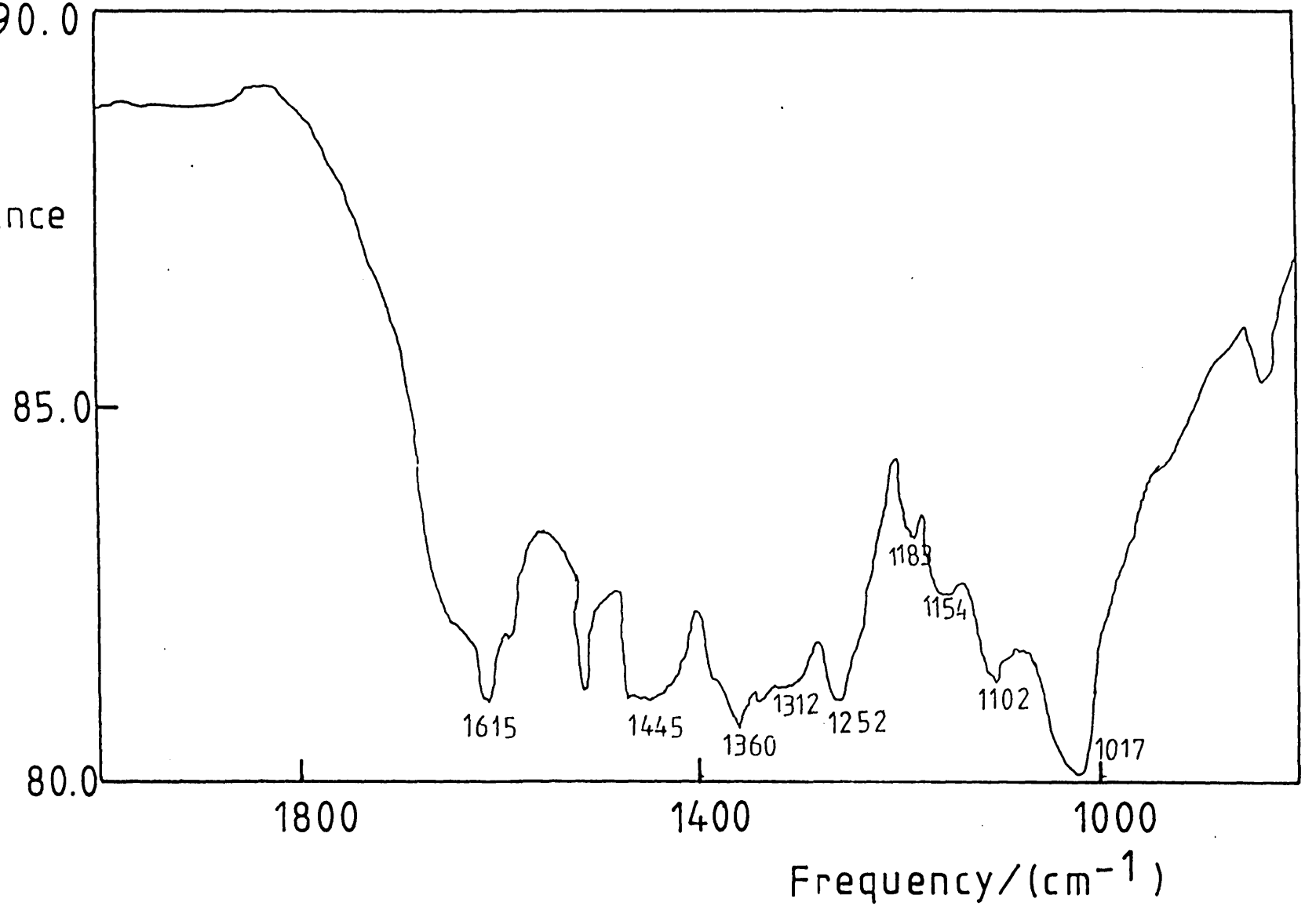
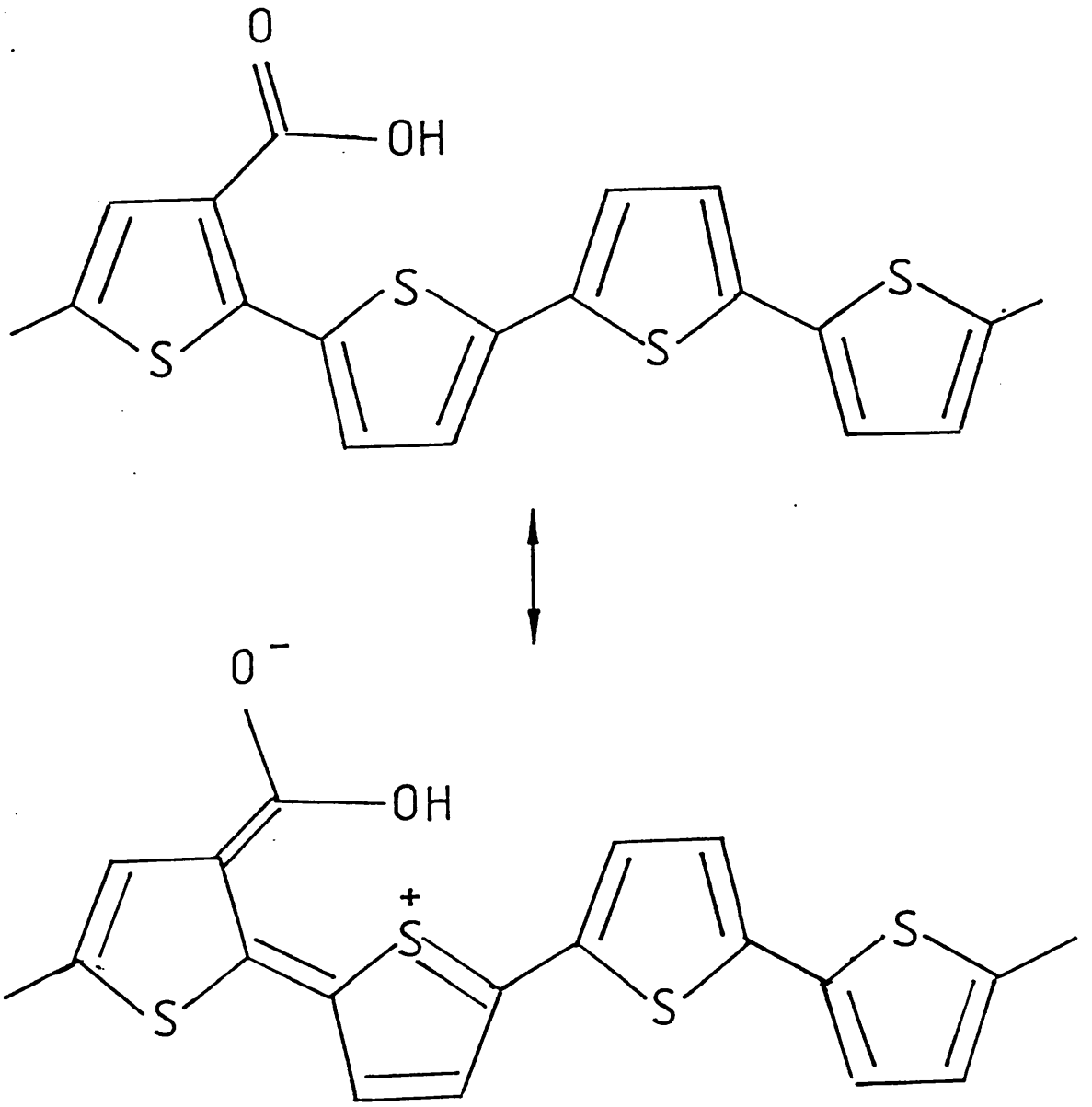


Figure 4.17 FTIR spectrum of a TP/TPCA copolymer.

Figure 4.18 The canonical forms of a TP/TPCA copolymer.



4.4 Incorporation Of Lead(II) Into TP/TPAA And TP/TPCA Copolymers

Lead(II) incorporation was achieved by soaking oxidised coats in aqueous $Pb(NO_3)_2$ solutions at neutral pH. The solubility of this salt is high[110]. The pK_a of acetic acid is 4.74[111] and that of TPAA would be expected to be similar. TPCA will probably have a lower pK_a value, due to resonance stabilisation of the resulting carboxylate anion. Hence, at this pH, the carboxylic acid groups would be expected to be present as carboxylate anion. Therefore it is expected that incorporation would take place according to the reaction

$$2\ P\text{-}CO_2^- + Pb^{2+} \longrightarrow (P\text{-}CO_2)_2Pb \qquad ....(4.1)$$

where P is the polythiophene backbone.

4.4.1 TP/TPAA Copolymers

Figure 4.19a shows the FTIR spectrum of a copolymer produced from 300mM TP/200mM TPAA solution after soaking for six hours in the lead solution. The electrode was rinsed in water and acetonitrile prior to spectroscopic analysis. Comparison of this spectrum with that for the copolymer prior to soaking (Figure 4.11a) shows significant change. The peak at 1705 cm^{-1}, assigned to the carbonyl stretch of the acetic acid side group, has completely disappeared. Two major new peaks at 1526 cm^{-1} and 1372 cm^{-1} can clearly be seen. The spectrum of lead(II) acetate trihydrate[112] (Figure 4.19b) has similar peaks. Therefore, complete conversion of the acetic acid groups to lead(II) acetate has occured.

Figure 4.19a FTIR spectrum of copolymer produced from a 300mM TP/200mM TPAA solution. The coat was soaked in saturated aqueous lead(II) nitrate solution for six hours.

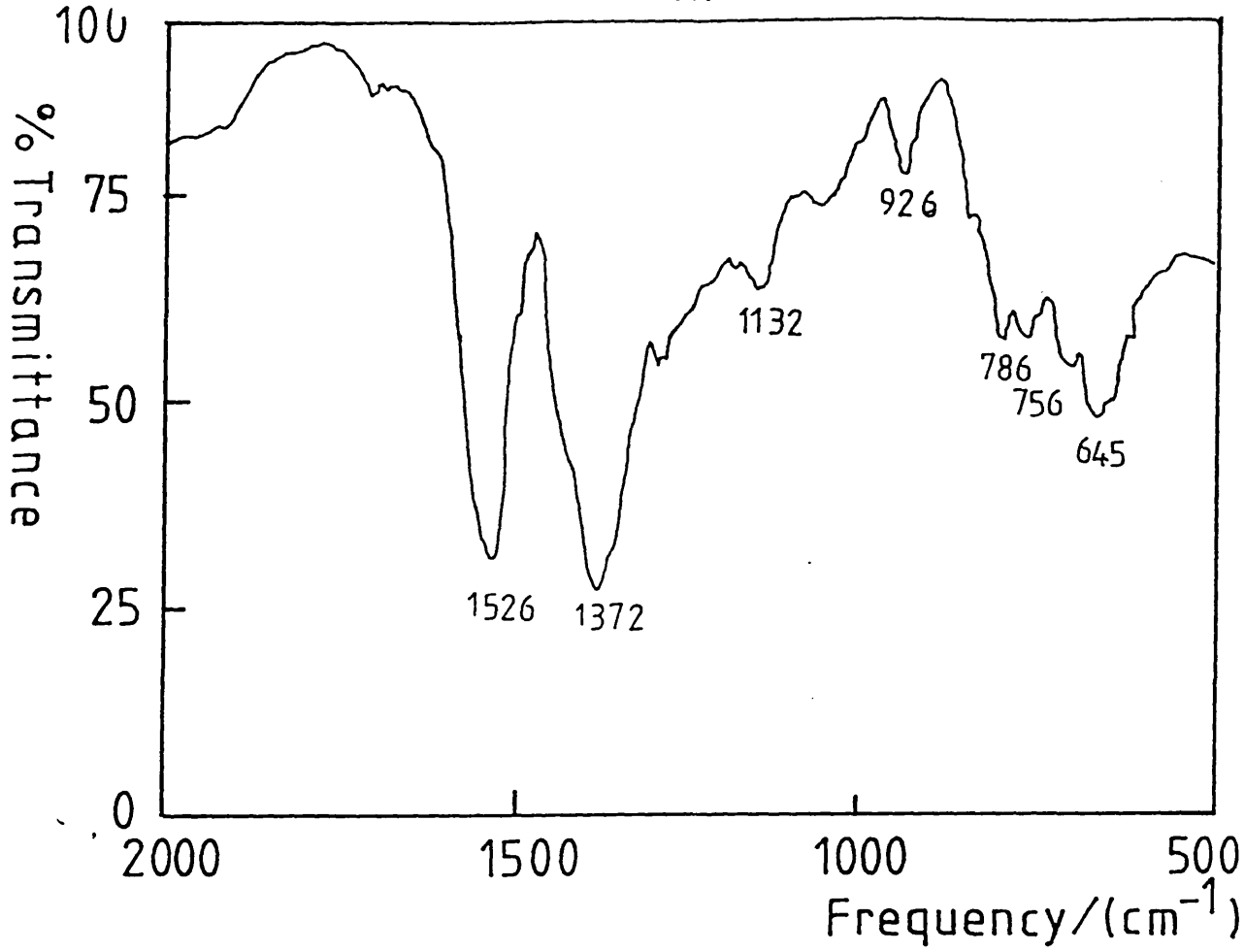
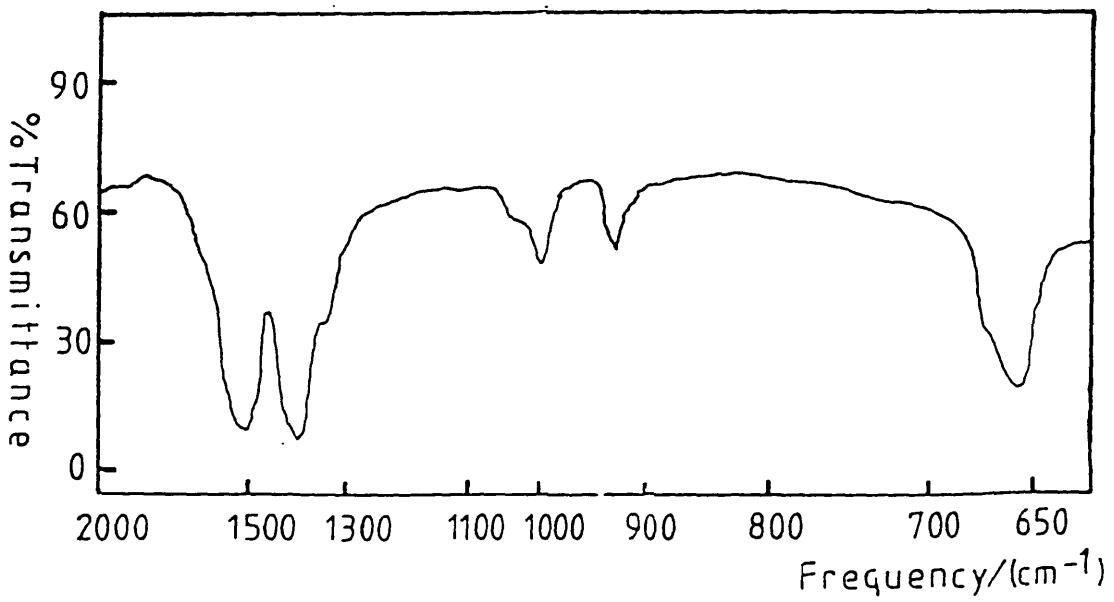
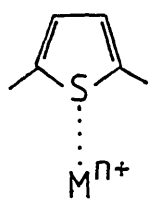


Figure 4.19b IR spectrum of lead(II) acetate.



ESCA spectra of these coats show a doublet at 415.1±0.1 eV and 439.0±0.1 eV, due to the $Pb(4d_{5/2})$ and $Pb(4d_{3/2})$ core electrons. The relative intensity of these and the C(1s) peaks, after correction for the different relative electron photoionisation cross-sections[113], indicates a ratio of lead:carbon of 1:2 in the film. This is a far greater incorporation of lead than is required for the complete derivatisation of TPAA, according to equation (4.1).

Previous work[114,115] on chemically synthesised polythiophenes using butyllithium and Grignard reagents found significant retention of magnesium and transition metal ions in the polymer. This was attributed to the formation of a cation-ring sulphur complex



where M^{n+} is the cation. It is here postulated that the excess of lead species in the coat over that required to derivatise the acetate groups is due to the formation of just such a complex. The stretching frequency of this type of complex would be expected to be low (<800 cm^{-1}) and confident identification of this absorption in the FTIR spectrum would be difficult. However, it cannot be ruled out from these results that the excess lead is due to the presence of excess $Pb(NO_3)_2$ which has not been removed by

the rinsing procedure. Further work is required, monitoring the intensity of the peaks due to the N core electrons, to resolve the relative contributions of these species to the observed spectrum.

SEM pictures of the film show little change in coat morphology on lead incorporation (Figure 4.20).

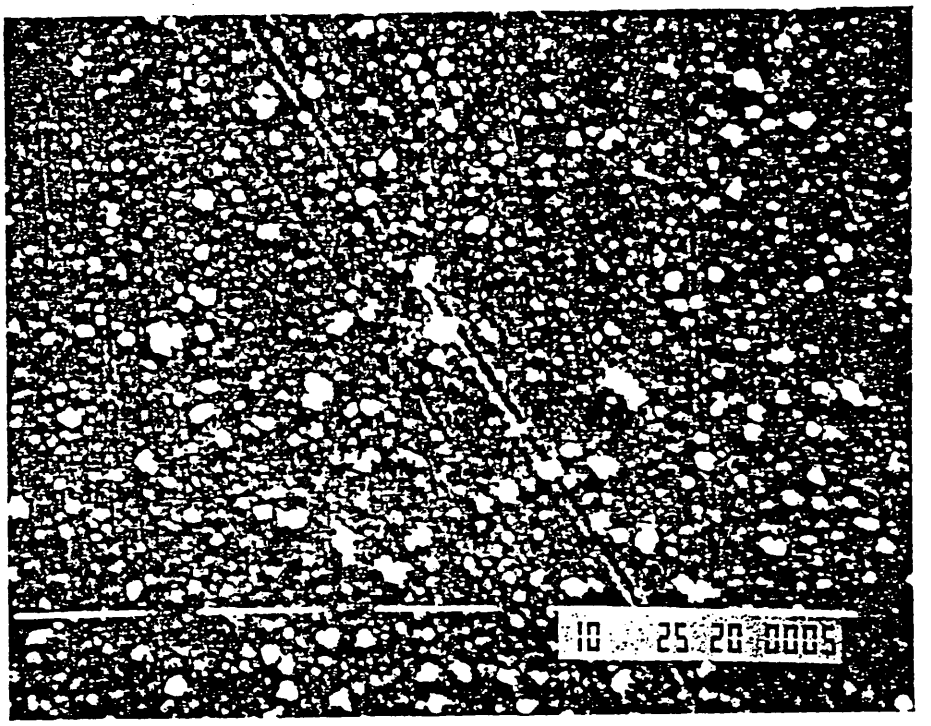
4.4.2 The Leading Of TP/TPCA Copolymers

In contrast to TP/TPAA, Figure 4.21 shows the FTIR spectrum of a TP/TPCA copolymer after soaking in aqueous lead nitrate solution for ten hours. There is little change in peak intensities or frequencies with respect to the original TP/TPCA copolymer. This indicates negligible derivatisation of the carboxylic acid group.

This can be attributed to the effect of delocalisation of the anionic carboxylate charge into the π-system of the polymer. This will stabilise the free carboxylate species. Thus, the equilibrium position of equation (4.1) will favour the reactants in this case.

Hence, it seems that the precursor to the catalytic lead(IV) carboxylate group cannot be formed for TP/TPCA copolymers.

Figure 4.20 Typical SEM photograph of a leaded TP/TPAA copolymer coated flag.



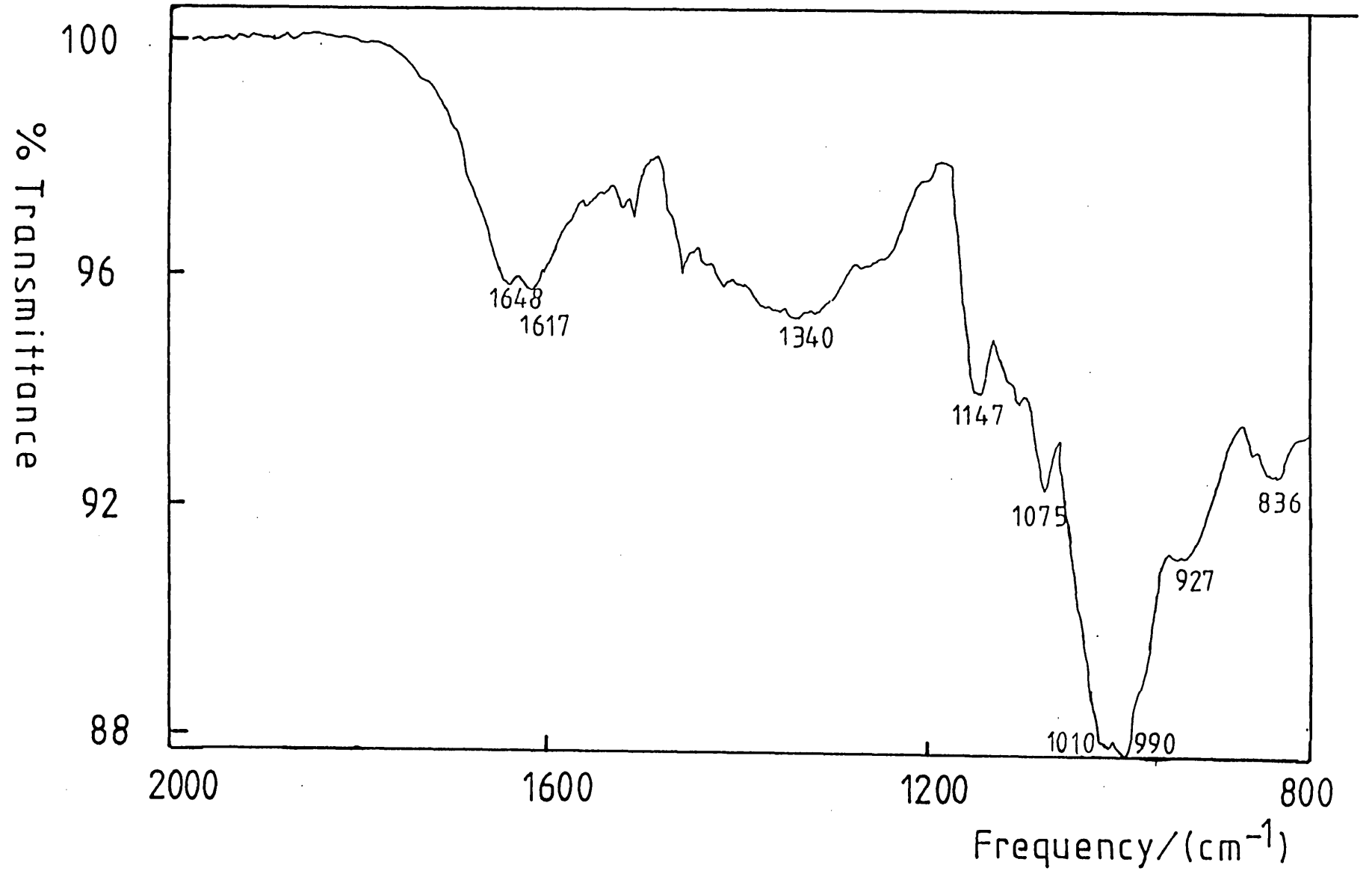


Figure 4.21 FTIR spectrum of a TP/TPCA copolymer after soaking in saturated lead(II) nitrate solution for ten hours.

4.5 Electrochemistry Of Leaded TP/TPAA Copolymers

Experiments to investigate the electrochemistry of the leaded TP/TPAA copolymers were generally performed in acetonitrile solutions. Lead(II) acetate is insoluble in this medium and so the dissociation of the $Pb(TPAA)_2$ complex is suppressed.

4.5.1 Cyclic Voltammetry

Cyclic voltammetric experiments were performed to observe the oxidation and reduction characteristics of these films (Figure 4.22). Lead incorporation results in a shift of the polymer oxidation and reduction reactions to more oxidising potential. This is due to the increase in electronegativity of derivatised polythiophene when it is co-ordinated to lead(II). The peak currents and total charge passed in these voltammograms increased initially with increasing sweep number. Also, an oxidation peak develops and the potential at which this peak occurs decreases. However after 20-30 cycles, no further change was observed. The currents were five to ten times less than those of an unleaded film. As in the case of unleaded polythiophene coats, further oxidation was observed at potentials greater than +1.3V, leading to a loss in coat electroactivity.

Figure 4.23 shows CV data for a TP coat after incorporating lead in an identical manner. Similar behaviour is observed. Again, a ten-fold decrease in the polymer oxidation/reduction peaks was observed, comparable to that for the leaded TP/TPAA copolymer. Similar CV data was

Figure 4.22 Cyclic voltammogram of a leaded TP/TPAA coat (v =50 mV s^{-1}) (a) first cycle (b) after 5 cycles (c) after 30-40 cycles.

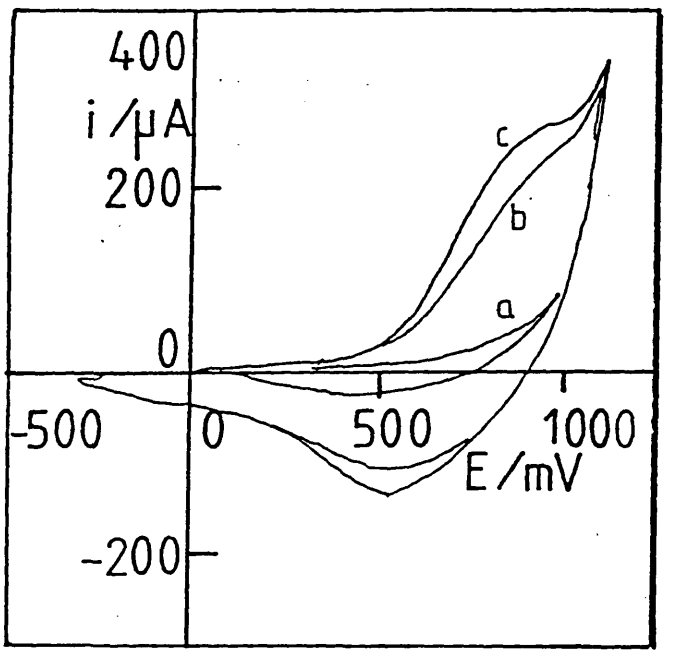
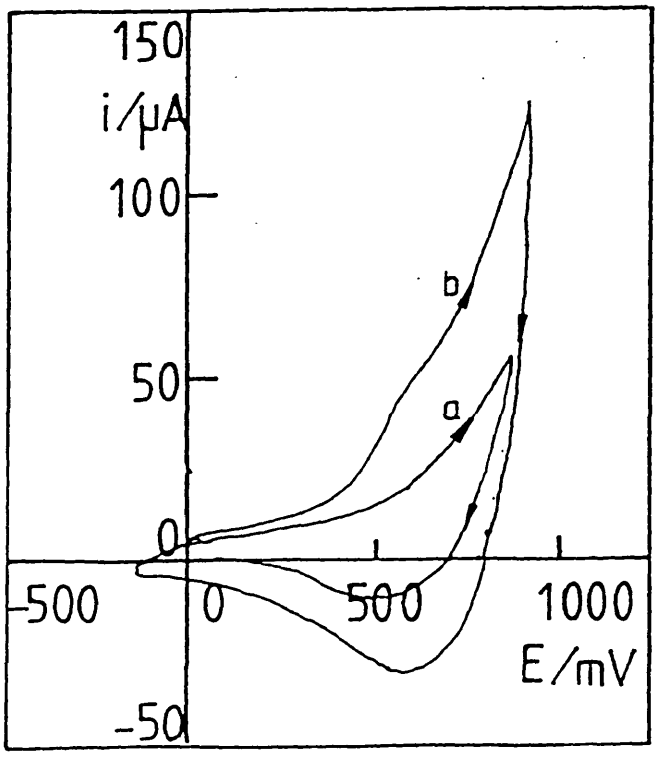


Figure 4.23 Cyclic voltammogram of a leaded TP coat (v = 50 mV s^{-1}) (a) first cycle (b) after 30-40 cycles. This coat was soaked in aqueous lead(II) nitrate for six hours.



obtained from TP/TPAA coats soaked in $Ca(NO_3)_2$ and $NaNO_3$ solutions. In contrast, prolonged soaking of TP/TPAA coats in distilled water had no effect on the observed oxidation and reduction reactions in background solution.

Thus, it is evident that the change in coat conductivity is due to the incorporation of ions into the coat, but not to those co-ordinated to the acetate groups. The changes can be attributed to the formation of the cation-ring sulphur complex postulated earlier (section 4.4.1)[115]. This would be expected to have a marked effect on the coat conductivity, as the ring sulphur forms part of the conjugated π-system of the polymer. The formation of such a complex may also result in a drop in conductivity by the loss of ring coplanarity[116].

4.5.2 Redox Reactions

4.5.2.1 The Oxidation Of Quinol

Comparative studies were also carried out on the oxidation of quinol(5 mM) solutions at leaded and unleaded TP/TPAA coated RDE's. In acetonitrile solutions, quinol undergoes a two-electron oxidation to p-benzoquinone[117]. Figure 4.24a and 4.24b presents Levich and modified Tafel plots (section 2.1) for the oxidation of quinol at TP/TPAA films. In contrast, reaction at leaded copolymer electrodes does not produce a straight Levich plot. A typical Koutecky-Levich plot for these results is given in Figure 4.24c. Data from these plots for clean platinum and TP/TPAA and leaded TP/TPAA copolymer films coated onto Pt are collected in Table 4.5.

Figure 4.24a Levich plot for the oxidation of quinol(5 mM) at a TP/TPAA copolymer film.

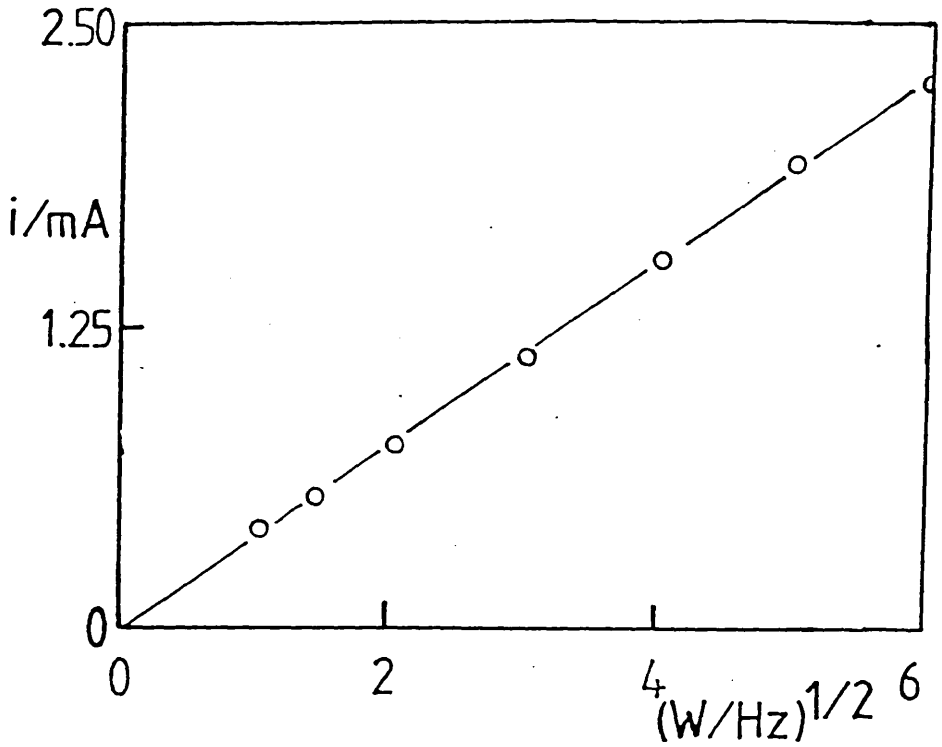


Figure 4.24b Tafel plot for the same data.

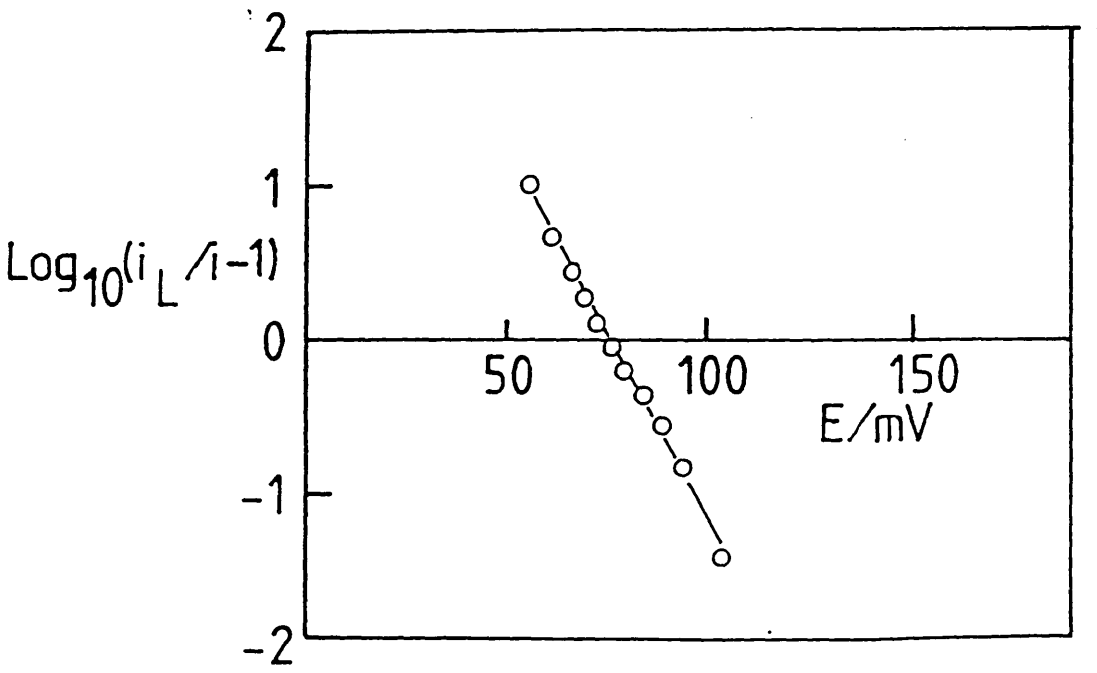


Figure 4.24c Koutecky-Levich plot for the oxidation of quinol (5 mM) at a leaded TP/TPAA copolyme film.

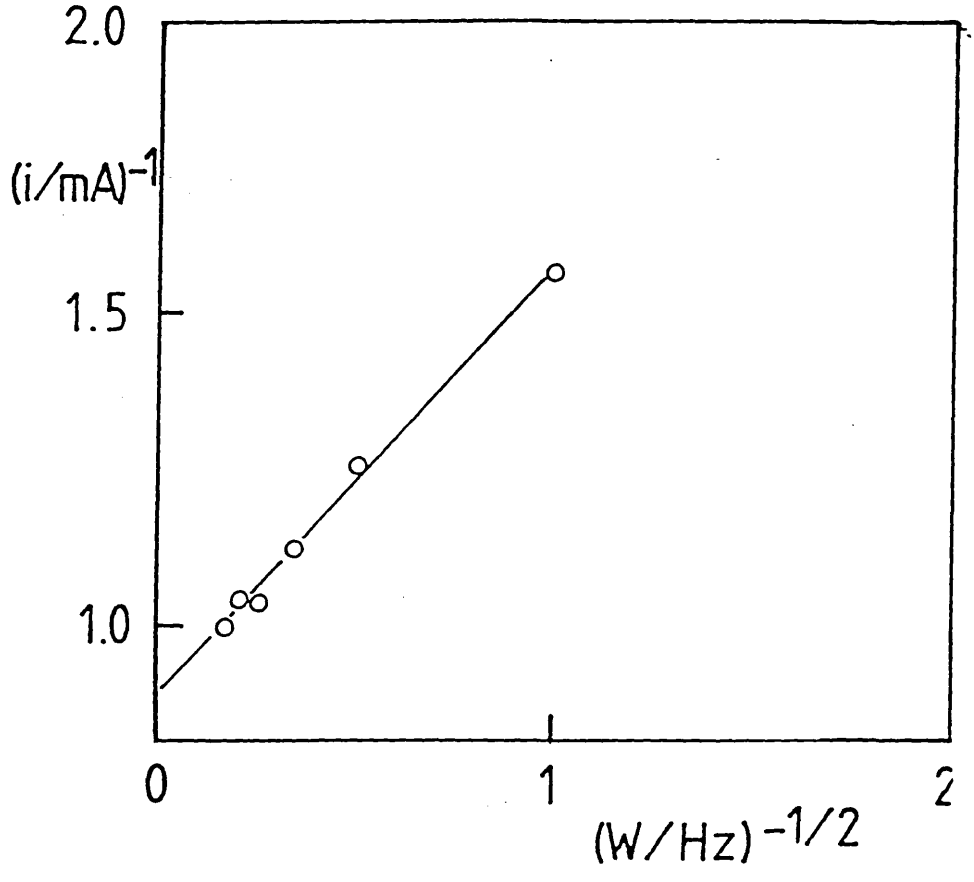


Table 4.5 Kinetic Data For The Oxidation Of Quinol (5 mM)

Electrode	Pt	TP/TPAA copol.	Leaded TP/TPAA copol.
$E_{1/2}$/mV	730±5	720±5	770±5
β	0.35	0.36	0.30
Levich Plot?	No	Yes	No
Koutecky-Levich Plot?	Yes	No	Yes
$10^3.k_f$/ cm s-1	39±3	-	2.9±0.2

All these results give a calculated diffusion coefficient for quinol of 7±2 x 10^{-5} cm^2 s^{-1}.

From these results, it is clear that this reaction has similar kinetic and thermodynamic characteristics at platinum and TP/TPAA electrodes. (The large but finite value of $k_?^{'}$ observed for Pt is probably due to poisoning of the electrode by solution impurities or oxidation products.) A possible explanation for this is that direct electron transfer between quinol and the Pt electrode is occurring. However, this cannot be the case, as complete blocking of ferrocene oxidation at TP/TPAA coated platinum was observed at potentials less than +450mV, where the coat is in its insulating form. This reaction occurs at clean platinum electrodes with $E_{1/2}$ = +100mV. This indicates that substrates do not penetrate these coats to react at the platinum electrode surface. Hence, mediated electron transfer between the film and the quinol must be taking place. That this reaction gives Levich behaviour indicates the transport of electrons through the coat to be fast. Unlike bare platinum, the coated electrode is not susceptible to poisoning. Levich behaviour is always observed for this oxidation at the modified electrode- this makes the coated electrode a better substrate for quinol oxidation.

It is apparent from Table 4.5 that for the oxidation of quinol at leaded TP/TPAA films, a mass transport independent surface process is of importance. This is further evidence of a decrease in the electronic conductivity of the coat. The small shift in the $E_{1/2}$ of +50

mV with respect to TP/TPAA polymers can be attributed to the shift in the CV peak assigned to polymer oxidation i.e. the shift in the potential required to form the oxidised coat species responsible for quinol oxidation. The standard electrode potential for the lead(II) acetate-lead(IV) acetate system in acetic acid is +0.92V[97]. These are the most favourable conditions for the formation of the lead(IV) acetate species. Thus, in these polymers, the potential required to oxidise lead(II) acetate would be even greater. Therefore, it appears that reaction is between the oxidised coat and quinol and does not proceed via a lead(IV)acetate intermediate.

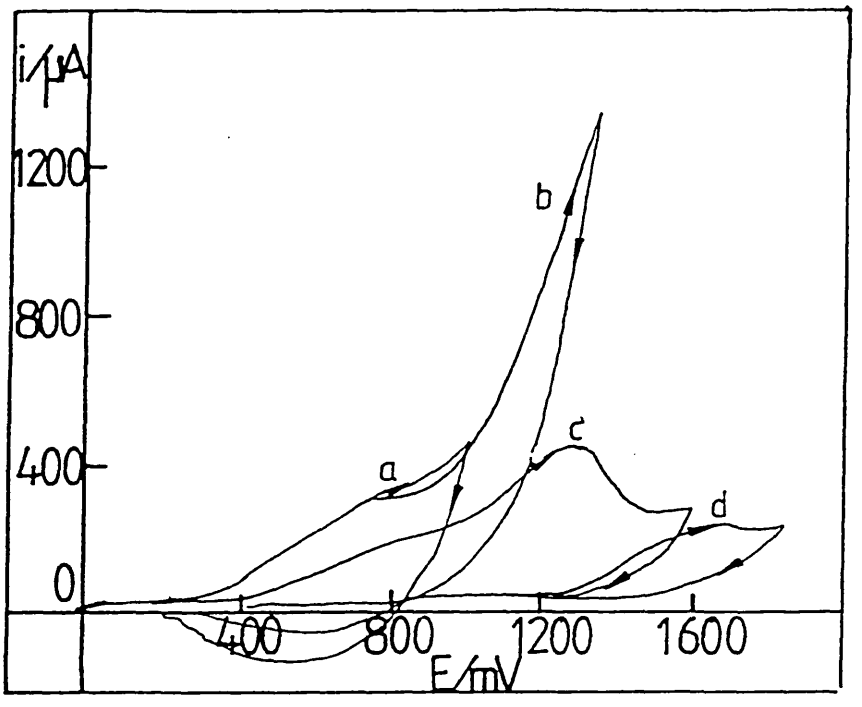
4.5.2.2 The Oxidation Of Ethylene Glycol And Other Diols

Data for the oxidation of ethlene glycol (1 M) at a leaded TP/TPAA copolymer electrode is presented in Figure 4.25(i). On sweeping the potential anodically, past the potential required to oxidise the coat, an oxidation current is observed. This decays and moves to more positive potentials on subsequent cycling, until after 30 -40 cycles, no further change in the CV is observed. Similar behaviour was observed for all diol concentrations between 55 mM and pure glycol. This behaviour was also observed on varying the lead incorporation time between six minutes and two days. Rapid decay of the oxidation peak after 1-2 cycles was seen in background acetonitrile solutions, indicating that the current is due to glycol oxidation.

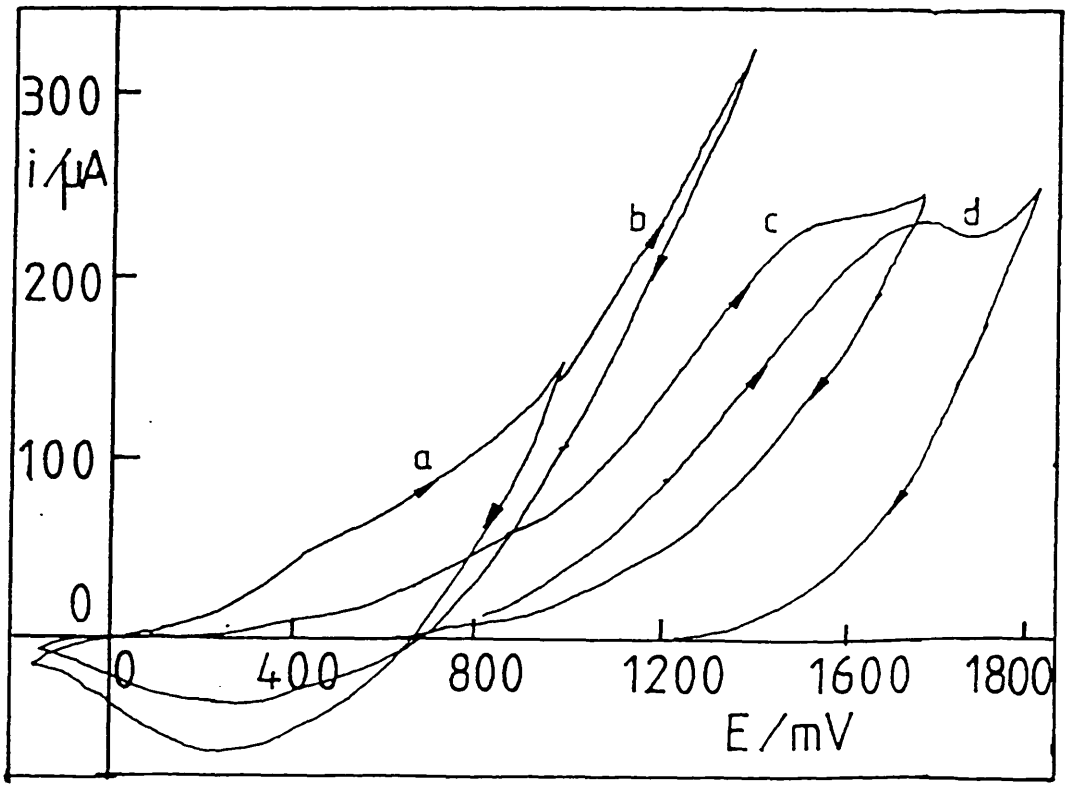
Figure 4.25(ii) shows similar data for a leaded TP coated electrode. Again, a peak was seen around +1.3V, which

Figure 4.25 Current-voltage data for the oxidation of ethylene glycol (1 M; v = 20 mV s^{-1}; W = 9 Hz; a, b, c, d refer to the first, second, third and thirtieth to fourtieth cycles)

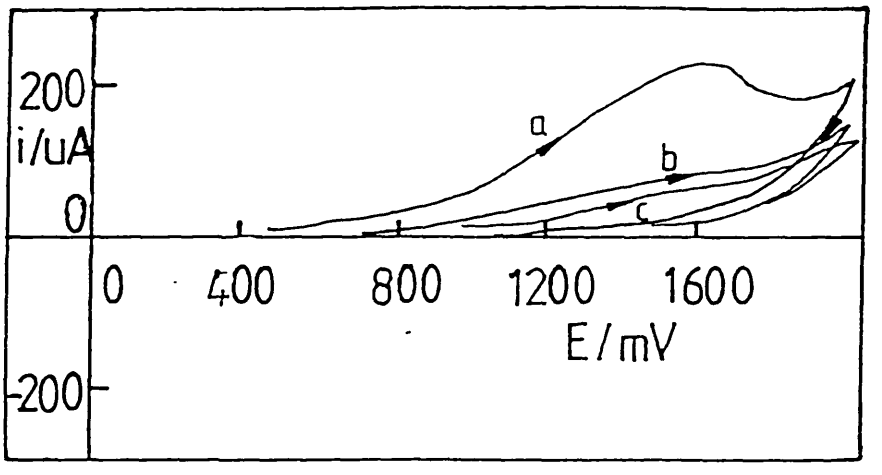
(i) at a leaded TP/TPAA electrode



(ii) at a leaded polythiophene electrode



(iii) at a platinum electrode.



decreased in size and shifted to more oxidising potentials on continued cycling. Unleaded TP coats show similar electrochemistry.

Glycol oxidation at bare platinum takes place with a peak oxidation potential of +1.6V (Figure 4.25(iii)). Complete passivation of the electrode rapidly occurs as a result of the adsorption of carbonaceous deposits[118].

These results indicate that the oxidation of glycol is due to mediated electron transfer by the polymer backbone. This dominates any oxidation via a lead(IV) acetate intermediate. The loss of oxidation current and evolution of the peak potential for oxidation is likely to be due to a decrease in coat electroactivity, as, at these potentials, complete loss of electroactivity is observed in background solutions. The destruction of the conjugated π-system will lead to a fall in the rate of electron transfer across the coat. Hence, a migrational field will be set up within the coat to speed this transport. This is indicated by the drop in oxidation current and the increase in oxidation potential. However, it is evident that oxidation at these coats is not inhibited by product absorption, as is the case for bare platinum. Thus, polythiophene coats appear better than platinum for electrooxidising glycols.

Similar behaviour was observed for the oxidation of pinacol and cyclohexane-1,2-diol.

4.6 Discussion

The incorporation of lead(II) acetate groups into a conducting polymer coat has been achieved. However, mediated electrooxidation reactions using these films do not involve lead(IV) acetate species. Rather, oxidation is mediated by the polythiophene backbone for all the redox systems studied.

At first glance, the expansion of this work to research the reaction of thallium(III) acetate groups in these coats seems desirable. Benzene substrates generally have high oxidation potentials and therefore should not be oxidised by TP coats[119]. Also, thallium(III) acetate is produced from thallium(I) acetate at lower potentials than the oxidation of lead(II) acetate to lead(IV) acetate[120]. However, this reaction involves attack by a nucleophile on a thallated aromatic molecule. Nucleophiles tend to be electron rich and easily oxidised. Therefore, it is likely that oxidation of these species by the coat will occur, rather than the oxidation of thallium(I) to thallium(III). For example, preliminary experiments show that iodide undergoes facile oxidation to iodine at these modified electrodes. A further complication is that thallium(III), if formed, would also be expected to oxidise these nucleophiles as well as the aromatic molecules present. This problem is overcome in batch synthesis by thallating the benzene prior to the addition of nucleophile- of couse, this is not possible in continuous electrocatalysis. For these reasons,

it appears that the electrocatalytic oxidation of organic molecules by the use of these two-electron inorganic ions incorporated into derivatised thiophene coats cannot be achieved.

However, the results presented in this chapter indicate that mediated electron transfer can occur via the polythiophene backbone. It has been shown that for both quinone and glycols, oxidation at these coated electrodes is not affected in the same way as platinum by electrode poisoning from product absorption. Albery and Jones[121] have recently studied the electrochemical oxidation and reduction of polypyrrole by cyclic voltammetry, whilst measuring the ESR signal due to the coat. A correlation of the number of spins with the amount of charge injected into the coat is found for the first half of the oxidation and the second half of the reduction reactions. This implies that the current is due to a one-electron oxidation of the polypyrrole, producing a localised radical species. Passage of the remaining oxidation charge results in the complete loss of this ESR signal. This can be attributed to the formation of a localised, two-electron, oxidised species in the coat with no unpaired electrons. Genies[122] has also explained spectroelectrochemical data for polypyrrole films in terms of two successive one-electron oxidation reactions. ESR experiments on polythiophene[123] have shown similar behaviour.

The cyclic voltammetric data presented by Albery and Jones indicates that these redox couples do not obey the

Nernst equation. Rather, the results are seen to fit a model where each redox couple has a Gaussian distribution of the standard electrode potential about a mean value[124]. This spread in E^{σ} can be attributed to the heterogeneity of the coat. (An alternative explanation for this effect would be the increased electrostatic repulsion of these redox centres on increasing the degree of coat oxidation.) This means that these redox centres would possess a range of abilities as oxidising or reducing agents.

Thus, it seems that in the fully oxidised form, *polythiophene and polypyrrole films possess two-electron* oxidants of varying oxidising power. This means that these themselves have potential as electrocatalytic oxidants of organic substrates, without the need for the incorporation of other redox species.

Appendix-Experimental Details For The TosMIC Reaction

Each synthesis was attempted four times. A solution of tosylmethylisocyanide (TosMIC, 20 mmol, 3.91 g) and the chosen vinyl substrate (20 mmol) was prepared in a mixture of diethyl ether and dimethyl sulphoxide (2:1 v/v, 25 ml). This was added dropwise to a stirred suspension of circa 1.2 equivalents of sodium hydride (1.2g) in diethyl ether (40 ml) under dry argon.

After refluxing for fifteen minutes, the mixture was diluted with water (50 ml). For the synthesis of DPDC, the product was then isolated as a yellow solid. This was purified by vacuum sublimation (200 °C, 0.05 mbar) to yield white needle crystals of DPDC (35%).

Physical Data:(Theoretical and Literature values in parentheses)

Microanalysis	C 52.45% (52.46%), H 4.95% (4.92%), O 7.59% (7.65%)
Melting point	246-247 °C (243-245 °C[103])
NMR	δ 7.40, 3.70 (7.43, 3.70[125])

For all other syntheses, the aqueous layer was extracted with diethyl ether and dried over sodium sulphate. The ether was removed in vacuo to yield an oil. This was purified by column chromatography. NMR spectra of the resulting fractions indicated that no substituted pyrrole was present. Extraction from the organic layer using a variety of solvents gave similar results.

CHAPTER 5-CHARGING AND DISCHARGING THE THIONINE COATED ELECTRODE

5.1 Introduction

5.1.1 Reaction Kinetics of Polymer Modified Electrodes

Polymer modified electrodes typically contain redox centres in high concentration (section 1.1). Thus, the electrochemical switching of these centres between their oxidised and reduced forms will permit the reversible storage of a high density of charge in a thin polymer layer. It is this feature which has led to the investigation of these electrodes for use in secondary cells.

There is considerable controversy over the exact kinetics and mechanism of these reactions[126,127]. Figure 5.1a shows the processes occurring in a typical modified electrode when the electrode potential is stepped such that the reaction

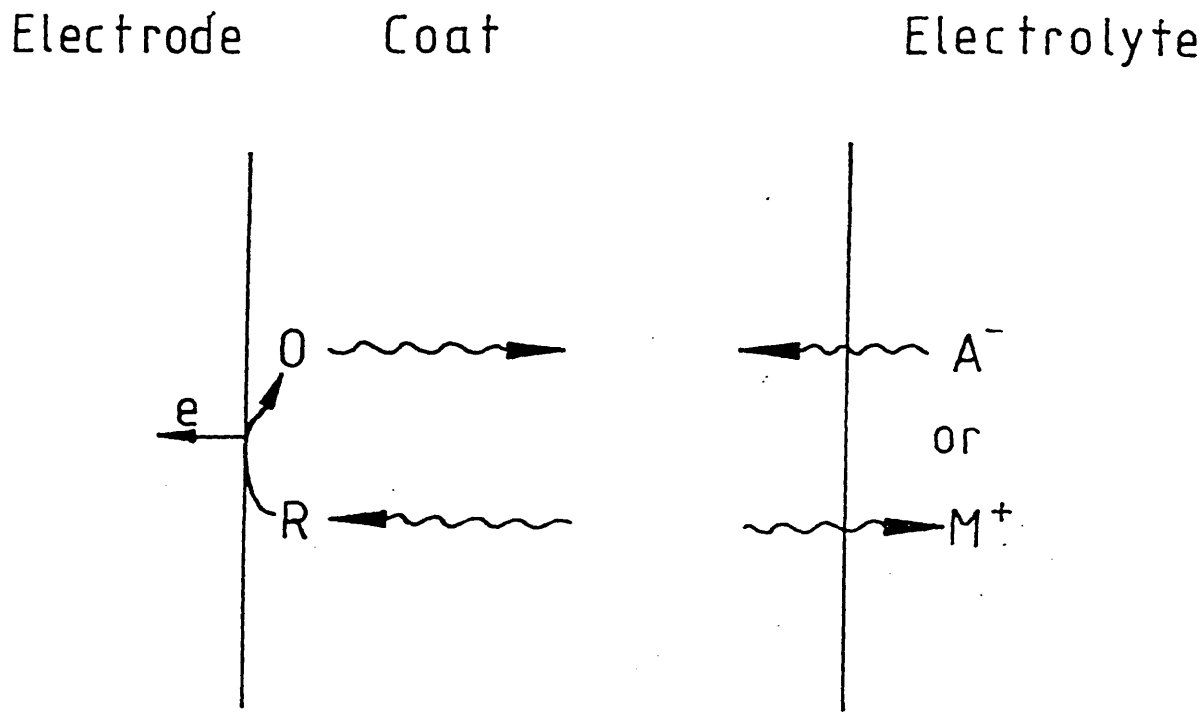
$$R \xrightarrow{-e^-} O$$

occurs.

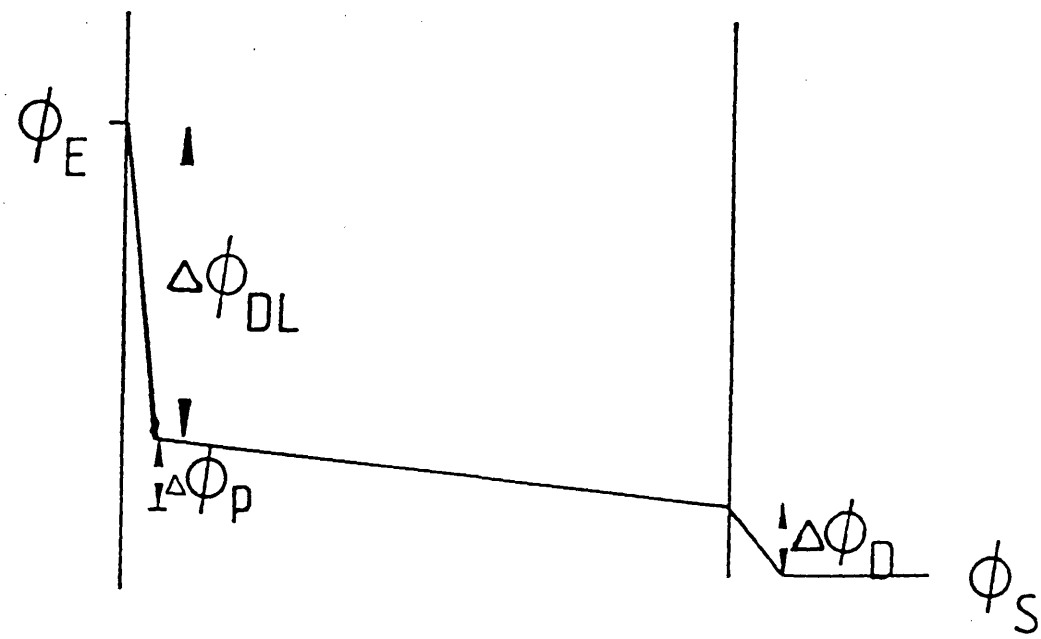
R transports to the electrode where it is oxidised. In order to maintain electroneutrality within the layer, a counterion must diffuse across the polymer/electrolyte interface. The counterion movement may be that of cation out or of anion into the polymer. This will obviously vary with the concentration of cation in the polymer relative to the concentration of anion in the solution and the permselectivity of the coat towards each ionic species. These factors will depend upon the structure of the coat and its net charge.

Figure 5.1 Schematic representation of the oxidation of a modified electrode in the absence of redox reaction with solution species.

(a) transport of polymer redox species and counterions.



(b) field distribution across the layer.



Transport of electrons and ions through the coat can be by both diffusion and migration. Thus the potential distribution throughout the layer is of importance. Figure 5.1b shows an idealised schematic illustration of this distribution. ϕ_E is the potential of the electrode and ϕ_S that of the bulk solution. (The magnitude of $\phi_E - \phi_S$ is fixed at any given potential.) At the electrode/polymer interface, there will be an electrical double layer across which a potential $\Delta\phi_{DL}$ is dropped. This double layer is analogous to that between an electrode and electrolyte. There may also be a potential drop, $\Delta\phi_p$, across the polymer layer. The relative magnitude of these potential differences and the thickness of the double layer will depend upon the activities of the ionic species in the polymer, by direct analogy with solution[128,129].

In addition to these voltages, there may also be a voltage at the polymer/electrolyte interface. For coats which have a net charge, molar counterion concentrations may be necessary in the polymer layer in order to preserve electroneutrality. However, in bulk solution, ionic concentrations are typically of the order of one-tenth molar. Thus, there may be a large concentration difference in the coat compared with solution, maintained by a potential at the interface. This is termed a Donnan potential[130].

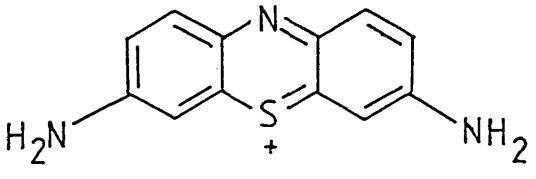
As the reaction proceeds, these concentration and potential profiles will change. It is therefore true that any mechanism may be complex and may change with time.

Hence, the kinetics of the reaction and the location of the reaction zone may also change. This explains the controversy in the literature concerning the modelling of these reactions[126,127].

With such complexity, it is necessary to combine data from various techniques to unravel the mysteries of any system. Current-time data is valuable in probing electron transfer at the electrode/polymer interface. Moreover, a knowledge of counterion flux and the position of the reaction zone is desirable. This chapter describes and applies such techniques for the accumulation of data for the thionine coated electrode.

5.1.2 The Thionine Coated Electrode - The Story So Far

Thionine is an organic phenothiazine dye:

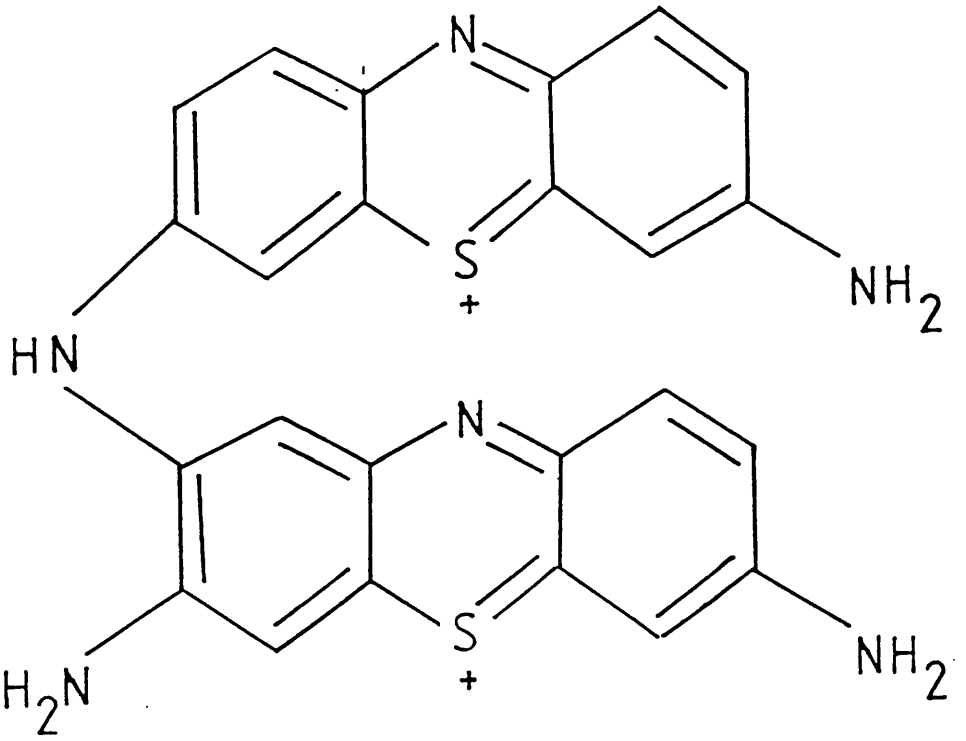


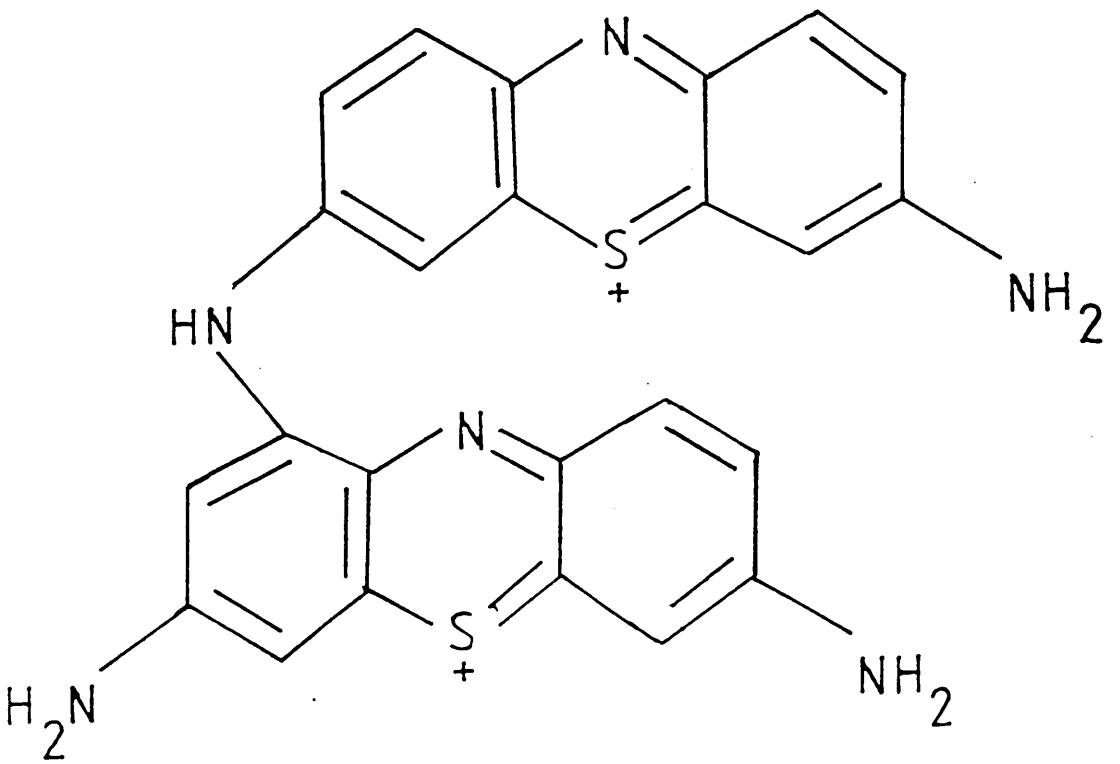
Thionine coated electrodes are produced by coating from a circa 30 μM solution in 50 mM sulphuric acid at +1.2V with respect to SCE for 900 seconds[61,131,132]. The mechanism of film formation is thought to be the coupling of thionine radical cations, linked via their amino nitrogens[85,133]. This results in the structures shown in Figure 5.2.

The thionine centres (Th) in the modified electrode undergo a two-electron reduction to a leucothionine species (L) according to the reaction

$$Th^{+} \xrightleftharpoons{2e^{-},nH^{+}} L^{(n-1)+} \qquad .....(5.1)$$

Figure 5.2 The two possible types of intermolecular bonding for thionine in the coat.





This is analogous to the electrochemistry of thionine in aqueous solution. Thus it can be seen that charging and discharging of the thionine electrode also involves protonic flux. A typical cyclic voltammogram (CV) of the thionine electrode in 50mM sulphuric acid supporting electrolyte (pH 1.2) is shown in Figure 5.3. The maximum peak currents vary linearly with sweep rate up to 100 mV/s, indicating the complete oxidation and reduction of a surface-bound species[81]. Integration of the CV peaks and use of an estimate of the area of a thionine molecule of 0.57 nm^2/molecule[134] gives a typical electrode coverage of ten monolayers. This area is calculated assuming the molecules lie flat on the electrode surface. Electron transfer is reversible, with a 90 mV peak-to-peak separation for the $3H^+,2e^-$ reaction at pH 1.2[62].

Experimental data has also been acquired for the variation of E' with the pH of the aqueous solution[81]. (E' is the mean of the oxidation and reduction peaks in a CV. This is the equivalent of the standard electrochemical potential of a species in solution.)

The gradient of this plot gives n/2 for reaction (5.1). This allows approximate pK_a values for the thionine and leucothionine species to be calculated[81]. This data is shown in Figure 5.4. Also shown are the pK_a values for the solution species, and the solution pK_a values of the one-electron semithionine (S) intermediate. The three leucothionine equilibria are henceforth designated as pK_{a1},

Figure 5.3 Typical cyclic voltammogram of polythionine in H_2SO_4 (50 mM; v = 50 mV s^{-1}).

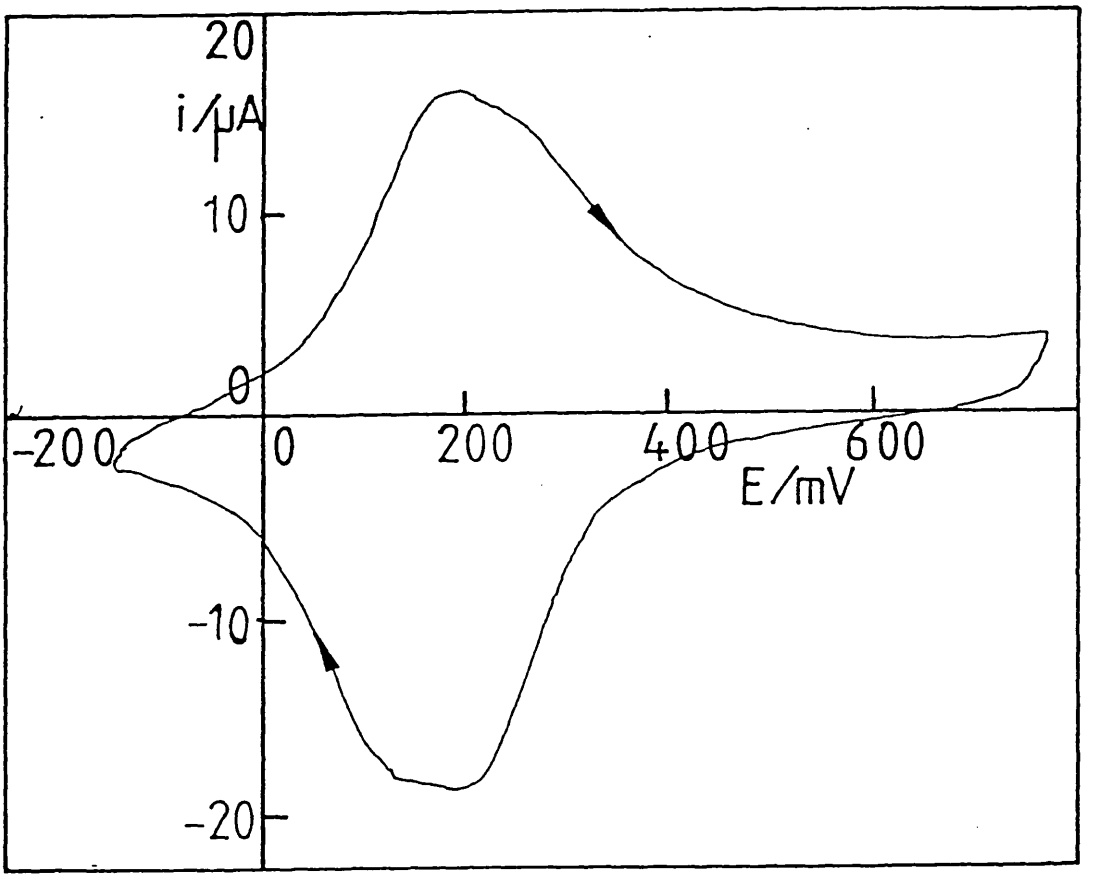
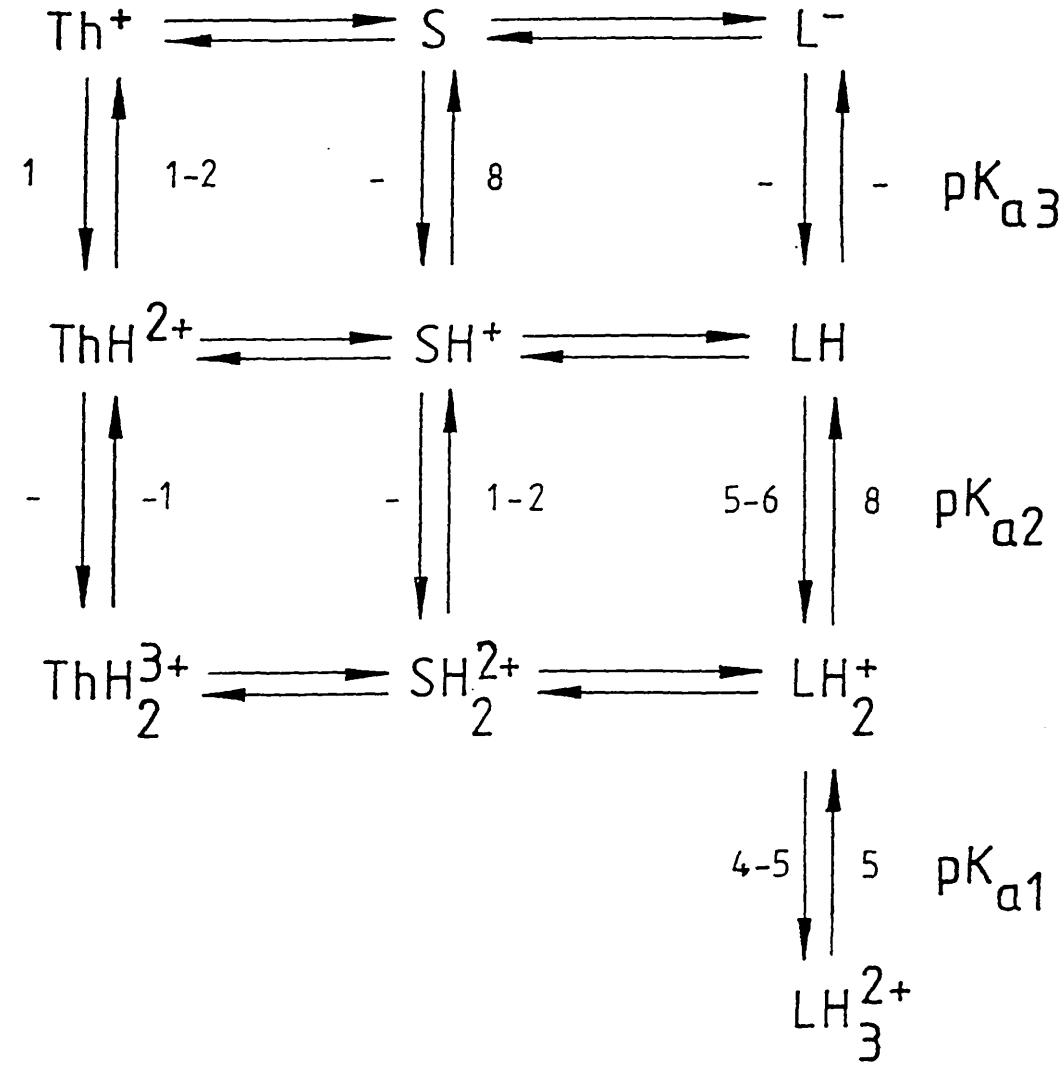


Figure 5.4 The scheme of squares for thionine. The values to the left of the equilibria are for the coated species. Those to the right refer to thionine in solution.



pK_{a2}, pK_{a3} as shown.

5.2 Chronoamperometric Studies

Some chronoamperometric studies have already been carried out on this electrode[79]. Small potential steps of ten to twenty millivolts around the E' of the coat were performed. These can be fitted to a modified Cottrell expansion:

$$i = \left\{ \frac{D}{\pi t} \right\}^{1/2} \frac{\Delta q}{l} \left[1 + 2 \sum_{m=1}^{\infty} (-1)^m \exp \left\{ - \frac{m^2 l^2}{Dt} \right\} \right] \quad \ldots.(5.2)$$

where Δq is the change in charge on performing the experiment.

This equation is derived by integration of Fick's Second Law of Diffusion for a thin layer of thickness l. The experimental time course is controlled by one characteristic parameter, D/l^2.

At pH 1.2, the observed values of this time constant were found to vary with the size of the background anion. With this evidence, it was proposed that the rate determining step for the coat redox reaction was the diffusion of anion within the coat. This would be the case if electron transport were fast.

At pH 5, the values of D/l^2 obtained were uniformly higher, and independent of anion size. Thus, electron transport was considered to be rate determining. At this pH, the redox reaction was proposed as being

$$Th^+ \xrightleftharpoons{2e^-, 2H^+} LH_2^+$$

This does not require anion incorporation.

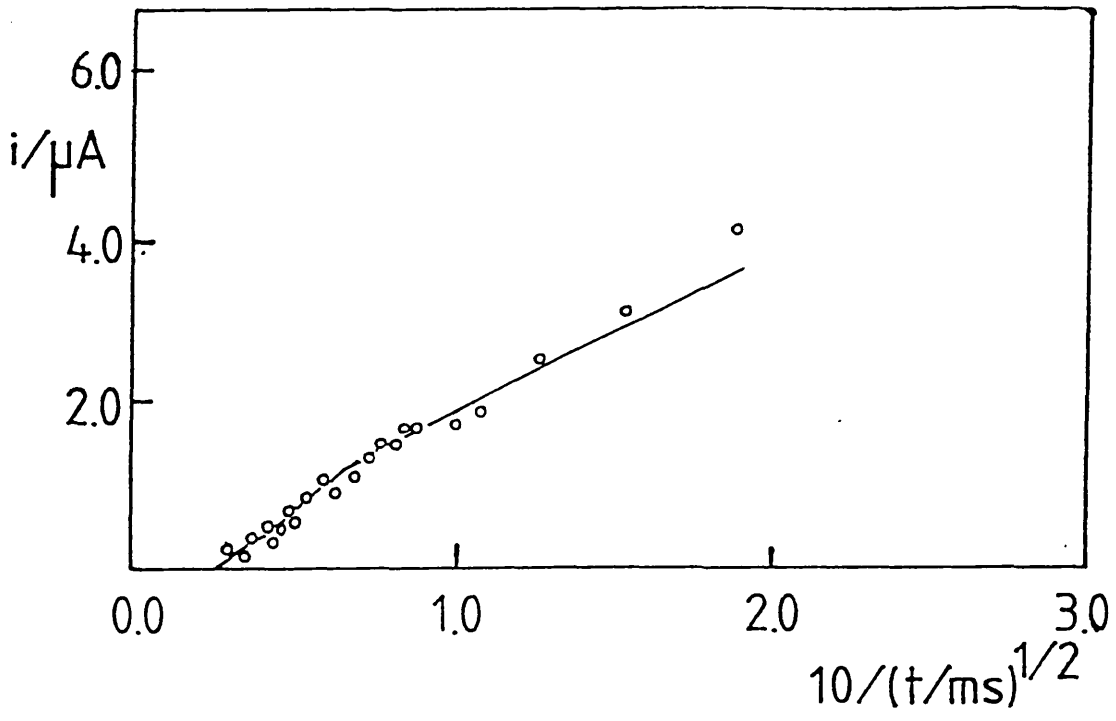
Figure 5.5 shows typical current versus $t^{-1/2}$ plots for 20 mV steps about the E' of a thionine coated electrode for small and large anion background electrolyte. Also shown is a theoretical line calculated from the first five terms of equation (5.2) for modified Cottrell behaviour. The close correlation of the data with this line and the variation of the measured value of D/l^2 with the size of the background anion is in good agreement with the aforementioned work. This is observed for all bulk pH values and for both buffered and unbuffered solutions.

Figures 5.6(a) and 5.6(b) show large step chronoamperometric experiments in unbuffered aqueous sodium perchlorate (0.1 M) at varying pH. The term large step, when used in this thesis, means that the potential jump is such that complete oxidation (or reduction) of the fully reduced (or oxidised) coat occurs. These current transients cannot be interpreted using simple modified Cottrell theory. Their shape is also not constant with bulk pH. This is in marked contrast to small step experiments.

The application of small potential steps should give results equivalent to relaxation experiments. Small changes in concentration of thionine and leucothionine are effected. This allows only small disc pH excursions thereby minimising changes in the protonation state of leucothionine. Migration in the layer would also be expected to be unimportant. However, for large step experiments, a rapid turnover of all the thionine centres is enforced. Thus, very large changes in the local

Figure 5.5 Current versus $t^{-1/2}$ plots for small step chronoamperometry at thionine modified electrodes.

(a) in H_2SO_4 (50 mM; step 190 mV to 210 mV; $D/l^2 = 1.82\ s^{-1}$)



(b) in glycylglycylglycine buffer (0.1 M, pH 8.0; step -75 mV to -175 mV; $D/l^2 = 0.66\ s^{-1}$)

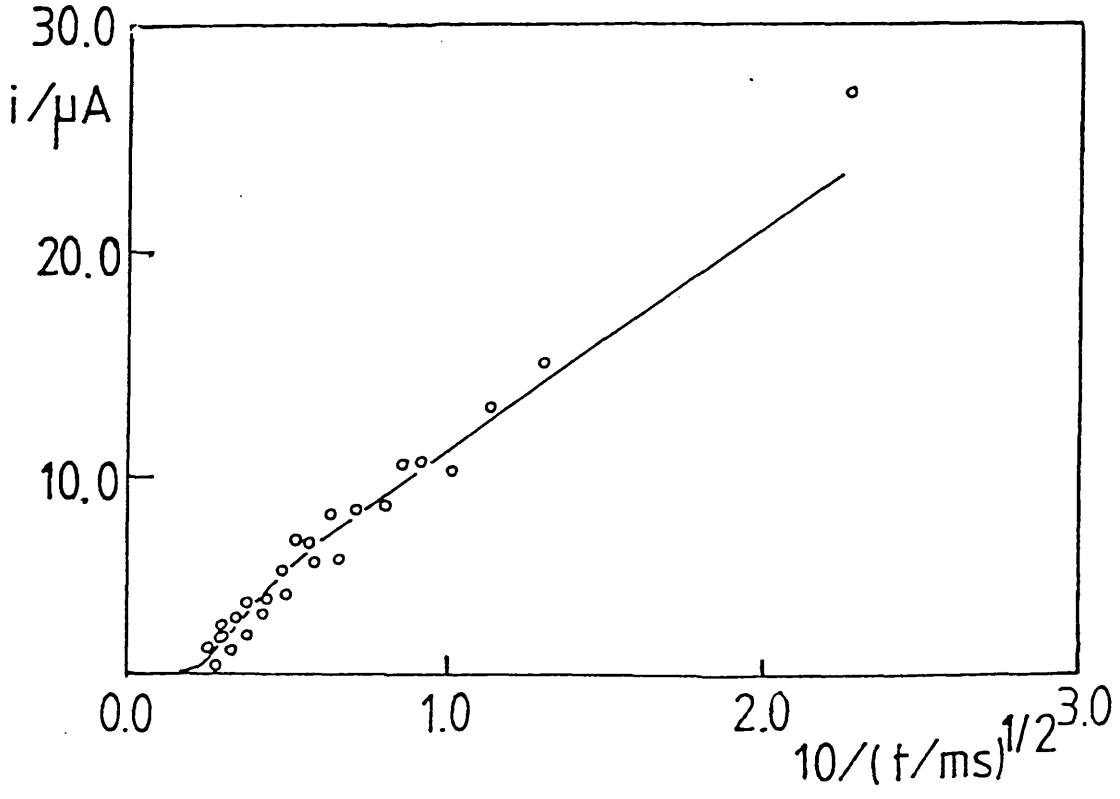
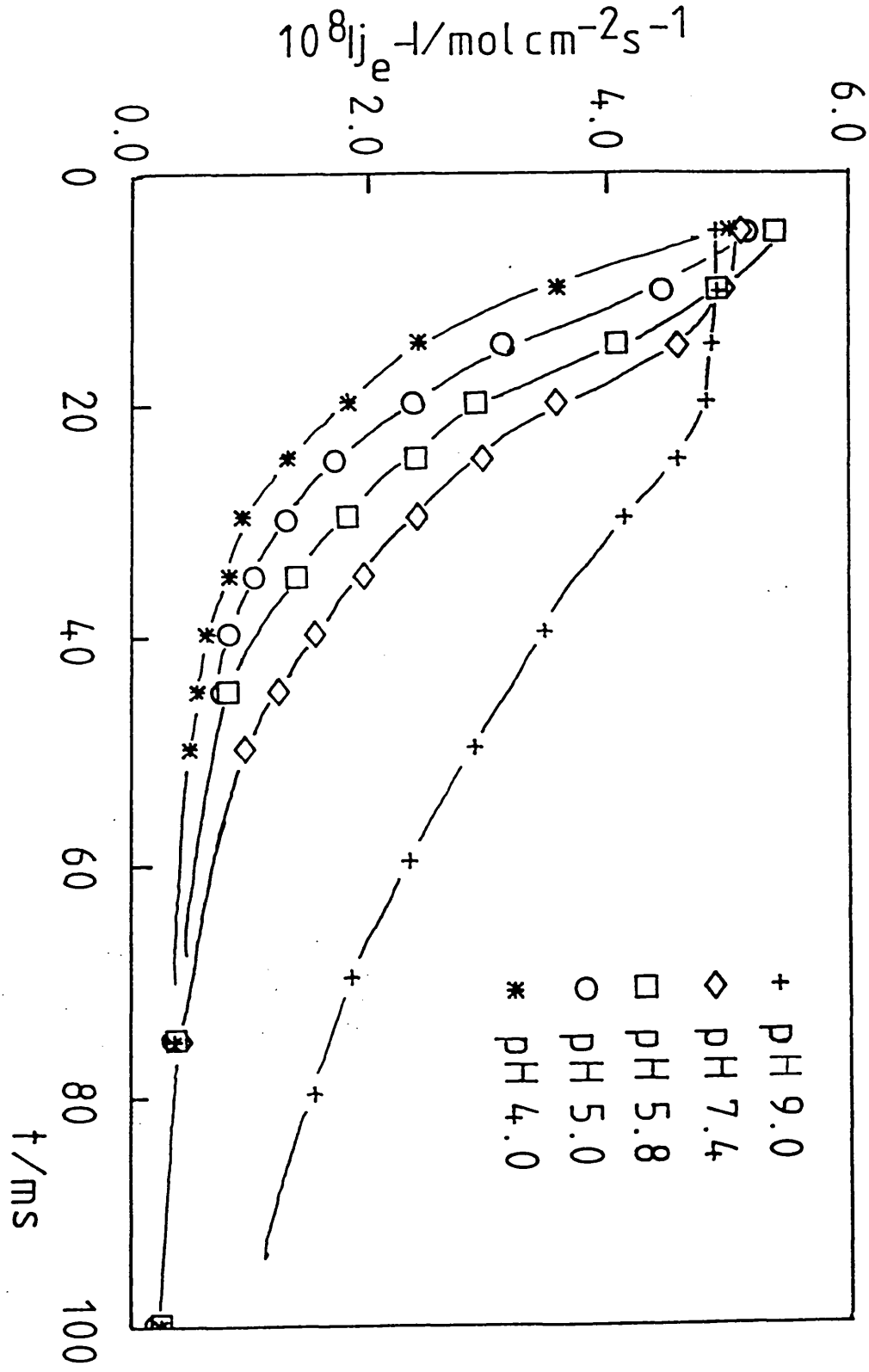
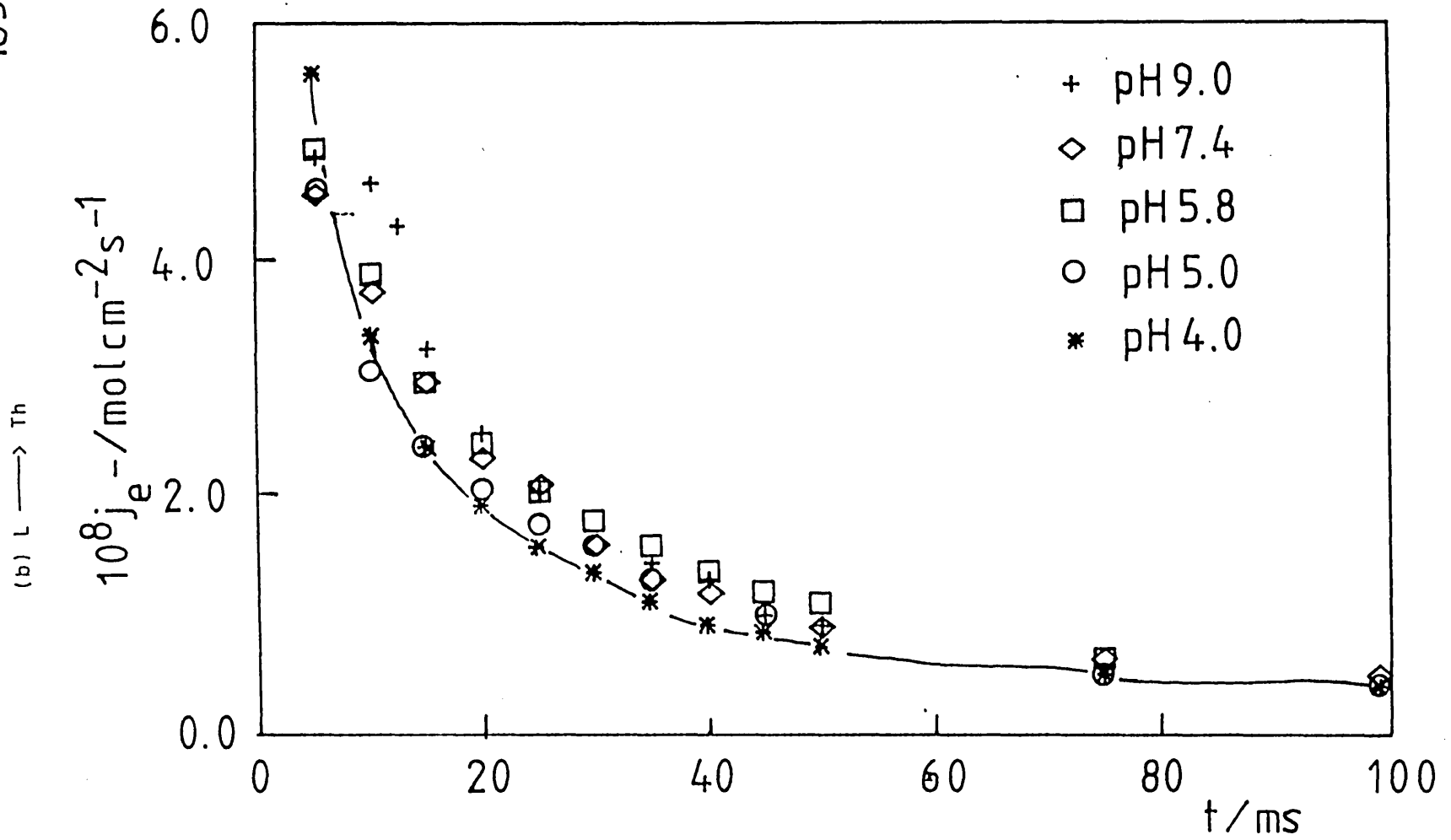


Figure 5.6 Large step chronoamperometry at a thionine modified electrode in aqueous $NaClO_4$ (0.1 M) solution.

(a) Th ——> L




6.0
4.0
2.0
0.0
0
20
40
60
80
100
t/ms
$10^8 j_e^-$/molcm^{-2}s^{-1}
pH 9.0
pH 7.4
pH 5.8
pH 5.0
pH 4.0
(b) L ⟶ Th

concentrations of thionine proton and anion are possible, resulting in a more complex reaction. The object of this work is to explain the observed kinetics of these coat redox reactions in terms of a general model.

5.3 Mechanisms of the Charging/Discharging Process

The elucidation of mechanisms for the charge/discharge process of the thionine modified electrode requires knowledge of the flux of protons and counterions throughout the electrode reaction. This has been accomplished by the use of bismuth/bismuth oxide and silver/silver chloride ring electrodes as downstream sensors of these species.

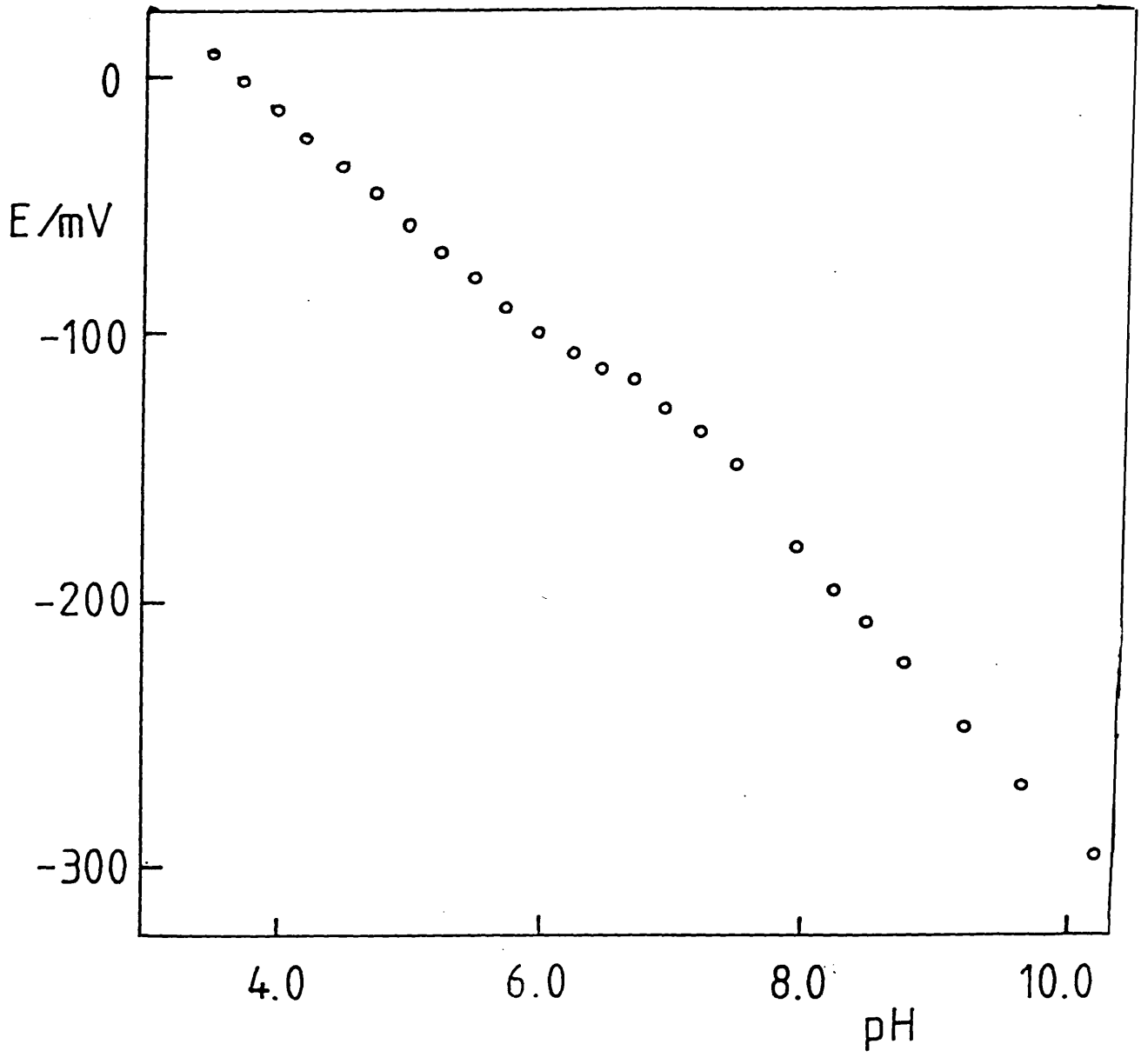
5.3.1 Bismuth/Bismuth Oxide Experiments

The typical response of a bismuth oxide ring electrode to solutions of varying pH is shown in Figure 5.7. The rotation speed of the electrode was 10 Hz. This complex response can be attributed to changes in the degree of protonation of the bismuth oxide layer. Typically the ring response to pH was measured before and after each experiment. This was found to be sufficient to enable easy conversion between measured potentials and pH.

Experiments involved the imposition of a potential of 600 to 700 mV about the E' to a thionine coated disc electrode. This effects a disc electrode conversion from the thionine to the leucothionine form, or vice versa.

However, the imposition of a fast voltage change over the period of a few milliseconds was found to produce a non-Faradaic voltage excursion at the ring. This effect has been observed for high frequency ac experiments[62] and is due to the charging of the ring electrode double layer through the solution resistance. The magnitude of the effect is directly proportional to the applied ac voltage.

Figure 5.7 Response of a bismuth/bismuth oxide ring electrode to solutions of varying pH (W = 10 Hz).



It is clear that an experiment involving a step (or fast ramp) in potential can be considered to be analogous to the application of a quarter of one cycle of an ac signal. Therefore, this non-Faradaic signal can be minimised by decreasing the ramp rate. Experiments have revealed that the effect is small for a ramp time of 100-200 ms.

Experimental fluxes of protons at the disc were calculated from observed bismuth ring voltages using the theory given in section 2.2.2.3.

Figure 5.8 shows the electron and proton fluxes for the conversion of thionine to leucothionine and the reverse reaction at a bulk pH of 3. In each case, the electron and proton fluxes are of a similar shape. The flux of protons is of the order of one and a half times greater than the flux of electrons. This is consistent with the three proton, two electron reaction implied by Colby[81]

$$Th^{+} \underset{\longleftarrow}{\overset{3H^{+},2e^{-}}{\longrightarrow}} LH_3^{2+}$$

The 'proton flux' observed after the completion of the electrochemical reaction is an experimental artefact, due to drift in the potential of the sensor at this pH. Small changes in this potential will produce large calculated 'fluxes' at low pH, where the ring is comparitively insensitive to proton flux.

Figure 5.9 shows typical experimental data collected at pH 4. The reaction L ——> Th is similar to that at pH 3. The most marked change is in the shape of the proton flux transient for the reduction of thionine. This

Figure 5.8 Electronic and protonic flux for the reactions Th ——> L and L ——> Th in unbuffered $NaClO_4$ (0.1 M) solution, bulk pH 3.

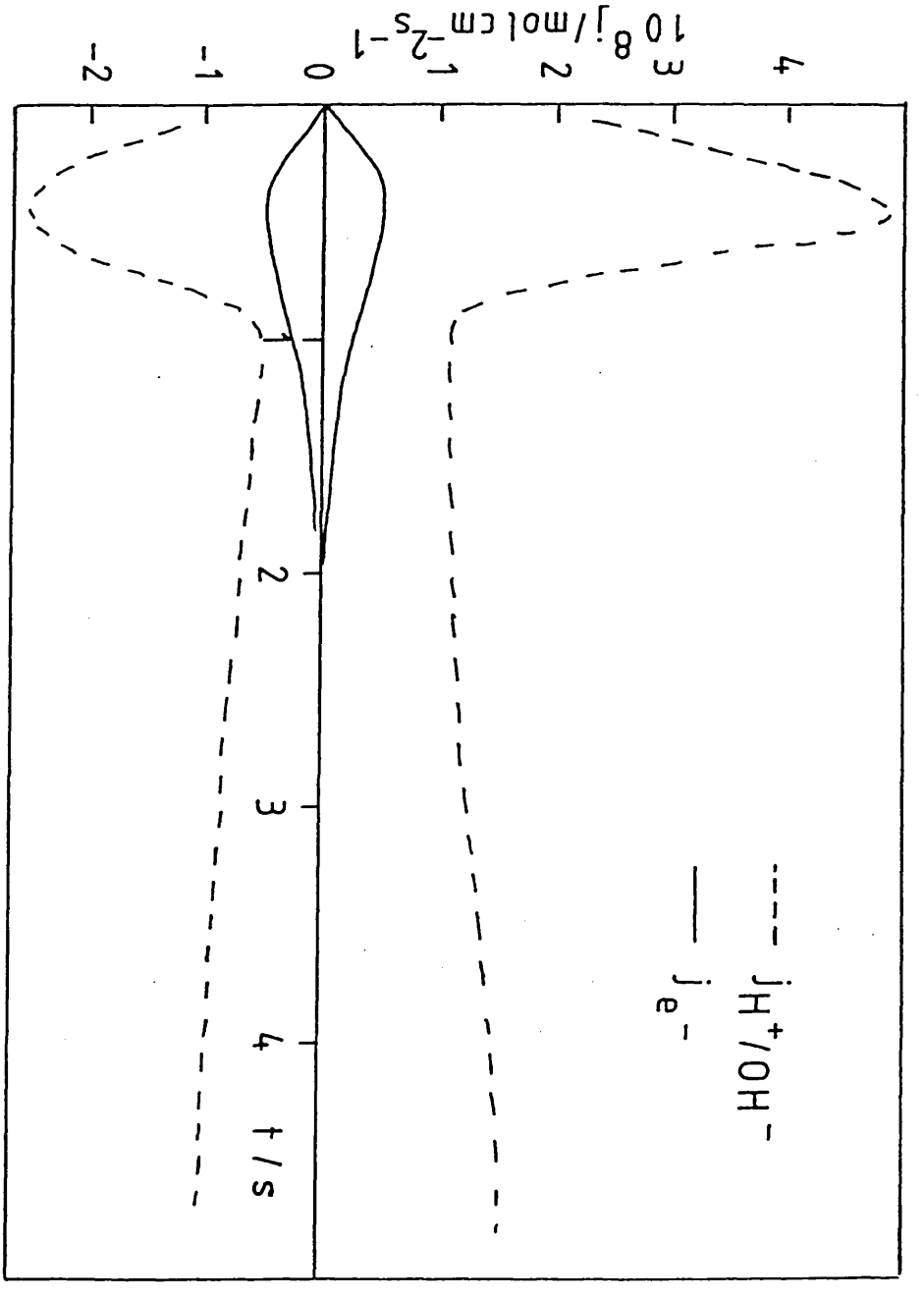
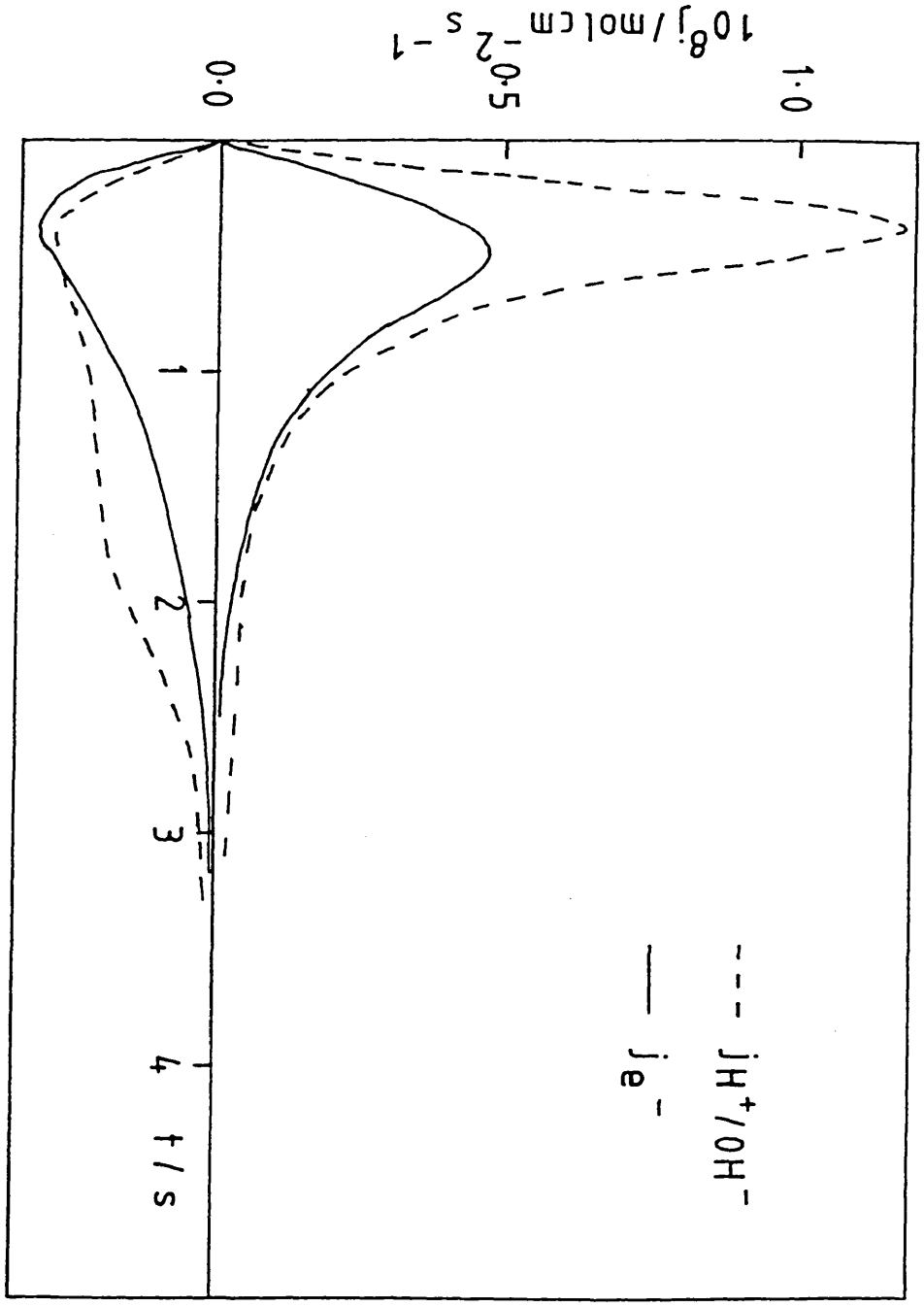


Figure 5.9 Electronic and protonic flux for the reactions Th ——> L and L ——> Th in unbuffered $NaClO_4$ (0.1 M) solution, bulk pH 4.



can be explained by considering the excursion in pH. As reaction proceeds, L is formed, consuming protons. The concentration of the redox sites in the coat is estimated to be 3 M[79]. Hence the pH at the disc (pH_0) becomes more alkaline, until pH_0 becomes greater than pKa_1. At this point, the reaction switches from

$$Th^+ \xrightarrow{2e^-,3H^+} LH_3^{2+}$$

to

$$Th^+ \xrightarrow{2e^-,2H^+} LH_2^+$$

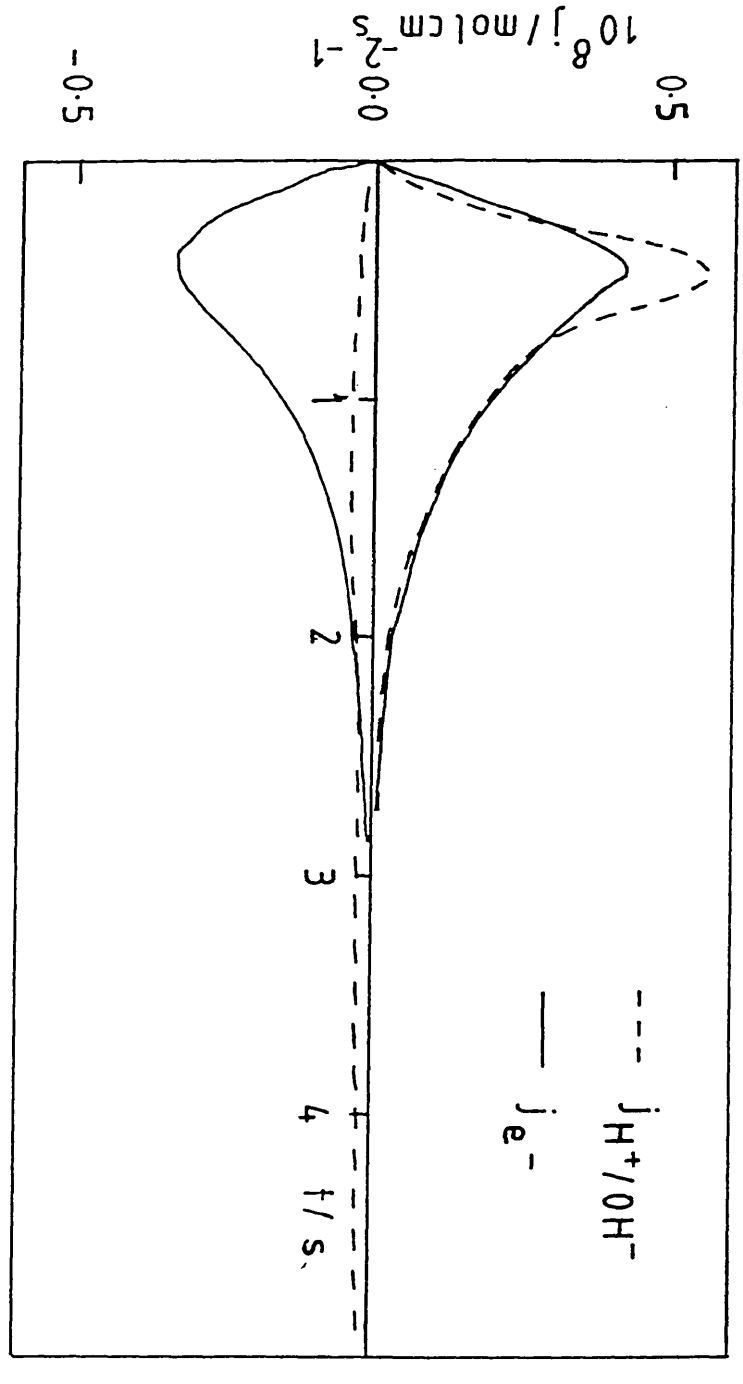
This produces a proton flux in time with the electron flux, but smaller in magnitude than at pH 3. As the reaction nears completion, pH_0 gradually relaxes to the bulk value, and proton is titrated into the coat, according to the reaction

$$LH_2^+ \xrightarrow{H^+} LH_3^{2+}$$

Thus, a large proton flux is still observed, even as electron transfer nears completion.

At pH 5 (Figure 5.10) the reaction L ——> Th still gives similar proton and electron flux transients. The Th ——> L reaction is similar to that at pH 4. The proton flux required to change the disc pH such that pH > pK_{a3} is much smaller and cannot be observed. Also, the comparatively small disc fluxes of proton or hydroxide ion suggests a rapid pH excursion such that pH > pK_{a2}, pK_{a3}, giving the reaction

Figure 5.10 Electronic and protonic flux for the reactions Th ——> L and L ——> Th in unbuffered $NaClO_4$ (0.1 M) solution, bulk pH 5.



$$Th^{+} \xrightarrow{2e^{-}} L^{-}$$

followed by slow titration of protons into the coat to restore bulk pH.

$$L^{-} \xrightarrow{3H^{+}} LH_3^{2+}$$

This smaller relaxation flux is due to the smaller concentration gradient between disc and bulk at pH 5, when compared with pH 4.

At pH 6, (Figure 5.11), even smaller fluxes are required to drive the disc pH more alkaline than pK_{a1}. However, the main new development is now in the L ——> Th transient. The proton flux transient is consistent with the reaction initially being

$$LH_2^{+} \xrightarrow{-2e^{-},2H^{+}} Th^{+}$$

with the evolved protons rapidly causing the disc pH to fall such that $pH_0 < pK_{a1}$, giving the simultaneous reaction

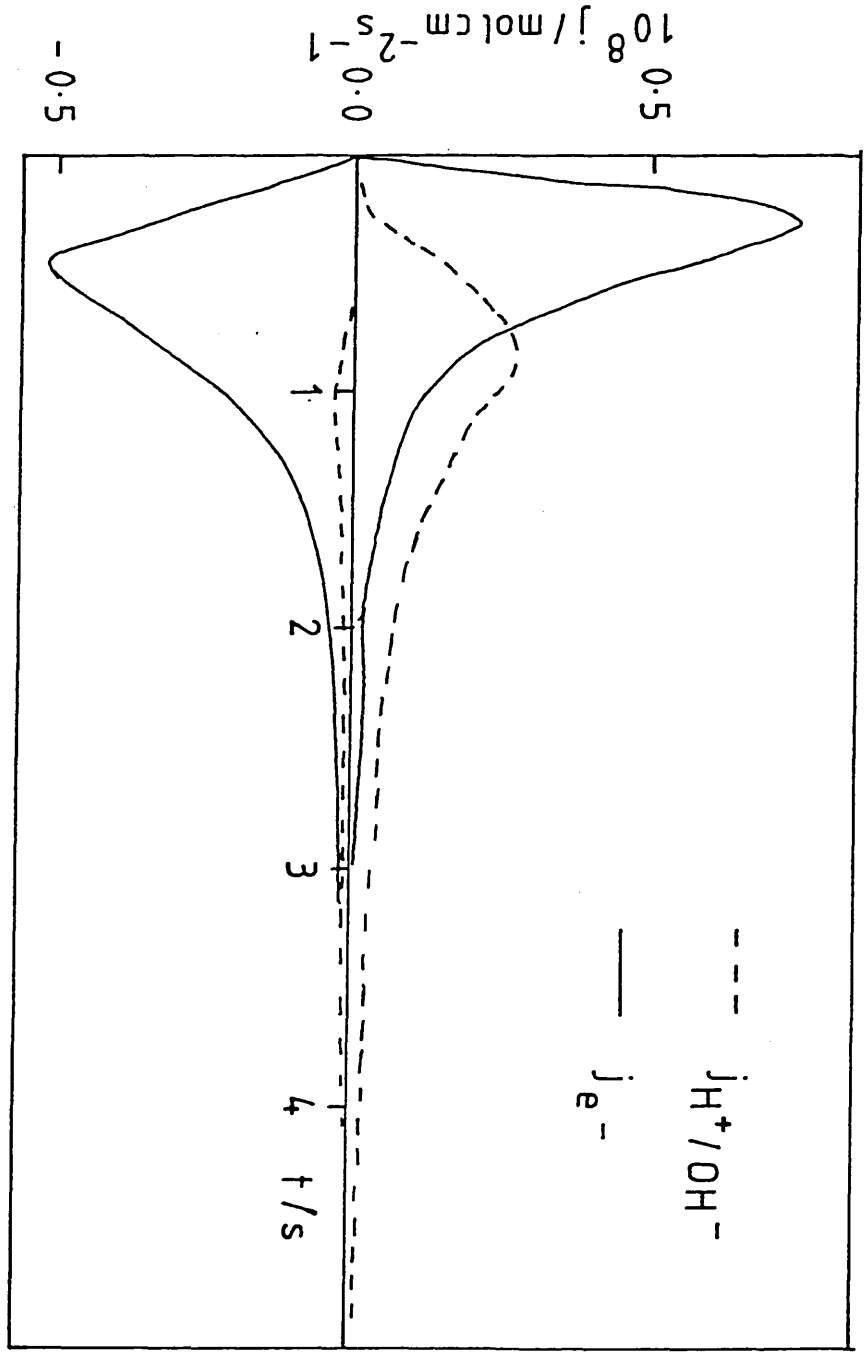
$$LH_2^{+} \xrightarrow{H^{+}} LH_3^{2+}$$

i.e. self-buffering by the coat. This process will continue until the buffer capacity of the layer is exceeded. This is when all L is present as LH_3^{2+}. This will require the turnover of one-third of the L sites. Then further oxidation will result in a proton flux being observed as LH_3^{2+} reacts to form Th^{+}. This data therefore implies

$$5 < pK_{a1} < 6$$

Data collected at pH values of 7 and 8 are similar

Figure 5.11 Electronic and protonic flux for the reactions Th ——> L and L ——> Th in unbuffered $NaClO_4$ (0.1 M) solution, bulk pH 6.



in form to that at pH 6. Figure 5.12 shows that at pH 9 no proton or hydroxide ion transients can be observed, indicating that the reaction is $Th^{+} \xrightarrow{2e^{-}} L^{-}$ and that

$$8 < pK_{a2} < 9$$

$$8 < pK_{a3} < 9$$

Values of the maximum disc pH were calculated from the T ——> L reactions at bulk pH's of 6, 7 and 8. This used the same procedure as the construction of Figure 2.13. This was found to be 8.4±0.1 in each case. (In crossing the pK_{a3} boundary, no further excursion in pH will occur, as the thionine/leucothionine reaction requires no protons.)

Therefore

$$8 < pK_{a2} < 8.4$$

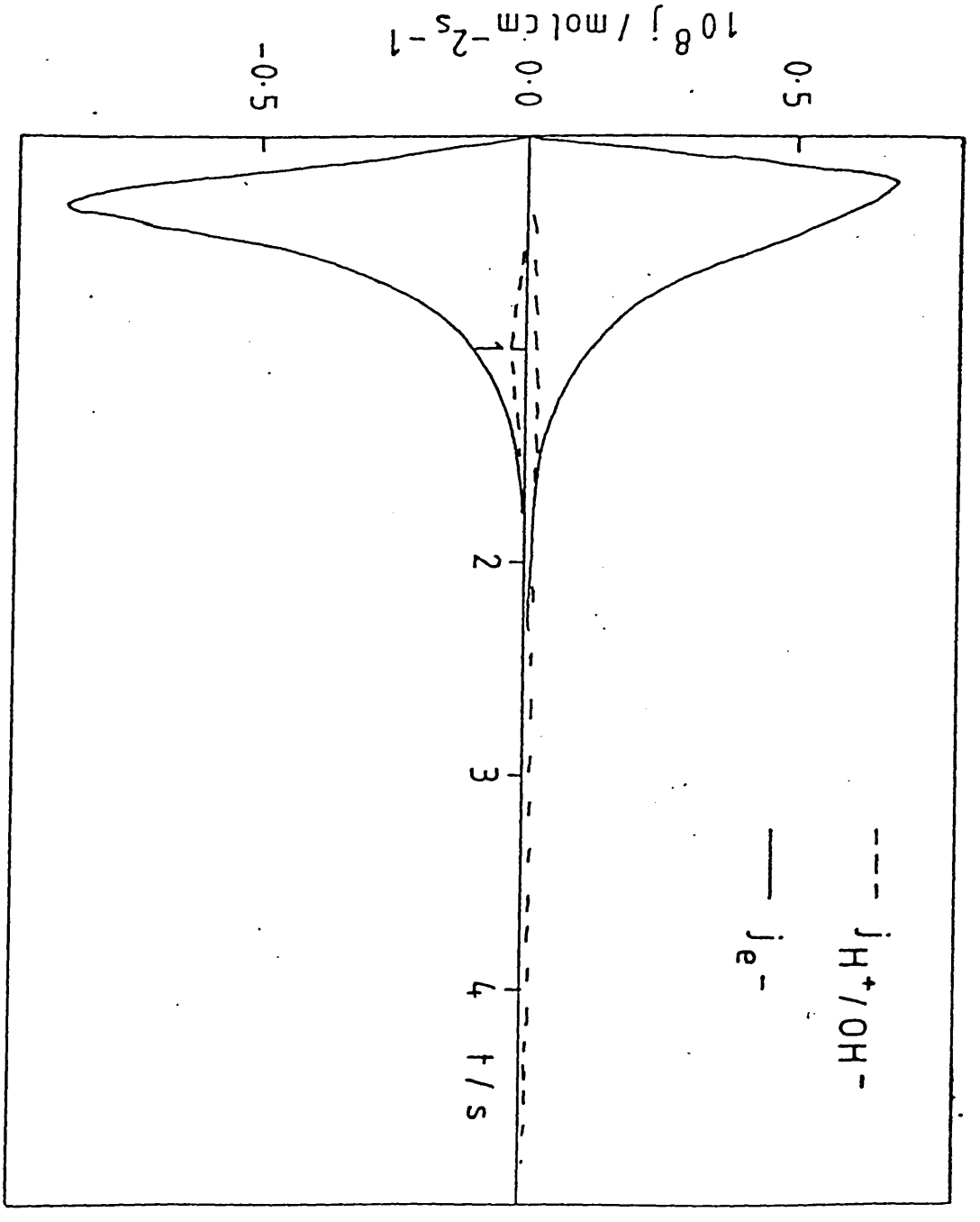
$$8 < pK_{a3} < 8.4$$

It is comforting that these values of pK_{a1} and pK_{a2} agree well with literature values given in Figure 5.4. K_{a2} and K_{a3} are each assigned to the intermolecular bridging amine groups. It is therefore not unreasonable that their values are similar.

These results indicate simultaneous electron and proton exchange for these reactions. The current transients have a similar time scale over many orders of pH and various protonations and deprotonations of the thionine and leucothionine species. This infers that the rate determining step of these reactions does not involve protons or hydroxide ions.

These experiments indicate the value of this novel

Figure 5.12 Electronic and protonic flux for the reactions Th ⟶ L and L ⟶ Th in unbuffered $NaClO_4$ (0.1 M) solution, bulk pH 9.



technique, which makes possible the direct measurement of the flux of proton or hydroxide ion at the disc throughout an electrochemical reaction. This method is generally applicable to the study of any electrode reaction involving simultaneous electron and proton transfer.

5.3.2 Silver/Silver Chloride Experiments

Most of the reaction schemes proposed in section 5.3.1 require a change in charge of the coat. Typically, the layer is positively charged and will therefore be permselective towards anions. This section describes the use of a potentiometric sensor to gain information about the disc flux of anion throughout the charging reactions.

Figure 5.13 shows a typical response of a silver/silver chloride electrode to the concentration of chloride ion in solution. The slope of the calibration plot is 55±5 mV/pH unit, indicating good Nernstian behaviour. Deviations from this behaviour occur at pH $\geq$ 9, where surface silver oxide is formed[72].

Experiments were performed in 100 μM sodium chloride solutions. This ensured that $[Cl^-] >> \sqrt{K_{sp}}$ throughout the experiment. Therefore the theory of section 2.2.2.2 may be applied. The effects of solution migration were minimised by the addition of excess sodium perchlorate (50 mM) as supplementary background electrolyte. That this electrode can detect changes in chloride flux in the presence of large excess of other anions demonstrates the sensitivity of the technique.

Fast potential steps were employed, of similar magnitude to the proton flux experiments. These produced similar, non-Faradaic ring voltage excursions (section 5.2). However, reducing the rate of change of the disc potential was found to have little effect. This is because the chloride ring potential is very much smaller than the non-

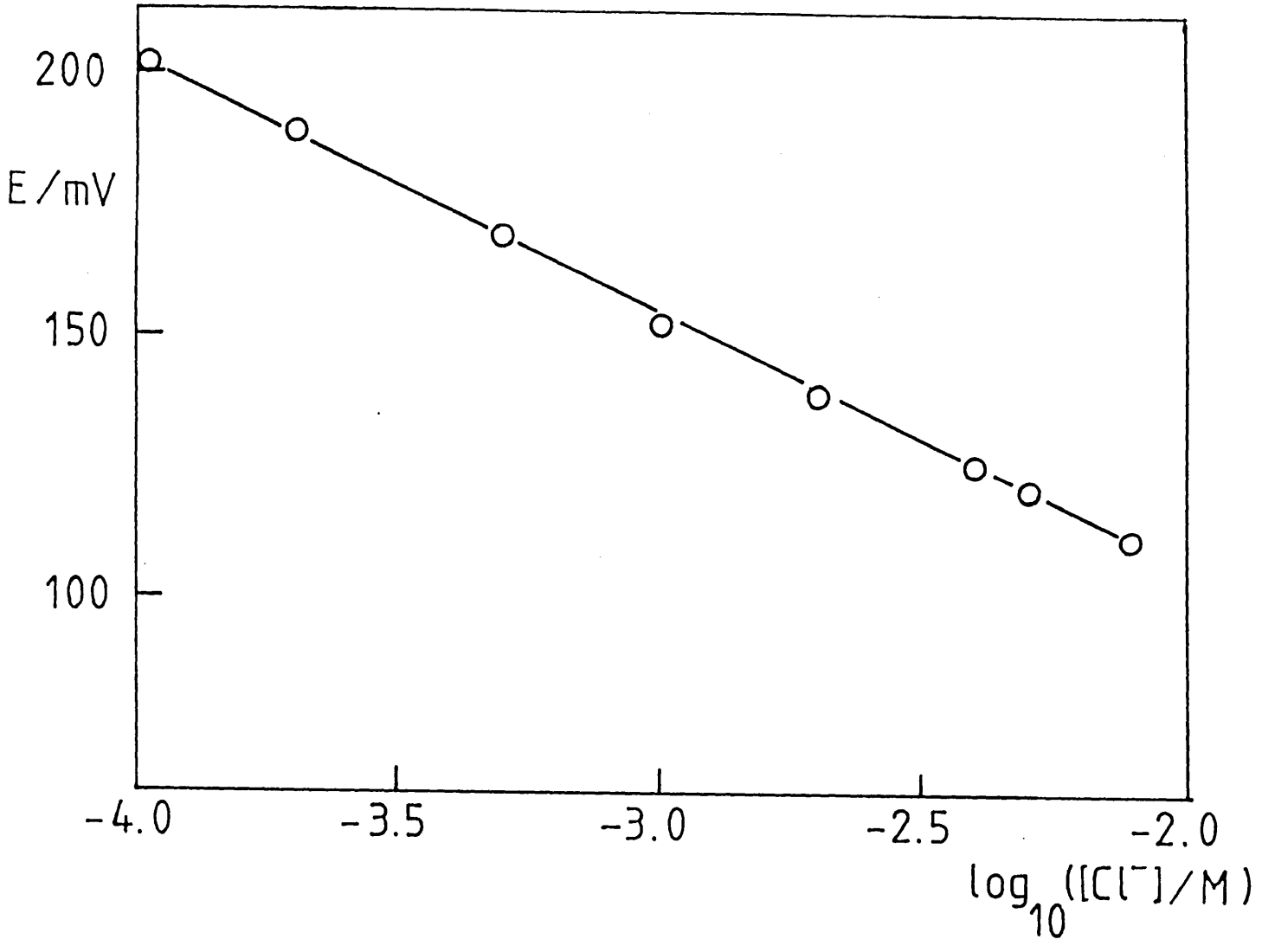


Figure 5.13 Typical response of an Ag/AgCl potentiometric ring sensor to variation of the bulk chloride concentration (W = 9 Hz).

Faradaic response in this case. Deconvolution of these signals was enabled by using slow rotation speeds of 1 or 2 Hz. This increases the ring disc transit time to greater than one second[135]. At these times, the non-Faradaic excursion, which is unaffected by rotation rate, is minimal. Unfortunately, this also means that equation (2.36) does not hold, for this assumes a fast transit time between disc and ring compared with the time scale of the disc current transient. But a combination of equations (2.36) and (2.19) gives

$$i_{R,Cl^-} = i^{\infty}_{R,Cl^-} \left[\exp \left\{ - \frac{\Delta EF}{RT} \right\} - 1 \right] \qquad ....(5.3)$$

where i_{R,Cl^-} is the amperometric flux of chloride ion and i^{∞}_{R,Cl^-} can be calculated from equation (2.14).

This allows easy conversion of the observed ring potential to an amperometric ring current. Firstly, deconvolution of this current to a disc chloride flux was attempted using the procedure outlined by Albery et al[81,136]. However, the disc transients typically last less than 0.3 s. This is far too fast for this procedure to produce accurate results.

The second approach was to predict the ring response to the disc current. Colby[81] has developed a simulation method in which the disc current is considered to be a series of galvanostatic steps joined to make a smooth transient. The ring current at any given time is given by the sum of the contribution of each disc current step

multiplied by its value of N_T, the time dependent collection efficiency[137]. A FORTRAN computer program, DECON, has been developed to provide this data manipulation[81]. This calculates a simulated amperometric ring response i_R^S. Therefore comparison of i_R^S and i_{R,Cl^-} allows a match between disc chloride flux and disc current.

Figure 5.14 shows the typical ring responses for the reactions Th ——> L and L ——> Th at a bulk pH of 7. It can be seen that the ring response for the reduction reaction is greater than that for the oxidation. That there is a response is indicative of the involvement of anions in this reaction. The direction of the potential excursions indicates an incorporation of anion into the coat during oxidation and an ejection on reduction. The normalised simulated ring response i_R^S for Th ——> L is shown in Figure 5.15. Also shown is the normalised amperometric ring 'current' of chloride ion i_{R,Cl^-} given by equation (5.3).

It is evident that i_R^S and i_{R,Cl^-} are closely matched in shape. Furthermore

$$i_R^S \approx 100\ i_{R,Cl^-}$$

The concentration ratio of perchlorate to chloride anion is 500.

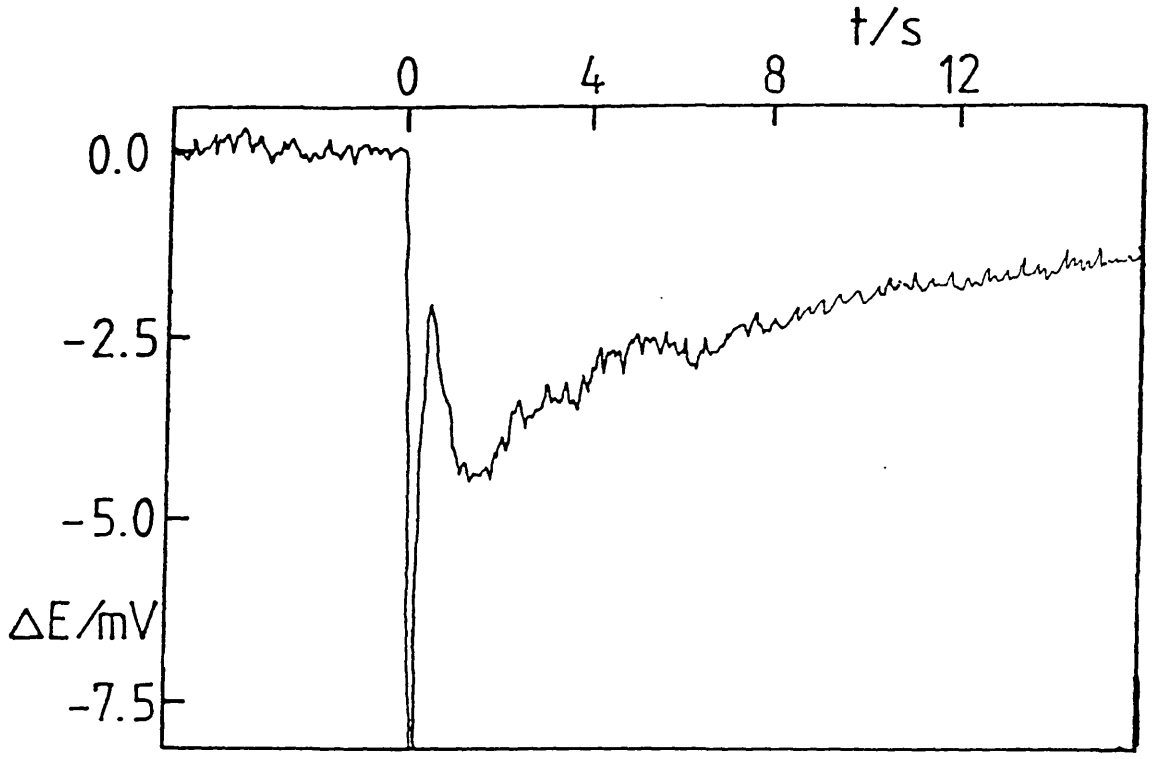
The Th ——> L reaction at a bulk pH 7 has been shown to be

$$Th^+ \xrightarrow{2e} L^-$$

since at the disc $pH_0 > pK_{a1}$ (section 5.3.1).
Therefore, in conjunction with these results, the reaction

Figure 5.14 Typical Ag/AgCl ring response to large step chronoamperometry at a thionine coated electrode in 100μM NaCl/50mM $NaClO_4$ solution (W = 2 Hz)

(a) Th ——> L



(b) L ——> Th.

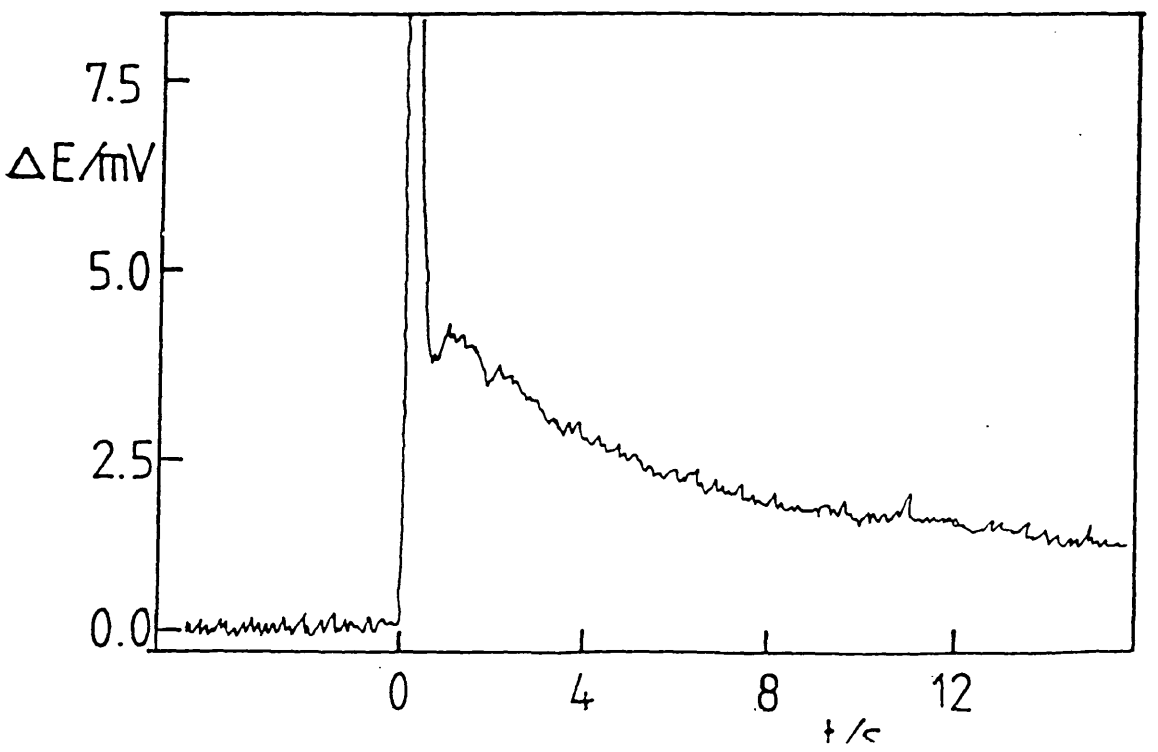
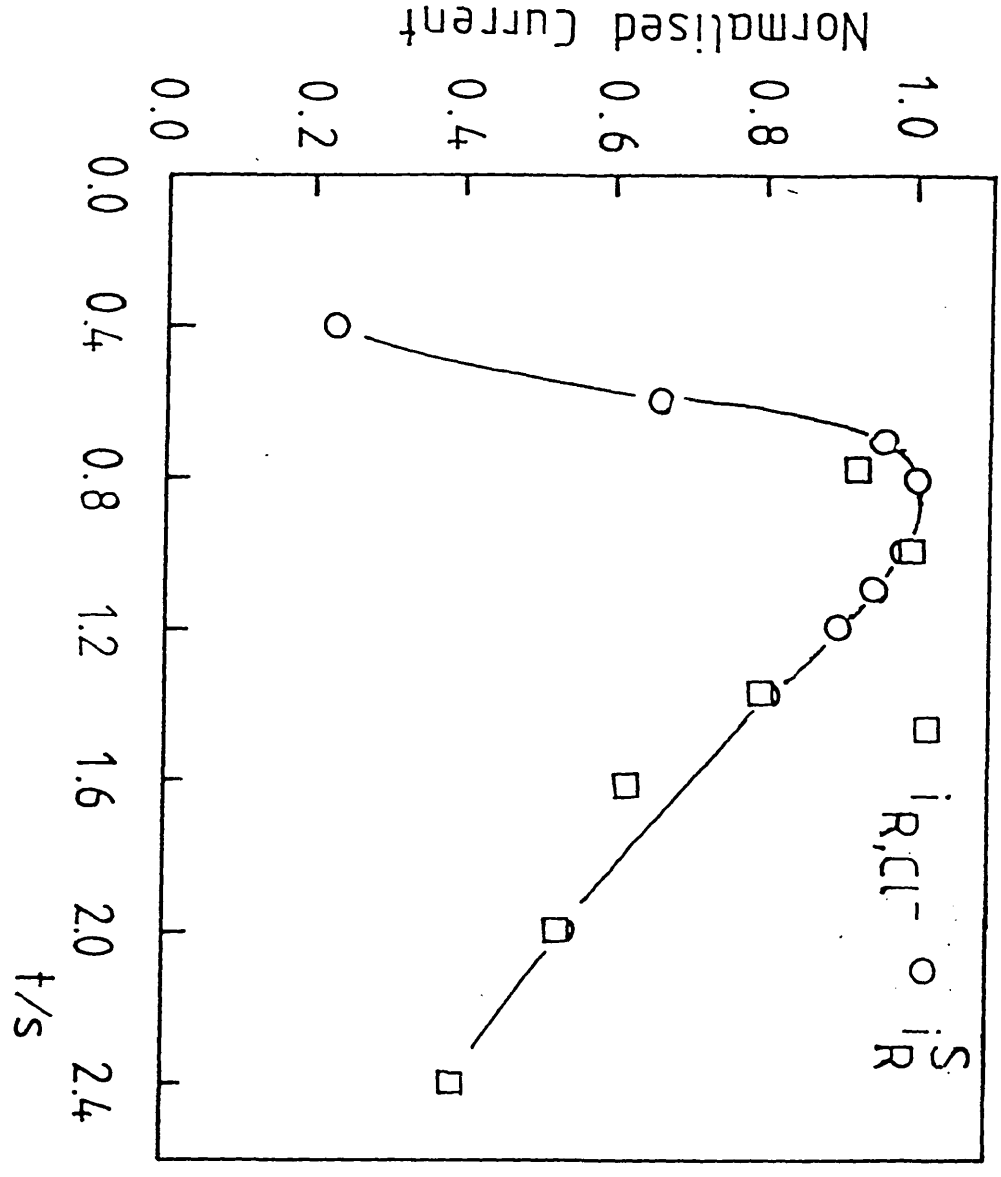


Figure 5.15 The normalised simulated ring response, i_R^S, and the normalised amperometric ring current, i_{R,Cl^-}, for the reaction Th ⟶ L from Figure 5.14.



is most likely to be

$$2Th^{+}A^{-} \xrightarrow{2e^{-}} Th^{+}L^{-} + 2A^{-}(aq)$$

with the ejection of one anion to preserve electroneutrality upon the injection of one electron. Therefore it appears that the permselectivity of the coat for Cl^{-} compared with ClO_4^{-} is 5. Further evidence for this reaction is presented in section 5.2.3. The reaction L ——> Th is (section 5.3.1)

$$LH_2^{+} \xrightarrow{-2e} Th^{+} + H^{+}_{coat} + H^{+}(aq)$$

and

$$LH_2^{+} + H^{+}_{coat} \longrightarrow LH_3^{2+}$$

The overall reaction requires one half of a counterion to be incorporated into the coat to maintain electroneutrality for each electron. Therefore, one sees a reduced chloride ion flux compared with the reduction process. This technique is not as sensitive as the bismuth/bismuth oxide sensor, and so the slow ejection of this counterion as the buffer capacity of coat is reached,

$$LH_3^{2+}2A^{-} \xrightarrow{-2e} Th^{+}A^{-} + 2H^{+}(aq) + A^{-}(aq),$$

cannot be detected. A further complication of the oxidation reaction is that the coat appears permselective to chloride ion. Permselectivity depends on coat thermodynamics rather than kinetics. Therefore, it is possible that for these experiments, which are under kinetic control, the amount of perchlorate ions incorporated initially is greater than that

required by thermodynamics. There would then be a slow relaxation of the system after electrochemical reaction has finished, with chloride diffusing into the coat and perchlorate diffusing out, in order to obtain the most stable coat configuration. This would also result in a lessening of the observed chloride flux resulting from the current transient, when compared to the reduction reaction.

Experiments at a pH of 4 show little potential excursion for Th ——> L. This is consistent with the results of section (5.3.1), where the predominant reaction is the removal of two electrons and two protons from the coat, leaving the overall oxidation state unchanged.

It is sensible that these reactions involve the incorporation of anion and not the expulsion of cation. This would be expected for a coat which carries positive charge.

This technique is a useful one for measuring the flux of anions during an electrochemical reaction. In particular, the great sensitivity of this method to small disc fluxes, when the solution concentration of chloride ion is small, is attractive. However, for these potential step experiments, it is necessary for the disc to ring transit time to be greater than the time course of the reaction. This means that deconvolution of ring transients to give changes in the magnitude of the disc chloride ion flux throughout the transient is not possible. Only the mean flux can be ascertained. In order for this technique to be of comparable sensitivity to the bismuth/bismuth oxide

experiments, the potential excursion at the ring due to chloride ion must be at least of similar magnitude to the non-Faradaic potential excursion. This requires a system for which a greater flux of chloride ion is produced upon reaction.

5.3.3 The Reactions Of Coated Thionine at pH > pK_{a3}

It has been proposed that the thionine to leucothionine reaction at pH > pK_{a3} (i.e. pH > 8.4) is

$$2Th^{+}A^{-} \longrightarrow Th^{+}L^{-} + 2A^{-}(aq)$$

This reaction scheme predicts the formation of a 50:50 mixture of thionine and leucothionine. Such a conformation would be expected to be a stable intermediate in charging/discharging reactions. The formation of these thionine-leucothionine "ion pairs" and the expulsion of counterion would lead to a compact hydrophobic organic layer. This change in structure would also show marked changes in permeability. Experiments were therefore undertaken to provide evidence of the formation of this intermediate. These were performed in 0.1 M glycine buffer (pH 9.4).

5.3.3.1 In Situ Visible Spectroscopic Experiments

Figure 5.16 shows the visible spectrum of a thionine coated electrode in its oxidised form in glycine buffer (0.1 M, pH 9.4). Coated thionine has a broad absorption band in the visible, with a maximum centred around 600 nm. Leucothionine is transparent in the visible. Therefore, the absorbance of the coat is directly proportional to the amount of thionine in the coat.

Figure 5.17a shows a typical transient on stepping the potential such that the reaction Th ——> L occurs. It can be seen that there is a fast decrease in absorbance to approximately one half of the original value. This is indicative of the formation of a $Th^{+}L^{-}$ intermediate. This intermediate has a lifetime of a few seconds. A similar intermediate, stable for about a second is observed for the reverse reaction L ——> Th (Figure 5.17b). This result is further discussed in section 5.4.

5.3.3.2 'Disconnect' Experiments

In this technique, the electrode is stepped from leucothionine to thionine and the applied potential removed. The potential of the disc is then monitored with time. An example is shown in Figure 5.18. The oxidising potential was applied for one second before disconnection. Upon isolation, the disc potential jumped to -130 mV and remained stable for a few minutes. This is the E' for the coat at pH 9.4[81]. Typically, the oxidation of leucothionine by potential step methods is completed in less than 0.2 seconds (section 5.3). Therefore, the experiment is diagnostic for

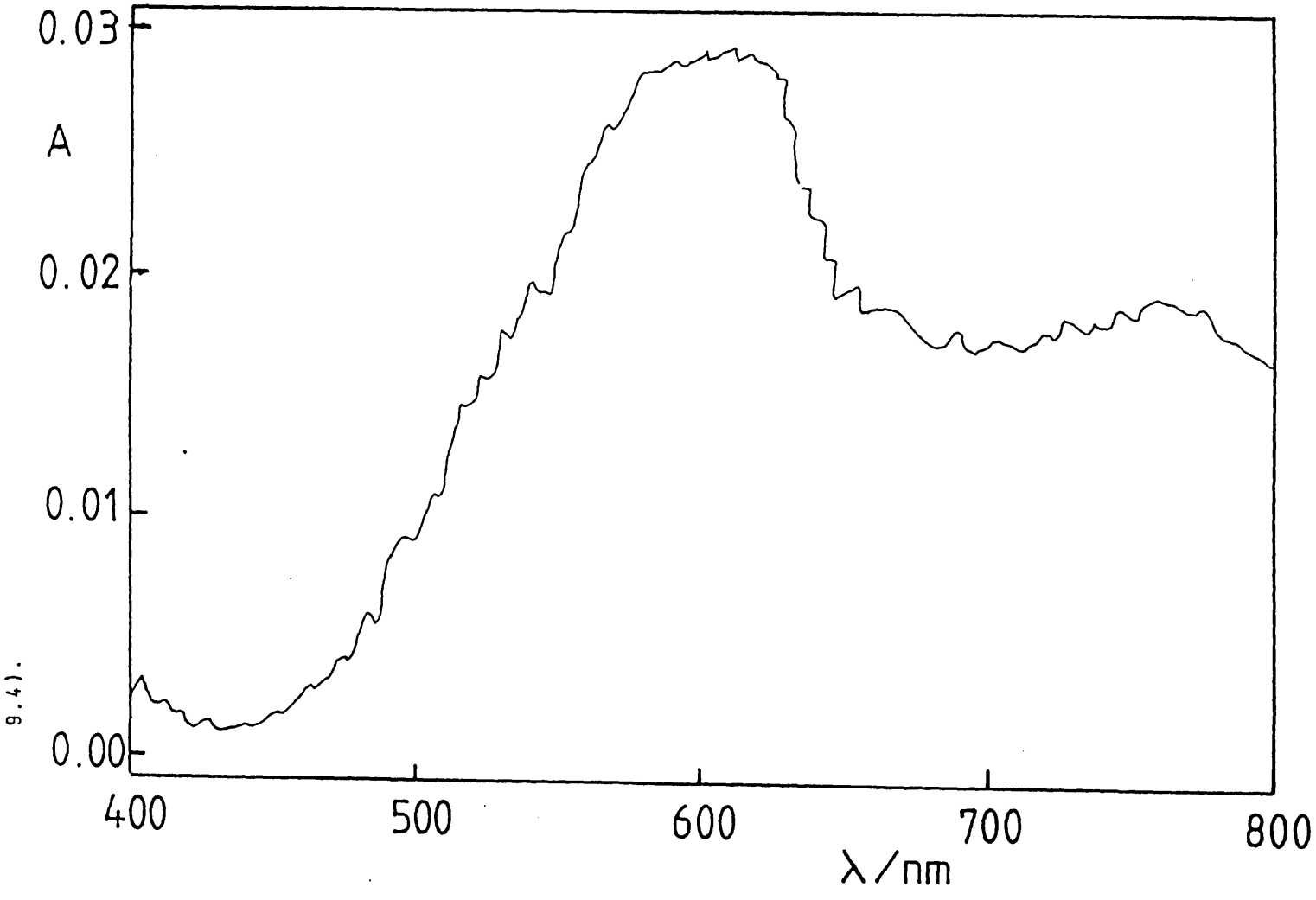
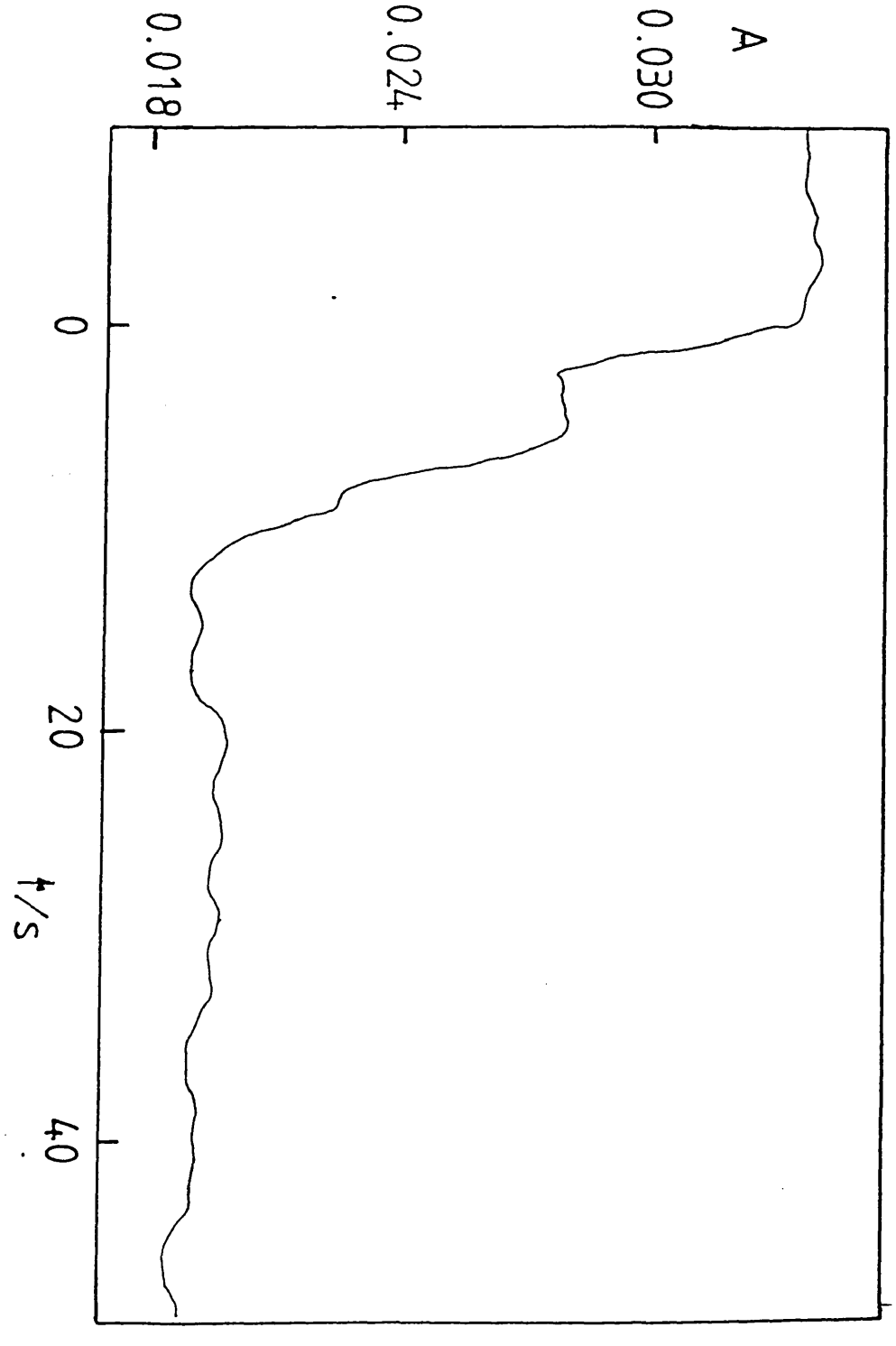


Figure 5.16 The visible spectrum of an oxidised thionine coated electrode in glycine buffer(0.1 M, pH 9.4).

Figure 5.17 Change in the absorption of a thionine coated electrode with time after the imposition of a potential step to bring about complete coat oxidation or reduction

(a) Th ⟶ L



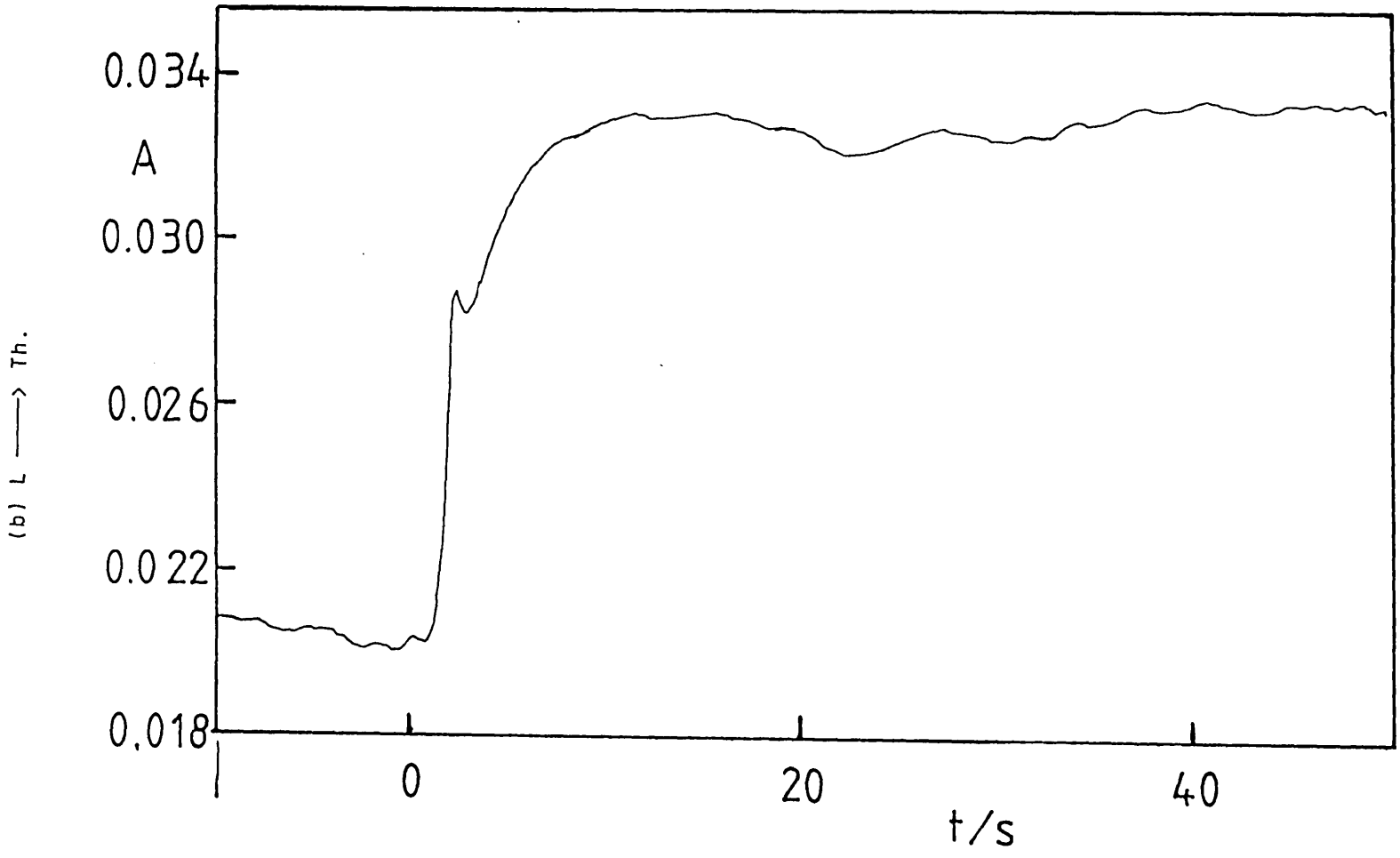
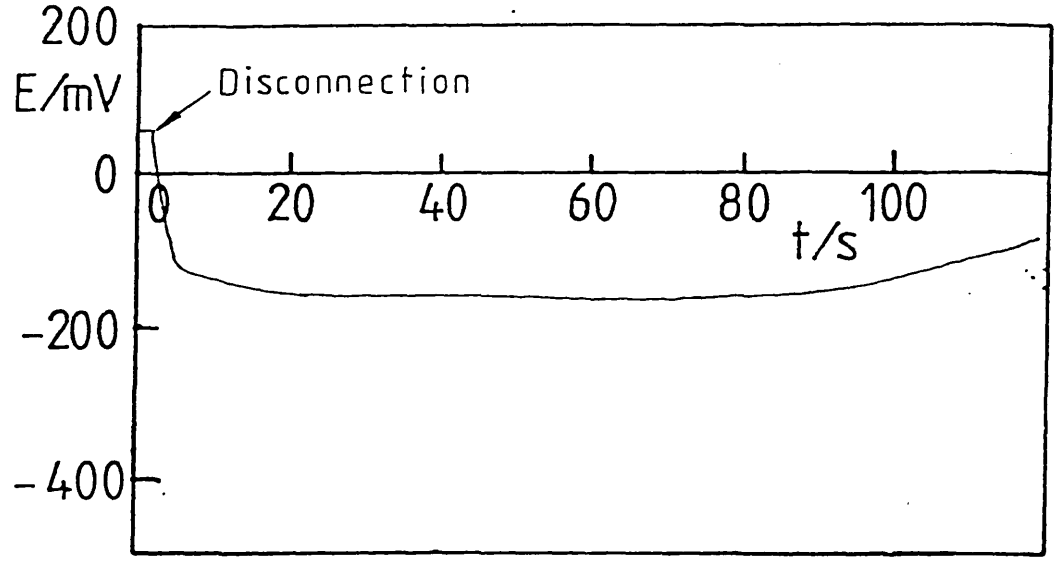
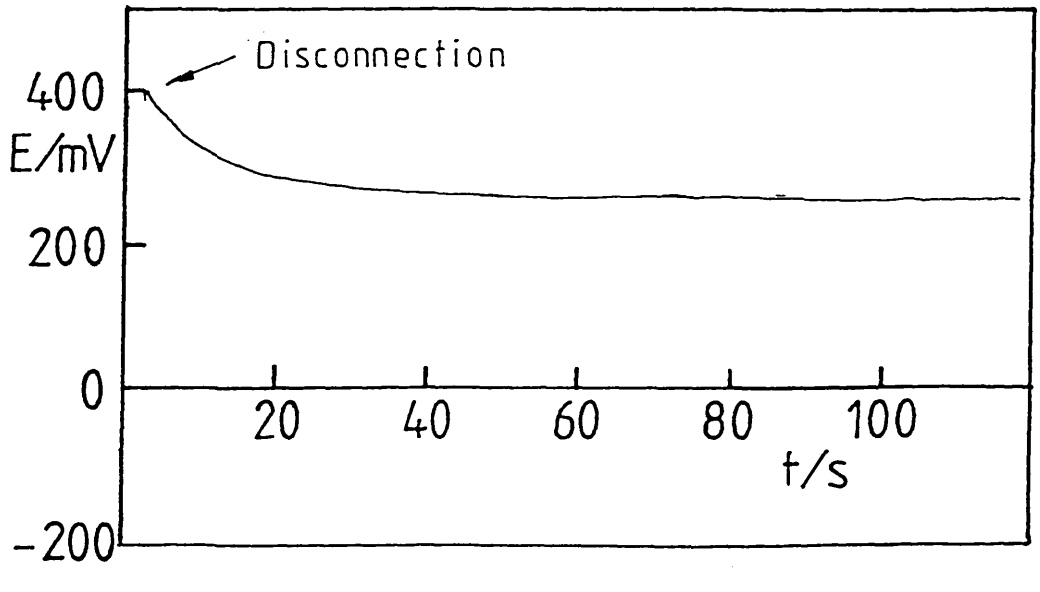

0.034
A
0.030
0.026
0.022
0.018
0
20
40
t/s
(b) L ⟶ Th.

Figure 5.18 Evolution of the potential of a thionine coated electrode with time after disconnection of the applied potential. The electrode had been oxidised for one second prior to disconnection by the application of a potential step to bring about the reaction L ——> Th.

(a) glycine buffer (0.1 M, pH 9.4)



(b) H_2SO_4 (50 mM).



the formation of a stable $Th^{+}L^{-}$ intermediate. The gradual increase in electrode potential with time is due to slow air oxidation of the coat. Similar experiments at pH 1.2 show the disc potential is unstable and remains hundreds of millivolts above E' upon disconnection. Variation of the time of application of the oxidation potential indicates that the lifetime of this intermediate is of the order of 2 seconds.

5.4 Kinetics Of Large Step Chronoamperometric Experiments

5.4.1 Effects of Mechanistic Change

The bismuth/bismuth oxide results presented in section 5.3 show that for a large step coat reduction, at bulk pH values between 5 and 8, pH > pK_{a2}, pK_{a3} at the disc. Thus the initial reaction is

$$2Th^{+}A^{-} \xrightarrow{2e^{-}} Th^{+}L^{-} + 2A^{-}$$

i.e. the formation of a 'locked' species of thionine-leucothionine pairs. Further reduction can be brought about by one of two methods.

Firstly, proton can diffuse into the coat such that at the disc, pH < pK_{a3}, and the reaction

$$Th^{+}L^{-} \xrightarrow{2e,2H^{+}} 2LH \qquad ....(5.4)$$

can occur. A second competing relaxation mechanism is

$$Th^{+}L^{-} \xrightarrow{2e,2Na^{+}} 2L^{-}Na^{+} \qquad ....(5.5)$$

The cation relaxation mechanism will occur exclusively in the experiment performed at bulk pH 9, where ion pair destruction by proton is not possible. This is shown in Figure 5.6a. The constant current at short time indicates the formation of a highly resistive layer. A large concentration of ion pairs is present throughout the coat and this is likely to produce a more compact, hydrophobic layer. Diffusion of sodium ions in the coat would be slow and effected by a migrational field.

For all other reduction experiments in which the ion pair species are formed, it can clearly be seen that as

the bulk pH is reduced, the time course of the current transient is also reduced. This can be explained by two processes. Firstly, there is the increased importance of reaction (5.4) in unlocking the coat. Initially, the disc pH for these experiments is less than 8. Therefore, the concentration of proton in the coat is low, and negligible compared with the bulk. Thus an increase in the bulk pH will result in a greater flux of proton to the coat. This will result in faster ion pair destruction leading to a more rapid reduction reaction. Secondly, as the bulk pH becomes more acidic, more leucothionine must be formed to push the disc pH to 8.4. This means that less ion pairs will be formed and faster coat diffusion will be possible.

The experiment performed at pH 4 does not involve the formation of any ion pairs - it is not surprising that this is the fastest reduction of all.

For the oxidation reaction (Figure 5.6b), only the experiment at bulk pH 9 will involve the formation of ion pairs. This transient is the slowest of all the oxidation transients. However, it is interesting to note that its time course is much faster than the reduction reaction. This indicates that the coat has a more open structure in this case. This result can be contrasted with potential step experiments performed in glycine buffer. The experiments reported in section 5.3.3 indicated that the coat has a more compact structure during oxidation, with the 50:50 ion pair intermediate being stable for about a second.

Figure 5.19 shows a typical current time transient for oxidation. It can be seen that reaction is indeed slower in this medium compared with sodium perchlorate. Hence, it appears that the porosity of the coat in its locked state is dependent upon the nature and concentration of the background counterions present. Such variations may explain the observed differences between the charging and discharging reactions.

Further work is required to investigate this effect for a wide variety of electrolytes.

With the exception of the oxidation experiment at bulk pH 4, all other oxidation reactions involve a disc pH traversal of the pK_{a1} boundary, and, therefore, a change in coat reaction. It is not surprising that such transients do not fit simple modified Cottrell theory.

5.4.2 Effect of Step Size

It is clear that changes in disc reaction mechanism due to coat buffering can have profound effects on the redox reaction rate. It is also desirable to investigate coat charge/discharge reactions of thionine in the absence of such a complication. This is the case for experiments performed in 0.1 M $HClO_4$ supporting electrolyte, at pH 1. Figures 5.20a and 5.20b show the effect of the magnitude of the large step upon the observed current transient, for both oxidation and reduction. Each potential is sufficient for coat reaction to go to completion. This means that the reactions are not under electrochemical control. Therefore, the increase in electrode kinetics

Figure 5.19 Large step chronoamperometric data for the reaction L ——> Th in glycine buffer (0.1 M).

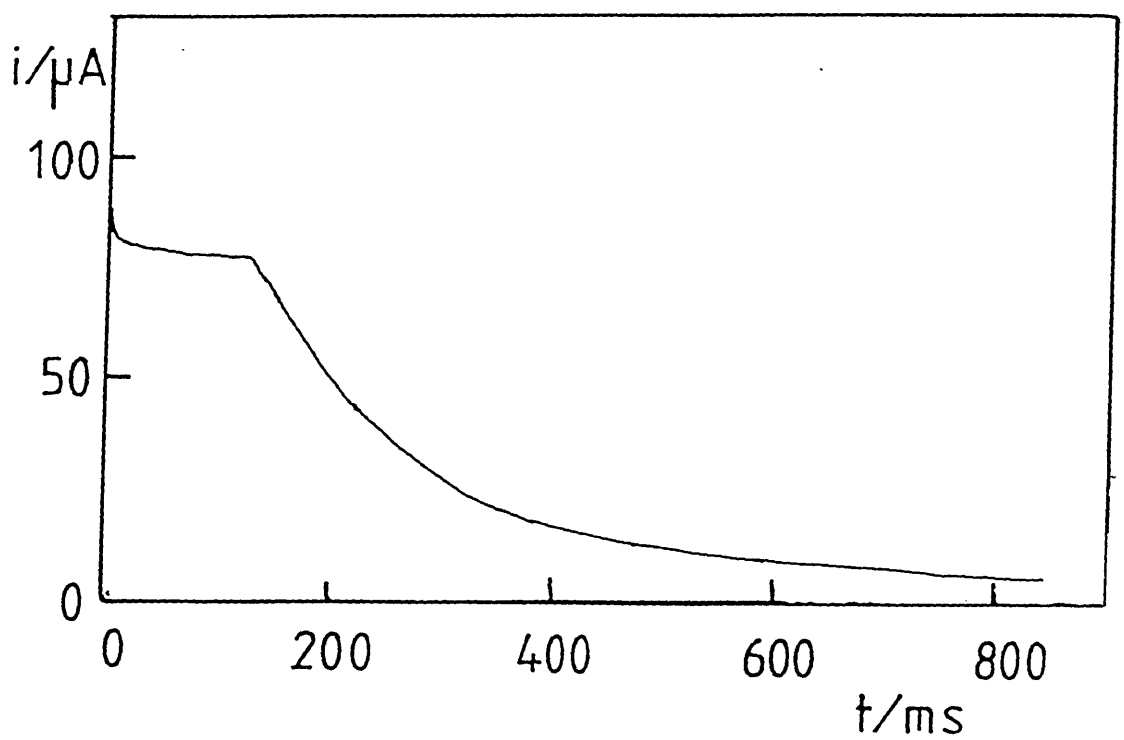
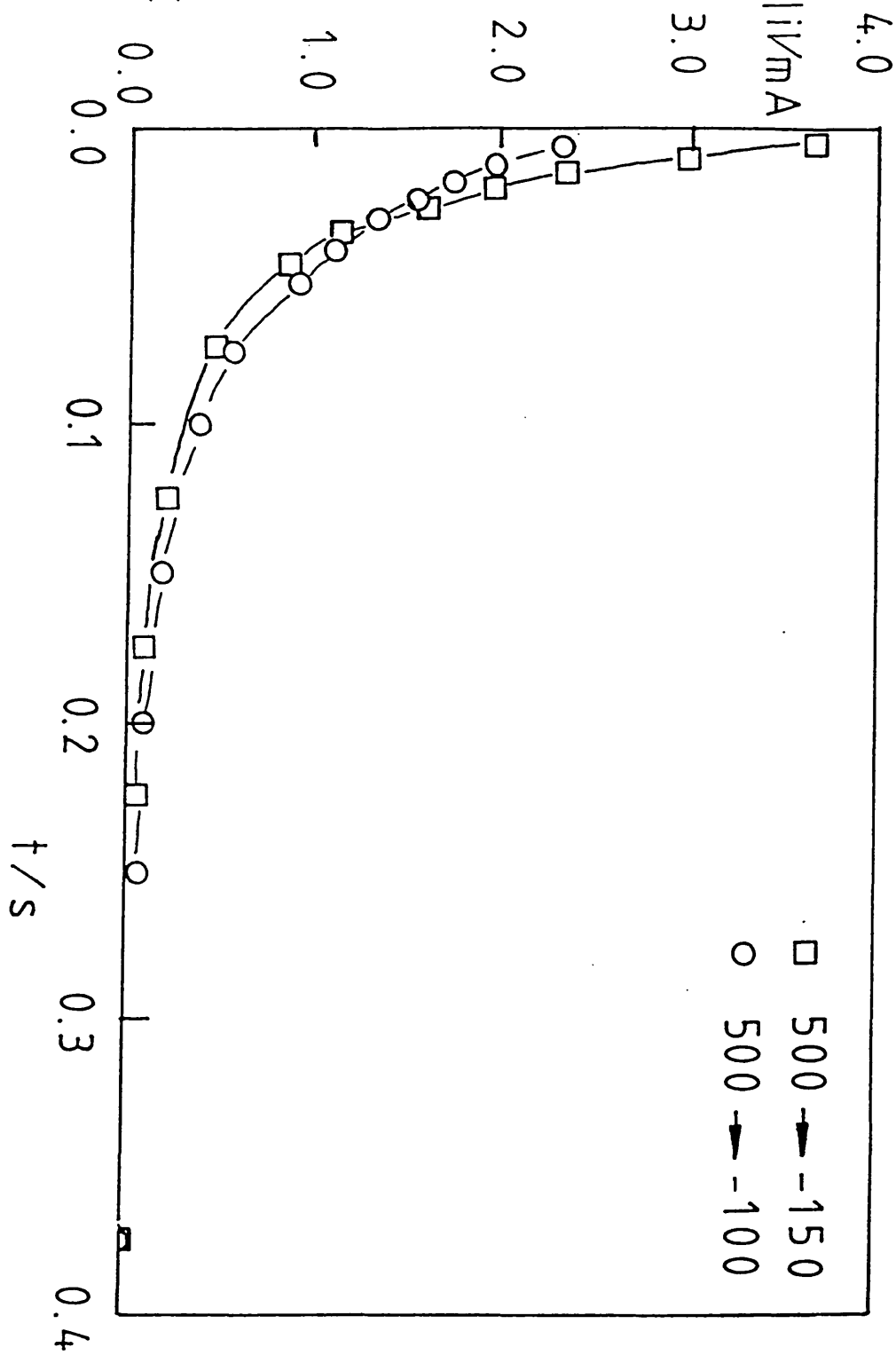
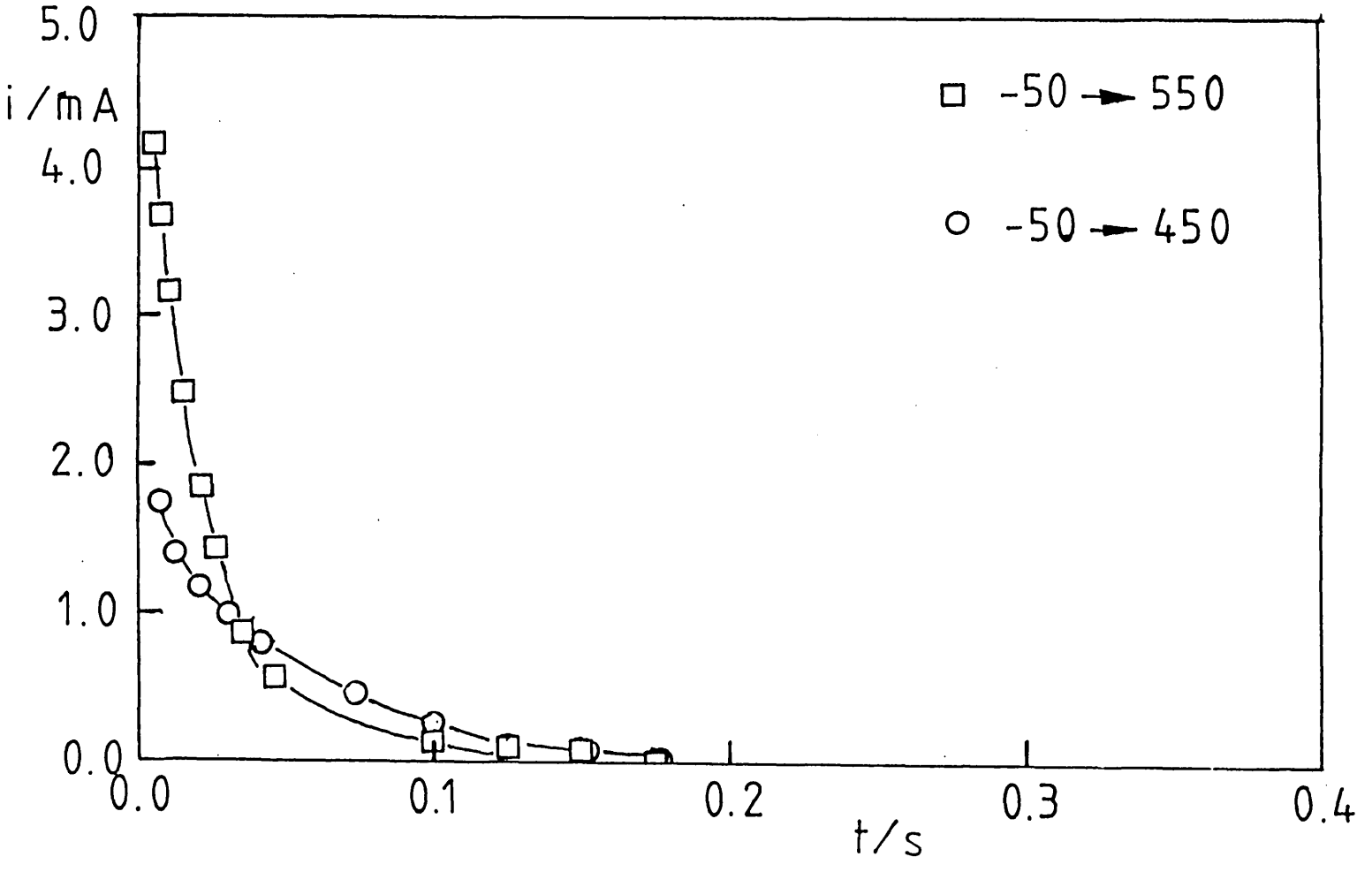


Figure 5.20 The effect of the magnitude of the potential step when performing large step chronoamperometry on a thionine coated electrode in $HClO_4$ (0.1 M) solution.

(a) Th ⟶ L




5.0
i/mA
4.0
3.0
2.0
1.0
0.0
0.0
0.1
0.2
0.3
0.4
t/s
□ -50 → 550
○ -50 → 450
(b) L ⟶ Th.

observed on increasing the step size is indicative of the importance of migration in the electrode reaction. No enhancement of reaction rate would be observed for a purely diffusional process.

5.4.3 Effect of Anion Size

Figure 5.21 shows the species used to make large anion buffer solutions. The pK_a values of these molecules were chosen to span the pH 3-8 range. Typically the transients produced were of a time scale 3-10 times slower than those for buffered ClO_4^- or Cl^- solutions and unbuffered ClO_4^- or Cl^- solutions of low pH (Figure 5.22). Thus, as with small step experiments, the rate of coat reaction is dependent upon anion size. Thus, as is the case for the small step experiments, it appears that anion transport is involved in the rate determining step.

Figure 5.21 The large anion biological buffers used in these experiments.

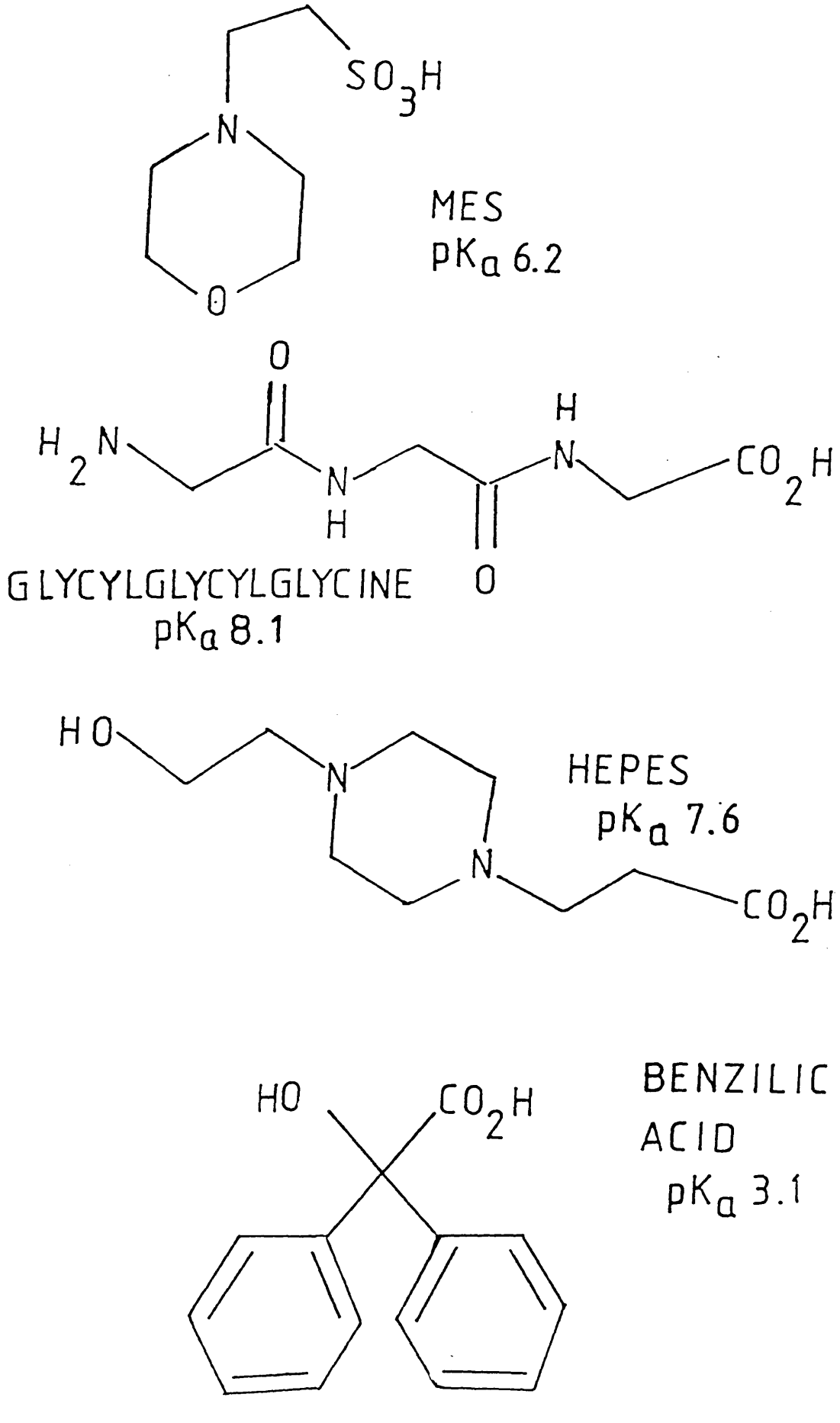
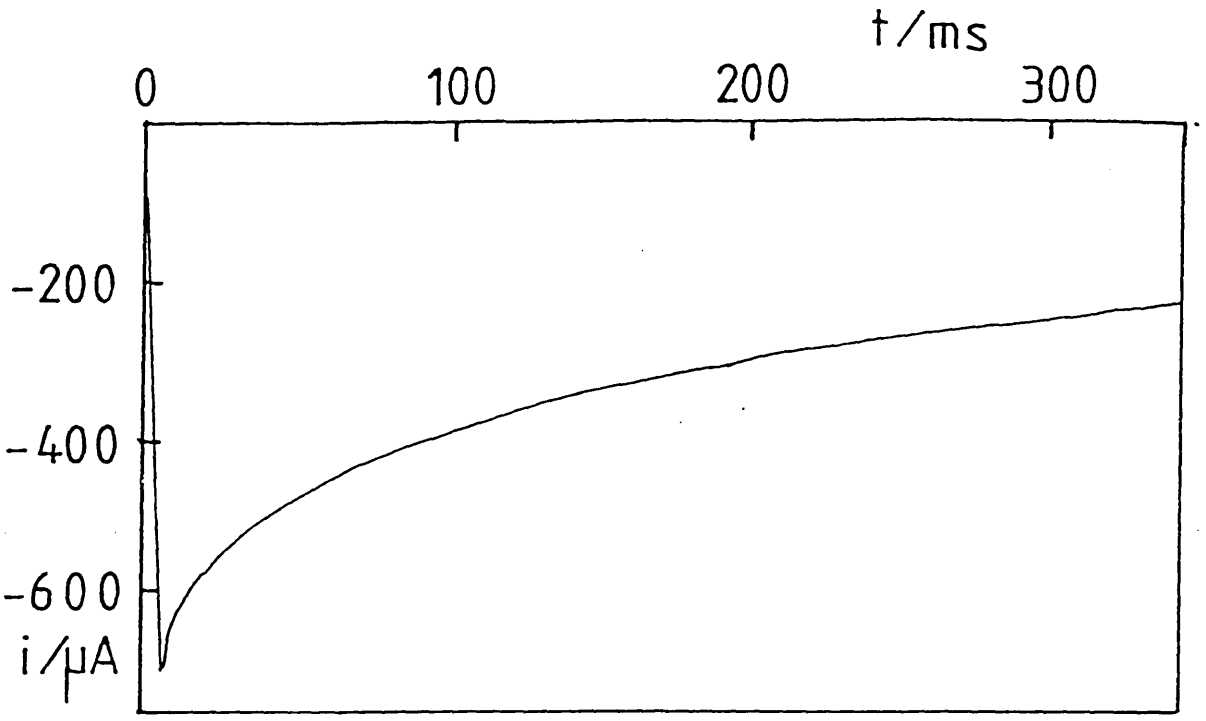
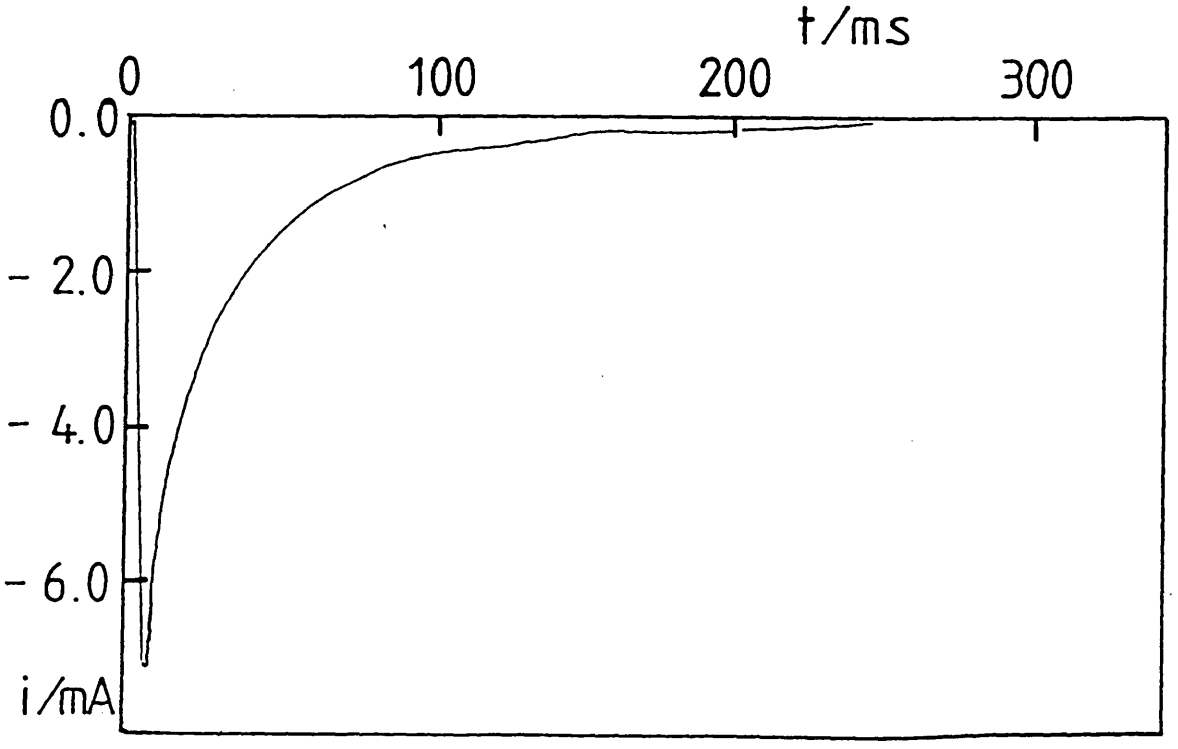


Figure 5.22 Large step chronoamperometric data for the reaction Th ——> L at a coated electrode.

(a) in MES buffer (0.1 M; pH 5.5)



(b) in $HClO_4$ (0.1 M).



5.5 In Situ Laser Raman Spectroscopic Studies

Thionine modified gold electrodes have been shown to exhibit a surface enhanced resonance Raman (SERR) signal when excited by 647.1nm laser radiation[85]. No signal was detected for the leucothionine form. The exact nature of the surface enhancement mechanism is still under debate[138]. However, observations on thionine[85] and other systems[138] have indicated that the Raman signal is due to the layers closest to the gold electrode. This is supported by the observation that similar Raman intensities are produced from electrodes coated with three layers and ten layers of thionine.

Figure 5.23 shows the in situ SERR spectrum of a thionine electrode held in the oxidised form at pH 1.2. The dominant feature is the strong, sharp peak at 479 cm^{-1}. This has been asigned to the δ(CNC) skeletal deformation of the thionine molecule. Therefore, the intensity of this peak was followed with time during chronoamperometric experiments. This allows one to probe the oxidation state of the innermost layers of the coat. Comparison of this data with the integrated current transient, which gives information on the oxidation state of all of the coat, will give information on the location of the reaction zone.

Figure 5.24 shows the variation in intensity of this peak during the charging and discharging reactions. For both oxidation and reduction, the change in the Raman signal is sharp and immediate, in marked contrast to the injection or removal of charge. This implies that reaction

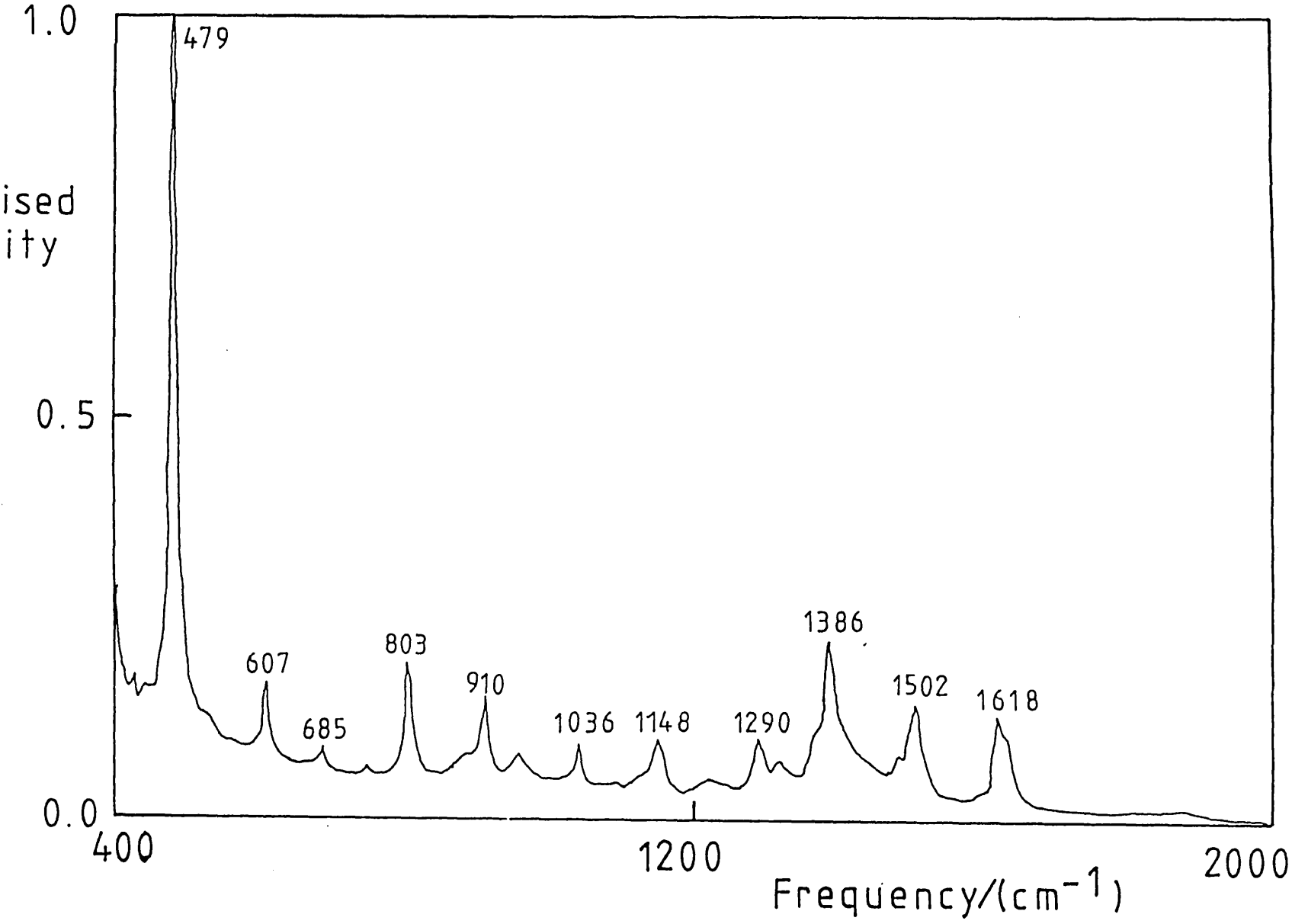
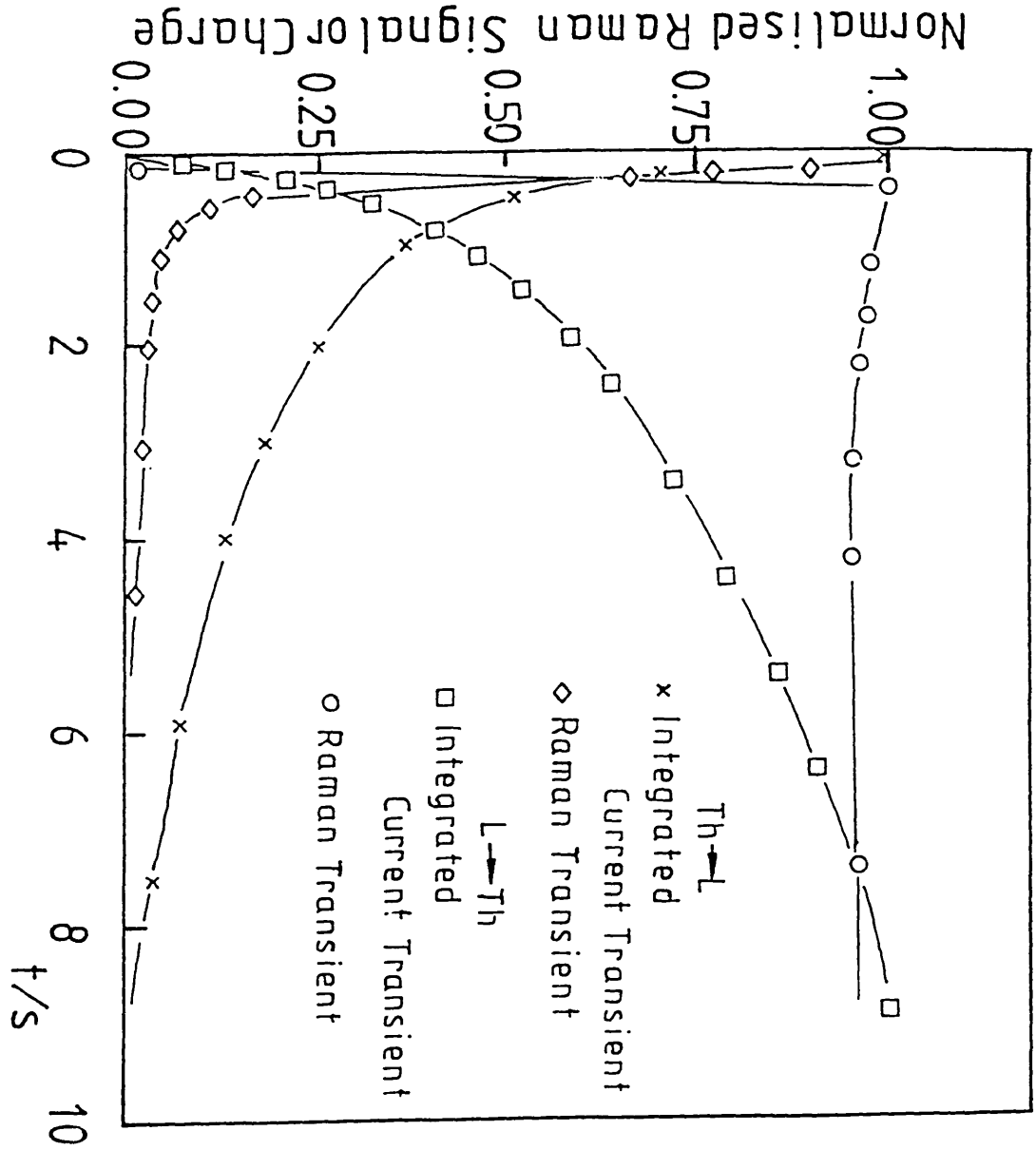


Figure 5.23 SERR spectrum of an oxidised thionine coat in H_2SO_4 (50 mM).

Figure 5.24 The variation in intensity of the 479 cm^{-1} Raman peak throughout the coat reactions Th ——> L and L ——> Th in H_2SO_4 (50 mM).



is initially located at the electrode/coat interface. A fast change in the Raman signal is observed at all pH values, implying that the layers closest to the electrode are all ways the first to react. This is in direct contradiction to the predicted location at the coat/electrolyte interface for reactions in which diffusion of anion into the coat is rate limiting. This will be further discussed in section 5.6. Figure 5.25 shows the SERR spectrum of the coat in 0.1M glycine at pH 9.4. The absolute intensity of the peak at 479 cm^{-1} has decreased while that of the complex structure at ~1400 cm^{-1} has risen dramatically. This set of peaks has been assigned to the asymmetric and symmetric CN stretches of the intermolecular thionine bonds[85]. Table 5.1 shows the variation of the relative intensities of the major Raman peaks due to the oxidised coat with pH. These have been normalised with respect to the intensity of the peak at 479 cm^{-1}.

These changes are not due to the change in electrode potential required to oxidise thionine upon changing the pH. Generally, the ratio of the spectral peak intensities vary with pH at any given potential, but show little dependence on potential at constant pH. Similarly, the peak intensities appear relatively insensitive to the nature of the background anion. This change is probably due to changes in coat stucture due to the creation and destruction of hydrogen bonds.

The largest changes in intensity can clearly be

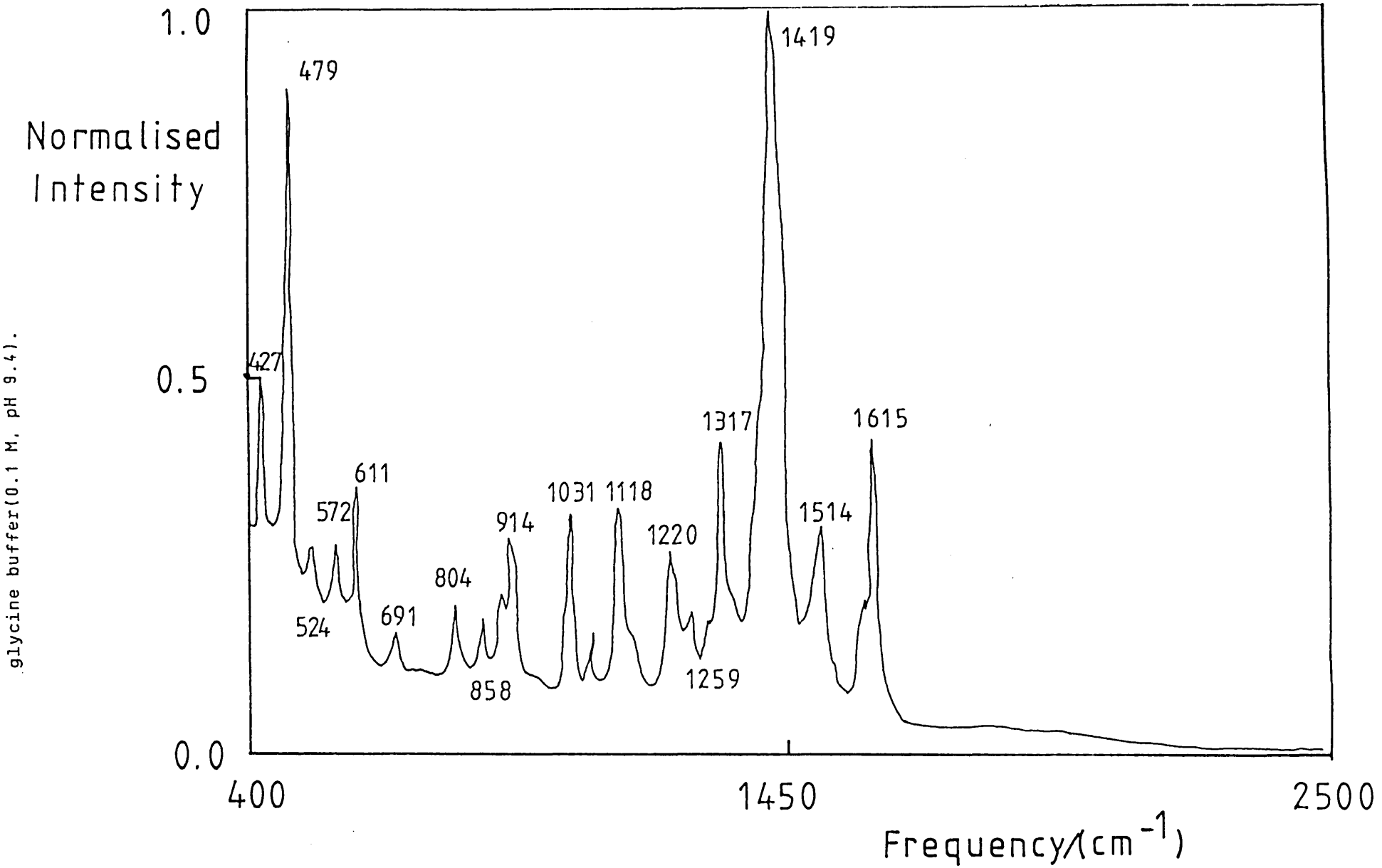


Figure 5.25 SERR spectrum of an oxidised thionine coat in glycine buffer(0.1 M, pH 9.4).

Table 5.1 In Situ SERR Data For Oxidised Thionine Coats Normalised With Respect To The Intensity Of The Peak At 479 cm^{-1}

Normalised Intensity

Peak pos. /(cm^{-1}) and Assignment	610 in pl. skel. def.	1040 β(CH)	~1400 ν(CN)	1502 $\delta(NH_2)$	1620 ν(CC)
Solution, pH					
0.01 M HCl, 2.0	.12	.09	.29	.17	.17
0.1 M Acetate Buffer, 4.1	.10	.10	.36	.17	.22
0.1 M Phosphate Buffer, 7.4	.11	.11	.44	.15	.24
0.1 M HEPES Buffer, 8.0	.20	.27	.82	.33	.60
0.1 M Glycine Buffer, 9.4	.14	.25	.88	.52	.58

observed above pH7. Therefore, in this region, calibration of these effects would allow the change in the Raman signals to act as a sensitive detector of the pH of the coat.

This effect can be seen for the potential step experiment shown in Figure 5.26 at pH 8. The reaction at this pH is

$$LH_2^+ \xrightarrow{-2H^+,2e^-} Th^+$$

The L ——> Th Raman signal rises sharply but the long time decay of signal can be assigned to the relaxation of disc pH from a value less than that in the bulk. That this behaviour has been observed in both buffered and unbuffered solution indicates that 0.1 M large anion buffer solutions are not able to buffer this coat reaction completely, because the rate of change of concentration of proton within the coat is too large.

Further changes in Raman intensity are also observed upon forming the Th^+L^- intermediate. Figure 5.27 shows data for the reaction Th ——> L at pH 6.2 in unbuffered solution. The initial rise in intensity of the Raman signal is assigned to the formation of the Th^+L^- complex. Evidence for this can be found by investigating the change in intensity with potential of this peak at pH 9.2. This can be seen to go through a maximum at E', where the stable Th^+L^- intermediate is formed.

Figure 5.26 The variation in intensity of the 479 cm^{-1} Raman peak throughout the coat reactions Th ⟶ L and L ⟶ Th in HEPES buffer (0.1 M, pH 8.1).

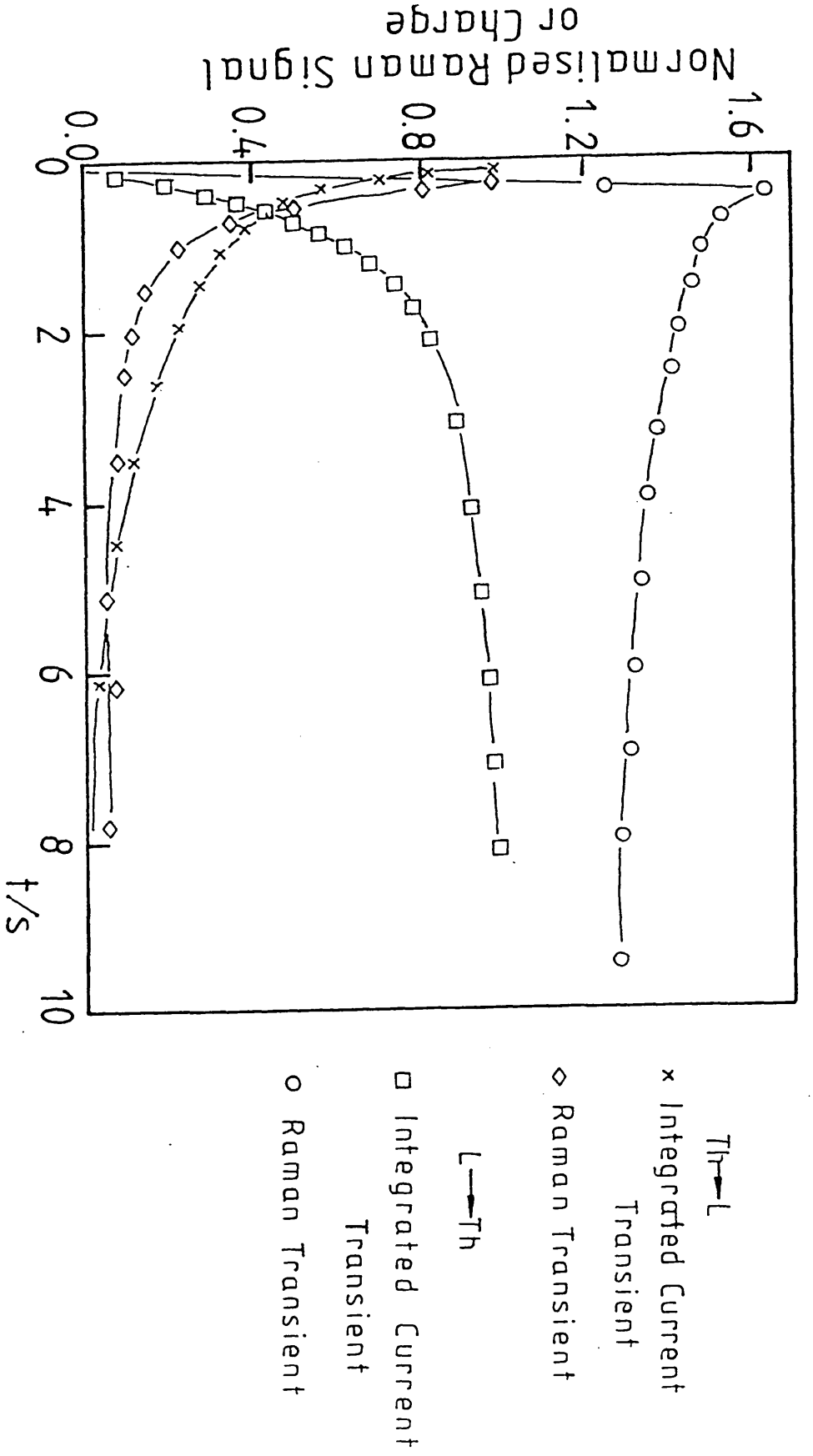
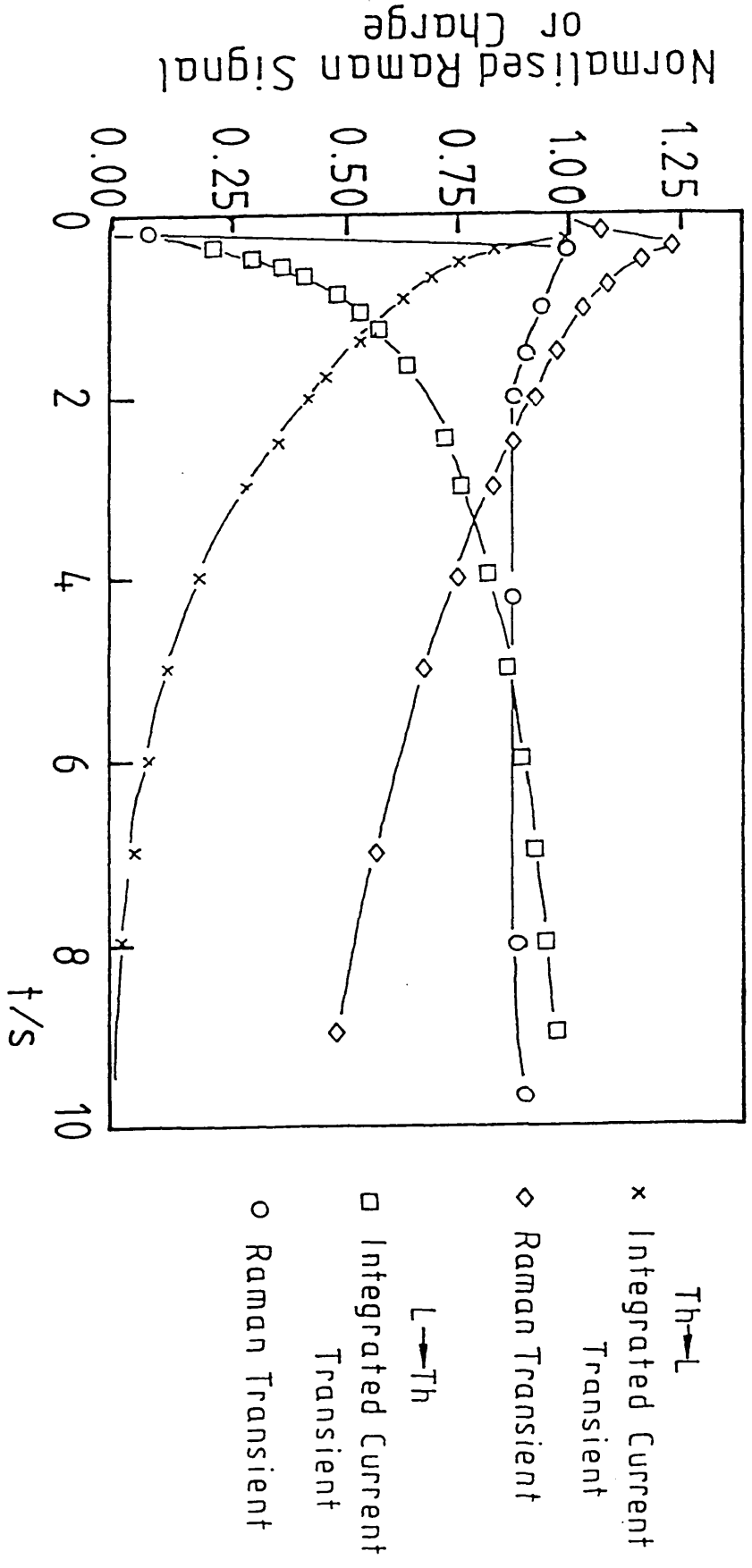


Figure 5.27 The variation in intensity of the 479 cm^{-1} Raman peak throughout the coat reactions Th ⟶ L and L ⟶ Th in KCl (0.1 M, pH 6.2).



5.6 Discussion- The Formulation Of A General Model For Chronoamperometry At The Thionine Modified Electrode

The experimental evidence of section 5.4.3 indicates that the time scale of the current transient observed for large step chronoamperometry is dependent upon the size of the counteranion present. This implies that the rate determining step for the coat reaction involves the incorporation of counteranion, in order to maintain coat electroneutrality. This is in agreement with small step chronoamperometric data (section 5.2). In this case, reaction would be expected to proceed at the coat/electrolyte interface. This is because electron transport across the the layer is fast compared to anion transport. Therefore, coat reaction would initially occur where the change in anion concentration is most rapid. This is at the polymer/electrolyte interface. This type of argument has been used to explain the observed hysteresis of the change in the Raman signal at 479 cm^{-1} with the degree of coat oxidation, on performing cyclic voltammetry[85].

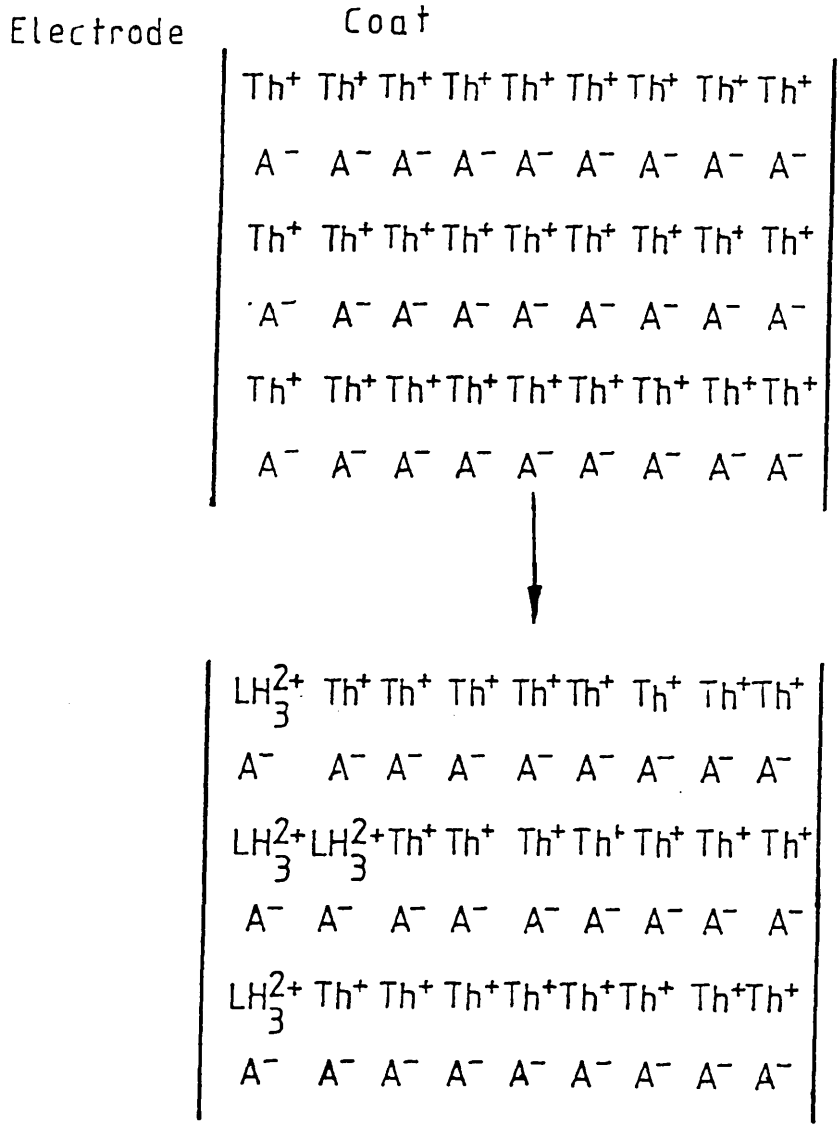
However, paradoxically, the results presented in section 5.4 for large step chronoamperometry are not consistent with this reaction scheme. For these experiments, the change in Raman signal is sharp and immediate. Since this technique is sensitive to the layers closest to the electrode, this indicates that these layers are the first to change. The results presented in this

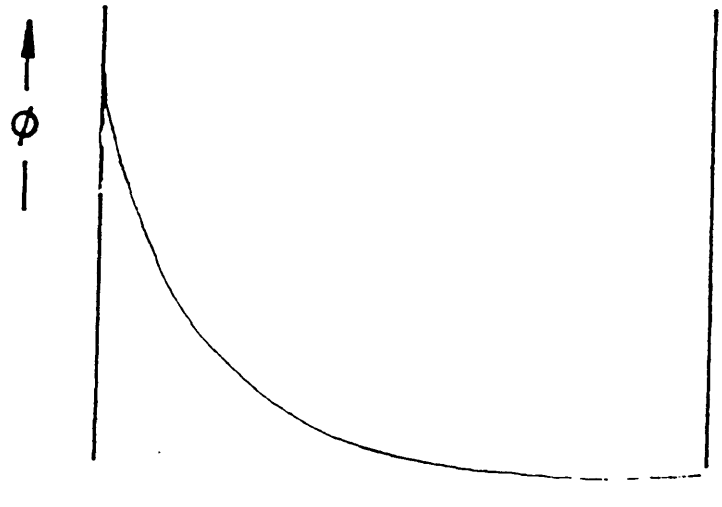
chapter also indicate that the large step experiments are more complex. Significant changes in the shape and time course of the current transients occur on varying the bulk pH, and the magnitude of the potential step. This makes the modelling of the reaction very difficult. However, a general hypothesis can be proposed to explain this behaviour. Further evidence is required to either confirm or deny this model.

It is proposed that the inner layers are indeed the first to change. This produces a breakdown of electroneutrality within the film. As an example, Figure 5.28 shows a schematic representation for the reduction of coated thionine at pH 1. Excess positive charge is produced at the electrode as $Th^{+}...A^{-}$ reacts to form $LH_3^{2+}...A^{-}$. The formation of this species will be thermodynamically less favourable than the production of $LH_3^{2+}...2A^{-}$. However, the magnitude of the large step provides of the order of 300-400 mV of overpotential over E',to enable this process to occur. It is not possible for the leucothionine species co-ordinated to two anions to be formed, as the concentration of anion in the coat is too small, initially. The production of this species will give rise to a field within the layer, as excess positive charge is present. This will speed the movement of counterion into the layer, as transport by migration as well as diffusion will be of importance.

The importance of migration in these large step reactions has been shown by the experiments presented in

Figure 5.28 Schematic representation of the proposed initial reaction on performing complete coat reduction at pH 1 and the electrostatic field produced across the layer.





section 5.4.2. This data shows that increasing the magnitude of the applied potential step increases the rate of the film redox reaction. Since, for each of these steps, complete conversion of the thionine centres occurs, this is unlikely to be due to a change in the electrochemical rate constant for electron transfer to and from the thionine species. Also, the small step experiments indicate that the rate determining step is not electron transfer. For these experiments, a reaction under pure diffusion control would show no dependence of the observed current on the size of the potential step. Such a dependence would be expected if migration in the layer were important. The increase in potential step will allow a still greater breakdown of electroneutrality, increasing the migrational field and speeding anion transport within the film. It is also pertinent that none of the large step experiments fit modified Cottrell theory, which is derived assuming a diffusional process. Generally, the time course of the large step reactions is less than that for the small step experiments. This is consistent with an increased rate of reaction due to the effects of migration.

Small potential steps of 10-20 mV about the E' of the coat result in much less perturbation of the concentrations of thionine and leucothionine. There is no driving force for any significant breakdown of electroneutrality, and as a consequence, migration across the layer is unimportant. This would explain the

observation that these transients show modified Cottrell behaviour. Cyclic voltammetric experiments would also not be expected to involve the formation of a significant amount of uncompensated charged centres in the layer, unless very fast sweep rates are involved. This is because the transport of anion into the layer to quench this excess charge should be faster than the rate of oxidation of the coat.

5.7 The Applicability Of The Techniques Presented In This Chapter

The results presented in this chapter have illustrated the value of in situ spectroelectrochemistry. The measurement of current, potential and charge provides information about the kinetics and mechanism of electrode reactions. However, this data is indirect, and one has little evidence concerning the nature of reaction intermediates, any changes in coat structure or the presence of more than one redox reaction. It is clear that such information can be provided by the use of in situ spectroscopy.

Further to this, it is evident that the potentiometric ring sensors developed in this work provide complementary information to spectroelectrochemistry. Knowledge of the flux of protons and counteranion has proved invaluable in probing the variation of the reaction mechanism of thionine coated electrodes with pH. This has proved invaluable in the interpretation of both chronoamperometric and spectroscopic data. Such data cannot be obtained spectroscopically, as these ions do not contain active chromophores. These sensors are specific and more sensitive than the amperometric ring techniques for the detection of these species. A combination of these techniques has led to the elucidation of a model for the charging and discharging of the thionine coat. Many modified electrodes contain chromophores and incorporate or

expel protons and/or anions upon reacting. In these cases, this application of these techniques to probe coat kinetics and mechanism should be of great value.

APPENDIX

The BASIC computer program, BISMUTH, for the calculation of the flux of proton or hydroxide ion at a rotating disc electrode from the potential of a bismuth/bismuth oxide ring sensor.

```
  10 REM ***THIS PROGRAM CALCULATES DISC PROTON/HYDROXIDE ION FLUX
  20 REM ***ACCORDING TO THE THEORY PRESENTED IN SECTION 2.2.2.3
  30 REM DATA IS INPUT IN THE FORM:
  40 REM t(s) and the measured bismuth/
  50 REM bismuth oxide ring potential(mV)
  60 REM ************************************************************************
  70 REM ************************************************************************
  80 REM
  90 *FX5,1
 100 *FX6,10
 110  MODE1:@%=&500
 120 GOSUB 1090
 130PRINT
 140DIM X(50),Y(50),Z(50):RO=3:FLAG=0
 150 REM ************************************************************************
 160 REM
 170 REM print main menu
 180PRINT TAB(5,15)"<1> ENTER NEW DATA":PRINT TAB(5,17)"<2> RECALL STORED DATA ":PRINTTAB(5,19)"<3>
CONTINUE WITH SAME DATA"
 190INPUTQQ:IF QQ<1 OR QQ>3 GOTO 190
 200ON QQ GOTO 240,920,910
 210 REM ************************************************************************
 220 REM
 230 REM keyboard data input
 240CLS:PRINT"ENTER / TO END DATA":PRINT:
 250 PRINT"ENTER t IN SECS AND Bi POT IN mV"
 260 INPUT LINE"TITLE";TITLE$
 270  FOR J=1TO50
 280 PRINT"t-VALUE FOR POINT ";J;" ";:INPUT X$:X(J)=VAL(X$):IFX$="/"THEN J=50:GOTO310
 290PRINT"Bi(mV)-VALUE FOR POINT ";J;" ";:INPUT Y$:Y(J)=VAL(Y$)
 300 PRINT:CT=CT+1
 310NEXTJ
 320 REM ************************************************************************
 330 REM
 340 REM linear regression calculation
 350 START=1:FINISH=CT
 360A=0:B=0:C=0:D=0:E=0:F=0
 370 PROCSORT:REM sort data in increasing t
 380CLS:VDU14;28,0,28,39,0
 390 REM ************************************************************************
 400 REM
 410 REM print data
 420 IF FLAG=0 THEN PRINTTITLE$:PRINT:  PRINT"  POINT      t            Bi(mV)" ELSE PRINTTITLE$:P
RINT:  PRINT"  POINT       t       j/molcm-2s-1  eq"
 430PRINT"----------------------------------------"
 440 FORJ=1TOCT
 450PRINT TAB(4);J;
 460 IF FLAG=0 THEN PRINTTAB(15);X(J);:PRINT TAB(24);Y(J) ELSE PRINTTAB(15);X(J);:PRINT TAB(24);Y(J
);:PRINTTAB(39);Z(J)
 470NEXTJ
 480PRINT:PRINT"----------------------------------------"
 490 VDU3;15;26
 500 REM ************************************************************************
 510 REM
 520 REM data editing
 530PRINTTAB(0,30)"     <1>ADD POINT <2>DELETE POINT     ":PRINT"     **Press RETURN to continue**
  ";
 540INPUT K$:IFK$=""THEN GOTO1130
 550 K=VAL(K$)
```

```
  560  IF K <1 OR K >2 THEN GOTO 540
  570 ON K GOTO 580,610
  580CT=CT+1:INPUT"X-VALUE";X(CT) :REM Add a point
  590 INPUT"Y-VALUE";Y(CT)
  600GOTO350
  610 INPUT"WHICH POINT";P :REM Delete a point
  620 FORJ=P TO CT-1
  630 X(J)=X(J+1)
  640 Y(J)=Y(J+1)
  650 NEXT J
  660 CT=CT-1
  670GOTO350
  680 REM ************************************************************************
  690 REM
  700 REM Print data table on printer
  710 VDU2: PRINT:PRINT:PRINT:GOTO420
  720 REM ************************************************************************
  730 REM
  740 REM Store data on disk
  750 IF FLAG=0 THEN GOTO 1130
  760 PRINT"FILENAME?ALL FILES START WITH B"
  770 INPUT F$:F$="B"+F$
  780Z= OPENOUT F$
  790 ONERROR GOTO 840
  800 PRINT£Z,TITLE$
  810FOR J=1TO CT
  820 PRINT£Z, X(J),Y(J),Z(J)
  830 NEXT J
  840 CLOSE£Z
  850 ONERROR OFF
  860 REM ************************************************************************
  870 REM
  880 REM call program to plot graph on screen and dump to printer
  890 IF QQ=5 AND FLAG=1 THEN CHAIN "SHUP1"
  900 GOTO1130
  910 F$="TTTT": GOTO 950
  920CLS:*CAT
  930 REM Recall data from disk
  940 INPUT"FILENAME";F$:IF LEFT$(F$,1)<>"B" THEN GOTO1130
  950 Z=OPENIN F$
  960 ONERROR GOTO 1030
  970 J=0
  980 INPUT£Z,TITLE$
  990 REPEAT
 1000 J=J+1
 1010 INPUT£Z,X(J),Y(J),Z(J)
 1020 UNTIL EOF£Z
 1030 CLOSE£Z
 1040 FLAG=1
 1050 ONERROR OFF
 1060 CT=J
 1070 GOTO350
 1080 GOTO360
 1090  PRINT TAB(6,6)"BISMUTH PH7 ANALYSIS":RETURN
 1100 REM ************************************************************************
 1110 REM
 1120 REM Display menu
 1130 CLS:PRINT TAB(5,3)"<1>LIST DATA":PRINT TAB(5,5)"<2>SAVE DATA":PRINTTAB(5,7)"<3>PRINT DATA":PR
NTTAB(5,9)"<4>CALCULATE FUNCTION":PRINTTAB(5,11)"<5>DRAW GRAPH"
 1140 PRINT:PRINT
```

```
 1150 REM ************************************************************************
 1160 REM
 1170 INPUTQQ:IF QQ<1 OR QQ>5 GOTO1170
 1180  ON QQ GOTO 380,740,700,1220,1270
 1190 REM ************************************************************************
 1200 REM
 1210 REM calculate proton and hydroxide fluxes
 1220 PROCCALCULATE: GOTO 360
 1230 END
 1240 REM ************************************************************************
 1250 REM
 1260 REM replace dummy file on disc
 1270 CLS:CLOSE£0:*DELETE TTTT
 1280F$="TTTT":GOTO780
 1290 REM ************************************************************************
 1300 REM
 1310DEF PROCSORT
 1320 LOCAL N,M
 1330 FOR N=CT-1 TO 1 STEP -1
 1340 FOR M=1 TO N
 1350 IF X(M)>X(M+1) THEN PROCSWAP(M)
 1360 NEXT M
 1370 NEXT N
 1380ENDPROC
 1390 REM ************************************************************************
 1400 REM
 1410DEF PROCSWAP(K)
 1420 LOCAL HOLD
 1430 HOLD=X(K):X(K)=X(K+1):X(K+1)=HOLD
 1440 HOLD=Y(K):Y(K)=Y(K+1):Y(K+1)=HOLD
 1450 ENDPROC
 1460 REM ************************************************************************
 1470 REM
 1480 REM input global data and calculate fluxes
 1490DEF PROCCALCULATE
 1500IF FLAG=1 THEN ENDPROC
 1510CLS
 1520PRINT"ENTER THE FOLLOWING VARIABLES"
 1530INPUT"pH";PH
 1540INPUT"BISMUTH CALIBRATION(mV/pH)";BCAL
 1550 INPUT"STARTING Bi pH VALUE";BS
 1560INPUT"Nd";ND
 1570INPUT"ROTATION SPEED(Hz)";W
 1580 INPUT"ARE THESE CORRECT(Y/N)";ZZ$
 1590IF ZZ$<>"Y" THEN GOTO 1520
 1600LET HINF=10^(-PH)
 1610LET OHINF=10^(PH-14)
 1620IF HINF>=OHINF THEN F1=0 ELSE F1=1
 1630FOR J=1 TO CT
 1640X=10^(-BS+Y(J)/BCAL)
 1650Y=1E-14/X
 1660 IF (F1=0 AND X>HINF) OR (F1=1 AND Y>OHINF) THEN PROCone:Z(J)=4:GOTO 1700
 1670 IF (F1=0 AND Y>X) OR (F1=1 AND Y<X) THEN PROCtwo:Z(J)=2:GOTO1700
 1680IF (F1=0 AND X<HINF*(1-ND) AND X>0) OR (F1=1 AND Y<OHINF*(1-ND) AND Y>0) THEN PROCthree:Z(J)=3:
GOTO 1700
 1690IF (F1=0 AND X>HINF*(1-ND) AND X<HINF) OR (F1=1 AND Y>OHINF*(1-ND) AND Y<OHINF) THEN PROCfour:Z
(J)=4:GOTO1700
 1700NEXT J
 1710FLAG=1
 1720ENDPROC
```

```
 1730 REM ************************************************************************
 1740 REM
 17500EF PROCone
 1760IF F1=0 THEN Y(J)=1.554*SQR(W)/ND/.466*(9.34E-5)^(2/3)*(X-HINF)/1000
 1770IF F1=1 THEN Y(J)=1.554*SQR(W)/ND/.466*(5.27E-5)^(2/3)*(Y-OHINF)/1000
 1780ENDPROC
 1790 REM ************************************************************************
 1800 REM
 1810DEF PROCtwo
 1820 IF F1=0 THEN ALPHA=5.27/9.34:YR=Y/HINF:PROCquad ELSE GOTO 1840
 1830Y(J)=(5.27E-5*Y+9.34E-5*HINF)/(1000*ND*.643*W^(-.5)*.466*9.34E-5^(1/3)*(1-(1-ALPHA^(-1/3))/(ND*
(1+.1*DOB))))
 1840IF F1=1 THEN ALPHA=9.34/5.27:YR=X/OHINF:PROCquad ELSE GOTO 1860
 1850Y(J)=(9.34E-5*X+5.27E-5*OHINF)/(1000*ND*.643*W^(-.5)*.466*5.27E-5^(1/3)*(1-(1-ALPHA^(-1/3))/(ND
*(1+.1*DOB))))
 1860ENDPROC
 1870 REM ************************************************************************
 1880 REM
 1890DEF PROCthree
 1900IF F1=0 THEN Y(J)=(HINF/1000-(5.27/9.34)^(1/3)*X/1000)/(.643*W^(-.5)*.466*(9.34E-5)^(-2/3)*(1-
5.27/9.34)^(1/3)*(1-ND)))
 1910IF F1=1 THEN Y(J)=(OHINF/1000-(9.34/5.27)^(1/3)*Y/1000)/(.643*W^(-.5)*.466*(5.27E-5)^(-2/3)*(1-
(9.34/5.27)^(1/3)*(1-ND)))
 1920ENDPROC
 1930 REM ************************************************************************
 1940 REM
 1950DEF PROCfour
 1960IF F1=0 THEN Y(J)=9.34E-5^(2/3)*(HINF-X)/(1000*.643*W^(-.5)*.466*ND)
 1970IF F1=1 THEN Y(J)=5.27E-5^(2/3)*(OHINF-Y)/(1000*.643*W^(-.5)*.466*ND)
 1980ENDPROC
 1990 REM ************************************************************************
 2000 REM
 2010 DEF PROCquad
 2020 A1=.1*ND*ALPHA^(4/3)
 2030 A2=ALPHA-ALPHA^(1/3)*(1-ND)*(.1+ALPHA)-.1*ALPHA^(4/3)*YR
 2040A3=-(ALPHA*YR+ALPHA^(1/3)*(1-ND))
 2050DOB=(-A2+SQR(A2^2-4*A1*A3))/2/A1
 2060ENDPROC
```

REFERENCES

1. A.J. Bard, L.R. Faulkner, 'Electrochemical Methods', Wiley, (1980): 'Instrumental Methods In Electrochemistry', Southampton Electrochemistry Group, Ellis Horwood, (1985)
2. P.R Moses, L. Weir, R.W.Murray, Anal. Chem., (1975), 45, 1882.
3. W.J. Albery, A.R. Hillman, Ann. Rep. C, (1981), 78, 377.
4. R.W. Murray, J. Electroanal. Chem., (1984), 13, 191.
5. P.J. Peerce, A.J. Bard, J. Electroanal. Chem., (1980), 114, 89.
6. J.B. Kerr, L.L. Miller, M.R. Van de Mark, J. Am. Chem. Soc., (1980), 102, 3383.
7. A. Akohoshi, S. Toshima, K. Itaya, J. Phys. Chem., (1981), 85, 818.
8. N. Oyama, K. Sato, F.C. Anson, J. Electroanal. Chem., (1980), 115, 49: N. Oyama, F.C. Anson, J. Electrochem. Soc., (1980), 127, 640.
9. R. Hernandez, A.F. Diaz, R. Waltman, J. Bargon, J. Phys. Chem., (1984), 88, 3333.
10. M.F. Dautartas, J.F. Evans, J. Electroanal. Chem., (1980), 109, 301.
11. K.K. Kanazawa, A.F Diaz, R.H Geiss, W.D. Gill, J.F.Kwak, J.A. Logan, J.F. Rabolt, G.B. Street, J. Chem. Soc. Chem. Commun., (1979), 854.
12. T. Ikeda, C.R. Leidner, R.W. Murray, J. Am. Chem. Soc., (1981), 103, 7422.

13. J. Schneider, R.W. Murray, Anal. Chem., (1982), 54, 1508.

14. W.J. Albery, M.G. Boutelle, P.J. Colby, A.R. Hillman, J. Electroanal. Chem., (1982), 133, 135.

15. J.C.M. Brokken-Zijp, M.S. De Groot, Chem. Phys. Lett., (1980), 76, 1

16. A.F Diaz, J. Castillo, K.K. Kanazawa, J.A. Logan, M. Salmon, O. Fajardo, J. Electroanal. Chem., (1982), 133, 233.

17. N. Cenas, A. Pocius, J. Kulys, Bioelectrochem. Bioenerg., (1984), 12, 583.

18. G. Arai, M. Matshushita, I. Yasumori, Nippon Kagaku Kaishi, (1985), 5, 894.

19. M.F. Dautartas, J.F. Evans, J. Electroanal. Chem., (1980), 109, 301.

20. J.C. Moutet, J. Electroanal. Chem., (1984), 161, 181.

21. G.J. Samuels, T.J. Meyer, J. Am. Chem. Soc., (1981), 103, 307.

22. K.W. Willman, R.W. Murray, J. Electroanal. Chem., (1982), 133, 211.

23. J.B. Kerr, L.L. Miller, M.R. Van de Mark, J. Am. Chem. Soc., (1980), 102, 3383.

24. M.F. Dautartas, K.R. Mann, J.F. Evans, J. Electroanal. Chem., (1980), 110, 379.

25. T.R. O'Toole, L.D. Margerum, T.D. Westmoreland, W.J. Vining, R.W. Murray, T.J. Meyer, J. Chem. Soc. Chem. Commun., (1985), 1416.

26. P.M. Hoang, S. Holdcroft, B.L. Funt, J. Electrochem. Soc., (1985), 132, 2129.

27. J.E. Dubois, M.C. Pham, J. Electroanal. Chem., (1986), 199, 153.

28. C. Degrand, J. Electroanal. Chem., (1984), 169, 259.

29. H. Behret, H. Binder, G. Sandstede, G.G. Scherer, J. Electroanal. Chem., (1981), 117, 29.

30. O. Ikeda, K. Okayabashi, H. Tamura, Chem. Lett., (1983), 1821.

31. D.J. Harrison, M.S. Wrighton, J. Phys. Chem., (1984), 88, 3932.

32. K.P. Parsons, PhD. Thesis, University Of London, (1986).

33. P.J. Nigrey, A.G. MacDiarmid, A.J. Heeger, Mol. Cryst. Liq. Cryst., (1982), 83, 309.

34. A.G. MacDiarmid, R.B. Kaner, R.J. Mammone, A.J. Heeger, J. Phys. Colloq., (1983), C3, 543.

35. A.G. MacDiarmid, M. Aldissi, R.B. Kaner, M. Maxfield, R.J. Mammone, Abstract 557, Proc. Electrochem. Soc. Ext. Abs., (1983), 83-1.

36. R.J. Waltman, A. F. Diaz, J. Bargon, J. Electrochem. Soc., (1984), 131, 1452.

37. M.S. Simon, P.T. Moore, J. Polym. Sci. Polym. Chem. Ed., (1975), 13, 1.

38. A. Factor, G.E. Heinsohn, Polym. Lett., (1971), 9, 289.

39. H. Sato, T. Tamamura, J. Appl. Polm. Sci., (1979), 24, 2075.

40. M. Yamana, T. Kawata, Nippon Kagaku Kaishi, (1977), 7, 941.

41. F. Garnier, G. Tourillon, M. Gazard, J.C. Dubois, J. Electroanal. Chem., (1983), 148, 299.

42. M. Gazard, J.C. Dubois, M. Champagne, F. Garnier, G. Tourillon, J. Phys. Colloq., (1983), C3, 537.

43. T. Skotheim, I. Lundström, J. Prejza, J. Electrochem. Soc, (1981), 128, 1625.

44. T. Skotheim, L.-G. Peterson, O. Inganas, I. Lundström, J. Electrochem. Soc., (1982), 129, 1737.

45. T. Skotheim, O. Inganas, J. Prejza, I. Lundström, Mol. Cryst. Liq. Cryst., (1982), 83, 1361.

46. A.J. Frank, Mol. Cryst. Liq. Cryst., (1982), 83, 1373.

47. F.R.F. Fan, L. Bob, A.J. Bard, R. Nuofi, J. Electrochem. Soc., (1981), 128, 2042.

48. R. Nuofi, D. Tench, L.F. Warren, J. Electrochem. Soc., (1981), 128, 2596.

49. R. Nuofi, A.J. Nozik, J. White, L.F. Warren, J. Electrochem. Soc., (1982), 129, 2261.

50. R. Nuofi, A.J. Frank, A.J. Novik, J. Am. Chem. Soc., (1981), 103, 1849.

51. G. Horowitz, F. Garnier, J. Electrochem. Soc., (1985), 132, 634.

52. A. Kuczkowski, Phys. Status Solidi A, (1985), 89(1), K109.

53. S. Glenis, G. Horowitz, G. Tourillon, F. Garnier, Thin Solid Films, (1984), 111, 93.

54. P.V. Kamat, M.A. Fox, A.J. Fatiadi, J. Am. Chem. Soc., (1984), 106, 1191.

55. P.C. Lee, M.S. Matheson, D. Meisel, Isr. J. Chem., (1982), 22, 133.

56. L.L. Miller, R.L. Blankespoor, J. Chem. Soc. Chem. Commun., (1985), 90.

57. R.B. Bjorklund, I. Lundström, J. Electron. Mat., (1984), 13, 211.

58. T. Von Karmen, Z. Angew. Math. Mech., (1921), 1, 233.

59. V.G. Levich, Acta Phys. Chim. URSS, (1942), 17, 257.

60. J. Koutecky, V.G. Levich, Zh. Fiz. Khim., (1956), 32, 1565.

61. W.J. Albery, A.W. Foulds, K.J. Hall, A.R. Hillman, J. Electrochem. Soc., (1980), 127, 654.

62. A.R. Hillman, PhD. Thesis, University Of Oxford, (1979).

63. A.N. Frumkin, L.I. Nekrasov, Dokl. Akad. Nauk. SSSR, (1959), 126, 115.

64. W.J. Albery, M.L. Hitchman, 'Ring-Disc Electrodes', Oxford University Press, (1971).

65. W.J. Albery, Trans. Faraday Soc., (1966), 62, 1915.

66. W.J. Albery, S. Bruckenstein, Trans. Faraday Soc., (1966), 62, 1920.

67. W.J. Albery, S. Bruckenstein, D.T. Napp, Trans Faraday Soc., (1966), 62, 1932.

68. W.J. Albery, S. Bruckenstein, Trans. Faraday Soc., (1966), 62, 2596.

69. W.T. Grubb, L.H. King, Anal. Chem., (1980), 52, 270.

70. D.J.G Ives, G.T. Janz, `Reference Electrodes, Theory And Practise', Academic Press, (1961), ch. 7.

71. H.M Sammour, A.A Moussa, J. Chem. Soc., (1952), 1762.

72. D. Midgeley, K. Torrance, `Potentiometric Water Analysis', Wiley, (1978).

73. T. Katan, S. Szpak, D.N. Bennion, J. Electrochem. Soc., (1973), 120, 883.

74. V.B. Aleskovski, E.V. Bairichnyi, E.G. Ivanov, V.A. Nikol'ski, Sb. Rob. Khim. Istochnikam Toka, (1969), 4, 241.

75. W.J. Albery, E.J. Calvo, J. Chem. Soc. Faraday Trans 1, (1983), 79, 2583.

76. `Handbook Of Mathematical Functions', ed. M. Abramovitz, I.A. Stegun, Dover, (1965), p. 260.

77. `Handbook Of Mathematical Functions', ed. M. Abramovitz, I.A. Stegun, Dover, (1965), p. 262-263.

78. `Instrumental Methods In Electrochemistry', Southampton Electrochemistry Group, Ellis-Horwood, (1985), p.31.

79. W.J. Albery, M.G. Boutelle, P.J. Colby, A.R. Hillman, J. Electroanal. Chem., (1982), 133, 135.

80. `Instrumental Methods In Electrochemistry', Southampton Electrochemistry Group, Ellis-Horwood, (1985), ch. 6.

81. P.J. Colby, PhD. Thesis, University Of London, (1983).

82. J.E. Przeworski, PhD. Thesis, University Of London, (1984).

83. C.K. Mann, J. Electroanal. Chem., (1969), 4, 57.

84. M. Fleischmann, P.J. Hendra, A.J. Mcquillan, Chem. Phys. Lett., (1974), 26, 163.

85. K. Hutchinson, R.E. Hester, W.J. Albery, A.R. Hillman, J. Chem Soc. Faraday Trans. 1, (1984), 80, 2053.

86. C.M. Pham, F. Adami, P.C. Lacaze, J.P. Doucet, J.E. Dubois, J. Electroanal. Chem., (1986), 201, 413.

87. P.A. Wilks, T. Hirschfield, Appl. Spectrosc. Rev., (1967), 1, 99.

88. M. Harbough, F.C. Mather, Trans. Electrochem. Soc., (1933), 64, 293.

89. C.P. Andrieux, J.M. Dumas-Bouchiat, J.M. Savèant, J. Electroanal. Chem., (1982), 131, 1.

90. A.F. Diaz, K.K. Kanazawa, G.P. Gardini, J. Chem. Soc. Chem. Commun., (1979), 635.

91. A.F. Diaz, Chem. Scr., (1981), 17, 5.

92. G. Tourillon, F. Garnier, J. Electroanal. Chem., (1982), 135, 183.

93. R.J. Waltman, A.F. Diaz, J. Bargon, J. Phys. Chem., (1984), 88, 4343.

94. J. Bargon, S. Mohmand, R.J. Waltman, IBM J. Res. Dev., (1983), 27, 330.

95. A.F. Diaz, J.J. Castillo, J.A. Logan, W.-Y. Lee, J. Electroanal. Chem., (1981), 129, 115.

96. R.J. Waltman, J. Bargon, A.F. Diaz, J. Phys. Chem., (1983), 87, 1459.

97. `Oxidation In Organic Chemistry 5-A', Academic Press, , pp. 398-405.

98. R.N. Butler in `Synthetic Reagents Vol. 3', ed. J.S. Pizey, (1977), Ch. 4.: A.S. Perlin, Adv. Carbohydrate Chem., (1959), 14, 9.

99. S. Uemura in `Synthetic Reagents Vol. 5', ed. J.S. Pizey, (1983), Ch. 3.

100. A.F. Diaz, W.-Y. Lee, A. Logan, D.C. Green, J. Electroanal. Chem., (1980), 108, 377.

101. A.F. Diaz, J. Castillo, K.K. Kanazawa, J.A. Logan, M. Salmon, O. Fajardo, J. Electroanal. Chem., (1982), 133, 233.

102. R.J. Waltman, J. Bargon, Can. J. Chem., (1986), 64, 76.

103. A.M. Van Leusen, H. Siderius, B.E. Hogenboom, D. Van Leusen, Tett. Lett., (1972), 53, 5337.

104. `Instrumental Methods In Electrochemistry', Southampton Electrochemistry Group, Ellis Horwood, (1985), Ch. 9.

105. A.R. Hillman, private communication.

106. C.J. Pochert, `*The Aldrich Library Of Infrared* Spectra', (1975), Spectrum 3,1211E.

107. K. Siegbahn et al, Nova Acta Reg. Sco. Sci. Upsaliensis Ser. IV, (1967), 20, 1.

108. D. Penn, J. Elec. Spec. Rel. Phem., (1976), 9, 2940.

109. V.M.Parikh, `Absorption Spectroscopy Of Organic Molecules', Addison-Wesley, (1974), p.250.

110. `Chemical Rubber Co. Handbook 60th. Ed.', CRC Press, (1979), B-90.

111. `Chemical Rubber Co. Handbook 60th. Ed.', CRC Press, (1979), D-164.

112. C.J. Pochert, `The Aldrich Library Of Infrared Spectra', (1975), Spectrum 3,325D.

113. S. Evans, R.G. Pritchard, J.M. Thomas, J. Elec. Spec., Rel. Phem., (1976), 8, 129.

114. T. Yamamoto, K. Samechika, A. Yamamoto, J. Polym. Sci. Polym. Lett., (1980), 18, 9.

115. H.B. Mark, A. Czerwinski, H. Zimmer, A. Amer, C. van Pham, S.Pons, J. Chem. Soc. Chem. Commun., (1985), 1158.

116. J.L. Brèdas, G.B. Street, B. Thémans, J.M. Andrè, J. Chem. Phys., (1985), 83, 1323.

117. V.D. Parker, Electrochim. Acta, (1973), 18, 519.

118. `Encyclopaedia Of The Electrochemistry Of The Elements', ed. A.J. Bard, (1978), Vol. XI-2.

119. `Encyclopaedia Of The Electrochemistry Of The Elements', ed. A.J. Bard, (1978), Vol. I.

120. `Encyclopaedia Of The Electrochemistry Of The Elements', ed. A.J. Bard, (1978), Vol. IV.

121. W.J. Albery, C.C. Jones, submitted for publication (1986).

122. E.M. Genies, J.-M. Pernaut, J. Electroanal. Chem., (1985), 111, 11.

123. C.C. Jones, private communication: L. Emsley, Third Year Report, Imperial College, (1986).

124. W.J. Albery, P.N. Bartlett, C.P. Wilde, J.R. Darwent, J. Am. Chem. Soc., (1985), 107, 1854.

125. J.K. Groves, N.E. Cundasawmy, H.J. Anderson, Can. J. Chem., (1973), 51, 1089.

126. C.M. Elliot, J.G. Redepenning, J. Electroanal. Chem., (1984), 181, 137.

127. S.W. Feldberg, J. Am. Chem. Soc., (1984), 106, 4671.

128. `Instrumental Methods In Electrochemistry', Southampton Electrochemistry Group, Ellis Horwood, (1985), Ch. 5.

129. W.J. Albery, `Electrode Kinetics', Clarendon Press, (1975).

130. K.J. Vetter, `Electrochemical Kinetics', Academic Press, (1967): J. Koryta, `Ion-Selective Electrodes', Cambridge University Press, (1975).

131. W.J. Albery, W.R. Bowen, F.S. Fisher, A.W. Foulds, K.J. Hall, A.R. Hillman, R.G. Egdell, A.R. Orchard, J. Electroanal. Chem., (1980), 107, 37.

132. W.J. Albery, A.W. Foulds, K.J. Hall, A.R. Hillman, R.G. Egdell, A.R. Orchard, Nature, (1979), 282, 793.

133. J.M. Bauldray, M.D. Archer, Electrochim. Acta, (1983), 28, 1515.

134. M.I.C. Ferreira, PhD. Thesis, University Of London, (1980).

135. S. Bruckenstein, G.A. Feldman, J. Electroanal. Chem., (1965), 9, 395.

136. W.J. Albery, M.G. Boutelle, P.J. Colby, A.R. Hillman, J. Chem. Soc. Faraday Trans. 1, (1982), 78, 2757.

137. W.J. Albery, J.S. Drury, M.L. Hitchman, Trans. Faraday Soc., (1971), 67, 2162.

138. `Surface Enhanced Raman Scattering', ed. R.K. Chang, T.E. Furtak, Plenum Press, (1982).